JOURNAL OF THE

Electrochemical Society

l. 105, No. 6 June 1958

Keeping Hooker Cells at their best

Making the best use of the remarkable efficiency of Hooker cells depends upon the skills of the men who operate them.

Also at work, with a skill all their own, are GLC ANODES, which are "custom made" to individual cell requirements.

FREE – *This illustration of keeping cells at peak efficiency has been handsomely reproduced with no advertising text. We will be pleased to send you one of these reproductions with our compliments. Simply write to Dept. J-6.*

ELECTRODE
GLC®
DIVISION

GREAT LAKES CARBON CORPORATION

18 EAST 48TH STREET, NEW YORK 17, N.Y. OFFICES IN PRINCIPAL CITIES

Journal of the Electrochemical Society

JUNE 1958 **VOL. 105 • NO. 6**

CONTENTS

Published monthly by The Electrochemical Society, Inc., from Manchester, N. H., **Executive Offices, Editorial Office** and **Circulation Dept.**, and **Advertising Office** at 1860 Broadway, New York 23, N. Y., combining the JOURNAL and TRANSACTIONS OF THE ELECTROCHEMICAL SOCIETY. Statements and opinions given in articles and papers in the JOURNAL OF THE ELECTROCHEMICAL SOCIETY are those of the contributors, and The Electrochemical Society assumes no responsibility for them. Nondeductible subscription to members $5.00; subscription to nonmembers $18.00. Single copies $1.25 to members, $1.75 to nonmembers.

Entered as second-class matter at the Post Office at Manchester, N. H., under the act of August 24, 1912.

Editorial

The Editor Makes Mistakes

GREMLINS sometimes find their way into the editorial inkwell and typewriter. In September 1956 Lake Michigan was placed at a somewhat greater elevation above sea level than has been established by the U. S. Coast and Geodetic Survey, and we were promptly informed of the error. Moral: while it is all right for the German farmers of eastern Maryland and Delaware to be convinced that salt water in the sauerkraut barrel rises and falls with the nearby ocean tides, any editor should be able to copy facts correctly.

In April 1957 we stated that publication in the JOURNAL was being delayed by lack of funds for printing and for editorial assistance. To be sure, this had been the case, but more careful examination would have shown that the situation was correcting itself. The Board of Directors had allotted more money to the JOURNAL, and a change of printer was effecting some saving. A few more technical articles were published each month; for some reason manuscripts came back more slowly from the review staff, and the backlog of accepted papers shrank rapidly. Delay now is largely due to the time taken for review and revision. It is difficult to handle promptly the number of manuscripts received, even with two Divisional Editors for some of the Divisions. Every technical journal of high standards has a similar problem: to induce capable and busy men to give high priority to review of its manuscripts. Authors can help a great deal, both by following the "Instructions to Authors" and the JOURNAL style closely, and by writing carefully, clearly, and concisely, keeping in mind that correspondence, revision, and additional reviewing take time.

The Editorial of February 1958 unfortunately stated that ocean vessels require more current for cathodic protection when in port than when under way at sea: the opposite is true. This statement brought prompt denial from representatives of both the Royal Canadian Navy and the U.S. Navy. Their letters are published elsewhere in the JOURNAL,* since they contain other information and comments of interest.

Last month's Editorial concerning translation from the Russian may have been misleading in some respects: a great many capable scientists in this country can, of course, read Russian with ease. In early March we sent a request to 21 laboratories: who could examine two Russian books dealing with problems in corrosion, and advise whether English translations would be useful? Eleven of the persons addressed replied yes, someone was available who would examine the books, possibly translate them. One correspondent was acquainted with both, pointed out that one is a collection of papers which has been translated from English into Russian!

No errors have been pointed out in the March 1957 comments concerning the prospects of mankind for the year 101,957. Writing science fiction should be interesting; it must be hard to make mistakes.

—CVK

* Letters to the Editor, 105, May issue, p. 97C, and June issue, p. 113C (1958).

Silver, Cobalt, and Positive-Grid Corrosion in the Lead-Acid Battery

J. J. Lander

The Electric Auto-Lite Company, Toledo, Ohio

ABSTRACT

Positive-grid corrosion rates measured at several temperatures over a range of potentials corresponding to overcharge conditions show that voltage depression at the positive plate of but a few hundredths of a volt can result in corrosion rates decreasing by factors of one-third to one-half or more. Silver and cobalt when added directly to the electrolyte of batteries on SAE Overcharge Life Test depolarize the positive plate overcharge voltage, resulting in increased overcharge life. An identical series of reactions is proposed to explain the depolarizing effects of silver and cobalt. Overcharge corrosion does not play a major role in governing the service life of passenger car batteries. The SAE Overcharge Life Test cannot be expected to evaluate the effects of silver and cobalt on service life.

In the past year or so there has been an intense reawakening of interest in the effects of silver and cobalt on positive-grid corrosion in the lead-acid battery, especially in automotive types. Considerable evidence exists to show that the addition of cobalt to the battery electrolyte is quite effective in reducing grid corrosion under certain overcharge conditions (1-3). More evidence is presented in this paper. A patent covering this protective aspect of Co was issued in 1931 (4). The use of Ag in grid alloys for the purpose of decreasing overcharge corrosion, first studied by Fink and Dornblatt (5), was suggested by earlier work in which Ag-Pb alloy anodes were used in various electrolytic processes (6). Several patents have been issued for the use of Ag in grid metal (7). Older and less well known, perhaps, is the claim that Ag, even as Co, is effective as an additive to the electrolyte in extending life (8). Under current-regulated overcharge conditions only, this claim is supported herein. An interesting feature of the use of Ag is that it does not seem to be effective except under overcharge conditions (5, 9, 10). There is some evidence that this is true of Co (2).

Along with the similarities between Co and Ag already noted, another effect has been observed, i.e., addition of Co to the electrolyte results in a lowering of the oxygen overvoltage at the positive plate (2, 3, 11). Silver does so as will be shown.

These parallels between the action of Co and Ag, in conjunction with thermodynamic data and measured corrosion rates of Sb alloys, lead to a simple, consistent explanation for their protective effect. Mechanisms of protection are identical for each element; they can be expected to be protective only under overcharge conditions; and, more specifically, they are especially protective under conditions imposed by the SAE Overcharge Test.

A tentative explanation for the effect of Ag has been offered (9) which tried to relate decreased corrosion to the catalytic activity of Ag in decomposing persulfate ion. No supporting evidence was offered. Other work (2, 3) attempted to treat the theory of the effect of Co, but led to proposals of conflicting and ill-defined mechanisms because the proper corrosion data were lacking and because part of the thermodynamic data was neglected.

Table I gives the standard electrode potentials (12) for the reactions concerned.

In this way, Co^{++} and Ag^{+} would be returned to solution and the concentration of Co^{+++} and Ag^{++} would not be allowed to build up to shut off the reaction. Co^{+++} does in fact oxidize water at appreciable rates (13). When a battery is on overcharge, substantially all the current that passes through the positive plate goes to evolution of oxygen. The higher the current, the higher is the overcharge

Table I

$PbSO_4 + 2H_2O = PbO_2 + SO_4^{=} + 4H^{+} + 2e$	$+1.685$	(I)
$Co^{++} = Co^{+++} + e$	$+1.82$	(II)
$Ag^{+} = Ag^{++} + e$	$+1.98$	(III)

Reaction (I) takes place at the positive plate of the lead-acid cell. On charge, as this reaction nears completion, the evolution of oxygen commences and, at the same time, positive plate potentials become more positive to extents sufficient for reactions (II) or (III) to go when Co^{++} or Ag^{+} is present in the electrolyte. If these reactions occur, Co^{+++} and Ag^{++} can oxidize water to H_2O_2 as in reactions (IV) and (V)

$$2H_2O + 2Co^{+++} = H_2O_2 + 2Co^{++} + 2H^{+}, \quad F^\circ = -1.5 \text{ kcal} \quad \text{(IV)}$$

$$2H_2O + 2Ag^{++} = H_2O_2 + 2Ag^{+} + 2H^{+}, \quad F^\circ = -9.5 \text{ kcal} \quad \text{(V)}$$

H_2O_2 decomposes in acid solution to give oxygen:

$$2H_2O_2 = O_2 + 2H_2O, \quad F^\circ = -50.4 \text{ kcal} \quad \text{(VI)}$$

potential at the positive plate, according to often observed empirical relationships. The effect of Ag and Co is to supply an alternate path for the evolution of oxygen; therefore, their presence should result in a decreased oxygen overvoltage, as has been mentioned. It will be shown that small amounts of either Ag or Co in the electrolyte produce voltage decreases of several hundredths of a volt at the positive plate on overcharge. It will also be shown that voltage depressions of this order of magnitude can lower corrosion rates of antimonial alloys by factors of 30-90% in the SAE Overcharge Life Test range of potential. Cobalt should be the more effective depolarizer according to the potentials of reactions (II) and (III).

The possibility of this depolarization mechanism for the effect of Co on corrosion has been pointed out in substance (3), but because the corrosion work was done with Pb rather than antimonial alloys, it has been concluded (2) that the voltage lowering produced by Co was incapable of decreasing corrosion to any appreciable extent. This led to favorable entertainment of an adsorption theory. In these works (2, 3) the mechanistic identity of the function of Ag and Co in overcharge protection was not considered.

Experimental

Corrosion rates of an antimonial alloy (6.75% Sb, 0.4 As, 0.35 Sn, balance Pb) were obtained by corroding bare grids at several constant potentials in the overcharge range in acid of 1.260 sp gr. Three temperatures were used and potential was measured with reference to a mercury-mercurous sulfate electrode in the electrolyte. Rates were obtained by stripping the corrosion product in a mannitol solution 10 g hydrazine dihydrochloride, 20 g mannitol, 100 g sodium hydroxide, per liter of solution, and obtaining weight losses as a function of time on test. Typical weight loss curves are shown in Fig. 1 for several potentials at 37.8°C and rates obtained for all potentials and temperatures are shown in Fig. 2. The potential scale has been converted to the cadmium reference electrode in all charts. The 26.6°C data is extended to lower voltages by including data on 6-8% Sb alloys obtained from other sources (14).

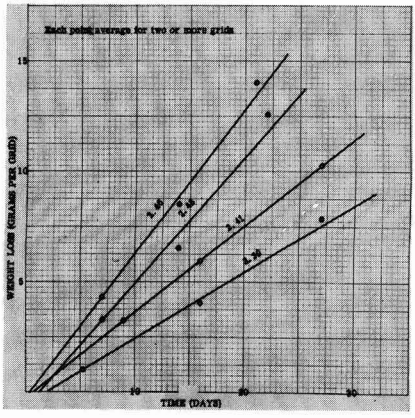

Fig. 1. Grid-corrosion at several overcharge voltages, 100°F

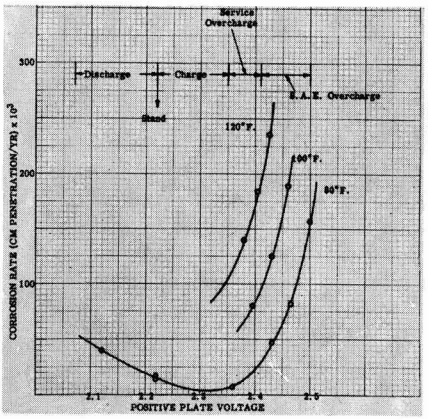

Fig. 2. Positive-grid corrosion rate vs. positive plate voltage

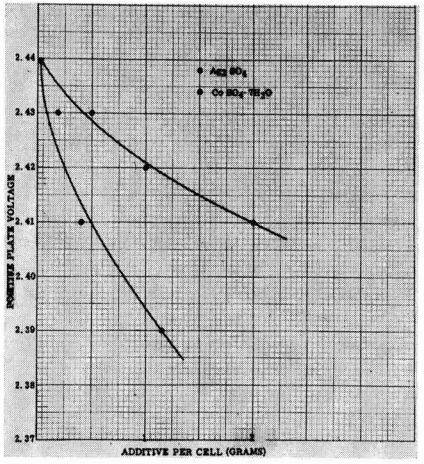

Fig. 3. Effect of Co and Ag on positive plate overcharge voltage. Group 1 Battery at 9 amp.

In another test, silver sulfate and cobalt sulfate were added in varying amounts to the electrolyte of Group 1—6-v batteries at the time they started on SAE Overcharge Life Test (15). The effect of these elements on the positive plate overcharge voltage is shown in Fig. 3. The voltage decreases exhibited persisted throughout the life test. The overcharge life of these batteries is given in Table II.

All batteries failed by positive grid corrosion.

Table II. Effect of silver and cobalt on SAE Overcharge Life

Ag_2SO_4 added/cell g	SAE Overcharge Life (Avg of 2 batteries) weeks
None	10
0.5	11.5
1.0	12.0
2.0	15.0
$CoSO_4 \cdot 7H_2O$ added/cell	
None	9.5
0.17	10.0
0.46	12.5
1.14	17.0

Table III. Estimated vs. actual increase in SAE Overcharge Life

Ag_2SO_4 added/cell g	Voltage depression v	% Life increase (Est'd.)	% Life increase (Expt'l.)
0	0	0	0
0.5	0.01	14	15
1.0	0.02	29	20
2.0	0.03	45	50
$CoSO_4 \cdot 7H_2O$ added/cell			
0	0	0	0
0.17	0.01	14	5
0.46	0.03	45	32
1.14	0.05	85	79

Discussion

SAE Overcharge Life Test

The positive cadmium voltages of various battery types on the SAE Overcharge Life Test fall in the range marked on Fig. 2. Internal temperatures of batteries on this test range around 43°-49°C. The slopes of the curves of Fig. 2 show that voltage depressions of but a few hundredths of a volt are quite sufficient to decrease the corrosion rate by 30-90%. From the measured decreases in voltage resulting from the use of Ag and Co shown in Fig. 3 the life increase can be estimated; for example, a voltage depression of 0.06 v at 49°C (2.43 to 2.37) cuts the corrosion rate in half which should double the SAE Overcharge life. Estimated increases for Ag and Co additions are compared with those actually obtained in Table III.

The calculated and experimental life increases are in as good agreement as can be expected considering that the usual variation in overcharge life runs about ±0.5 week when hand-pasted selected grids are used for positives. There is no doubt that voltage depressions of the values measured are quite capable of extending SAE Overcharge Life by the values found.

Whether or not the reactions go as explained in the theory needs demonstration of one step, i.e., that Co^{+++} and Ag^{++} are formed electrochemically at rates sufficient to by-pass appreciable amounts of current from the usual oxygen-producing reaction. The voltage depression is an indirect indication that they are formed at sufficient rates. In the absence of direct knowledge, however, it is not impossible that another mechanism could be operating. Regardless of the mechanism of voltage depression, the relation between voltage depression and increased overcharge life has been demonstrated quantitatively within experimental error, i.e., if other factors were operating in appreciable measure to decrease corrosion and increase life, this quantitative agreement would not have been produced. This is further illustrated by Fig. 4 which shows life increase as a function of voltage depression for both Ag and Co; it seems to be immaterial which element does the job. Therefore, it may be concluded that Ag and Co act to increase overcharge life by depressing the positive plate overcharge voltage at constant current, thus reducing the grid corrosion rate under constant current conditions.

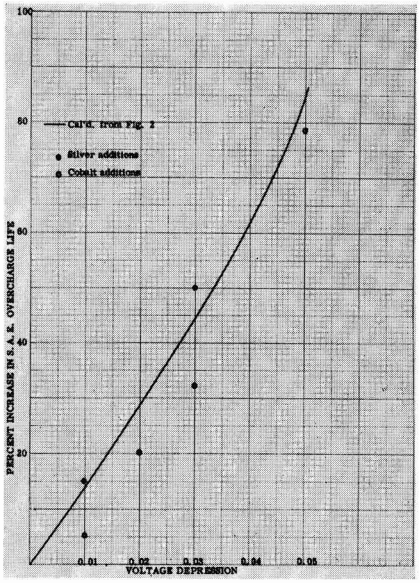

Fig. 4. SAE Overcharge Life vs. positive-plate voltage depression. Calculated vs. experimental.

Automobile Battery Service

At one time it was more or less generally accepted in the automobile battery industry that in-service failure of positive grids was due to overcharge corrosion. It has been pointed out (16) that, because of the large fraction of time spent in idle periods, positive grids of automobile batteries should approach the life of the same batteries on float, their life being governed largely by grid corrosion rates on stand. There is still disagreement, however, as to which area or areas of service operation affect grid corrosion most importantly (17). This question can be resolved using the data of Fig. 2. Inasmuch as the ordinate of this graph is a rate, the curves of the graph show the important variables affecting grid corrosion to be: time, potential, and temperature. If it were known what fractions of time are spent by the positive plate in the various voltage ranges, the relative effects of the various operating conditions could be determined.

For purposes of calculation, the time distribution for passenger car service can be fixed if it is supposed that the ordinary car travels to and from work once a day for two hours, six days a week. For city driving, perhaps 20% of this time will be spent in overcharging the battery. Also let the car be driven for two hours in the country once a week, during which the battery is on overcharge, say, 75% of the time. The remainder of time the car is parked and the battery is idle. If the driving time not spent on overcharge is arbitrarily divided into 10% discharge time and 90% charge time, the above breakdown per week results in the time distribution shown in the first column of Table IV.

If these percentages of time are multiplied by their corresponding corrosion rates as determined from Fig. 2, an index of corrosion for each condition is

Table IV. Voltage-time corrosion of positive grids in service

Voltage condition	% of time	Corrosion rate	Index	% Corrosion
Discharge	0.6	35	21	2.1
Charge	5.4	6	32	3.1
Overcharge	2.3	25	58	5.6
Stand	91.7	10	917	89.2

obtained. These results are shown in Table IV for 26.6°C.

On the basis of this analysis only 6% of the total grid corrosion occurs during overcharge; 89% occurs while the battery is idle. Certainly, the time schedule on which this analysis is based can be varied within limits for passenger car service, but it is clear that the bulk of the grid corrosion will occur while the battery is standing idle, because the stand time far outweighs the driving time.

It can be shown in another way that overcharge corrosion is of minor influence on positive grid life. Twelve-volt, 50 A.H. batteries containing 60 mil positive plates exhibited an average of 16 weeks on the SAE Overcharge Life Test. On this test, about five days a week are spent on overcharge; therefore, the overcharge life of these batteries is about 1920 hr. In the previous time analysis, overcharge time was estimated to be about 4 hr/week. If it is true that batteries fail in service by overcharge corrosion, the service life of this battery should be $1920 \div 4 =$ 480 weeks or 9.2 years. This is a minimum value because overcharge conditions of potential and temperature are not nearly so severe in service as they are on the overcharge test. The warranty on this battery is three years.

The foregoing analysis shows that elements which act as depolarizers at the positive plate can have little or no favorable effect on grid corrosion in service life in passenger cars; indeed, there is some reason to believe that both Ag (9) and Co (10) may hasten grid corrosion at the stand potential and thus shorten grid life. The simple addition of Co may be expected to increase self-discharge at the positive plate (18) and it definitely does decrease charging efficiency at the positive plate (19).

While it has been concluded that service life of positive grids can be affected but slightly by overcharge conditions in passenger car service, it may be worthwhile to consider the implications arising from the voltage regulator system. Depolarization at either plate will result in logarithmic increases in overcharge current and, since water-loss and temperature increase are linearly related to overcharge current, these will increase logarithmically also. If both Ag and Co were to depolarize the negative as well as the positive and if the effect were equal at the negative, no decrease in positive plate voltage could occur and hence no improvement in overcharge corrosion could accrue, because current would have to increase enough to make up the voltage loss. If Ag and Co were to stay at the positive plate, a decrease in overcharge corrosion would result which might contribute as much as 2-3% increase in life, based on Table IV, unless heating caused by the extra current due to depolarization should increase corrosion enough to overbalance the beneficial effect of depolarization.

On the basis of the conclusion that overcharge corrosion is incapable of a large influence on service life and the considerations arising from the voltage-regulated system, the SAE Overcharge Test cannot be expected to evaluate the effect of Ag and Co on service life.

Acknowledgments

Mr. Dwayne Spoon obtained the grid corrosion data and the Battery Test Section, under Mr. P. A. Cherenzia, obtained the SAE Overcharge Life data.

Manuscript received June 26, 1957. This paper was prepared for delivery before the Buffalo Meeting, Oct. 6-10, 1957.

Any discussion of this paper will appear in a Discussion Section to be published in the December 1958 JOURNAL.

REFERENCES

1. G. W. Vinal, *et al.*, R.P. 1335, *J. Research Nat'l. Bur. Standards*, **25**, 417 (1940).
2. E. V. Krivolapova and B. N. Kabanov, *Trudy Soveshchaniya Elektrokhim, Akad. Nauk S.S.S.R., Otdel. Khim. Nauk*, **1950**, 539 (1953).
3. L. I. Antropov, *et al.*, *ibid*, **1950**, 549 (1953).
4. F. Booss and R. N. Chamberlain, U.S. Pat. 1,826,724, Oct. 13, 1931.
5. C. G. Fink and A. J. Dornblatt, *Trans. Electrochem. Soc.*, **79**, 269 (1941).
6. C. G. Fink and L. C. Pan, *ibid.*, **46**, 349 (1924); **49**, 85 (1926); C. G. Fink and R. E. Lowe, U.S. Pat. 1,740,291, Dec. 17, 1929. Many references quoted in footnotes 17 and 18 in reference 5.
7. L. E. Lighton, U.S. Pat. 2,333,072, Oct. 26, 1943; H. Stoertz, U.S. Pat. 2,678,340, May 11, 1953; A. Kawabe, Japanese Pat. 3459 ('54) (1954); W. P. Carroll, U.S. Pat. 2,694,628, Nov. 16, 1954.
8. J. Luthy, U.S. Pat. 1,161,398, Nov. 23, 1915.
9. W. H. Power, *et al.*, Naval Research Laboratory Report P-2908 (1947).
10. J. J. Lander, Unpublished work, Naval Research Laboratory.
11. H. M. Wood, CEO 22545, Sept. 1953. The Electric Auto-Lite Company.
12. W. M. Latimer, "Oxidation Potentials," 2nd ed., p. 345, Prentice-Hall, New York (1952).
13. R. S. Young, "Cobalt," p. 61, A.C.S. Monograph No. 108, Reinhold Publishing Corp., New York (1948); C. E. H. Bawn and A. G. White, *J. Chem. Soc.*, **1951**, 331.
14. J. J. Lander, *This Journal*, **99**, 467 (1952); reference 10; and unpublished work in this laboratory.
15. G. W. Vinal, "Storage Batteries," 4th ed., p. 347, John Wiley & Sons, Inc., New York (1954).
16. J. J. Lander, *This Journal*, **103**, 1 (1956); Naval Research Laboratory Report 4475, Jan. 1955.
17. E. Willihnganz, Discussion, p. 86, in "Life Testing of Automobile Batteries and Related Subjects," The Electrochemical Society, New York (1956).
18. M. Rey, *et al.*, *Trans. Electrochem. Soc.*, **73**, 324, (1938).
19. W. T. Abel, ED-5496, Aug. 1957. The Electric Auto-Lite Company.

A Film Lining for High-Capacity Dry Cells

N. C. Cahoon and M. P. Korver

National Carbon Research Laboratories, National Carbon Company,

A Division of Union Carbide Corporation, Cleveland, Ohio

ABSTRACT

The use of cereal paste is shown to contribute, to a considerable degree, to the deterioration observed in experimental dry cells made with synthetic MnO_2 depolarizers. The mechanism involves the hydrolysis of the cereal to form a reducing compound which then reacts chemically with the MnO_2 to consume a part of the available oxygen content of the depolarizer. A group of chemically inert hydrophilic colloids, including methyl cellulose, was selected for evaluation as separators. The application of methyl cellulose in a two-film lining for a dry cell is described. The anode film, to be placed next to the anode, is formulated from methyl cellulose and a mercury salt. The barrier film used to separate the anode from the depolarizer mix is formulated from methyl cellulose insolubilized to a limited degree with citric acid. Experimental cells incorporating the composite film lining show keeping qualities far surpassing those of paste-type cells.

Since the introduction of the commercial dry cell in the middle 1880's the cell liner has shown a gradual evolution through cloth, papers and pasted papers to the cereal paste used in many present-day cells. The trend has continually been toward thinner liners as a means both of reducing the internal resistance of the cell and of increasing the quantity of active depolarizer.

During recent years, the use of active electrolytic manganese dioxide has become widespread (1). However, certain early types of experimental cells prepared with this material have shown unexpected cell deterioration during storage. Table I shows the service levels of experimental cells assembled with an electrolytic MnO_2 depolarizer and cereal paste separators. It is clear that a serious drop in battery capacity (22-31%) occurs in the relatively short storage period of about two months at 70°F. The cells made with both flour and starch showed such a significant decrease in service that it caused serious concern.

The investigation of the cause of cell deterioration established that the hydrolysis of the separator was responsible for the reduced battery capacity. To correct this condition, a separator medium was needed which would not hydrolyze and react with the active MnO_2 depolarizer.

Table I. Service of experimental "D"-size cells made with electrolytic MnO_2 and paste*

Cell age†	Separators: Minutes service to 0.9 v on 4-ohm HIF test at 70°F — 3 Weeks	3 Months	6 Months
Separator Cereal			
Flour	928	635	640
Cornstarch	1108	866	792

* The cells described above were experimental units designed only for the study of the reaction between the depolarizer and the cereal content of the paste.

† These cells were stored at 70°F.

Experimental

Experimental attention was, therefore, directed to other hydrophilic materials which could be considered for dry-cell separators. A considerable number of materials were selected which, in general, were synthetically prepared and free of many of the variations that develop in naturally occurring materials. The alkyl cellulose ethers, the hydroxy alkyl cellulose ethers, the salts of cellulose glycolic acid, and a number of vinyl compounds, e.g., polyvinyl alcohol, were the most attractive of the groups studied. It was found that no reaction occurs between the above materials and electrolytic MnO_2 under simulated dry-cell conditions.

The film-forming properties of methyl cellulose permitted the easy preparation of sheets. A horizontal glass plate was coated with an aqueous solution of this material and allowed to dry. Such sheets or films were well suited to the manufacture of experimental dry cells.[1] A comparison of the performance of cells made with methyl cellulose and cereal paste separators showed that, until the cells were about six weeks old, similar results were obtained. A sudden voltage drop in the methyl cellulose cells, beginning at this point, was found to result from the slow solution of the methyl cellulose film in the electrolyte followed by its absorption into the cathode mix. This left the anode unprotected and resulted in serious corrosion.

One method of attaining the desired film permanence appeared to be a treatment which could be applied to only one surface of the methyl cellulose film. Such a protective layer should be insoluble in electrolyte, yet still permit rapid diffusion of

[1] Methyl cellulose also appeared applicable as an improvement over the cereal coatings frequently applied to cellulosic or paper layers.

Table II. Effect of the tannic acid content of methyl cellulose films on the performance of "D" size cells

Amount of tannic acid in film liner* g		70°F 4-Ohm HIF† service to 0.9 v % of control
Control	0	100
	0.10	104
	0.20	98
	0.40	98
	0.60	100
	0.80	91

* The amount of tannic acid combined with 14.0 g methyl cellulose is given above.
† The abbreviation HIF is used to indicate the Standard Heavy Industrial Flashlight test, accepted throughout the industry.

zinc chloride from anolyte to catholyte. At the same time, it should prevent the migration of the dissolved methyl cellulose from the anode surface. A large group of substances (2), including tannic, trichloroacetic, and phosphotungstic acids, will react with methyl cellulose to reduce its solubility. Tannic acid was chosen for study. Experimental films were surface-tanned by exposing one surface to a tannic acid solution for a definite time and at a given temperature. However, the precise control of conditions necessary to attain the desired result from this process appeared difficult and alternative methods were investigated.

An improvement on the above process was the incorporation of the tannic acid into the methyl cellulose solution used for the preparation of the film lining. A series of films were prepared in which amounts of tannic acid ranging from 0.10 g to 0.80 g were combined with 14.0 g of methyl cellulose in solution. The dry films were used in the preparation of experimental cells which were placed on test with the initial results shown in Table II. These data illustrate that the presence of tannic acid in the film lining does not materially reduce the initial service capacity of the cell on the 4-ohm HIF test at 70°F. Cells made with the above films have given satisfactory shelf and service maintenance for periods up to several months. However, these films lacked the desired permanence, since the insolubilizing agent dissolved slowly, and other materials were investigated.

A considerable number of reagents, in addition to those mentioned previously, have been described for insolubilizing alkyl cellulose ethers and related compounds. These include organic polybasic acids (3) such as citric, tricarballylic, tartaric, malic, phthalic, and similar compounds. Another group of reagents is that including aldehydes, such as glyoxal (4) and formaldehyde, aldehyde resins such as phenol formaldehyde (5), condensation products such as urea or melamine with formaldehyde (6) and isocyanates (7). Citric acid was chosen as representative of the first group for an experimental study.

It was found expedient to incorporate the citric acid into the aqueous solution of the methyl cellulose used for film preparation. The dry film, formed by the evaporation of the water, was exposed to heat to react the acid with the methyl cellulose. It was desired to employ the minimum amount of acid and to react it as completely as practical to prevent residual amounts of acid in the film from reacting with the MnO_2. It was soon found that, when mercuric chloride was incorporated with citric acid and methyl cellulose, heat treatment gave a charred useless material. Apparently the mercury salt catalyzed the thermal decomposition of methyl cellulose in some manner. This observation suggested the development of two separate films for a composite lining. That portion of the film to be placed next to the anode, formulated from methyl cellulose and a mercury salt, was termed the "anode film." The other portion of the separator, visualized as a partially insolubilized methyl cellulose layer, was termed the "barrier film." Whereas, the earlier films had been about 0.0076 cm thick, each layer of the improved film was made 0.0038 cm thick. This division of the separator into two parts with separate functions permitted a direct approach to the formulation of each part of the separator.

The requirements of a suitable barrier film now could be defined. A film was needed which would be highly permeable to electrolyte salts and ions, and yet which would prevent the migration of the methyl cellulose from the anode layer under a wide variety of dry cell discharge conditions. This film should be highly bibulous and yet retain an elastic gel structure which would not itself be dispersed in electrolyte. A great deal of experimental work was required to establish the conditions under which the above desired properties would be obtained. The composition chosen consists of a combination of 0.0025 equivalent, (1.52 g) of citric acid per C_6 unit (182.5 g) of methyl cellulose. An aqueous solution of these ingredients is cast on a glass plate to give a dry film 0.0038 cm thick. Heat treatment for 8-10 min at 205°C (401°F) produces the desired barrier film characteristics. Cells made with this barrier film and an anode film comprising methyl cellulose with an appropriate amount of mercury salt give excellent initial and delayed service as shown in Table III. For comparison with the data on the film-lined cells, service levels of paste cells of comparable composition are also given. It may readily be seen that the maintenance of service, voltage, and amperage of the film-lined type is far superior to that of the paste-separator cells.

Discussion

The double film lining, described herewith, features two film layers which together contribute greatly to the maintenance of high service levels of the dry cell described in this paper. The anode film, although dry when used in the cell assembly process, absorbs electrolyte to become a viscous, highly adhesive layer. The zinc anode is thoroughly wetted by this adhesive and an efficient metal-electrolyte contact is obtained. Determinations of wasteful corrosion in experimental cells made with film linings show lower values than those found in comparable cells made with cereal paste construction. The concentrated corrosive attack at the air-separator-zinc interface, so characteristic of cells made with cereal

Table III. A comparison of the service and keeping quality of "D"-size citric acid insolubilized barrier film-lined cells with paste-lined cells containing electrolytic MnO_2

Separator type		70°F Shelf Readings						
		Initial	3 Months	6 Months	12 Months	18 Months	24 Months	30 Months
Cereal paste	Volts	1.74	1.58	1.53	1.48	1.45	—	—
	Amperes	7.4	5.7	4.9	3.3	1.6	—	—
Film lining	Volts	1.80	1.66	1.63	1.61	1.63	1.60	1.60
	Amperes	6.7	6.5	6.1	5.8	5.5	5.2	4.9

Separator	Minutes on 4-Ohm HIF* to 0.9 v				Minutes on 4-Ohm LIF* to 0.9 v			
	Initial	3 Months	6 Months	12 Months	Initial	3 Months	6 Months	12 Months
Film lining	922	719	750	591	623	616	—	433
Cereal paste	1072	—	1122	1084	1372	—	1179	896

* The abbreviations HIF and LIF are used to indicate the Standard Heavy Industrial Flashlight and Light Industrial Flashlight tests, respectively.

paste, is greatly lessened by the use of the film lining. Zinc can perforation is also reduced as a result of the lessened wasteful attack on the anode.

The success of the film lining in providing a high-capacity cell of good keeping quality seems due in part to the unique properties of the barrier film. The reaction between methyl cellulose and an insolubilizing reagent, such as citric acid, appears to be the formation of a complex involving both materials. The resulting insolubilized film is an elastic, gelatinous layer when saturated with electrolyte and shows some evidence of cross-linkage. Because of the reduction in solubility, it can be concluded that a considerable increase in molecular size is obtained by the reaction. The behavior of the cells containing the double film lining is considered strong evidence for the ready diffusion of electrolyte salt solutions and ions through the film during discharge and rest periods.

The early indications of stability of methyl cellulose films in contact with MnO_2 have been confirmed by the excellent keeping quality of experimental film-lined cells stored at 35°C (95°F) and 45°C (113°F). The maintenance of service levels under such severe conditions probably indicates a trend toward the use of such linings in cells destined for tropical and similar applications. It is probable that the success of methyl cellulose film linings in this application is, in part, related to the reduced solubility of this material at the elevated temperatures. In contrast to cereal paste which becomes less viscous at elevated temperatures, methyl cellulose coagulates when the temperature exceeds the "gel point." Even when so coagulated, the separator maintains an excellent adhesive contact with the anode and effectively prevents air access to the anode surface.

The techniques developed in this work have provided an easier method of commercial manufacture (8, 9) of certain small sizes of cells than those customarily used with conventional paste separators. Thus, in the present trend toward small cell sizes, the film-type lining appears destined to play an important role.

Acknowledgment

The authors gratefully acknowledge the valuable help and assistance given by Mr. G. W. Heise, who directed the work described in this paper.

Manuscript received Nov. 7, 1955. This paper was prepared for delivery before the Boston Meeting, Oct. 3-7, 1954.

Any discussion of this paper will appear in a Discussion Section to be published in the December 1958 JOURNAL.

REFERENCES

1. J. A. Lee, *J. (and Trans.) Electrochem. Soc.*, **95**, 2P-13P (1949).
2. L. Lilienfeld, U. S. Pat. 1,505,044, Aug. 12, 1924.
3. R. M. Upright, U. S. Pat. 2,270,200, Jan. 13, 1942.
4. A. E. Broderick, U. S. Pat. 2,329,741, Sept. 21, 1943.
5. D. D. Lanning, U. S. Pat. 2,467,436, April 19, 1949.
6. R. M. Upright and S. L. Bass, U. S. Pat. 2,270,180, Jan. 13, 1942.
7. G. D. Jones, U. S. Pat. 2,467,832, April 19, 1949.
8. N. C. Cahoon, U. S. Pat. 2,534,336, Dec. 19, 1950; M. R. Hatfield, U. S. Pat. 2,551,799, May 8, 1951.
9. G. W. Heise, E. A. Schumacher, and N. C. Cahoon, *J. (and Trans.) Electrochem. Soc.*, **94**, 99 (1948); N. C. Cahoon and G. W. Heise, U. S. Pat. 2,612,-538, Sept. 30, 1952; H. M. Zimmerman and N. C. Cahoon, U. S. Pat. 2,572,296, Oct. 23, 1951.

Cathode Reactions in the Leclanche Dry Cell

N. C. Cahoon, R. S. Johnson,[1] and M. P. Korver

National Carbon Research Laboratories, National Carbon Company,

A Division of Union Carbide Corporation, Cleveland, Ohio

ABSTRACT

The reactions at the cathode of the Leclanché-type dry cell are considered in terms of three heterogeneous chemical reactions for which there is advanced a plausible mechanism, leading to a unified theory of the cathode process. When reviewed in terms of this theory, the numerous observations of others that formerly have appeared to be incongruous are correlated and rationalized in terms of the over-all cathode reaction.

The identification of the reaction products formed in the dry cell cathode during cell discharge has been the subject of considerable work. An examination of the literature indicates that perhaps more effort has been spent on the identification of the products of the electrolyte reaction than on those involving manganese compounds. Until recently, the over-all reaction in the Leclanché cell was written thus:

$$Zn + 2MnO_2 + 2NH_4Cl \rightarrow ZnCl_2 \cdot 2NH_3 + Mn_2O_3 + H_2O \quad (I)$$

Although the above reaction indicates the reduced product is trivalent manganese oxide, the representation of it as bixbyite, Mn_2O_3, is now considered incorrect. Both manganite (1), MnOOH, and hetaerolite (2), $ZnO \cdot Mn_2O_3$, have been identified by x-ray diffraction techniques as the solid reaction products formed in cathodic reaction. In addition to these solid products, soluble manganese has been found in the electrolyte of a discharged cathode (3). It is the purpose of this paper to extend the co-ordination of part of these findings already presented (4) to include all the above reaction products and to offer a rational theory of the cathodic reaction process.

Experimental

The analysis of the cathode mix of discharged dry cells for manganite, hetaerolite, and dissolved manganese was undertaken. Briefly, the analytical procedure involves the suspension of a weighed aliquot portion[2] (e.g., 25 g of the total cathode mix) in a 500 ml volume of a 25% aqueous solution of ammonium chloride buffered at a pH of 5.2-5.4, followed by stirring of the suspension at about 40°C for 2 hr. This step insures the solution of the soluble manganese together with the diammino zinc chloride and/or zinc oxychloride usually present.

It has been reported (5) that the zinc content of hetaerolite, $ZnO \cdot Mn_2O_3$, is not soluble in ammonium chloride solution under these conditions. The authors' findings confirm this observation. Thus, leaching the cathode mix with the ammonium chloride solution removes the soluble zinc compounds without attacking the hetaerolite and permits their separate determinations.

The pH of the slurry is initially adjusted to between 5.2 and 5.4 by the addition of a 40-45% aqueous zinc chloride solution in quantity sufficient to prevent the soluble manganese from reacting with any residual MnO_2 (1) during the course of the analysis. At the end of the leaching step the slurry is then filtered and the filter cake well washed, first with ammonium chloride solution and finally with water. The combined filtrate and washings are diluted with water or ammonium chloride solution to an appropriate standard volume, e.g., 1 liter. Aliquot samples of this solution are quantitatively analyzed for manganese.

From the manganese content of the aliquot sample, the dilution involved, and the sample weights, the amount of divalent manganese in the discharged bobbin can be calculated. From the reaction,

$$MnO_2 + 4H^+ + 2e \rightarrow Mn^{++} + 2H_2O \quad (II)$$

it can be calculated that 1 amp-hr of electrical energy involves the consumption of 1.62 g of MnO_2 and the formation of 1.02 g of divalent manganese. The latter value enables the conversion of the divalent manganese content of the cathode to equivalent ampere hours of energy represented by the formation of this product and is designated as item (a). From the above ratio the divalent manganese content of the cathode can also be calculated as an equivalent loss of MnO_2 in grams per cell, shown as item (b).

The filter cake is dried at 110°C and its weight and composition determined. Standard methods of quantitative analysis (6) for manganese, zinc, and available oxygen are employed. From the content of manganese and available oxygen in the filter cake, the weights of the ingredients involved and the initial weight and composition of the manganese dioxide used in the cell, the loss in available oxygen which occurred in the cathode of the cell during the particular discharge can be calculated. This can be expressed conveniently as the loss of an equivalent

[1] Present Address: Riegel Textile Corporation, Ware Shoals, South Carolina.

[2] The cell being studied is removed from test when it reaches its cutoff voltage and is immediately subjected to analysis.

weight of MnO_2 and designated item (c). From the reaction,

$$2MnO_2 + 2H^+ + 2e \rightarrow 2MnOOH \qquad (III)$$

it can be calculated that 3.24 g of MnO_2 are required to produce 1 amp-hr of energy. From the zinc content of the filter cake and the aliquot weights, the total zinc content of the discharged cathode can be calculated. On the basis of the reaction (2),

$$2MnO_2 + Zn^{++} + 2e \rightarrow ZnO \cdot Mn_2O_3 \qquad (IV)$$

and the fact that the MnO_2 is reduced to a trivalent oxide, 3.24 g of MnO_2 are converted to 4.46 g hetaerolite in which 1.22 g of zinc are combined for each ampere hour of electrical energy obtained. The zinc content of the discharged cathode can thus be converted readily to equivalent ampere hours output, and designated item (f).

The results of the cathode analysis are expressed in the following manner: (*a*) ampere hour output equivalent of Mn^{II} found in the cathode; (*b*) weight of MnO_2 consumed equivalent to Mn^{II} found in the cathode; (c) weight of MnO_2 consumed during the discharge of the cell; (*d*) weight of MnO_2 converted to trivalent oxides, (*d*) = (c) − (*b*); (*e*) ampere hour output in form of trivalent manganese oxides, (*d*) ÷ 3.24; (*f*) ampere hour equivalent of hetaerolite; (*g*) ampere hour equivalent of manganite, (*g*) = (*e*) − (*f*).

Total chemically determined output of cell, (*h*) = (*a*) + (*f*) + (*g*).

Typical analytical data for a group of representative cells appear in Table I. Item (*k*), the electrical output of the cell, is mathematically calculated from the discharge curve, and is expressed in ampere hours.

Discussion

It has been suggested (4) that two types of reactions occur at the cathode in a Leclanché dry cell. The first is the electrochemical reaction by which electrical energy is produced; it is given as (II) above. This reaction operates only during the actual delivery of current by the cell. The divalent manganese formed in this reaction, present as a soluble manganous salt in the electrolyte, then reacts with residual manganese dioxide thus,

$$MnO_2 + Mn^{++} + 2OH^- \rightarrow 2MnOOH \qquad (V)$$

to form the product manganite.

A parallel reaction,

$$MnO_2 + Mn^{++} + 4OH^- + Zn^{++} \rightarrow ZnO \cdot Mn_2O_3 + 2H_2O \qquad (VI)$$

forming hetaerolite appears a distinct possibility. Both reactions (V) and (VI) are chemical reactions and may occur during both cell discharge and rest periods.

If the above reasoning is correct, the total energy output calculated from the amounts of chemical products found in a discharged cell will agree with the energy output measured electrically. The data presented in Table I show that a reasonable correlation exists between these two values given by items (h) and (k), respectively, for cells with two different oxides discharged on three types of tests. Further argument for this viewpoint is added by the fact that it has been found previously that the energy which would be derived simply from the reduction of MnO_2 to the trivalent stage does not account for all the energy actually produced. The possibility of air depolarization to explain this discrepancy has been suggested (8). However, in the present case, it is believed that air depolarization was not a factor since the difference is readily accounted for by the divalent manganese that is produced during reaction (II) and not reacted to form trivalent oxides of manganese, shown in Table I as item (b).

The fact that this correlation exists between outputs as determined by both chemical and electrical means strongly suggests that reactions (V) and (VI) may occur simultaneously. The final product usually found is a mixture of the two oxides rather than either component alone. The relative quantities of the two types of trivalent oxide appear to be the result of several factors.

The Manganite-Hetaerolite Ratio

Examples of typical cell analyses are shown in Table I. A "D" size cell made with a cathode mix containing African ore and discharged on a 4 ohm continuous test forms a solid product that is substantially all manganite. On lighter drains, represented by the HIF and LIF (7) tests, the quantity of hetaerolite formed amounts to one-thirteenth and one-sixth, respectively, of the amount of maganite developed. Although the amounts of hetaerolite present are still small, the fact that the quantity increases with a reduction in the severity of the test appears significant.

Tests have shown that, if zinc salts are present in solution in the cathode mix, hetaerolite, $ZnO \cdot Mn_2O_3$, may be formed (1). If this is not the condition, then MnOOH will be the final reduction product. The amount of dissolved zinc salts in the cathode mix is determined by such factors as original cell composi-

Table I. A comparison of the chemically determined and electrical outputs of "D" size experimental cells

Oxide type	4 Ohm test (7)	Chemically determined output values: Soluble manganese (Mn^{++}) Item (a)	Hetaerolite ($ZnO \cdot Mn_2O_3$) Item (f)	Manganite (MnOOH) Item (g)	Total Item (h)	Electrical output Item (k)
African	Continuous	0.06	0.001	1.27	1.33	1.33
African	HIF*	0.43	0.13	1.74	2.30	2.15
African	LIF*	1.15	0.61	3.16	4.92	4.91
Electrolytic	HIF	2.02	4.41	1.65	8.08	8.19

Data above expressed in ampere hours.
* The abbreviations HIF and LIF are used to indicate the standard Heavy Industrial Flashlight and Light Industrial Flashlight tests, respectively.

tion, diffusion from the anode, and solution pH (9). Also, the type of MnO_2 determines, to a certain extent, the pH of the operating cathode. It has been pointed out that the primary reaction consumed hydrogen ions. This tends to increase the pH. The secondary reactions consume hydroxyl ions and thus increase the acidity in the electrolyte at the cathode. This restoration of the pH will be faster with the more efficient types of MnO_2, such as electrolytic oxide.

The equations presented herewith seem to apply to all types of manganese dioxide: natural oxides, beneficiated ores, and the various types of synthetic depolarizers. Although the formation of hetaerolite is generally associated with highly reactive oxides (2), the oxide type will not necessarily determine the nature of the final product. The African Ore cells in Table I show how the hetaerolite to manganite ratio is altered when the type of test is changed.

Stoichiometry of the Electrode

At an operating MnO_2-carbon electrode, it is obvious that the system is not at equilibrium. Furthermore, during most of the time the electrode is not even under conditions of steady state. Hence, any application of the Nernst equation and similar thermodynamic relationships are totally invalid. The one rule that is applicable is Faraday's law. This can be correctly applied to the primary reaction (II). Although the final solid products, manganite and hetaerolite, are represented as MnOOH and $ZnO \cdot Mn_2O_3$, they rarely appear in the true stoichiometric proportion (2). For example, it is possible for the manganese-oxygen ratio in manganite to range from 1.4 to 1.6 and the solid can still be considered to be manganite (10). Recent work in the field of solid-state physics shows that these nonstoichiometric solids are real entities and such studies may throw further light on the mechanism of their formation.

It should be noted that the three equations used to describe the cathode process involve solids and ions in solution. Due recognition is thus given to the fact that the reactions occur in a heterogeneous system. Although Mn^{++} and Zn^{++} are discussed as ions, they are no doubt actually present as hydrated complex ammines of varying composition. However, the mechanism of the reactions is the same in both cases, so that simplification of the ions does not invalidate the presentation.

Acknowledgment

The authors gratefully acknowledge the valuable help and assistance given by Mr. G. W. Heise, who directed the work described in this paper.

Manuscript received Nov. 7, 1955. This paper was prepared for delivery before the Boston Meeting, Oct. 3-7, 1954.

Any discussion of this paper will appear in a Discussion Section to be published in the December 1958 JOURNAL.

REFERENCES

1. H. F. McMurdie, D. N. Craig, and G. W. Vinal, *Trans. Electrochem. Soc.*, **90**, 509 (1946).
2. L. C. Copeland and F. S. Griffith, *ibid.*, **89**, 495 (1946); H. F. McMurdie, *ibid.*, **86**, 313 (1944).
3. J. M. Cowley and A. Walkley, *Nature*, **161**, 173 (1948); D. T. Ferrell Jr., and W. C. Vosburgh, *This Journal*, **98**, 334 (1951).
4. N. C. Cahoon, *This Journal*, **99**, 343 (1952).
5. E. Otto, discussion H. F. McMurdie, *Trans. Electrochem. Soc.*, **86**, 325 (1944).
6. W. W. Scott, "Standard Methods of Chemical Analysis," 5th ed., D. Van Nostrand and Co. (1939).
7. American Standard Specifications for Dry Cells and Batteries, Circular of the National Bureau of Standards, No. C435, U. S. Government Printing Office, Washington, D. C. (1942); No. C559 (1955).
8. K. Arndt, H. Walter, and E. Zender, *Z. Angew. Chem.*, **39**, 1426 (1926); C. Drotschmann, "Trockenbatterien," 3rd ed., p. 10, Akademische Verlagsgesellschaft, Becker and Erler Kom.—Ges., Leipzig (1945); R. C. Kirk, P. F. George, and A. B. Frey, *This Journal*, **99**, 323 (1952).
9. N. C. Cahoon, *Trans. Electrochem. Soc.*, **92**, 159 (1947).
10. W. Feitknecht and W. Marti, *Helv. Chim. Acta*, **28**, 129 (1945).

Investigation of the Electrochemical Properties of Organic Compounds

I. Aromatic Nitro Compounds

R. Glicksman and C. K. Morehouse

RCA Laboratories, Radio Corporation of America, Princeton, New Jersey

ABSTRACT

A study of the electrochemical characteristics of aromatic nitro compounds shows that the cathode potential of these compounds during current flow is dependent on the type and position of substituent groups on the aromatic ring, as well as the composition and *p*H of the electrolyte.

The high theoretical ampere-minute capacity of the aromatic dinitro compounds, along with their practical operating potentials, high electrode efficiencies, and favorable physical and chemical properties, show these materials to have considerable promise for use as cathode materials in primary cells, when coupled with a magnesium anode.

Previous work by the authors (1) disclosed a class of organic compounds, the N-halogens, which had many of the desirable electrochemical characteristics of a cathode material for primary cells. A further consideration of organic oxidizing agents suggested the use of aromatic nitro compounds as cathode materials in primary cells because of their high theoretical electrode potentials and coulombic capacities.

For example, from the free energy values of aniline and nitrobenzene (2), Latimer (3) calculates the potential of the $C_6H_5NO_2$-$C_6H_5NH_3^+$ couple to be:

$$C_6H_5NO_2+7H^++6e^-=C_6H_5NH_3^++2H_2O,\ E^\circ=+0.87 \quad (I)$$

This potential compares favorably with those of inorganic oxidizing agents. In addition, it has been shown that the aromatic nitro compounds can be reduced to the amino stage by both chemical and electrolytic methods in both acid and neutral electrolyte. This indicates the possibility of attaining high coulombic capacities from these compounds through the high resultant electron change per molecule of nitro compound undergoing reduction.

In this paper a systematic study of the electrochemical characteristics of aromatic nitro compounds is presented, with a view toward employing these compounds as cathodes in primary cells.

Experimental Data and Discussion of Results

Apparatus and technique.—Because of the irreversible nature of the electrode reaction and polarization effects encountered during current flow, the electrochemical characteristics of many inorganic and organic compounds cannot be predicted by thermodynamic calculations and a knowledge of their physical and chemical properties. A technique, previously described by the authors (4), has been used to measure the operating potential during current flow and the coulombic capacity of various aromatic nitro compounds. This technique consists in discharging at a constant current, in a large volume of electrolyte, a 0.5-g sample of the aromatic nitro cathode material mixed with 0.05 g of Shawinigan acetylene black. The change in cathode potential with time was measured with a L&N Type K potentiometer using a saturated calomel reference electrode. The measured potentials were corrected for the *IR* drop associated with the apparatus and electrolyte by means of an oscillographic technique (5).

All half-cell potential data reported in this paper are referred to the normal hydrogen scale and include a liquid junction potential, which in most cases is small and can be neglected. The variation of the saturated calomel electrode potential with temperature over the course of the measurements was less than 0.01 v, usually lower than 0.005 v, and no correction was made for this factor, i.e., all measured results were calculated using a value of 0.246 v for the potential of this reference electrode.

For most of the measurements an aqueous magnesium bromide electrolyte and a magnesium anode were used, while, in studying the effect of *p*H on potential, a zinc anode was employed with the acidic NH_4Cl-$ZnCl_2$-H_2O and basic NaOH-H_2O electrolytes.

Half-Cell Studies of Nitrobenzene and Its Reduction Products

Comprehensive studies have been made of the process of electrolytic reduction of nitrobenzene by Haber and Schmidt (6); they proposed a scheme, which, with subsequent modification (3), became the following:

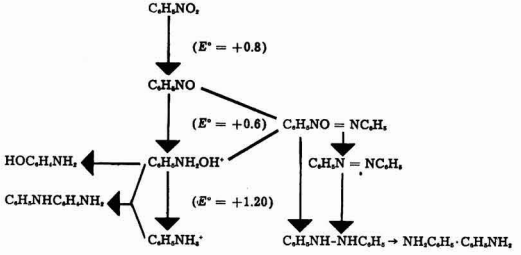

The results reported indicate that, in acid solution, the sequence of primary reduction is through the nitrosobenzene and phenylhydroxylamine stage to aniline. In strongly basic solution, nitrosobenzene can react with both phenylhydroxylamine and aniline to form azoxybenzene and azobenzene, respectively, so that a number of side products are possible. Products such as azobenzene and hydrazobenzene are also made possible by the reduction of azoxybenzene itself, as indicated by the vertical lines in the above scheme. Aniline is formed on prolonged reduction only, hydrazobenzene being the main product obtained when nitrobenzene is reduced in an alkaline solution.[1]

Half-cell discharge studies made on nitrobenzene and some of its reduction products, in various electrolytes, are shown in Fig. 1. These compounds were discharged as cathode materials in three electrolytes of different *p*H at a rate of 0.030 amp/g of material.[2] The data show that only nitrobenzene and nitrosobenzene operate at sufficiently high potentials to enable these materials to be coupled with a compatible anode, to yield a galvanic cell which operates at practical voltages.[3] In addition, these two compounds exhibit a desirable flat voltage discharge curve and have high theoretical coulombic capacities.

Among the lower oxidation state compounds, only azoxybenzene gives some capacity in the $MgBr_2$ and NH_4Cl-$ZnCl_2$ electrolytes, while its reduction products, azobenzene, hydrazobenzene, and aniline, have discharge potentials of −0.75 v or lower in the NH_4Cl-$ZnCl_2$ electrolyte, and −0.95 v or lower in the $MgBr_2$ electrolyte. The −0.75 and −0.95 v values are the potentials characteristic of the discharge of hydrogen ions on the carbon electrode in these electrolytes at a current drain of 0.030 amp/g of cathode material. In the NaOH electrolyte, capacity is obtained from both azobenzene and azoxybenzene, the azobenzene operating at a lower potential than the azoxybenzene. Despite the low potentials of the azoxybenzene in these three electrolytes, it exhibits a desirable flat voltage discharge curve, and might be useful if coupled with an anode of higher potential than magnesium.

Of most interest, however, are nitrobenzene and nitrosobenzene. Since each of these compounds represents only one of a large class of materials, extensive studies were made of the electrochemical properties of both classes. This paper deals with the work on the aromatic nitro compounds, while a subsequent paper will treat the data obtained on the aromatic nitroso compounds.

Effect of Substituted Groups on the Electrode Potential of Aromatic Nitro Compounds

The effect of para substituted groups on the electrode potential of aromatic nitro compounds was studied at a current drain of 0.030 amp/g of cathode material in an aqueous magnesium bromide electrolyte. From the data presented in Fig. 2 and 3,

[1] An extensive review has been given by Swann (7) for the whole field of electrolytic organic oxidation and reduction reactions, which includes the reduction of aromatic nitro compounds in various media.

[2] Liquid compounds, such as nitrobenzene, were tested by mixing 0.5 ml of the compound with Shawinigan acetylene black, and discharging the resultant mix at a rate of 0.030 amp/ml of material, and making half-cell potential measurements in the usual manner.

[3] Magnesium in a $MgBr_2$ electrolyte operates at a potential of approximately 1.3 v, while zinc operates at potentials of approximately 0.7 and 1.3 v in NH_4Cl and NaOH electrolytes, respectively.

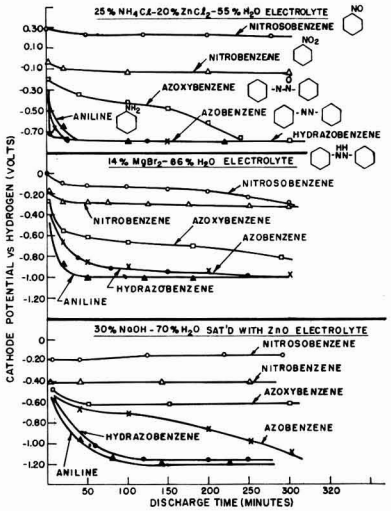

Fig. 1. Cathode potentials of nitrobenzene and its derivatives discharged in various electrolytes at 0.030 amp/g.

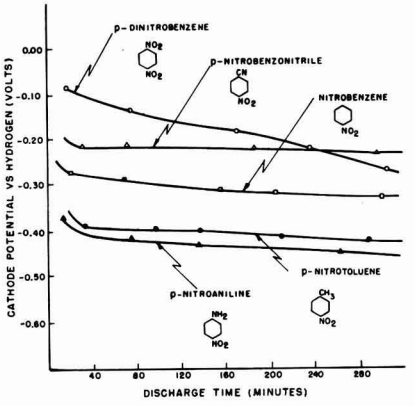

Fig. 2. Effect of para substituted groups on the cathode potential of nitrobenzene discharged in 250 g/l $MgBr_2 \cdot 6H_2O$ electrolyte at 0.030 amp/g.

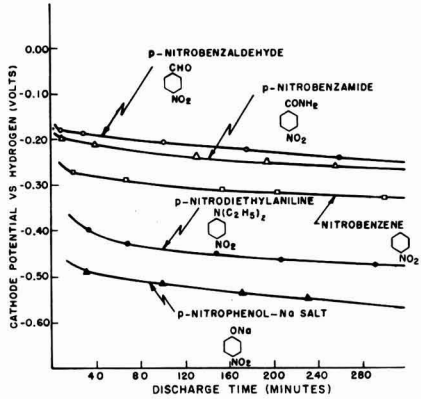

Fig. 3. Effect of para substituted groups on the cathode potential of nitrobenzene discharged in 250 g/l $MgBr_2 \cdot 6H_2O$ electrolyte at 0.030 amp/g.

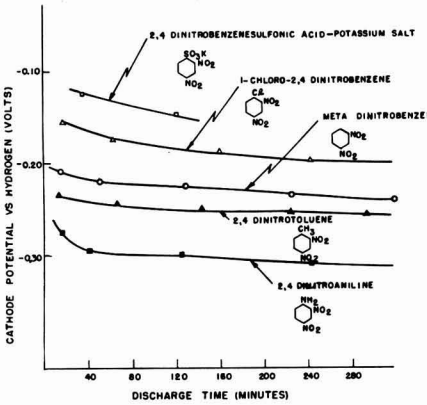

Fig. 4. Effect of substituted groups on the cathode potential of m-dinitrobenzene discharged in 250 g/l $MgBr_2 \cdot 6H_2O$ electrolyte at 0.030 amp/g.

it is seen that those compounds having electron-attracting groups, such as $-NO_2$, -CN, -CHO, and $-CONH_2$ substituted in the para position, initially operate at potentials 0.05-0.20 v higher than that of nitrobenzene. Conversely, electron-repelling groups, such as $-NH_2$, $-N(C_2H_5)_2$, $-CH_3$, and -ONa substituted in the para position, result in compounds having 0.10-0.20 v lower operating potentials than the parent nitrobenzene. In addition, it is seen that a strongly electron-attracting group, such as $-NO_2$, raises the operating potential to a greater extent than the more weakly electron-attracting groups such as -CN, -CHO, and $-CONH_2$, while the strongly electron-repelling $-NH_2$ and -ONa groups lower the operating potential to a greater extent than the weakly electron-repelling $-CH_3$ group.

The same type of behavior is noted for substituted dinitrobenzene compounds, as evidenced by the discharge curves presented in Fig. 4. However, it is significant to note that the potential lowering effect of the $-CH_3$ and $-NH_2$ groups on meta dinitrobenzene is less than that found for their addition to nitrobenzene.

The addition of more than one electron-attracting or electron-repelling group to nitrobenzene affects the potential still further, as seen by the data in Fig. 5. The effect is especially noticeable in the case

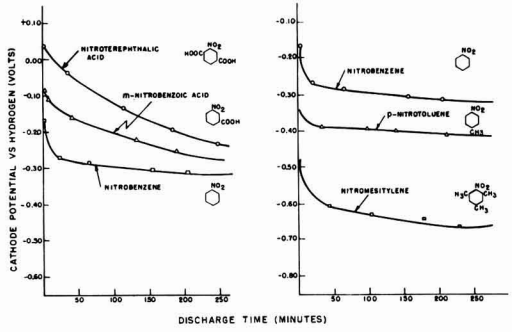

Fig. 5. Effect of the substitution of successive electron attracting and repelling groups on the cathode potential of nitrobenzene discharged in 250 g/l $MgBr_2 \cdot 6H_2O$ at 0.030 amp/g.

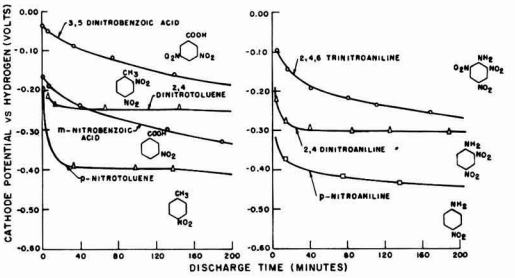

Fig. 6. Effect of an added nitro group on the cathode potential of aromatic nitro and dinitro compounds discharged in 250 g/l $MgBr_2 \cdot 6H_2O$ at 0.030 amp/g.

of nitromesitylene, which operates at a potential 0.3 v lower than nitrobenzene and 0.2 v lower than p-nitrotoluene. Conversely, the addition of successive -COOH groups to nitrobenzene, to form m-nitrobenzoic acid and nitroterephthalic acid, respectively, results in compounds with successively higher operating potentials.

In Fig. 6, it is seen that the effect of an added nitro group on the potential of p-nitrotoluene and m-nitrobenzoic acid is to raise the potential approximately 0.15 v. The further addition of a nitro group to a dinitro compound raises the potential still more, as evidenced by the discharge curves for mono, di, and trinitroaniline.

The addition of another nitro group to an aromatic nitro compound has a further advantage in that the theoretical ampere-minute capacity is increased through the addition of another reducible group. For example, assuming a six-electron change per nitro group, nitrobenzene has a theoretical capacity of 78.4 amp-min/g, as compared to 114.9 for dinitrobenzene and 136 for trinitrobenzene. Thus it would appear that, on the basis of their high electrode potential and coulombic capacity, the aromatic trinitro compounds show the most promise for use as cathode materials in primary cells. However, despite their attractive electrochemical properties, trinitro compounds in general are difficult to handle, and for that reason their use in primary cells would be limited.

Theoretical interpretation of data.—In order to explain the effect of substituted groups on electrode potential it is necessary to use some of the current theories of electronics, resonance, and molecular structure (8-10) pertaining to organic reactions. These theories show that the activation of an organic molecule is largely through active or incipient electron displacements leading to the development of a center of high or low electron density.

In a benzene molecule the six carbon atoms are equal to each other with respect to electron distribution. However, the addition of certain groups to the benzene ring results in an increase or decrease of electron density in the ring, depending on the substituted group. This change in electron density affects the various ring positions unequally. It has been verified by quantum-mechanical calculations that the ortho and para carbons are about equally affected, the meta carbon atoms being affected to a much smaller extent. This distribution of electron

density can be explained by theories involving the inductive and resonance effects.

Since the cathodic reaction of an electrochemical cell involves the ability of the material to accept electrons, it would be expected that the distribution of electron density in an aromatic nitro compound would have a distinguishable effect on its discharge potential. For example, in substituted nitrobenzenes the introduction of electron-attracting groups should decrease the electron density in the vicinity of the nitro group, thus increasing its affinity for electrons and facilitating its reduction. On the other hand, electron-repelling groups would increase the electron density around the nitro group, thus resulting in compounds which are reduced with more difficulty.

It is recognized that the reduction of aromatic nitro compounds involves the acceptance of hydrogen ions as well as electrons, and either or both might be involved in the rate-determining step. However, the data presented in Fig. 2-7 can be explained readily on the basis of a rate-determining electron transfer step.

This effect was first pointed out by Shikata and Tachi (11), who studied the polarographic reduction of ketones and nitro compounds and found that the ease of reduction of these compounds depends on the electronegativity of the groups combined with the reducible groups. It has been verified subsequently by other polarographic studies (12, 13). A similar effect was observed by Fieser (14) in the oxidation-reduction potentials of quinone type compounds.

Effect of Position of Substituted Groups on the Electrode Potential of Aromatic Nitro Compounds

According to theory, electron-attracting groups such as -CHO, -CN, and $-NO_2$ lower the electron density in the ring, but they affect the various positions unequally, the density in the ortho and para positions being decreased to the greatest extent. Therefore, one would expect compounds having a nitro group ortho or para to an electron-attracting group to be reduced more easily than those having a nitro group in the meta position, and they should thus have a higher cathodic electrode potential. The half-cell discharge data for the para and meta isomers of nitrobenzaldehyde, nitrobenzonitrile, and dinitrobenzene presented in Fig. 7 confirm the above reasoning. In each case the para substituted compound has a higher potential than the corresponding meta isomer.

Conversely, electron-repelling groups such as $-NH_2$, -OH, and $-CH_3$ increase the electron density in the ortho and para position to a greater extent than in the meta position. In this case, one would expect a nitro group in the meta position to be reduced more readily than one in an ortho or para position, and, therefore, the meta isomer should have a higher cathodic electrode potential. Half-cell discharge data for the meta and para isomers of nitroaniline, nitrophenol, and nitrotoluene are presented in Fig. 8 and, as expected, the meta isomers have higher potentials than their corresponding para compounds.

This effect is further illustrated by the discharge curves of 2,5 and 3,5 dinitrobenzoic acid and 2,5 and 2,4 dinitrophenol shown in Fig. 9. It is seen that in both cases the para dinitro compounds have higher potentials than their corresponding meta dinitro isomers.

From these data, it is seen that the position of a substituent group can alter the cathode potential of an aromatic nitro compound by 0.05-0.15 v, the effect being greatest with the more strongly electron-attracting and repelling groups, such as $-NO_2$ and $-NH_2$.

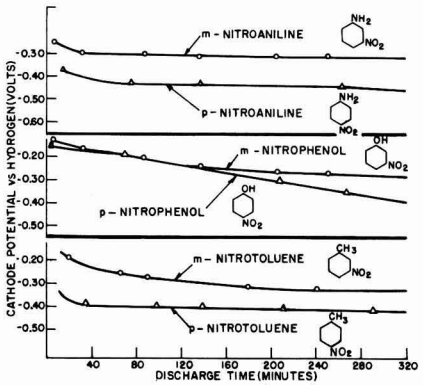

Fig. 8. Effect of the position of various groups on the cathode potential of aromatic nitro compounds discharged in 250 g/l $MgBr_2 \cdot 6H_2O$ electrolyte at 0.030 amp/g.

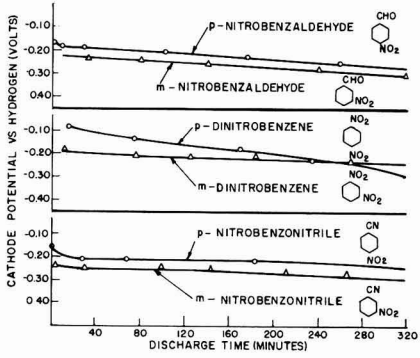

Fig. 7. Effect of the position of various groups on the cathode potential of aromatic nitro compounds discharged in 250 g/l $MgBr_2 \cdot 6H_2O$ electrolyte at 0.030 amp/g.

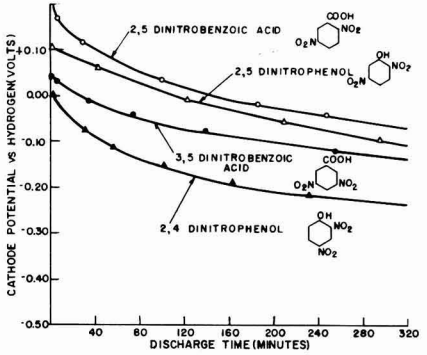

Fig. 9. Effect of the position of the nitro groups on the discharge potential of various dinitroaromatic compounds discharged in 250 g/l $MgBr_2 \cdot 6H_2O$ electrolyte at 0.030 amp/g.

Effect of Electrolyte pH on the Electrode Potential of Aromatic Nitro Compounds

Since hydrogen ions participate in the reduction of aromatic nitro compounds, it would be expected that the electrode potentials of these compounds are *p*H dependent. In Fig. 10 are presented discharge curves of 2,4 dinitroaniline and 2,4 dinitrotoluene in three different dry cell electrolytes of varying *p*H. It is seen that the cathode potentials of the nitro compounds increase as the *p*H of the electrolyte is decreased, a result in agreement with theory. This type of behavior is typical of the aromatic nitro compounds in general; however, the true effect of *p*H on the potential is, in some cases, masked by chemical reactions between the cathode material and the electrolyte or the discharge products.

For example, the *p*H of the medium often influences the intensity and direction of the inductive and resonance effects operating in a molecule by changing the nature of the molecule which is reduced. A case in point is the amino group, which is electron attracting in acid media because it acquires a proton and becomes positively charged, $-NH_3^+$, while in an alkaline medium it is a strongly electron-repelling group.

Another example of how the effect of *p*H on potential of a nitro compound is altered by the reaction between the electrolyte and the compound is shown in Fig. 11, where it is seen that the discharge potentials of p-nitrophenol and p-nitrophenol-Na salt are approximately the same in the acidic NH_4Cl-$ZnCl_2$ and basic NaOH electrolytes. It is reasoned that in a strongly basic solution p-nitrophenol reacts with the electrolyte to give the Na salt, whereas in acid solution the p-nitrophenol-Na salt hydrolyzes to give p-nitrophenol. The difference between the behavior of the two compounds in a magnesium bromide electrolyte is believed due to a neutralization reaction which occurs with time between p-nitrophenol and the magnesium bromide electrolyte, which has become saturated with $Mg(OH)_2$ as a consequence of the cathodic reduction reaction. The neutralization of the aromatic hydroxyl group could lower the potential in two ways: first, through the removal of the acidic hydrogen ion and corresponding rise of *p*H at the electrode surface; second, the formation of the very strongly electron-repelling phenoxide ion would lower the discharge potential of the parent nitro compound by replacing the more weakly electron-repelling hydroxyl group (15).

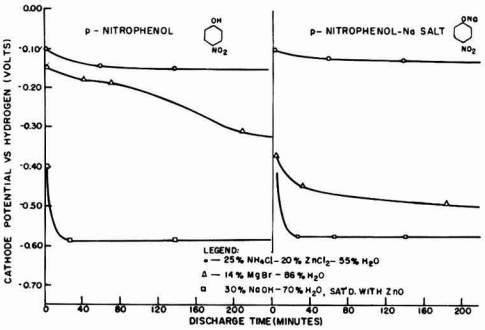

Fig. 11. Cathode potential of p-nitrophenol and its sodium salt discharged in various electrolytes at 0.030 amp/g.

The acidity of the cathode material itself can also influence the operating potential as evidenced by the discharge curves for p-nitrobenzenesulfonic and p-nitrobenzoic acids shown in Fig. 12. It is seen that these acidic compounds operate initially at higher potentials than comparable nitro compounds containing a more strongly electron-attracting group on the ring. These anomalous results are attributed to an increased hydrogen ion concentration at the electrode surface, caused by the ionization of these acidic compounds. As a result of the decreased *p*H at the electrode surface, the electrode potential is initially high. However, the potential of these compounds falls off with time and soon reaches a steady value, which corresponds more closely to what one would expect from these groups on the basis of their electron-attracting and repelling strengths. It is reasoned that the drop of potential with time as these compounds are discharged is due to the neutralization of the acidic groups by the hydroxide ion, formed as a consequence of the cathodic reduction reaction.

The high potential of p-nitrobenzenesulfonyl chloride may be explained by a combination of effects. The first is the inherently strong electron-attracting property of the $-SO_2Cl$ group, while the second is

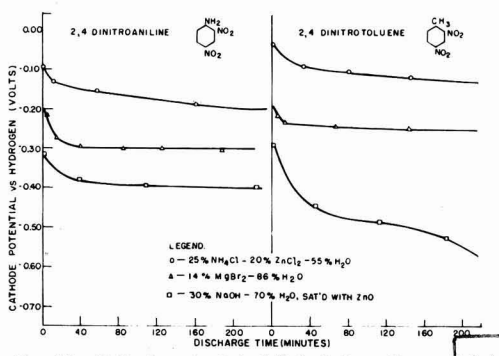

Fig. 10. Cathode potential of 2,4 dinitroaniline and 2,4 dinitrotoluene discharged in various electrolytes at 0.030 amp/g.

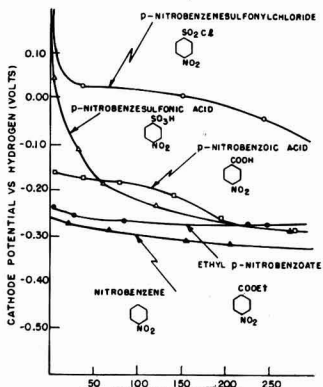

Fig. 12. Effect of acidic groups on the cathode potential of aromatic nitro compounds discharged in 250 g/l $MgBr_2 \cdot 6H_2O$ electrolyte at 0.030 amp/g.

Table I. Theoretical capacities and physical properties of various cathode materials

Cathode material	Physical properties	Melting* point, °C	Boiling* point, °C	Density*	Theoretical capacity amp-min/g	Theoretical capacity amp-min/cm³
Conventional dry cell cathode materials						
Manganese dioxide	Solid	—0, 230	—	5.03	18.5	93.1
Mercuric oxide	Solid	d. 100	—	11.14	14.9	166
Aromatic nitro compounds						
Nitrobenzene	Liquid	5.7	210.9	1.2	78.4	94.1
m-Dinitrobenzene	Solid	89.8	300-2	1.58	114.9	181.5
1,3,5 Trinitrobenzene	Solid	121	Decomposes	1.69	136	229.8
2,4 Dinitrobenzaldehyde	Solid	69-70	190-210	—	98.6	—
2,4 Dinitrotoluene	Solid	70	sl.d.300	1.32	105.8	139.6
2,4 Dinitroaniline	Solid	187-8	—	1.62	105.8	171.4
2,4 Dinitroanisole	Solid	94-5	—	1.341	97.4	129.5

* Lange's Handbook of Chemistry, 8th edition.

the decreased pH at the electrode surface, caused by the hydrolysis of the sulfonyl chloride compound, with the formation of p-nitrobenzenesulfonic acid and HCl.

In addition to the above considerations, the formulation of a pH-potential relationship for aromatic nitro compounds is dependent on a knowledge of the electrode reaction as well as the activities of the reactants and products. Since these reduction reactions are irreversible, the nature of the reduction product is often unknown and identification of the resultant products along with kinetic studies are needed in interpreting the electrode reaction.

Thus it is seen that the effect of the medium on cathode potential is a complex one and has to be considered anew for each individual case.

Coulombic Capacity of Aromatic Nitro Compounds

Tabulated in Table I are theoretical capacity and physical property data for a few aromatic nitro compounds compared with two of the cathode materials now used in commercial dry cells. The theoretical capacities of the nitro compounds were computed by means of Faraday's law, with the assumption that each nitro group is reduced to the amino stage with a corresponding 6-electron change.

It is seen that the listed nitro compounds have from 4 to 7 times greater theoretical ampere-minute capacity per unit of weight than manganese dioxide, and 5-9 times greater capacity than mercuric oxide. Because of the low densities of the nitro compounds, their theoretical capacities per unit of volume range from the same as to twice that of MnO_2, while some are even slightly superior to HgO, despite the high density of the latter compound. In addition most of the aromatic dinitro compounds are stable solids with sufficiently high melting and boiling points to enable them to be used as cathode materials in primary cells.

Coulometric studies made on meta and para dinitrobenzene and meta and para nitroaniline in a $MgBr_2$ electrolyte are shown in Fig. 13. The results were obtained by discharging 0.5-g samples of these compounds at a constant current drain of 0.005 amp/g, and measuring the change in half-cell potential with time by the same technique as described previously. Also included for purposes of comparison are curves of electrolytic manganese dioxide and mercuric oxide, discharged at a similar rate in aqueous $MgBr_2$ and NaOH electrolytes, respectively.

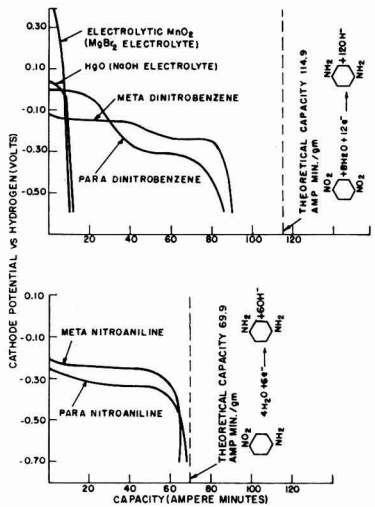

Fig. 13. Capacity curves for meta and para dinitrobenzene and nitroaniline discharged in 250 g/l $MgBr_2 \cdot 6H_2O$ electrolyte at 0.005 amp/g.

The reduction of meta and para dinitrobenzene is seen to take place stepwise, corresponding to two stages of reduction, the para dinitrobenzene having the higher cathode potential for the first stage of reduction and the meta dinitrobenzene having a greater cathode potential for the second reduction step. This is in agreement with the previous findings, relating the cathode potential of aromatic nitro compounds with the type and position of group substitution on the aromatic ring.

Although analyses were not made of the reduction products, it is believed that the reduction goes to the amino stage, as evidenced by the fact that the potentials of para and meta nitroaniline have approximately the same value as the cathode potentials corresponding to the second reduction step of para and meta dinitrobenzene. In addition, the capacities of the nitroaniline compounds indicate reduction takes place with a 6-electron change per nitro group.

Calculations based on Fig. 13 show para and meta dinitrobenzene to have capacities[4] of 78 and 88 amp-min/g, corresponding to efficiencies of 68% and

[4] Capacities reported are to a −0.40 v end point.

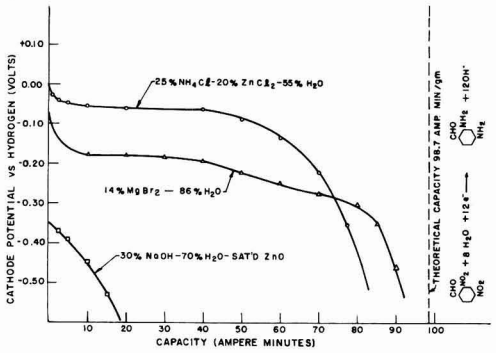

Fig. 14. Capacity curves for 2,4 dinitrobenzaldehyde discharged in various electrolytes at 0.002 amp/g.

77%, respectively, while under similar conditions of discharge the capacities of electrolytic MnO_2 and HgO are 10.3 and 10.4 amp-min/g, which correspond to efficiencies of 66%[5] and 70%. For the nitroaniline compounds, capacities of 61 and 63.5 amp-min/g were obtained for the para and meta isomers, respectively, corresponding to efficiencies of 87% and 91%. Thus it is seen that, under the aforementioned conditions of discharge, para and meta dinitrobenzene give 7 to 8 times greater ampere-minute capacity per unit of weight than HgO or electrolytic MnO_2 at comparable cathode efficiencies.

Additional coulometric studies were made on 2,4 dinitrobenzaldehyde in electrolytes of different *p*H in order to study the effect of *p*H on capacity. From the scheme of Haber and Schmidt previously described, it would be expected that the use of a strongly basic electrolyte should result in a loss of capacity due to the formation of side products such as azoxybenzene and azobenzene, which are formed by the condensation of the primary reduction products in the alkali electrolyte. The data presented in Fig. 14 for 2,4 dinitrobenzaldehyde discharged at a 0.002 amp/g rate in various electrolytes support this reasoning, as it is seen that little capacity is obtained from this compound in the strongly alkaline electrolyte. In the $MgBr_2$ and acidic NH_4Cl electrolytes, reduction apparently takes place to the diamino stage as evidenced by the fact that efficiencies of 80.5% and 88.9% were obtained.

It is seen from Fig. 14 that the use of a compatible zinc anode in either the acidic NH_4Cl-$ZnCl_2$ or strongly basic NaOH electrolytes would result in galvanic couples which operate at voltages too low for practical use. Coupling the aromatic nitro compound with an anode of higher potential, such as magnesium, however, would result in a couple which operates at practical voltage levels. Since magnesium corrodes too readily in an acid solution and polarizes in strongly basic solution, the most favorable anode-electrolyte combination to use with these aromatic nitro compounds appears to be magnesium with a $MgBr_2$ electrolyte. In a 2*N* $MgBr_2$ electrolyte, magnesium operates at a potential of approximately 1.3 v and when coupled with a compound such as 2,4 dinitrobenzaldehyde would give galvanic couples having operating voltages of 1.00-1.10 v during current drain.

[5] Efficiency calculation based on an 85% MnO_2 content.

Summary

1. A theory based on the effect of substituent groups on the electron density in the vicinity of a reducible nitro group is presented, which explains the effect of these groups on the operating potential of aromatic nitro compounds.

2. The cathode potential during current flow of mononitrobenzene compounds containing para substituted groups such as $-NO_2$, -CN, -CHO, and $-CONH_2$, which can cause a displacement of electrons toward the added group, is 0.05 to 0.20 v higher than the unsubstituted nitrobenzene, whereas mononitro compounds containing para substituted groups such as $-NH_2$, $-N(CH_3)_2$, -ONa, and $-CH_3$, which result in displacement of electrons away from the substituted group, operate at potentials 0.10 to 0.20 v lower than nitrobenzene.

3. The cathode potential is also affected by the position of the substituent group, and differences of 0.05-0.15 v are found for various meta and para isomers of the aromatic nitro compounds. For substituted electron-attracting groups, the para isomer is found to operate at higher potentials than the meta isomer, while the converse is found to hold for substituted electron-repelling groups.

4. In general, the cathode potentials of the aromatic nitro compounds increase as the *p*H of the electrolyte is decreased. However, the effect of the medium on the cathode potential is often a complex one and has to be considered for each individual case.

5. Coulometric reduction studies of various mono and dinitroaromatic compounds indicate that reduction of these compounds takes place to the amino stage, with a resultant 6-electron change per-NO_2 group, at electrode efficiencies of 70-90%.

6. On the basis of the data presented in this paper, the aromatic nitro and dinitro compounds show considerable promise for use as cathode materials in primary cells, the most outstanding feature of these compounds being their high theoretical ampere-minute capacities, both on a weight and volume basis.

Manuscript received Oct. 2, 1957. This paper was prepared for delivery before the Buffalo Meeting, Oct. 6-10, 1957.

Any discussion of this paper will appear in a Discussion Section to be published in the December 1958 JOURNAL.

REFERENCES

1. C. K. Morehouse and R. Glicksman, *This Journal*, **104**, 467 (1957).
2. G. S. Parks and H. M. Huffman, "Free Energies of Some Organic Compounds," Chemical Catalogue Co., New York (1932).
3. W. M. Latimer, "Oxidation Potentials," p. 136, Prentice-Hall, Inc., New York (1952).
4. C. K. Morehouse and R. Glicksman, *This Journal*, **103**, 94 (1956).
5. R. Glicksman and C. K. Morehouse, *ibid.*, **102**, 273 (1955).
6. F. Haber and C. Schmidt, *Z. physik. Chem.*, **32**, 271 (1900).
7. S. Swann, Jr., *Trans. Electrochem. Soc.*, **69**, 287 (1936); **77**, 459 (1940); **88**, 103 (1945); **99**, 219 (1952).
8. C. K. Ingold, *Chem. Revs.*, **15**, 225 (1934).

9. L. Pauling, Gilman's "Organic Chemistry," Vol. II, pp. 1975-1979, John Wiley & Sons, Inc., New York (1943).
10. G. W. Wheland, "The Theory of Resonance," pp. 256-272, John Wiley & Sons, Inc., New York (1947).
11. M. Shikata and I. Tachi, *J. Chem. Soc. Japan*, **53**, 834 (1932); *Collection Czeckoslov. Chem. Commun.*, **10**, 368 (1938).
12. J. Pearson, *Trans. Faraday Soc.*, **44**, 683 (1948); **45**, 199 (1949).
13. S. F. Dennis, A. S. Powell, and J. Astle, *J. Am. Chem. Soc.*, **71**, 1484 (1949).
14. L. F. Fieser, *ibid.*, **51**, 3101 (1929); L. F. Fieser and M. Fieser, *ibid.*, **57**, 491 (1935).
15. C. R. Noller, "Chemistry of Organic Compounds," p. 441, W. B. Saunders Co., Philadelphia, and London, England (1951).

Dry Cells Containing Various Aromatic Nitro Compounds as Cathode Materials

C. K. Morehouse and R. Glicksman

RCA Laboratories, Radio Corporation of America, Princeton, New Jersey

ABSTRACT

The class of aromatic nitro compounds has been found to have properties suitable for the design of improved dry cells when coupled with a magnesium anode. The performance characteristics of these cells are dependent on the type of aromatic nitro compound used as a cathode material.

The AA-size magnesium-meta dinitrobenzene dry cell has been fully characterized and shown to give superior performance to the commercial Leclanché cell on a number of discharge tests.

The use of organic nitro compounds in primary batteries was first mentioned in the patent literature by Bauer (1). He describes a wet-type battery, similar to the Lalande cell, composed of a zinc anode, an alkaline electrolyte, and a cathode consisting of a metal oxide such as copper oxide, and a nitro compound. More recently Arsem (2) and Sargent (3) make reference to the use of nitro compounds as organic oxidizing agents in dry cells. Arsem describes a cell consisting of a zinc anode, an electrolyte of an aqueous solution of boric acid and sodium chloride, and a nitro compound as a cathode. Sargent, on the other hand, employs an organic nitro compound as cathode with an aluminum anode, and an electrolyte composed of an aqueous solution of an alkali metal hydroxide and an alkali metal zincate.

Despite the references to the use of organic nitro compounds in the patent literature, no practical dry cell containing these compounds has been reported. From previous data gathered by the authors (4), one can attribute this to several factors: First, an aromatic nitro compound coupled with a zinc or an aluminum anode would result in a dry cell which would operate at too low a voltage to be competitive with existing commercial cells. Second, it has been found that electrolytes such as strongly alkaline solutions do not enable the aromatic nitro compound to be used at optimum efficiency. In addition, half-cell discharge studies have shown that certain types of aromatic nitro compounds have better cell operating characteristics than others. Finally, it has been found that the cathode mix formulation differs from the usual practice for conventional dry cells in that greater amounts of conductive carbon and electrolyte per quantity of cathode material are required.

In this paper, the performance characteristics of cells containing a magnesium anode coupled with various aromatic nitro and dinitro compounds as cathodes are presented.

Experimental

Experimental dry cells containing various aromatic nitro and dinitro cathodes were assembled using an impact extruded magnesium AA-size (height 1.82 in., O.D. 0.521 in., I.D. 0.441 in.) can, composed of an AZ10A Dow Chemical Company alloy. The magnesium cans were lined with a piece of Nibroc salt-free paper (2¼ in. x 2¼ in. x 0.002 in. thick), after which an extruded slug of cathode mix (weighing approximately 5 g) was inserted and consolidated in the lined can. A carbon rod (ht 1.787 in., diam. 0.159 in.) containing a brass cap was then inserted in the center of the cathode mix, and the cells sealed in the conventional manner with a rosin base wax seal. Two cathode mix formulations listed below were used in this study, the first describing the formulation of the cells discussed in the first section of this paper, and the second describing that of the magnesium-m-dinitrobenzene cells discussed in the second section.

Cathode Mix Formulation No. 1

	% by weight
Aromatic nitro or dinitro compound	26.5
Shawinigan acetylene black	13.3
Barium chromate	1.2
Electrolyte (aqueous solution of 500 g/l $MgBr_2 \cdot 6H_2O$ and 1.0 g/l $Li_2CrO_4 \cdot 2H_2O$)	59.0

Cathode Mix Formulation No. 2

	% by weight
m-Dinitrobenzene	14.6
Darco carbon black G-60	29.2
Barium chromate	1.3
Electrolyte (aqueous solution of 500 g/l $MgBr_2 \cdot 6H_2O$ and 1.0 g/l $Li_2CrO_4 \cdot 2H_2O$)	54.9

The voltage-discharge and capacity data shown in the following sections were obtained by discharging the cells through fixed resistances, and measuring the closed circuit voltage after various time intervals of discharge. All capacity data were gathered at 70° ± 2°F, 50 ± 5% relative humidity (R.H.).

Voltage-Discharge Characteristics of Dry Cells Containing Various Aromatic Mono- and Dinitro Compounds as Cathodes

A previous paper (4) dealt with the effect of various functional groups and their positions on the operating potential of the aromatic nitro and dinitro compounds. It was shown that when electron-attracting groups such as $-NO_2$, $-CO_2H$, $-CONH_2$, $-CN$, etc., are substituted in an aromatic nitro or dinitro molecule, the cathode potential of the parent compound during current flow is raised, the effect being more pronounced when the substitution is in the ortho or para position. Conversely, the substitution of electron-repelling groups such as $-CH_3$, $-NH_2$, etc., lowers the cathode potential during current flow.

The 150-ohm continuous-discharge data obtained on AA-size dry cells containing a magnesium anode and various substituted dinitrobenzene compounds as cathodes are shown in Fig. 1. These data illustrate the effects of substituted groups on the cell discharge potential. For example, cells containing m-dinitrobenzene with electron-attracting -Cl, and $-SO_3K$ groups substituted in the position which is both ortho and para to the nitro groups operate at voltages 0.03 and 0.06 v higher than comparable cells containing the unsubstituted m-dinitrobenzene as the cathode reactant. The addition of an electron-repelling $-CH_3$ group lowers the cell potential 0.05 v below that of the m-dinitrobenzene cell, while the substitution of an $-NH_2$ group lowers the cell potential approximately 0.14 v. This difference in magnitude of effect is expected, since the $-NH_2$ group is more strongly electron repelling than the $-CH_3$ group.

The effect of group substitution is further illustrated in Fig. 2 by the discharge data for cells containing m-dinitrobenzene compounds with electron-attracting $-COOC_2H_5$ and $-CONH_2$ groups in a position meta to the nitro groups. The pronounced two-step voltage-time discharge curve for these cells indicates that the reduction of the dinitro compound

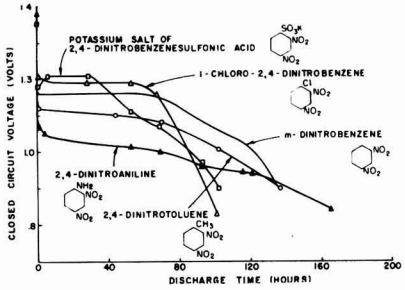

Fig. 1. AA-size dry cells containing a magnesium anode and various substituted dinitrobenzene cathodes discharged continuously through 150-ohm resistances.

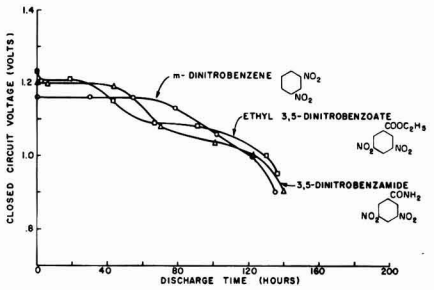

Fig. 2. AA-size dry cells containing a magnesium anode and substituted dinitrobenzene compounds as cathodes discharged continuously through 150-ohm resistances.

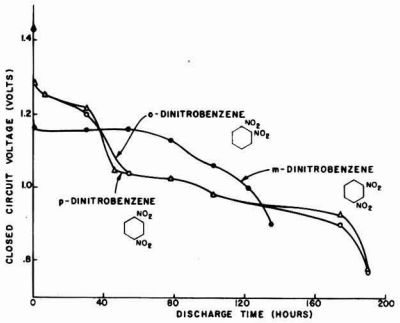

Fig. 3. AA-size dry cells containing a magnesium anode and various isomers of dinitrobenzene as cathodes discharged continuously through 150-ohm resistances.

takes place one nitro at a time. The lower operating potential of the second step is attributed to the formation of a strongly electron-repelling $-NH_2$ group as a result of the reduction of the first nitro group.

The effect of group position on the discharge potential of aromatic nitro compounds is shown in Fig. 3 by the discharge data obtained on cells containing the three isomers of dinitrobenzene. It is evident from the data that the cells have a two-step discharge curve, giving additional evidence that the nitro groups in the molecule are reduced one at a time. In accordance with theory, cells containing the ortho and para isomers have comparable discharge curves and operate at higher potentials than those with the meta isomer during the first part of the discharge. If one assumes that the first nitro group is reduced to the amino stage, the lower potential level of the second step can be explained. It has been shown (4) that a cathode of meta nitroaniline operates at a higher potential during current flow than para nitroaniline.

The effect of both position and type of substitution on operating potential is further illustrated by the discharge data in Fig. 4 for dry cells containing mono nitrobenzene derivatives. The voltage levels of the nitroaniline isomers are seen to correspond to those of the second discharge step of their corresponding dinitrobenzene isomers, giving evidence that the initial cathode reaction involves the reduction of one nitro group to the amino stage, with subsequent reduction of the second nitro group. Also

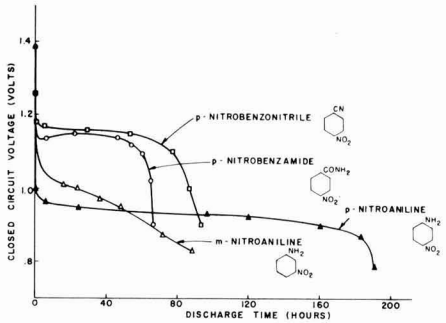

Fig. 4. AA-size dry cells containing a magnesium anode and various substituted nitrobenzene compounds as cathodes discharged continuously through 150-ohm resistances.

shown in Fig. 4 are the different voltage levels obtained when the electron attracting -CN and $-CONH_2$ groups and an electron-repelling $-NH_2$ group are substituted in the para position of nitrobenzene. A curve for a comparable cell containing nitrobenzene is not included, since nitrobenzene is a liquid, which property presents some difficulties in cell assembly. However, from half-cell discharge data (4) it would be expected that a magnesium-nitrobenzene cell would operate at approximately 1.05 v.

Performance Characteristics of Magnesium-m-Dinitrobenzene Dry Cells

There are a large number of aromatic nitro compounds which are stable solids and have theoretical ampere-minute capacities per unit of weight several times greater than the manganese dioxide and mercuric oxide cathode materials used at present in commercial dry cells (4). In addition, when these nitro compounds are coupled with a magnesium anode, dry cells can be made which have a flat discharge curve and operate over a wide range of current drains within the voltage limits of conventional dry cells.

It is beyond the scope of this paper to characterize fully all types of magnesium-aromatic nitro dry cells because of the vast number of such electrochemical systems. Instead, the magnesium-m-dinitrobenzene couple was selected for a more thorough study to determine some of the factors which affect cell performance, as well as to compare its cell characteristics with those of known dry cells.

Cell reactions.—m-Dinitrobenzene, which is produced at present at low cost in tonnage quantities, theoretically has more than 6 times the ampere-minute capacity per unit of weight of manganese dioxide, and 7 times that of mercuric oxide. In addition, it has been found from half-cell coulometric studies, that m-dinitrobenzene cathodes operate at efficiencies in excess of 75%. On this basis, together with the discharge data of the meta and para dinitrobenzene dry cells presented in the previous section, the electrode reactions which are believed to occur during the discharge of a magnesium-m-dinitrobenzene dry cell are shown below.

Although the detailed mechanism has not been worked out for the cathodic reaction, the above

Cathode reaction:

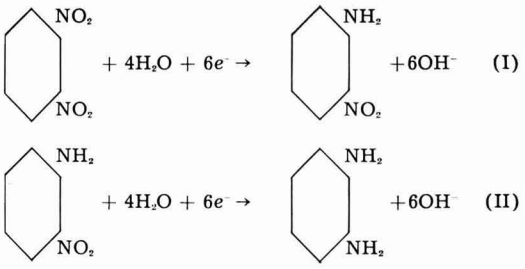

Anode reaction:

$$Mg \rightarrow Mg^{++} + 2e^- \qquad \text{(III)}$$

Over-all energy producing reaction:

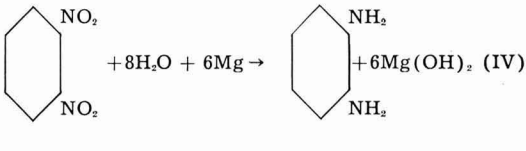

equations offer an explanation for the two-step voltage-discharge curve obtained from these dry cells, showing that reduction takes place one nitro group at a time. In addition, the over-all reduction of an aromatic nitro compound involves a six electron transfer per nitro group which accounts for the high theoretical ampere-minute capacity per unit of weight of these compounds.

Cell discharge data.—Experimental magnesium-m-dinitrobenzene AA-size dry cells were assembled using an impact-extruded AZ10A magnesium alloy can. It was found from a cathode mix formulation study that the type of carbon mixed with the m-dinitrobenzene affects cell performance, as well as the ratio by weight of carbon and electrolyte to m-dinitrobenzene. A formulation, previously described, containing a 1 to 2 ratio by weight of m-dinitrobenzene to Darco G-60 carbon black has been found to give favorable results. The performance characteristics of cells of this formulation are discussed below.

Initial capacity data obtained on these cells discharged continuously through 4- and 150-ohm re-

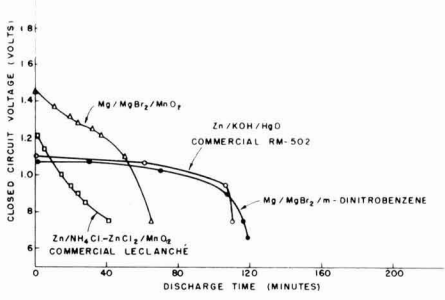

Fig. 5. AA-size dry cells discharged continuously through 4-ohm resistances.

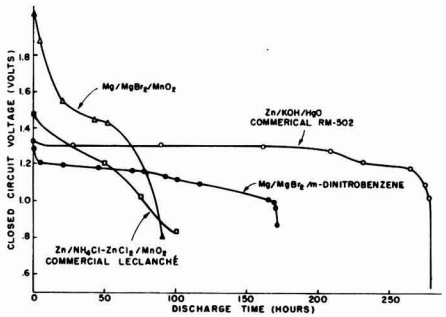

Fig. 6. AA-size dry cells discharged continuously through 150-ohm resistances.

sistances are shown in Fig. 5 and 6. The 4-ohm test represents a drain encountered in a flashlight application, while the 150-ohm test simulates a current drain encountered in a "B" battery or a transistor radio receiver application. Included in Fig. 5 and 6 are discharge data for comparable size Leclanché, zinc-mercuric oxide, and magnesium-manganese dioxide dry cells. The latter cells contained an impact extruded AZ10A magnesium alloy can and are of the type under development by the Dow Chemical Company (5).

The 4-ohm continuous-discharge data show that the m-dinitrobenzene dry cells have a flatter discharge curve than the two manganese dioxide dry cells, being comparable to that of the mercuric oxide cell. It is also seen that, on this test to a 0.90-v end voltage, the m-dinitrobenzene cells give comparable minutes of service to the mercuric oxide cell, and approximately 2 and 4 times the service of the magnesium-manganese dioxide and Leclanché dry cells, respectively.

The data for the 150-ohm continuous-discharge tests also illustrate the flat discharge curve of the m-dinitrobenzene dry cell. On this test, the organic cell gives approximately 90% more hours of service to a 0.90-v end voltage than the two manganese dioxide dry cells, and 38% less hours of service than the mercuric oxide cell.

Capacity data for the four cells obtained from continuous-discharge tests are summarized in Fig. 7 and 8. In Fig. 7 the capacity in hours of service to a 0.90-v end voltage is plotted against load resistance. It is seen that the m-dinitrobenzene cells give considerably more hours of service over a wide range of current drains than the two manganese dioxide dry cells, but are inferior to the mercuric oxide cell, except at high continuous-discharge rates.

In order to normalize the voltage differences between the four cells, watt-minute capacities per unit of weight and volume to a 0.90-v end voltage were plotted vs. average power output. The data in Fig. 8 show that under these conditions of evaluation the m-dinitrobenzene cells have a comparable watt-minute capacity per unit of volume to the magnesium-manganese dioxide dry cell, and 25-230% higher capacity than the commercial Leclanché cell over an average power output range of 5 to 270 mw. At low power output levels, the organic cell gives approximately 45% of the capacity

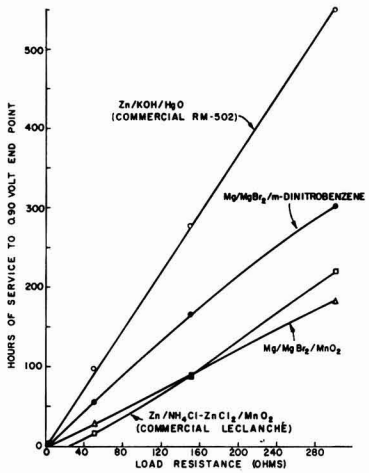

Fig. 7. Capacity in hours of service vs. load resistance of AA-size dry cells discharged continuously through various resistances.

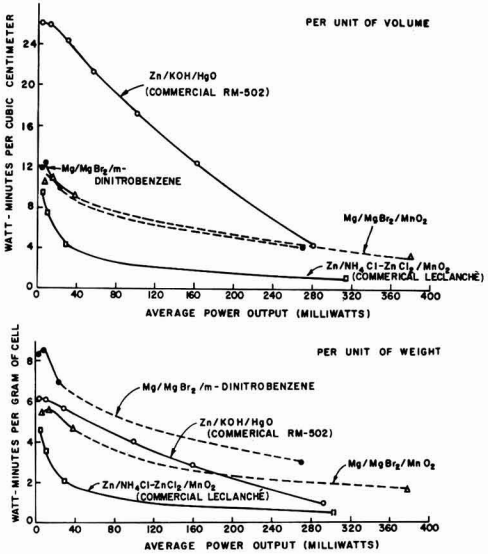

Fig. 8. Capacity in watt-minutes per unit weight and volume vs. average power output for AA-size dry cells discharged continuously through various resistances. (Watt-minute capacity and average power computed to 0.90 v end voltage.)

of the mercuric oxide cell and comparable watt-minute capacities at a power output level of 270 mw.

On the weight basis the m-dinitrobenzene cells give approximately 30% more capacity than the mercuric oxide and magnesium-manganese dioxide cells, and 80-400% greater capacity than the Leclanché cells over a wide range of power output levels.

An additional analysis of the four cells is shown in Table I in which are presented the approximate theoretical ampere-minute capacities and cathode efficiencies computed from the continuous cell discharge data. These data were calculated with the assumption that the cathode material is the limiting cell component.

Table I. Theoretical capacity and cathode efficiency of various AA-penlight size cells

	Theoretical capacity per gram of cathode material	Approx. wt of cathode material in cell	Approx. theor. cell capacity	Cathode efficiency* of cells discharged continuously through following resistances (ohms)			
				4	50	150	300
	(amp-min)	(g)	(amp-min)	%			
$Zn/NH_4Cl\text{-}ZnCl_2/MnO_2$							
Commercial Leclanché	18.5	3.3	60.5	11.1	40.5	60.6	89.3
Zn/KOH/HgO	14.9	10.	149.	19.3	94.6	95.2	95.4
$Mg/MgBr_2/MnO_2$	18.5	3.9	72.2	25.6	62.9	72.6	71.9
$Mg/MgBr_2$/m-Dinitrobenzene	114.9	0.73	83.9	33.1	76.5	91.2	84.4

* Data based on ampere-minute capacity to 0.90-v end voltage.

It is seen from the efficiency data in Table I that the m-dinitrobenzene cathode operates at high efficiencies approaching its theoretical limit on the 150-ohm continuous-discharge test, followed by a slightly lower efficiency on the 300-ohm test. This fall-off in cathode efficiency is also observed with the magnesium-manganese dioxide cell and is attributed to a decrease in magnesium efficiency at the lower current densities. The wasteful corrosion of magnesium consumes water in the cell, which component is essential to the cathodic reaction [Eq. (I) and (II)].

In addition, it is seen that the m-dinitrobenzene cell has a higher theoretical capacity than the two manganese dioxide cells, despite the fact that it has considerably less cathode material. Further performance gains should be possible if a way can be found to put more m-dinitrobenzene in the cell and still obtain the same cathode efficiency.

A significant feature of the m-dinitrobenzene cathode is its high efficiency advantage over the manganese dioxide cathode on heavy continuous-drain tests as seen in Table I. The favorable high-drain characteristics are illustrated also for C-size cells by the 4-ohm continuous and intermittent discharge data presented in Fig. 9. On the continuous test to a 0.90 v end voltage the m-dinitrobenzene cells last 2 and 4 times as long as the comparable size magnesium-manganese dioxide and Leclanché cells, respectively. Some of this capacity advantage, however, is lost on the intermittent test, as the manganese dioxide electrodes become more efficient under these discharge conditions.

Shelf Life Data for Various Magnesium-Aromatic Dinitro Compound Dry Cells

Listed in Table II are shelf life data for some AA-size dry cells containing various organic dinitro compounds as cathodes. These cells comprised an impact extruded magnesium can, a Nibroc salt-free paper separator, a $MgBr_2$ electrolyte, and were sealed with a rosin wax seal. The data presented in Table II represent single cell results. Each cell

Table II. Shelf life data obtained on "AA"-penlight size cells containing a magnesium anode and various aromatic dinitro compounds as cathodes

	Hr of service to 0.90 v*	Storage time at 70°F 50% R. H.			Storage time at 113°F 90% R. H. (Cells packaged in 6 mil polyethylene bags)	
		6 Mos.	9 Mos.	12 Mos.	3 Mos.	6 Mos.
		Capacity retention in % of initial				
Cells containing various unsubstituted aromatic dinitro cathodes						
m-Dinitrobenzene	147	94	95	—	93	80
o-Dinitrobenzene	139	—	93	95	92	114(5)†
p-Dinitrobenzene	176	90	—	100	93	72
Crude dinitrobenzene (Mixture of isomers)	110	110	72	112	97	100
Cells containing cathodes of various aromatic dinitro compounds with electron-repelling substituted groups						
2,4-Dinitroaniline	117	114	91	90	100	108(83@11 mos.)†
2,4-Dinitrotoluene	123	100	111	92	93	100(5) (73@11 mos.)†
2,4-Dinitroanisole	131	106	90	—	—	100
2,4-Dinitrophenetole	142	49	106	95	100	88
Cells containing cathodes of various aromatic dinitro compounds with electron-attracting substituted groups						
3,5-Dinitrobenzamide	140	102	100	98	91	94(5)†
3,5-Dinitrobenzonitrile	107	33	28	57	85	100(5)†
Ethyl-3,5-dinitrobenzoate	136	71	79	—	—	—
2,4-Dinitrobenzaldehyde	120	83	—	69	100	100(5)†
2,4-Dinitrobenzene sulfonate, potassium salt	97	78	54	92	100	100
1-Chloro-2,4-dinitrobenzene	80	115	88	75	115	—
1-Bromo-2,4-dinitrobenzene	128	83	94	83	—	—
6,8-Dinitro-2,4-(1H,3H) quinazoline dione	110	80	55	36	100	55

* Capacity measured at 70°F as hours of service to 0.90 v on 150-ohm continuous-discharge test.
† Figures in parentheses are storage time in months.

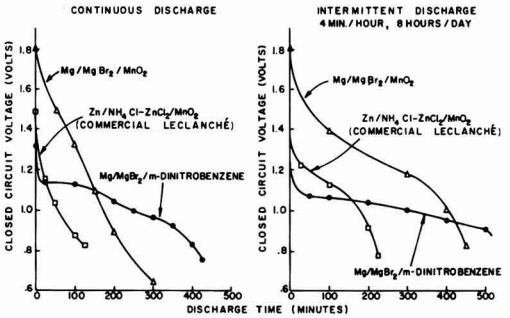

Fig. 9. C-size dry cells discharged through 4-ohm resistances.

tested was from a large group of cells assembled under controlled conditions. It is recognized that a larger test sample is preferred in order to make firm quantitative conclusions by normal statistical methods. However, the results while qualitative do indicate that many of these organic dry cells will have a satisfactory shelf life when stored at temperatures of 70° and 113°F. In several cases there is a difference between the 70°F and high temperature storage data, the cells showing a more favorable shelf life when stored at the elevated temperature. This difference is due to poor seal efficiency which resulted in greater drying out of cells stored at the lower relative humidity. The loss in water would be expected to result in a drop in capacity as water is essential to the cathode reaction as shown in Eq. (I) and (II).

Conclusions

At the present stage of development, the magnesium-aromatic nitro dry cells have problems primarily associated with the magnesium anode. These are loss in capacity on light intermittent tests, "delayed action," and higher impedance than comparable size commercial dry cells.

Acknowledgment

The authors wish to express their appreciation to Mr. G. R. Ganges and Dr. G. S. Lozier for assisting in gathering some of the cell data and their many helpful comments made during this study.

Manuscript received Oct. 2, 1957. This paper was prepared for delivery before the Buffalo Meeting, Oct. 6-10, 1957.

Any discussion of this paper will appear in a Discussion Section to be published in the December 1958 JOURNAL.

REFERENCES

1. W. C. Bauer, U.S. Pat. 1,134,093, April 6, 1915.
2. W. C. Arsem, U.S. Pat. 2,306,927, Dec. 29, 1942.
3. D. E. Sargent, U.S. Pat. 2,554,447, May 22, 1951.
4. R. Glicksman and C. K. Morehouse, *This Journal*, **105**, 299 (1958).
5. R. C. Kirk, P. F. George, and A. B. Fry, *ibid.*, **99**, 323 (1952).

Corrosion of the Zinc Electrode in the Silver-Zinc-Alkali Cell

T. P. Dirkse and Frank De Haan

Department of Chemistry, Calvin College, Grand Rapids, Michigan

ABSTRACT

A study has been made of the factors that affect or bring about the corrosion of the zinc electrode in a silver-zinc-alkali cell. Cells containing 30% potassium hydroxide as electrolyte were used and kept at room temperature. Special attention was centered on open circuit or stand conditions. This corrosion is affected primarily by oxygen and by dissolved silver oxides.

Although the silver-zinc-alkali cell has been produced for a relatively short time, its applications are increasing and it is becoming a rather widely used system. It is now being marketed as a secondary cell having a fairly good life. It is especially remarkable that these advances and developments have been made without a thorough understanding of the mechanisms of the electrode reactions. Relatively little work of a more or less theoretical or fundamental nature has been reported on this system.

It has been noted (1) that the anodic dissolution of zinc in KOH solutions proceeds in two steps. However, when this reaction takes place in a silver cell the mechanism is undoubtedly more complex since there is then the additional complicating factor of the presence of the silver oxides. It was the purpose of this study to investigate the effect of silver oxides and other factors on this anodic zinc process.

The effect of the silver oxides on the anodic dissolution of zinc in KOH solutions is especially obvious when one studies the relationship of this process to Faraday's laws. Two solutions, 15% and 30% KOH, were used as the electrolyte in cells containing zinc anodes and nickel screen cathodes. Two silver coulometers were connected in series with these cells and a small current density was used for about 2 hr. Comparing the amount of zinc oxidized (dissolved) with that prescribed by Faraday's laws, there were deviations of +4% and +0.1%. When a similar test was made on a cell containing a silver oxide cathode in place of the nickel screen and 30% KOH as the electrolyte, the deviation was +93%, i.e., the loss of zinc was about twice as great as that expected from Faraday's laws. A good deal of this

loss was due to the fact that during passage of current a heavy coating of spongy material formed on the anode (zinc) and fell off when the electrode was removed from the solution. This latter fact, aside from the deviation from Faraday's laws, prompted a further investigation of this process or phenomenon. A similar phenomenon was produced under open circuit conditions, and x-ray analysis showed that the spongy metallic product was the same in each case. Therefore an attempt was made to determine the origin and nature of this deposit. This was done by using only open-circuit conditions.

Experimental

Samples of zinc sheet, better than 99.9% pure, furnished by the New Jersey Zinc Sales Company, were cut into strips about 1 cm wide. These were degreased and then treated briefly with dilute HCl. In some cases such a zinc electrode, together with another electrode made by pasting silver oxide on a silver screen, was placed in a large test tube containing about 50 ml of 30% KOH solution. The electrodes were electrically insulated from each other, about 2 cm apart. After being in the cell for 24 hr, the zinc was withdrawn, briefly immersed in 6M acetic acid, then in distilled water, in ethanol, and finally in acetone. Following this the electrode was dried by heating for a short while. Each run was carried out in a constant temperature bath held at 25° ± 0.1°C. The loss of zinc was determined by the difference in weight. The surface area of the immersed zinc was about 10 cm^2. In some runs the silver oxide electrode was omitted, and in others a smaller test tube and a smaller volume of electrolyte were used. X-ray diffraction patterns were obtained by the use of copper radiation with a nickel foil filter.

Results

It soon became apparent that even on open circuit several factors were involved in the corrosion of the zinc. When cells were assembled using silver oxide, the zinc sheet, and 30% KOH solution, the zinc electrode always became covered with a dark black film. This film had a velvety appearance when viewed with a microscope. A black film is sometimes noted on the zinc electrodes after a discharge; then it is often due to a form of zinc oxide (1). In this case, however, the black film did not appear to be the zinc oxide. It did contain varying, but appreciable, amounts of silver or its oxides. This was noted by dissolving a portion of the electrode in nitric acid and then adding HCl to precipitate the silver as the chloride. X-ray diffraction patterns obtained from this film contained the lines due to zinc, but there were other additional lines as well, particularly at about 2.25 and 2.15Å. These extra lines were found in all such samples. Furthermore, these same lines were found in the spongy material that peeled off the zinc electrode when it was removed from the solution after having received a 24-hr anodic treatment. They were also produced by the dark colored film that forms on the zinc shortly after the discharge of a silver oxide-zinc-alkali cell is begun. These two lines are not due to silver or its oxides. The indications then, are that, although silver or its oxides were found on the zinc electrode, they were not present in appreciable quantities as metallic silver or oxides of silver. This black film was formed only when the silver oxide was present in the cell, not when zinc alone was immersed in the KOH solutions. Thus the silver oxide electrode is in some manner related to this film on the zinc. However, the effects of other conditions were also studied.

Table I gives a summary of the results obtained. Column 2 indicates the conditions under which each run was made. In some runs no electrode of silver oxide was present, but rather some silver oxide powder was placed in the test tube with the electrolyte and the zinc was placed on glass beads in the bottom of the test tube. This is indicated in column 3. In other cases the zinc specimen was given a silver coating by dipping it in a silver nitrate solution before it was assembled in the cell. This is indicated in Column 5. Column 7 refers to the nature of the coating formed on the zinc specimen. The term "light black" indicates a thin deposit of the black material.

From these results several conclusions can be drawn as to the nature of the process taking place. First of all it appears that under the conditions prevailing in these experiments the amount of electrolyte had but little effect (*see* runs 17 and 21).

A significant factor is oxygen, either dissolved in the electrolyte, or present in the atmosphere above

Table I. Factors contributing to the corrosion of zinc in 30% KOH at 25°C

		Silver present as				
No.	Conditions*	silver oxide powder in electrolyte	silver oxide electrode	metallic coating on zinc	Wt loss of zinc in mg	Color of film
1	a, g		x		337	spongy
2	a, c, g		x		130	black
3	g		x		52	black
4	c, g		x		55	black
5	c, f, g		x		26	black
6	b, g		x		136	black
7	b, c, g		x		145	black
8	e, g		x		138	black
9	h	x			18	light black
10	h	x			31	light black
11	f, h	x			3	light black
12	d, h			x	78	clear
13	d, f, h			x	29	clear
14	d, h			x	65	clear
15	a, g				46	clear
16	h				39	clear
17	h				43	clear
18	b, g				8	clear
19	e, h				31	clear
20	d, h				6	clear
21	g				43	clear

* The various conditions are: a, air bubbled through electrolyte throughout experiment; b, nitrogen bubbled through electrolyte throughout experiment; c, electrolyte saturated with zinc oxide; d, zinc completely submerged, i.e., no "water line" effect; e, electrolyte contains 0.2% hydrogen peroxide; f, electrolyte was not fresh but had just been used for another run; g, 50 ml of electrolyte used; h, 6 ml of electrolyte used.

the electrolyte. There is no doubt that such oxygen affects the corrosion of zinc. In these experiments white deposits of zinc oxide were sometimes formed at the electrolyte surface. This oxide is soluble in KOH solutions and hence such oxide formation offers no protection against corrosion. The effect of oxygen is noted by comparing run 1 with 3 and run 2 with 4. In each pair all the conditions were alike except for the bubbling of air through the electrolyte. However, even when air was not bubbled through the solution, the effect of oxygen could be noted. Comparison of run 4 with 5, 10 with 11, and 13 with 14, shows the effect of dissolved oxygen. In runs 5, 11, and 13, the electrolyte was not fresh. Consequently, dissolved oxygen had already been consumed. Comparing these with otherwise identical runs it is seen that in each case the corrosion of zinc was considerably less with the oxygen-deficient electrolyte. This was true whether silver oxide was present or not.

Still more evidence for this is found by comparing runs 17 and 20. In run 20 the zinc was completely submerged, whereas in 17 part of the zinc was out of the electrolyte. The zinc was attacked to a greater extent in the latter case where atmospheric oxygen as well as dissolved oxygen was available for reaction. Furthermore, in run 18 nitrogen was bubbled through the electrolyte thus removing the oxygen. Here again the weight loss of zinc was less than in run 21.

Thus the oxygen does attack the zinc. The mechanism of this reaction probably involves local cells containing zinc and oxygen electrodes. In effect, the oxygen transforms the zinc to zinc oxide or hydroxide which then dissolves in the KOH solution. If this is the course of the process, then, if the electrolyte were saturated with zinc oxide, the oxidation product of the zinc would not dissolve as readily and this product might then offer some protection to the remaining zinc. In run 2 an electrolyte saturated with zinc oxide was used and the attack on zinc was definitely less than in run 1. In both these runs air was bubbled through the electrolyte, thus heightening the effect of oxygen. Where this was not done the effect of zinc oxide-saturated potassium hydroxide was negligible, e.g., runs 3 and 4, runs 6 and 7.

However, under certain conditions, passing air through the electrolyte made very little difference. In run 15 the loss in weight of zinc was about the same as that in run 21. This may indicate that the oxygen attack is primarily by the dissolved oxygen. This difference may have been more pronounced if the run had continued longer.

Oxygen attacks and corrodes the zinc electrode, but this attack by itself does not produce the black film referred to earlier. Silver oxide is necessary for this and it produces the black film even in the absence of oxygen, run 6. Thus the actions of oxygen and of silver oxide are different, but they often occur simultaneously.

The effect of silver oxide electrodes on the corrosion of zinc is readily seen by comparing run 1 with 15, 3 with 21, and 6 with 18. In each case the corrosion of zinc was greater in the presence of the silver oxide electrodes. The difference was not the same in each of these three cases. The reasons for this are: (*a*) the weight loss is not accurate in each case since, especially in run 1, a large amount of spongy metallic material was formed which fell off when the electrode was removed; (*b*) in some cases the electrolyte was agitated with air or with nitrogen. When no agitation was used, runs 3 and 21, the difference was significant but not large. When the electrolyte was agitated by bubbling nitrogen through it, the corrosion loss of zinc due to the presence of silver oxide electrodes was greater (runs 6 and 18). In each case the zinc received a velvety black coating or a spongy metallic deposit.

An explanation for this phenomenon involves the ready dissolution of silver oxide in KOH solutions. This is shown on Fig. 1. Small amounts of silver oxide were placed in stoppered flasks containing 25% KOH solution. These mixtures were kept at room temperature and shaken occasionally; from time to time samples were withdrawn, filtered through glass wool, and analyzed for silver by titrating potentiometrically with a potassium iodide solution. The results show that the silver oxide dissolves rapidly in KOH solutions. When zinc was added to these solutions the dissolved silver was removed rather rapidly.

Quite likely then, the silver oxide from the electrode dissolves in the KOH electrolyte. When this dissolved silver oxide reaches the zinc electrode it reacts with the zinc and precipitates there, the reactions probably being

$$Ag_2O + H_2O + 2\,OH^- \rightarrow 2\,Ag(OH)_2^- \qquad (I)$$

$$2\,Ag(OH)_2^- + Zn \rightarrow Zn(OH)_2 + 2\,Ag + 2\,OH^- \qquad (II)$$

$$Zn(OH)_2 + 2\,OH^- \rightarrow Zn(OH)_4^{--} \qquad (III)$$

This mechanism accounts for the presence of silver found in the black film or metallic deposit on the zinc specimens. It also accounts for the effect of agitation, e.g., compare run 3 with 6 where no oxygen was present but the solution was agitated with nitrogen. This agitation hastens the diffusion

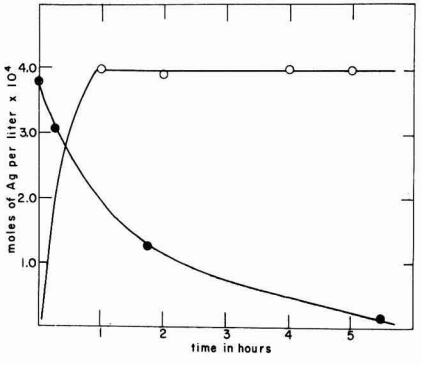

Fig. 1. Dissolution and precipitation of silver oxide from 25% KOH solution. Open circles, dissolution of silver oxide; closed circles, precipitation of dissolved silver oxide by metallic zinc.

of silver oxide to the zinc specimen; thus reaction (II) takes place more rapidly. Comparison of run 4 with 7 supports this hypothesis.

Further support for this mechanism is found in the fact that the appearance of the dark film on the zinc when the silver-zinc cell is discharged is more rapid as the temperature increases and as the concentration of the KOH increases. Increasing the temperature would increase the solubility of silver oxide and also the rate of diffusion of dissolved ions. The solubility of silver oxide also increases with increasing hydroxyl ion concentration (2).

When a little silver oxide was added to the electrolyte in the absence of silver oxide electrodes, the effect was slight (runs 9 and 10). This was undoubtedly due to the fact that the silver oxide rested on the bottom of the test tube with the zinc specimen suspended above it. In this case the dissolved silver oxide would have had to diffuse upward. That some of it did was shown by the fact that the zinc did become covered with a light black film. This was heaviest at the bottom of the electrode.

The dissolved silver oxide is largely in the form of a negative ion. Therefore, it is obvious that reaction (II) will be hastened during the discharge of the cell, since then the zinc functions as the anode. The silver ions will then migrate more rapidly to the zinc. For this reason too the same kind of film is formed on the zinc during discharge of the cell as during stand.

There still remains the question of the origin of the spongy metallic deposit on the zinc, especially in run 1. As has been noted, this deposit contained silver, but no silver lines were found in the x-ray pattern. Instead there were zinc lines plus others. A possible mechanism for this phenomenon is given below.

When reaction (II) takes place it may do so only at certain sites in the zinc lattice. The reduced silver atom then replaces the oxidized zinc atom. This gives the ordinary zinc lattice with silver atoms substituted for zinc atoms at certain points. The result is a solid solution of silver in zinc. Many studies have been made of the silver-zinc system. Of particular help is the work of Westgren and Phragmen (3), Owen and Pickup (4), and Owen and Edmunds (5), where the zinc-rich phases are discussed. Westgren and Phragmen give much information on the x-ray patterns of this system. The designation of the various phases differs, so such phases will be designated here by composition.

On Fig. 2 are given the x-ray lines for zinc, some silver-zinc alloys or solid solutions, and for a representative film obtained in our work. The lines obtained from the black film on the zinc specimens consist of those of zinc plus some of those of the silver-zinc solid solution having a composition varying from 50 to 80% zinc. The lines in Fig. 2b vary somewhat with the amount of zinc present (3). The region 51-60% zinc consists of a mixture of the two phases represented in Fig. 2b and 2c (4). These x-ray data lend support, then, to the hypothesis that, when the dissolved silver oxide reacts with the

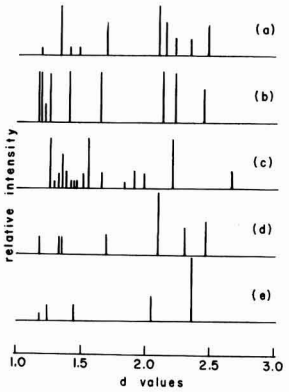

Fig. 2. X-ray patterns: (a) representative dark film obtained in this work; (b) Ag-Zn solid solution ranging from 60 to 78% Zn, ref. (3); (c) Ag-Zn solid solution ranging from 48 to 51% Zn, ref. (3); (d) zinc, ref. (6); (e) silver, ref. (6).

zinc, a solid solution of silver in zinc is formed on the surface of this zinc.

Furthermore, with this hypothesis one also has an explanation for the spongy metallic deposit formed on the zinc specimen in a few of the runs. As has been noted, analysis showed that this deposit contained zinc and silver. The potential of the silver-zinc solution is less anodic than that of zinc and hence the solid solution can be deposited by the emf of zinc itself. This explanation was also suggested by Straumanis and Fang (7) who studied a similar phenomenon in acid solutions.

There is also other evidence that metallic silver as such is not involved in this process. When zinc was covered wtih silver before being assembled in the cell (runs 12, 13, and 14) there was an increase in corrosion (compare with run 20) but there was no visible film on the zinc. Furthermore, when a silver electrode and a zinc specimen were electrically connected in a 30% KOH solution the zinc dissolved and hydrogen was evolved, vigorously at first, on the silver, but after 24 hr no zinc appeared on the silver electrode. The reaction probably was

$$Zn + 2\,H_2O + 2\,OH^- \rightarrow Zn(OH)_4^= + H_2 \qquad (IV)$$

Two runs were also made to test the effect of hydrogen peroxide on this corrosion of zinc. The presence of the HO_2^- ion increases the corrosion of zinc considerably when silver oxide is present (*see* runs 3 and 8). On the basis of thermodynamic considerations this could be expected since the free energy decrease for reaction (V) is about 25 kcal greater than for reaction (VI).

$$Ag_2O + HO_2^- + 2Zn + 2H_2O \rightarrow 2Ag + 2Zn(OH)_2 + OH^- \qquad (V)$$

$$2Ag_2O + 2Zn + 2H_2O \rightarrow 4Ag + 2Zn(OH)_2 \qquad (VI)$$

However, the mechanism is likely not as simple as indicated.

In the absence of silver oxide, the effect of hydrogen peroxide is less, (*see* runs 17 and 19). In fact, the presence of the HO_2^- ion seems to reduce the corrosive loss of zinc. The effect, however, is small.

Conclusion

In a silver-zinc-alkali cell the zinc electrode is attacked and oxidized by oxygen. When no diaphragm is present to reduce or eliminate diffusion, dissolved silver oxide migrates to the zinc electrode where it is reduced and forms a solid solution with the zinc, or else is deposited as such. This enables zinc or silver-zinc solid solution to precipitate from the electrolyte in a spongy form on the zinc electrode during open-circuit conditions and this may act as a short between the plates.

Acknowledgment

The authors wish to express thanks to the Office of Naval Research for sponsoring this project, to the New Jersey Zinc Sales Company for furnishing some of the materials, and to Mrs. Jeanne Burbank for her help in interpreting the x-ray work.

Manuscript received Nov. 4, 1957.

Any discussion of this paper will appear in a Discussion Section to be published in the December 1958 JOURNAL.

REFERENCES

1. T. P. Dirkse, *This Journal*, **102**, 497 (1955).
2. H. L. Johnston, F. Cuta, and A. B. Garrett, *J. Am. Chem. Soc.*, **55**, 2311 (1933).
3. A. Westgren and G. Phragmen, *Phil. Mag.*, **50**, 311 (1925).
4. E. A. Owen and L. Pickup, *Proc. Roy. Soc. London*, **140A**, 344 (1933).
5. E. A. Owen and I. G. Edmunds, *J. Inst. Metals*, **57**, 297 (1935); **63**, 265, 279, 291 (1938).
6. H. E. Swanson and E. Tatge, "Standard X-ray Diffraction Powder Patterns," National Bureau of Standards Circular 539, Vol. I, Washington, D. C. (1953).
7. M. E. Straumanis and C. C. Fang, *This Journal*, **98**, 9 (1951).

Diffusion of Oxygen in Zirconium and Its Relation to Oxidation and Corrosion

J. Paul Pemsler

Nuclear Metals, Inc., Cambridge, Massachusetts

ABSTRACT

The diffusion of oxygen in zirconium and dilute zirconium alloys has been studied in the temperature range of 400° to 585°C by observing the rates of dissolution of anodically deposited interference oxide films. The diffusion coefficient of oxygen in zirconium depends on the grain orientation and varies by a factor of two among different orientations. Macroscopically observed average values obey the equation

$$D, \text{cm}^2/\text{sec} = 9.4 \exp\left[(-51{,}780 \pm 220)/RT\right]$$

where the activation energy for the diffusion of oxygen in zirconium is 51.78 kcal/mole. No macroscopic differences were observed in the diffusion coefficients of the various dilute alloys. Oxidation and corrosion rates have been observed to have an orientation dependence similar to that observed in the diffusion study. The mechanism of oxidation and corrosion is discussed in terms of diffusion of oxygen and adherence of oxide films.

Zirconium shares with titanium and hafnium the unusual ability to dissolve large amounts of oxygen in interstitial solid solution. The oxygen is strongly bound to the lattice, as evidenced by the fact that the metal can be heated beyond its melting point without oxygen evolution. Few data exist concerning the rate of diffusion of oxygen in zirconium metal, especially at temperatures where its corrosion properties are of interest in nuclear reactor applications.

Investigators have defined the zirconium-oxygen phase diagram and made observations on the nature of the oxygen in the zirconium lattice. De Boer and Fast (1) studied the solution of oxygen in the zirconium lattice and concluded that all the oxygen in the metal is present in solid solution. They observed the migration of oxygen as negative oxygen ions under the influence of a potential drop. The binary phase diagram of the zirconium-oxygen system has been studied by Hansen, McPherson, and Domagala (2), who showed that the equilibrium solubility of oxygen in alpha zirconium is independent of temperature and has a value of 29 at. %.

The only other definitive study on the diffusion of oxygen in zirconium was carried out simultaneously with this work by Mallett, Albrecht, and Wilson (3) who determined the diffusion coefficient of oxygen in alpha and beta Zircaloy by the moving boundary and concentration gradient techniques, respectively. Over the temperature range studied, 1000°-1500°C, the equations for diffusion coefficients in the alpha and beta phase were:

$$D_\alpha = 0.196 \exp\left[(-41{,}000 \pm 1500)/RT\right]$$

and

$$D_\beta = 0.0453 \exp\left[(-28{,}200 \pm 2400)/RT\right]$$

Misch (4), whose technique was similar to that used here, studied the rate of oxide film dissolution over a temperature range of 450°-600°C. He reported a linear rate of dissolution at 450°C cor-

responding to 0.6 Å/min, and measured an energy of activation for the process of 43.5 kcal/mole. The results and interpretation in this investigation differ from those of Misch.

Experimental

In this investigation the diffusion of oxygen in zirconium and zirconium alloys was studied by following the rate of dissolution of anodically deposited interference oxide films when annealed *in vacuo*. The thickness of the oxide film was determined periodically during the experiment by observing its color.

Materials.—The alloys used in this study are listed below.

Zirconium—high purity, low hafnium crystal bar
Zircaloy-2 (1.5 weight per cent [w/o] Sn, 0.12 w/o Fe, 0.05 w/o Ni, 0.10 w/o Cr)
Zircaloy-3A (0.25 w/o Sn, 0.25 w/o Fe)
Zirconium—0.62 w/o Ni
Zirconium—0.93 w/o Cr
Zirconium—0.82 w/o Fe, 0.13 w/o Ni, 0.95 w/o Cr

Sample preparation.—Samples of zirconium and alloys, about 7 cm x 1 cm x 0.2 cm, were cut from rolled stock, annealed for 1 hr at 800°C, and furnace cooled. They were then polished on 400 grit Carborundum on a wet wheel and etched for 2 min in a bath of 50% HNO_3, 5% HF, and 45% H_2O.

Anodic deposition of oxide film.—Oxide films were deposited anodically from a 1% KOH solution in distilled water, with the sample as anode and a platinum wire as cathode. Samples were anodized for 15 min in steps of the desired voltage increment in a manner similar to that used by Misch in his study (4). Except for one end attached to an alligator clip, the suspended specimen was entirely submerged in the bath. After anodizing for 15 min the current was stopped, the sample withdrawn, rinsed with distilled water, and reimmersed to within 1 cm of the previous immersion. The voltage was increased by the desired increment and anodization started. In this way a step gauge strip was produced with a number of successively thicker oxide films. Table I lists the colors observed for different increasing voltages. In order to study the variation in thickness of anodically deposited oxide films with applied voltage, samples were weighed on a microbalance between successive anodizations. In these cases the same length of sample was immersed during each anodization.

Table I. Variation of color with applied voltage for anodically deposited ZrO_2 films

Voltage	Color
5	Light yellow
7½	Amber
15	Dark blue
22½	Light blue
30	Silver
37½	Yellow
50	Orange
65	Wine
80	Green
95	Yellow

Film dissolution.—Film dissolution was carried out in two different systems. In the first, a dynamic vacuum was maintained throughout the experiment. The specimen was contained in a tantalum or zirconium boat placed in a Vycor tube which was sealed at one end and had a ground glass joint at the other end. The tube was attached to a vacuum system and evacuated for at least 1 hr after a pressure of 10^{-6} mm Hg was attained. A thermocouple sealed into the tube was in contact with the specimen. A ball and socket ground glass joint enabled the tube to be swung into a horizontal tube furnace which had been preheated to the desired temperature and controlled to ±3°C by a temperature controller. The thermocouple indicated that the sample reached temperature in about 5 min. Periodic examination of the specimen was made under fluorescent light by lifting the top half of the furnace. The examination could be made quickly so that the temperature of the specimen, as indicated by the thermocouple, was not affected at all, or only slightly affected for a brief period. The color of each zone changed with time in the direction of decreasing film thickness, so that any given color corresponding to a particular oxide thickness would go through all the colors in Table I corresponding to films thinner than it. At any given time, the decrease in film thickness was found to be independent of the original thickness of a particular zone; thus, identical results were obtained using any one of the color zones as indicator. However, certain colors corresponding to a narrow range of thickness, and easy to detect, were used to decide when a given film thickness was reached within a smaller range of error. The approach to these colors could be estimated to within as little as ±0.5 v or 15Å.

The second system used for film dissolution involved a static vacuum. The sample, contained in a boat, and a wad of zirconium turnings were placed at opposite ends of a 15-in. Vycor tube sealed at one end. The tube was evacuated to 10^{-6} mm Hg or better and sealed off. The end containing the zirconium turnings was placed into the tube furnace and kept at 800°C for 1 hr, while the end containing the specimen extended far enough out of the furnace to prevent it from becoming heated. This treatment served to getter any remaining atmosphere in the tube. From this point on, the procedure was similar to the dynamic vacuum system, except that the thermocouple was external to the tube and the time required for the sample to reach temperature could not be estimated with the accuracy attainable in the first method.

Results and Discussion

The Anodic Film

The relation between the weight gain and applied voltage during the anodization of three different zirconium specimens was determined. The weight gain is linear with applied voltage from 0 to 65 v. An increase in slope corresponding to a higher rate of weight gain with voltage was obtained above 65 v. This latter increase may have been due to impurities in the anodizing bath. The majority of

studies were made using a maximum film thickness corresponding to values less than 65 v. Assuming a value of 5.7 for the density of ZrO_2, the oxide film thickness deposited during anodization corresponds to 29.0Å/v in the range of 0-65 v. This result is in good agreement with studies by Polling and Charlesby (5) and Misch (4), who obtained conversion factors of 27Å/v and 30Å/v, respectively.

Difficulty was observed during the anodization of several iron-containing alloys when there occurred an appreciable "creepage" of oxide film from the water line into the color zone above. Anodizations of these specimens at high voltages produced a dull film, and there was a great deal of bubbling compared to that observed while pure zirconium was being anodized. Further, during the subsequent vacuum anneal of these alloys, there was a dullness and fading of color compared to the bright reflecting film on pure zirconium and other alloys. The failure to form a suitable anodic film in these alloys is believed to be due to the low oxygen overvoltage on iron intermetallics. The vigorous liberation of oxygen in many areas during anodization prevented the formation of an adherent oxide film. Alloys containing appreciable amounts of iron present as finely divided second-phase particles are not amenable to this type of investigation.

Polling and Charlesby (6) report that, with respect to rate effects, anodically formed films are equivalent to air-formed films. Misch (7) criticizes this viewpoint, stating that anodic films are formed under high field strength which subjects the film to a very large pressure. In the corrosion reaction the formation field is much lower than in anodization except when anodizing at very low voltages.

In order to ascertain whether anodically deposited films are comparable to oxidation films, a zirconium sample was oxidized slowly in an oxygen atmosphere until a thin interference film oxide was formed. Subsequent vacuum annealing of this sample gave results in good agreement with the data obtained using anodically deposited films. While these anodic oxide films may differ initially from corrosion films, it appears that at elevated temperatures, in a short time compared to the time of the diffusion experiment, the mobility of oxygen in the metal and oxide causes the anodic film to behave similarly to a corrosion film, at least insofar as its dissolution rate is concerned.

Diffusion Coefficients

Data obtained using the dynamic vacuum suffered from a lack of reproducibility. Samples run side by side and at the same time gave identical results, but repetitions at a different time did not always agree with the previous data. During certain runs, a yellow tinge on some of the samples was noticed, especially at the end that had no original anodic deposit. This was undoubtedly due to the formation of yellow zirconium nitride, with the sample acting as a continuous getter for the residual atmosphere in the system. The nitride persisted during the diffusion, indicating that the mobility of nitrogen in zirconium is small compared to that of oxygen at the temperatures used in the diffusion anneal. On one occasion when the vacuum system suffered a small leak during an experiment, there was actually a reversal in the film dissolution process and the film thickened with time. However, in cases where the surface was free from nitride, results of the dynamic and static methods were in good agreement. The second technique of gettering the remaining atmosphere in a static system provided a method of obtaining consistently reproducible data.

Microscopic examination of samples which have been anodized and subsequently vacuum annealed revealed that the dissolution process was not homogeneous, and that, macroscopically, an average process was being observed. A wide range of colors, sharply defined by grain boundaries, was observed under a microscope. Under similar magnification an anodized specimen, before vacuum annealing, was homogeneous in color, except for small differences in the tints of some grains. These differences may have been due to small differences in the reactivity or reflectivity of the variously oriented grains. The results presented in this section are then based on a macroscopic, average estimate of color. Variation in diffusion coefficient from grain to grain depending on orientation is discussed in detail in the next section.

The decrease in thickness of oxide film as a function of time has been measured at five different temperatures. The results are plotted in Fig. 1, 2,

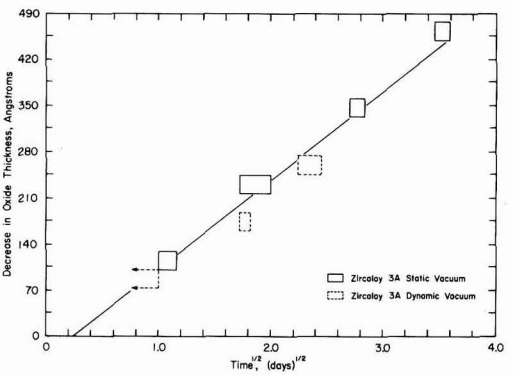

Fig. 1. Decrease in thickness of oxide film as a function of time, at 400°C.

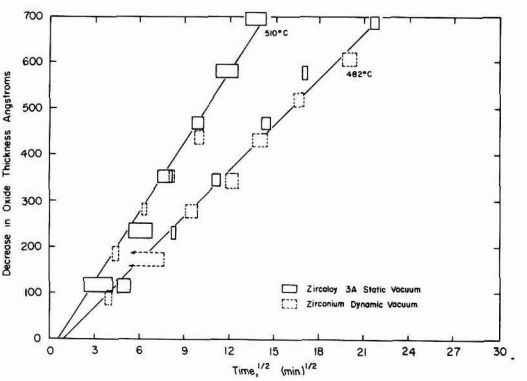

Fig. 2. Decrease in thickness of oxide film as a function of time, at 482° and 510°C.

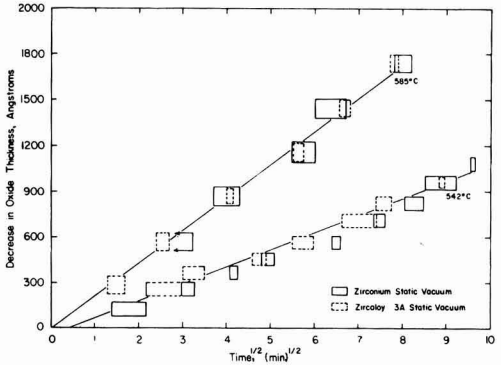

Fig. 3. Decrease in thickness of oxide film as a function of time, at 542° and 585°C.

and 3. Since the samples were examined intermittently, and the thickness estimated visually, each experimental observation is indicated by a rectangle whose dimensions correspond to estimates of the error in the observation. A plot of the decrease in film thickness vs. the square root of time is linear. Extrapolations of some of these lines miss the origin by a small amount, possibly corresponding to very small errors in estimation of the time when the sample came to temperature. Since the equilibrium partial pressure of oxygen over ZrO_2 is of the order of 10^{-58} atm at 600°C, the disappearance of oxide film must be due to solution of oxygen in zirconium metal, with a consequent growth of metal at the expense of oxide. Misch (4) measured the time dependence of dissolution of anodic oxide films at a single temperature. His points, based on a single observation of each sample after a given time interval, show appreciable scatter. Although he suggests a linear rate of dissolution, his data when replotted appear to fit a parabolic function about as well as they fit a straight line. The reproducibility in this study is better than is Misch's, and repeated observation of the same sample shows that a linear time-dissolution relationship is definitely excluded.

The parabolic rate of disappearance of the oxide film on zirconium suggests that the rate-determining step in the dissolution process is the diffusion of oxygen in zirconium metal. An alternative rate-determining step, the transfer of oxygen across the oxide-metal interface, would be expected to lead to a linear rate of disappearance of oxide. The consumption of oxide, generating additional metal, is accompanied by an outward motion of the oxide-metal boundary until the oxide is entirely consumed. Mathematically, this case falls within a limited class of moving-boundary diffusion problems, for which solutions are readily found. The diffusion equation is discussed in detail elsewhere (8). From the solution found on the assumption of constant diffusivity, D can be found as

$$D = \frac{1}{4b^2}\left(\frac{x'}{\sqrt{t}}\right)^2$$

where b is found to satisfy the equation

$$b\,(1 + \operatorname{erf} b) = \frac{1}{\sqrt{\pi}}\frac{C_o}{m_o}e^{-b^2}$$

Here in time t, there is a displacement of the oxide-metal boundary x', which is related to the observed decrease ΔL in thickness of oxide film by the following expression involving the respective molecular volumes:

$$x' = \frac{\rho ZrO_2}{\rho Zr \text{ saturated}}\,\frac{\text{Formular weight (Zr sat)}}{\text{Formular weight } (ZrO_2)}\,\Delta L$$

The quantity ρ is the density, and C_o is the difference between the saturated concentration C_s, and the initial concentration, of oxygen in the metal. The quantity m_o represents the weight of oxygen removed from the ZrO_2 consumed in the generation of unit volume of saturated zirconium ($ZrO_{0.41}$). It may be expressed as

$$m_o = \frac{\text{Formular weight } (O_{1.59})}{\text{Formular weight } (ZrO_{0.41})}\,\rho_{Zr\ sat}$$

In this work the values used are: $C_o = C_s = 0.450$ g/cm³ (the initial concentration was taken as zero); $m_o = 1.75$ g/cm³; $x' = 0.676\ \Delta L$, cm; $\rho_{Zr\ saturated} = 6.72$ g/cm³ (9); $\rho_{ZrO_2} = 5.73$ g/cm³ (10); $b = 0.126$. The densities of saturated zirconium and ZrO_2 were taken as the best available data at room temperature. No effort was made to correct these data to higher temperatures.

The solution is unique if D is constant. The agreement of the experimental results with the expression derived on the basis of constant D does not establish that D is, in fact, independent of concentration. Evidence for the constancy of D, at least in beta zirconium, is found in the work of Mallett, *et al.* (3). They found that the concentration distribution of oxygen diffused into specimens of beta zirconium could be fitted with constant-diffusivity solutions of the diffusion equation.

The diffusion coefficients of oxygen in zirconium at five temperatures are listed in Table II. A plot of the logarithms of the diffusion coefficient vs. the reciprocal of the absolute temperature over the range studied here is shown in Fig. 4. The resulting straight line is in excellent agreement with an Arrhenius temperature dependence, and an energy of activation of 51.8 kcal/mole is calculated. The equation for the diffusion coefficient of oxygen in zirconium in the temperature range of 400°-585°C is given by D, cm²/sec $= 9.4 \exp\,[(-51{,}780 \pm 220)/RT]$.

In the results of Mallett, *et al.* (3), the diffusion coefficient of oxygen in alpha Zircaloy-2 has been determined over the temperature range 1000°-

Table II. Diffusion coefficients of oxygen in zirconium

D, cm²/sec	T, °C
1.34×10^{-16}	400
1.21×10^{-14}	482
2.79×10^{-14}	510
1.38×10^{-13}	542
5.62×10^{-13}	585

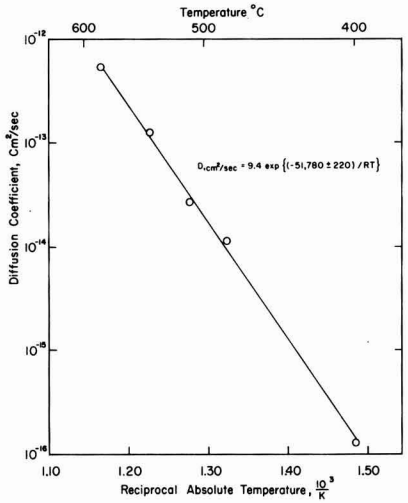

Fig. 4. Temperature dependence of the diffusion coefficient of oxygen in zirconium.

1500°C by the moving boundary technique, which makes use of the stabilization of alpha zirconium at high temperatures. The Arrhenius plot of Mallett's data together with the results of this study are presented in Fig. 5. Mallett calculated an energy of activation for diffusion of 41.0 kcal/mole. The agreement between these data is excellent considering the large differences in temperature ranges studied and in the techniques used. Extrapolation of Mallett's equation to the temperature range studied here would estimate a value for the diffusion coefficient which is high by a factor of about ten. Extrapolation of the equation obtained here to high temperatures gives excellent agreement with Mallett's data. One is tempted to draw a single least squares line through all the data from 400°-1500°C which is represented by the following equation:

$$D, \text{cm}^2/\text{sec} = 5.2 \exp\ (-50{,}800 \pm 870)/RT$$

The activation energy obtained using all the data is in excellent agreement with that derived from the low temperature data alone.

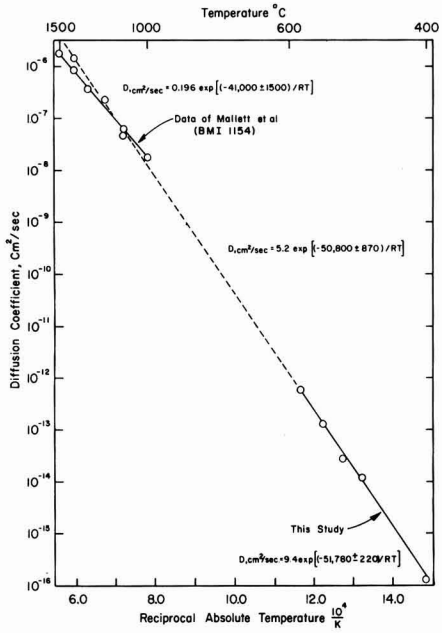

Fig. 5. Combined data for the temperature dependence of the diffusion coefficient of oxygen in zirconium.

Orientation Dependence of the Diffusion Coefficient

The results presented above are based on a visual estimation of the over-all extent of the diffusion. Microscopic examination of a particular color zone on a sample, after the diffusion anneal was completed, showed that a wide variation of colors was visible. For example, an area that appeared homogeneously light blue to the naked eye resolved under magnification into an approximately equal number of areas of dark blue, medium blue, light blue, silver, and light yellow color. These colors are sharply defined by grain boundaries. As previously discussed, the anodization produced a homogeneously colored oxide film.

The relation of grain orientation to diffusion coefficient was studied with the aid of a zirconium strip with very large grain size. Twenty-five separate grains, with an average grain size of 4 mm, were counted on one face of the strip. The strip was anodized, diffusion annealed, and examined with a low power microscope. The variation in color from grain to grain was very sharply defined by grain boundaries, and corresponds to a variation in the diffusion coefficient by a factor of two. Examination of numerous other specimens diffused over the range of temperatures examined in this study reveal the variation in diffusion coefficients by a factor of about two to be a constant. The orientations of eight grains exhibiting wide differences in oxygen diffusion coefficients were determined by x-ray diffraction. The continuity of these grains could be traced visually around the edges of the original face to the sides perpendicular to it. From a knowledge of the orientations of one face of the eight grains, the orientations of eight additional perpendicular faces could be calculated. The results of the examination of the relative diffusion coefficients of fifteen areas (one being the area used to attach the sample to the source of potential) are presented in Fig. 6, which shows one-twelfth of the stereographic projection of the hexagonal crystal system. The symmetry properties of the hexagonal system make this sufficient to describe all orientations.

In orientation, the c-axes of the grains range from being parallel to being within 28° of perpendicular to the plane of the sample. Relative diffusion coefficients of oxygen in zirconium are indicated by the degree of darkening of the circles indicating the orientation; the darkest circle is given a value of unity. The diffusion coefficient is a minimum when the c-axis is parallel to the reference plane, rises to a maximum when the c-axis is about 70° from the normal to the reference plane, and has inter-

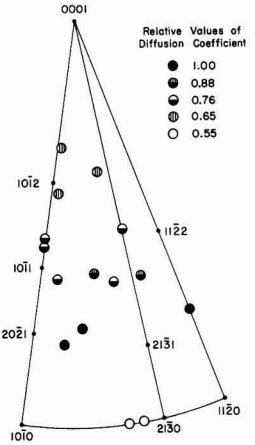

Fig. 6. Effect of orientation on the diffusion coefficient of oxygen in zirconium.

mediate values as it approaches the normal to the reference plane.

Oxygen has been postulated to diffuse through the hexagonal zirconium lattice interstitially. Size considerations (1) lead to the belief that the oxygen must be contained in octahedral rather than tetrahedral interstices. These octahedral interstices run parallel to the c-axis of the hexagonal lattice, and for this reason one would expect a maximum rate of diffusion when the c-axis is perpendicular to the plane of the sample, falling to a minimum rate when it is parallel to the sample plane. Experimental observations do not agree with this simple picture, and no explanation for the experimental observations is offered at this time.

Effect of Alloying Additions and Heat Treatment on the Diffusion Coefficient

No difference could be detected in the macroscopically observed rate of diffusion of oxygen in the various alloys listed in the Materials section. Microscopic examination revealed differences in rates of diffusion of different grains in accordance with observations of the orientation dependence as discussed above. The variation of diffusion coefficients for different grains was identical for the different specimens tested.

No difference could be detected in the macroscopically observed oxygen diffusion rate of alloys annealed in the alpha and water quenched from the beta region. Microscopically, annealed specimens showed the typical color variation due to orientation differences sharply defined by grain boundaries. In the water quenched alloys the macrostructure determined the over-all tint of the macrograin, but the structure within the grains showed additional color variations. The effect on the diffusion coefficient of the fine structures due to the water quench was therefore superimposed on the effect of the orientation of the macrograins resulting from the heat treatment in the beta region.

Anisotropy of Oxidation and Corrosion

In order to determine whether there is an orientation dependence on the rate of oxidation, similar to that observed in diffusion, a zirconium alloy was heated to 415°C in an oxygen atmosphere and examined periodically. An interference film formed quickly and the color changed with time in a manner analogous to that of anodic film growth with increasing voltage. Microscopic examination of the sample after the experiment was completed revealed a situation similar to that observed after a diffusion anneal: a distribution of color sharply defined by grain boundaries, indicating a variation of oxide thickness from grain to grain. The oxidation temperature used here was too low for any color changes due to anisotropic oxygen diffusion to occur in the time interval of the experiment. Such variations in interference color films on different grains have been observed previously by Schwartz, Vaughan, and Cocks (11) during the corrosion of zirconium samples in 316°C water. In order to compare the results obtained in oxygen with those in water the above experiment was repeated in a water vapor atmosphere at 415°C and in liquid water in an autoclave at 316°C. In both water vapor and liquid water the results were similar to that obtained in oxygen. However, in the latter two cases there was a decided tendency for certain areas to stain, i.e., preferentially oxidize so as to mask out any effects due to orientation. This phenomenon was not noticed during oxidation by oxygen gas.

The effect of grain orientation on the extent of oxidation was studied using the large grain zirconium sample used in the diffusion study. The sample was oxidized in an oxygen atmosphere for about 1 hr at 415°C. The effect of orientation on the extent of oxidation is shown in Fig. 7, which is a stereographic projection of the zirconium lattice as discussed above. The results parallel those observed for the orientation dependence of the oxygen diffusion coefficient: the rate of oxidation is a minimum when the c-axis is parallel to the plane of the sample, rises to a maximum when the c-axis is inclined about 20° from the sample plane, and decreases again at higher inclinations. An orientation effect similar to this has been observed in the extent of growth of anodic films on zirconium in nitric acid (12). In order to determine whether the orientation dependence of the corrosion rate persists be-

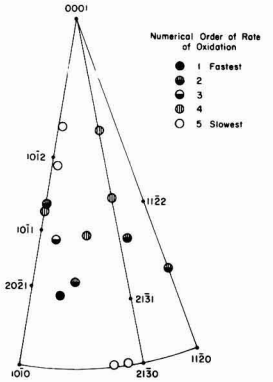

Fig. 7. Effect of orientation on the rate of oxidation of zirconium.

yond the initial stages of the reaction, a sample of pure zirconium of fairly large grain size was placed in 400°C steam at 1500 psi in an autoclave. After 20 hr the thickness of the oxide layer varied enormously from grain to grain in this single sample: some grains had interference film oxide layers of the order of a few thousand angstroms thick, while others had films ranging from dense black oxide to white blistering oxide, presumably spalling.

During the useful life of zirconium alloys in water at high temperature, before spalling occurs, weight gains of the order of 100 mg/dm^2 are obtained. Assuming an average grain size of the order of 0.05 mm, this weight gain corresponds to the formation of the entire oxide film from a fraction of the depth of the uppermost grains. In samples with good corrosion properties one must then reconcile the formation of a single continuous adherent oxide film (before spalling) from oxides growing at different rates on neighboring grains. The effect of this differential growth rate may lie in either of two directions:

1. Additional strains may develop between films on neighboring grains, resulting in spalling at a smaller weight gain than if there was no anisotropy of growth rate.

2. Some of the strain caused by the oxide having a greater molar volume than the metal (Pilling-Bedworth ratio 1.56) may be alleviated. A thick oxide layer under compression growing on one grain might relieve some of its stress by spreading over an adjacent grain having a thinner oxide layer under less compression. This merging of oxide above different metal grains might relieve the stress in those oxide zones under greatest compression. This relief would increase the weight gain before spalling occurred. Any mechanism purporting to explain the oxidation or corrosion of zirconium and zirconium alloys must account for the anisotropic nature of the reaction. It is obvious that more experimental work is needed before conclusions may be drawn regarding differential film growth.

Effect of Alloying Elements on Oxidation

The effect of alloying elements on the corrosion resistance of zirconium has been discussed in terms of the conductivity of the oxide according to the Wagner mechanism by other authors (13), and no attempt is made to evaluate these ideas. It is desired, however, to call attention to the role that second-phase inclusions may play in the film building process. Intermetallics such as Fe_2Zr and Zr_2Ni have been shown in themselves to have poor corrosion resistance, and yet it has been observed that a fine dispersion of these particles in an alpha matrix enhances the corrosion resistance of zirconium (14). These inclusions may serve in some way to anchor the oxide film to the metal, or alleviate stresses in the growing oxide film. Here, too, much experimental work remains.

Relation of Diffusion to Oxidation and Corrosion

In the initial stage of oxidation or corrosion a freshly exposed zirconium surface will dissolve oxygen in solid solution until an oxygen concentration is established at the interface which is in equilibrium with the composition of zirconium oxide. After that time, in the presence of an oxidizing atmosphere, an oxide scale will exist on the metal. As the reaction proceeds, oxygen will react with metal saturated with oxygen at the interface, and will continue to dissolve in the metal beyond the interface. If the solution to the diffusion equation given above is examined and one assumes that: (*a*) the concentration of oxygen at the metal-oxide interface is a constant, representing the solubility limit of oxygen in metal, (*b*) the concentration of oxygen is constant at the oxide-gas or liquid interface, probably representing a saturation value, and (*c*) the dimensions of the sample are very large compared to $\sqrt{Dt}$, several conclusions about the oxygen content of corroding zirconium may be drawn:

(*a*) Oxygen will be diffusing into metal at all times.
(*b*) The flux in the oxide will decrease with time as oxide thickness increases.
(*c*) The flux in the metal will decrease with time.
(*d*) The "depth of penetration", which is the distance beyond the metal-oxide interface that the oxygen has penetrated and reached some arbitrary concentration, will increase with time.

The ratio of the molar volumes of ZrO_2 to Zr (Pilling-Bedworth number) is 1.56 so that the growing oxide film is considered to be under compression. As the oxidation proceeds, the increasing extent of oxygen penetration in advance of the metal-oxide interface will lead to an increasing extent of embrittlement of the metal supporting the oxide film. This embrittlement may lessen the ability of the metal substrate to withstand the stress necessary to constrain the oxide film. At some point when the depth of penetration reaches a critical value, the metal may no longer be able to support the oxide and spalling will ensue.

The interpretation of weight-gain data for zirconium oxidation and corrosion should be re-examined in view of: (*a*) the appreciable dissolution of oxygen in zirconium during oxidation, (*b*) the anisotropy of the oxidation of zirconium grains, and (*c*) the agreement between the orientation dependence of diffusion and oxidation.

Acknowledgments

The author is indebted to Dr. Wayne Lees for valuable discussions on the theory of diffusion. Appreciation is also expressed to Dr. Erwin Parthé of the Massachusetts Institute of Technology for the x-ray diffraction determination of grain orientation in the coarse grain zirconium sample. This work was performed under AEC Contract No. AT(30-1)-1565.

Manuscript received Aug. 14, 1957. This paper was prepared for delivery before the Buffalo Meeting, Oct. 6-10, 1957.

Any discussion of this paper will appear in a Discussion Section to be published in the December 1958 JOURNAL.

REFERENCES

1. J. H. de Boer and J. D. Fast, *Rec. trav. chim.*, **59**, 161 (1940).

2. M. Hansen, D. J. McPherson, and R. F. Domagala, "Phase Diagrams of Zirconium-base Binary Alloys," Report COO-123 (1953).
3. M. W. Mallett, W. M. Albrecht, P. R. Wilson, "The Diffusion of Oxygen in Alpha and Beta Zircaloy-2 and Zircaloy-3 at High Temperatures," Report BMI-1154 (1957).
4. R. D. Misch, *Acta Met.*, **5**, 179 (1957).
5. J. J. Polling and A. Charlesby, *Proc. Phys. Soc.*, **67B**, 201 (1954).
6. J. J. Polling and A. Charlesby, "The Inhibition of Gas-phase Reactions of Zirconium by Anodic Oxide Films," Report AERE M/R-1040 (1953).
7. R. D. Misch, "Electrode Reactions of Zirconium Metal," in "The Metallurgy of Zirconium," p. 663, McGraw-Hill Book Co., New York (1955).
8. J. Paul Pemsler, "The Diffusion of Oxygen in Zirconium and Its Relation to Oxidation and Corrosion," Report NMI-1177 (1957).
9. W. Rostoker, "Phase Diagrams of Zirconium-base Binary Alloys," Report COO-181 (1953).
10. C. Curtis, Oak Ridge National Laboratory, Private communication.
11. C. M. Schwartz, D. A. Vaughan, and G. G. Cocks, "Identification and Growth of Oxide Films on Zirconium in High-Temperature Water," Report BMI-793 (1952).
12. R. D. Misch, *Acta Met.*, **4**, 222 (1956).
13. J. Chirigos and D. S. Thomas, "The Mechanism of Oxidation and Corrosion of Zirconium," Report WAPD 53 (1952).
14. W. K. Boyd, D. J. Maykuth, R. S. Peoples, and R. J. Jaffe, "Compositional Factors Affecting Corrosion Resistance of Zirconium in High-Temperature Water and Steam," Report BMI 1056 (1955).

The Reaction between Iron and Water in the Absence of Oxygen

V. J. Linnenbom

Naval Research Laboratory, Washington, D. C.

ABSTRACT

The reaction between pure iron and oxygen-free water has been investigated at 25°, 60°, and 300°C. At room temperature, the primary product of reaction appears to be $Fe(OH)_2$; no evidence was found to indicate the presence of Fe_3O_4. Formation of Fe_3O_4, however, occurs readily in the iron-water system at both 60° and 300°C. The possibility that this Fe_3O_4 is produced via formation and subsequent decomposition of $Fe(OH)_2$ is discussed; the conclusion is reached that the mechanism of formation of Fe_3O_4 from the reaction of iron and water cannot be decided definitely at this time.

The nature of the product which results when pure iron reacts with water in the absence of oxygen is a matter of fundamental importance in corrosion studies. At elevated temperatures, there is general agreement that the end product is Fe_3O_4. However, conflicting reports have appeared in the literature as to whether this product at room temperature is $Fe(OH)_2$ or Fe_3O_4. A number of investigators (1-3) have employed the reaction of iron with oxygen-free water to measure the solubility of ferrous hydroxide, on the assumption that this compound is the end product of the reaction, and that the *p*H and solubility values obtained are characteristic of a saturated solution of $Fe(OH)_2$. On the other hand, it has also been reported (4-6) that Fe_3O_4 is the end product of the reaction. In this connection, Schikorr (7) also claimed that ferrous hydroxide at room temperature slowly transforms into magnetite, according to what is now known as Schikorr's reaction:

$$3Fe(OH)_2 \rightarrow Fe_3O_4 + H_2 + 2H_2O \qquad (I)$$

The occurrence of such a reaction would appear to confirm the claim that Fe_3O_4 is the end product of the iron-water reaction. However, Evans and Wanklyn (8) and Shipko and Douglas (9) found no evidence that reaction (I) occurs at room temperature unless certain substances are present to catalyze the reaction.

It is the purpose of this communication to report some experimental work carried out here on the iron-water reaction in the absence of oxygen, the results of which indicate that $Fe(OH)_2$ is formed by this reaction at room temperature, and that Fe_3O_4 is formed only at higher temperatures.[1]

Experimental

The samples of iron used in this work came from three different sources. One was a specimen of pure iron foil obtained from the National Bureau of Standards, containing less than 0.01% impurities. The second was an iron powder prepared by the reduction of reagent grade ferric oxide. The third was a commercially available reduced iron powder, also certified to be reagent grade; however, an aqueous suspension of this latter material as received was found to be slightly alkaline, and it was necessary to wash it exhaustively by decantation before use to remove this impurity. In all cases the powder samples just prior to use were reduced in purified hydrogen at 900°C for a period of 24 hr; this produced a sintered mass of reduced iron powder which was bright and silvery in appearance and which tarnished very quickly if exposed to air. The iron foil was alternately oxidized and reduced several times to produce a very reactive surface, the final reduction with purified hydrogen again being

[1] These experiments are reported in more detail in Naval Research Laboratory Report 4824, September 1956.

carried out at 900°C for 24 hr. All water used in the experiments was doubly distilled and stored in quartz containers, the second distillation being made from an alkaline permanganate solution.

The reaction was investigated at three different temperatures, 25°, 60°, and 300°C. At room temperature the reaction was carried out in both Pyrex and quartz containers, since Corey and Finnegan (5) reported different results for these two materials. Each flask was fitted with an internal filter through which samples could be withdrawn at periodic intervals for solubility and *p*H measurements. Before adding the iron, the water was first deoxygenated by bubbling purified hydrogen through the water for a period of 48 hr. The transfer of the freshly reduced iron to the flask containing the oxygen-free water was then carried out in a dry box under an atmosphere of purified helium. During the course of the experiment a stream of hydrogen was passed continuously through the solution; it was allowed to exit through a mercury trap to prevent back diffusion of air into the flask. The mercury trap thus produced a slight positive pressure inside the flask for the entire duration of the experiment.

The experiments at 60°C were carried out in the same apparatus by encasing the flask in a heating jacket and controlling the heat input manually by means of a voltage regulator.

The experiments at 300°C were carried out in a gold-plated nickel autoclave equipped with an internal gold filter element. The doubly distilled water was deoxygenated as described above, the reduced iron sample added under a helium atmosphere, and the autoclave sealed off. During the initial period of heating from room temperature up to 300°C, a vent plug was opened periodically to flush excess helium and hydrogen from the system with the steam being generated inside the autoclave.

Results

At room temperature there was no visible evidence that magnetite was formed. The surface of the reduced iron remained bright and silvery in appearance, even after 42 days contact with water. The solution after only a few hours showed a strong Tyndall effect (absent at the start), indicating the presence of suspended colloidal material. In some of the experiments a definite trace of turbidity developed. After four days' reaction time, samples of solution withdrawn through the filter showed a *p*H of 9.30 and a soluble Fe content of 0.4 ppm. These results agree with those reported by Murata (3) for the same reaction time interval. The *p*H remained constant with time; however, the soluble iron content showed a slow decrease, finally reaching a constant value of 0.08 ppm Fe after approximately 30 days. This may have been due to (*a*) increased filtering efficiency with time due to particle size growth of the colloidal ferrous hydroxide, or (*b*) a change in the nature of the colloidal species due to aging, with a consequent change in solubility. The visible absence of any black magnetite in the system, together with the *p*H and solubility values, indicate that $Fe(OH)_2$ is the species existing in contact with oxygen-free water at 25°C. In one or two cases where some magnetite did form, the reason was traced to leakage of air into the system. This was confirmed by experiments in which, after several days reaction time, the hydrogen flow was stopped and air was deliberately admitted to the flask. The flask was then sealed, and after a sufficient time lapse to allow diffusion of air through the water, the submerged sintered mass of iron powder began to darken. Eventually, an appreciable quantity of loose, black Fe_3O_4 powder was formed. However, when oxygen was carefully excluded, no visible signs of magnetite formation were noticeable at room temperature. There was no significant change in experimental results when quartz reaction flasks were substituted for Pyrex, contrary to the report of Corey and Finnegan (5).

At 60°C the formation of black Fe_3O_4 proceeded fairly rapidly, even in the absence of oxygen. Experiments which had been allowed to proceed at room temperature for several days showed almost immediate formation of the black oxide on the surface of the submerged iron when the temperature was raised to 60°. At this temperature the soluble iron content was found to be approximately 0.008 ppm after 10 days' contact between iron and water.

During the course of the experiments carried out at 300°C visual observations could not be made. However, at the conclusion of all of the experiments the autoclave was always found to contain large quantities of black Fe_3O_4. Solubility values in these high temperature runs showed a definite decrease with time and tended to approach a lower limit of about 0.05 ppm Fe.

Discussion

Thermodynamic data (10) show that both $Fe(OH)_2$ and Fe_3O_4 may be formed spontaneously in the reaction between iron and oxygen-free water at room temperature, and that $Fe(OH)_2$ can further react spontaneously to form Fe_3O_4:

$$Fe+2H_2O \rightarrow Fe(OH)_2+H_2 \quad \Delta F^\circ_{298^\circ K} = -2190 \text{ cal} \quad \text{(II)}$$

$$3Fe+4H_2O \rightarrow Fe_3O_4+4H_2 \quad \Delta F^\circ_{298^\circ K} = -15{,}640 \text{ cal} \quad \text{(III)}$$

$$3Fe(OH)_2 \rightarrow Fe_3O_4+2H_2O+H_2 \quad \Delta F^\circ_{298^\circ K} = -9070 \text{ cal} \quad \text{(I)}$$

However, these data tell us nothing about the relative rates of the reactions, nor of the mechanism by which Fe_3O_4 may be formed. From the experimental work described here it would appear likely that reaction (II) predominates at room temperature. Solubility and *p*H values, as well as visual evidence, indicate that $Fe(OH)_2$ is the solid species in equilibrium with solution at 25°C. The absence of Fe_3O_4 would indicate that reactions (I) and (III), although thermodynamically favored, are too slow to be measurable at room temperature within the time (40 days) of these experiments.

Heat capacity data as a function of temperature (11, 12) allow calculations to be made on the free energy change of reaction (III) at 60° and 300°C. At both temperatures this reaction is still thermodynamically possible; hence, direct formation of

Fe_3O_4 via (III) remains possible. Unfortunately, heat capacity data on $Fe(OH)_2$ necessary to make similar calculations for reactions (I) and (II) at these temperatures are lacking, so that the possibility of Fe_3O_4 formation via prior formation of $Fe(OH)_2$ cannot be eliminated. Such calculations, therefore, offer no significant clues as to the reaction mechanism. In this particular case, further experimentation is needed in order to learn the mechanisms involved.

One further point should be emphasized. This is the extreme sensitivity of reaction (I) to the presence of other materials. Excess hydroxyl ion, for example, markedly inhibits the reaction, even at elevated temperatures (9). On the other hand, Evans and Wanklyn (8) reported the decomposition of precipitated ferrous hydroxide at room temperature in the presence of nickel powder, copper powder, colloidal platinum, platinum chloride, and nickel sulfate; in the absence of these materials, no decomposition occurred. Similarly, Shipko and Douglas (9) found it necessary to co-precipitate nickel hydroxide with the ferrous hydroxide in order to observe decomposition of the latter at room temperature; in the absence of the nickel hydroxide, reaction (I) did not proceed at a measurable rate below 100°C. The formation of Fe_3O_4 at 60°C in this work may therefore have been due to the catalyzing effect of excess iron powder in promoting reaction (I). It is appropriate to mention here a report by Gould and Evans (13) that in the absence of oxygen boiling water reacts with steel to first form $Fe(OH)_2$, which then decomposes to give Fe_3O_4 as the end product. These observations are pertinent to the problem of the corrosion of iron and steel in oxygen-free water. Any impurity or added substance which is effective in promoting reaction (I) might well affect corrosion rates by preventing formation of a possible protective film of ferrous hydroxide.

To summarize, the evidence reported here (solubility, pH, and visual observation) indicates that $Fe(OH)_2$ is the primary product of the reaction between pure iron and oxygen-free water at room temperature. No evidence was found to indicate the presence of Fe_3O_4. The mechanism of the formation of Fe_3O_4 at higher temperatures cannot be definitely decided. Whether magnetite formation is necessarily preceded by the formation of $Fe(OH)_2$, or whether it is formed directly from the water reacting on the iron, is not clear.

Acknowledgment

The writer wishes to acknowledge the assistance of Howard S. Dreyer in performing some of the experimental work described.

Manuscript received Aug. 8, 1957.

Any discussion of this paper will appear in a Discussion Section to be published in the December 1958 JOURNAL.

REFERENCES

1. J. W. Shipley and I. R. McHaffie, *Canadian Chem. Met.*, **8**, 121 (1924).
2. W. G. Whitman, R. P. Russell, and G. H. Davis, *J. Am. Chem. Soc.*, **47**, 70 (1925).
3. K. Murata, *J. Soc. Chem. Ind. Japan*, (Suppl. Binding), **35**, 523 (1932).
4. G. Schikorr, *Z. Elektrochem.*, **35**, 62 (1929).
5. R. C. Corey and T. J. Finnegan, *Proc. Am. Soc. Testing Materials*, **39**, 1242 (1939).
6. M. Thompson, *Trans. Electrochem. Soc.*, **78**, 251 (1940).
7. G. Schikorr, *Z. anorg. u. allgem. Chem.*, **212**, 33 (1933).
8. J. R. Evans and J. N. Wanklyn, *Nature*, **162**, 27 (1948).
9. F. J. Shipko and D. L. Douglas, *J. Phys. Chem.*, **60** 1519 (1956).
10. F. D. Rossini, D. D. Wagman, W. H. Evans, S. Levine, and I. Jaffe, *Nat. Bureau Standards Circ. 500* (1952).
11. K. K. Kelley, "Data on Theoretical Metallurgy, X. High-Temperature Heat-Content, Heat-Capacity, and Entropy Data for Inorganic Compounds," Bureau of Mines Bull. 476 (1949).
12. U.S.A.E.C., "The Reactor Handbook," Vol. 2, Chap. 2, AECD-3646, U.S. Govt. Printing Office (1955).
13. A. J. Gould and U. R. Evans, *J. Iron Steel Inst. London*, **155**, 195 (1947).

Chemical Factors Affecting Stress Corrosion Cracking of 18-8 Stainless Steels

H. H. Uhlig and John Lincoln, Jr.[1]

Corrosion Laboratory, Department of Metallurgy, Massachusetts Institute of Technology, Cambridge, Massachusetts

ABSTRACT

Transgranular stress corrosion cracking of 18-8 Type 304 specimens in boiling 42% $MgCl_2$ does not depend on rate of stressing (<1 sec to 10 min) nor on small variations in degree of plastic deformation. Cold worked specimens fail in shorter times than annealed, sheared specimens. Addition of HCl to $MgCl_2$ decreases cracking time whereas addition of NaOH increases the time. Pre-exposure of unstressed specimens to $MgCl_2$ slightly decreases cracking times of the same specimens subsequently stressed. Cracks occur along sheared edges of unstressed specimens despite stress relief anneal at 375°C for 2 hr.

Cracks propagate along sheared edges of U-bend specimens at 0.5 to 1 cm/hr through that portion of the specimen cross section in tension, the rate being much slower through the remaining cross section. No induction time for cracks to initiate was observed.

Sizeable pits are not necessary for cracking in $MgCl_2$, but appear to be essential in media like NaCl which in absence of pitting is not particularly active in causing cracking. The pitting mechanism produces concentrated low *p*H metal chlorides (e.g., $FeCl_2$) within the pit, which like $MgCl_2$ cause immediate cracking. Oxygen is required for pitting of 18-8 by NaCl solutions as shown by Uhlig and Morrill, and hence also for stress corrosion cracking as observed by Williams and Eckel, but oxygen is not necessary in $MgCl_2$ or $FeCl_2$.

Cracking can be prevented by cathodic protection at a C.D. of 0.03 ma/cm^2 or higher. Anodic C.D. up to 0.01 ma/cm^2 were found to have no effect on cracking tendency, nor did coupling of 18-8 to Pt.

Transgranular cracking of austenitic stainless steels occurs whenever the alloys stressed in tension are exposed simultaneously to a critical chemical environment. Failures of this kind occur with all the common 18-8 stainless steels, including the stabilized (A.I.S.I. Type 321 and 347), molybdenum-containing (Type 316), and low carbon (ELC Type 304) grades, and also the higher nickel grades (Types 309 and 310). The time required for cracking can be a matter of hours under severe conditions, or of years for less severe exposures. Avoidance of failure can be approached by changing the environment, which is discussed herewith, or by certain metallurgical alterations which will be discussed in another paper. Relief of residual stress does not appear to be more than a temporary expedient because cracking occurs eventually at applied stresses, for example in a $MgCl_2$ solution, no greater than 10,000 psi (1), or in water at elevated temperatures at a stress as low as 5,000 psi (2).

Chemical media most apt to cause cracking are those containing chlorides at a *p*H slightly on the acid side of neutral. Hence boiling concentrated magnesium chloride constitutes a severe environment and cracking occurs within a few hours. General corrosion in such media is only slight. In media for which general corrosion is pronounced, cracking may not occur at all.

Although chlorides are the common constituent of a variety of environments which induce cracking, their presence does not seem to be altogether necessary. Transgranular cracking of 18-8 has been observed, for example, in caustic soda solutions at 350°C (660°F) under pressure (1), in acid sulfite cooking liquors (1), in 12% hydrofluoric acid plus 0.2% fluosilicic acid at 80°C (180°F) (3) and in molten NaOH (4) at 370°C (700°F). Furthermore, cracking of 18-8 has been observed in hot water containing very little chloride (5), in steam condensate containing less than 0.5 ppm total solids (6), and in cooling waters containing 25 ppm or more of chloride (7). Williams and Eckel (2) report that oxygen is necessary for cracking of 18-8 in hot water or in steam containing small quantities of chloride. They also report an instance of cracking in a severely cold worked 18-8 exposed to hot pure water.[2] Many additional examples are cited in the literature.

[1] Present address: Esso Standard Oil Company, Everett, Massachusetts.

[2] There is a possibility that the mechanism of transgranular cracking in chloride-free environments occurring with 18-8 that is severely cold worked, and hence has been transformed in part from austenite to ferrite, differs from that occurring with totally austenitic alloys in chloride solutions. The mechanism, for example, may be related to cracking of ferritic and martensitic stainless steels in chloride-free environments by a mechanism that appears to require interstitial hydrogen rather than electrochemical reaction at the apex of a growing crack. This particular matter requires further study.

The object of the present investigation was to outline chemical factors affecting time of cracking of 18-8 stainless steel in a boiling 42% magnesium chloride test solution, and to correlate these effects with a plausible mechanism of cracking.

Test Apparatus

Spring-loaded, U-bend, Type 304 stainless steel specimens stressed beyond the elastic limit were used for all the tests. The test solution was boiling 42% $MgCl_2$ at 154°C, as suggested by Scheil (8), in which complete failure by cracking occurred in about 4 hr.[3]

Our choice of test specimens stressed beyond rather than below the elastic limit was based on the observation by several investigators and by our own work that specimens so stressed are more susceptible to cracking, they fail in a shorter time, and reproducibility from one run to another is reasonably good. Furthermore, any steps which can be taken to avoid stress corrosion cracking are more significant if they succeed with specimens stressed sufficiently to cause plastic deformation.[4]

The test apparatus was constructed of 5/16-in. square 18-8 stainless steel stock to which was attached a sliding arm of ⅛ x ⅜ in. 18-8 stainless steel strip, both stress relieved. The test specimen was held under stress by a strong compression spring and an adjustable screw located at the top of the holder. Two notched porcelain blocks insulated the specimen itself from the sliding arm. An adjustable screw attached to the sliding arm operated a normal-open microswitch which, in turn, stopped an electric time recorder when the specimen failed.

Two types of test cells were constructed from 2-liter, wide-mouth Erlenmeyer Pyrex flasks which were fitted at the neck with 71/60 ground glass outer joints. Condensers of ⅞-in. I.D. were fitted with 71/60 ground glass inner joints to permit easy removal from the cells.

The first type of test cell was adapted to the study of weight loss and cracking of stressed specimens (Fig. 1); the other was adapted to the study of cracking when specimens were anodically or cathodically polarized. Heat was supplied to both types of cells by electric hot plates.

The polarization cell contained platinum foil electrodes in the side arms separated from the center portion by means of sintered glass disks. For electrical contact with the test specimen, a piece of platinum wire, 0.016 in. in diameter, was spot welded to the upper surface of the stressed specimen and then led up through the condenser. In order to minimize current flow through electrolyte to the wire, the latter was almost totally encased in sections of 2 mm Pyrex glass tubing. The lower portion of the test apparatus (that part immersed in the solution), although insulated from the specimen, was tightly wrapped with thin Teflon ribbon in order to avoid any slight current leakage both onto and off the metal components.

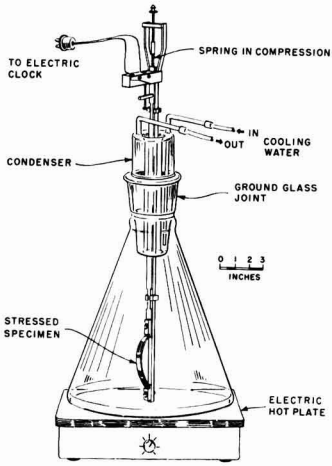

Fig. 1. Apparatus for study of stress corrosion cracking

The test solutions were prepared by using reagent grade $MgCl_2 \cdot 6\,H_2O$ crystals which were melted and dissolved in their own water of crystallization. Just enough distilled water was added to lower the boiling point of the solution to 154°C. Although very little evaporation loss was encountered, more distilled water was added daily, if necessary, so as to maintain this boiling point.

Since the $MgCl_2$ solutions gradually became contaminated with corrosion products, the solutions could be used for only a limited time. The main contaminant was probably ferric ion which is known to accelerate stress corrosion cracking of stainless steels in $MgCl_2$ (9). In general, it was found possible to use a single solution for 30-40 hr of actual test, during which time the solutions acquired a yellowish or orange color.

Different batches of fresh analytical grade $MgCl_2 \cdot 6\,H_2O$, particularly from different suppliers, were in themselves found to vary in performance. This necessitated correcting the results to take care of the variations. Corrections were made by running 5 or 6 specimens in a given new batch of salt, and determining the average time for cracking compared with the average time for many batches of salt (4.0 ± 1 hr). Data of Fig. 3 and 5, for example, were corrected in this manner. Maximum corrections amounted to 1.5 hr, and average corrections for Fig. 3 were 1.3 hr and for Fig. 5 were 1.2 hr.

Specimen Preparation and Stressing

The 18-8 stainless steel, Type 304, was supplied by courtesy of the Carnegie-Illinois Steel Corporation, who also provided the following analysis: 18.42% Cr, 8.63% Ni, 1.16% Mn, 0.08% C, 0.024% P, 0.018% S, 0.30% Si, balance Fe. The rolled 1/16-in. thick sheet, as received, was sheared into specimens measuring 5 in. long and ⅜-in. wide. Each specimen was stenciled at the extreme end with an identifying number.

[3] Other boiling solutions were tried, e.g., [1] ethylene glycol containing 2.5% to 12% $MgCl_2$ or [2] ethylene glycol, 0.1*N* in HCl, [3] 65% aqueous $CaCl_2$, [4] ditto with 2 ml/l concentrated HCl, [5] glycerine, 0.7*M* in NH_4Cl, [6] 9*M* aqueous NH_4Cl. However, of all these, only $CaCl_2$ produced cracking in 6.0 hr for solution [3] and in 4.0 hr for solution [4].

[4] Since surface stresses alone determine susceptibility to initiation of stress corrosion cracking, and these cannot be measured easily, a specimen stressed beyond the elastic limit defines surface stresses in general more satisfactorily than is the case for a totally annealed specimen. This probably explains the authors' observation that reproducibility is better for plastically deformed specimens.

Specimens were cleaned by first removing any edge burrs with a metal file. They were then degreased in boiling benzene for 3-5 min, after which they were ready for heat treatment or pickling.

The majority of the specimens were used either in the as-sheared condition, or they were stress relieved at 375°C for approximately 2 hr, followed by air cooling. Some specimens were heat treated by annealing for 20-30 min at 1050°C, followed immediately by water quenching. A helium atmosphere was used during the annealing to prevent excessive surface oxidation.

Specimens after heat treatment were pickled in a 15 vol % HNO_3-5 vol % HF, based on the commercial acid concentrations, at a temperature of 90°C. To achieve optimum surface reproducibility, specimens were pickled individually for exactly 5 min in Pyrex test tubes immersed in a water bath at 90°C after which they were brushed under tap water to remove any loose scale. This was followed by rinsing in acetone, then in benzene, and drying in warm air.

The 5-in. test specimens were stressed beyond the yield point by bending in a vise until the ends of the specimen just fitted into a notched stainless steel holder which allowed a span of 4⅛ in. The specimen was then transferred to the test apparatus by sliding the two ends into the porcelain holding blocks and the sliding arm tightened until the notched holder was just released. The specimen was finally centered and adjusted to a span of exactly 4 in.

In all of the bending operations, extreme care was taken not to allow any spring-back. Once the specimens were loaded in the test apparatus, they were immediately immersed in the test solution.

Results

Corrosion rate determinations in 42% $MgCl_2$.—The weight losses of both stressed and unstressed 18-8 test specimens, previously stress relieved, then pickled and weighed, and immersed into the boiling 42% $MgCl_2$, were determined as a function of time. Upon removal from the test solution, the specimens were brushed under tap water, rinsed in acetone, next in benzene, dried in air, and again weighed. Fresh $MgCl_2$ solutions were used in all these tests.

Results are given in Fig. 2 showing corrosion rates in mg/dm²/day (mdd) as a function of hours of exposure to $MgCl_2$, each point representing an average of 2-3 specimens. For unstressed specimens, a high initial corrosion rate falls off to a lower relatively steady state after about 4 hr. The same trend takes place for stressed specimens except that weight loss is somewhat higher and failure occurs before steady-state conditions are achieved. A few similar measurements by D. Triadis of this laboratory on specimens previously annealed at 1050°C and water quenched also showed a high initial rate followed by a lower final rate after about 4 hr exposure.

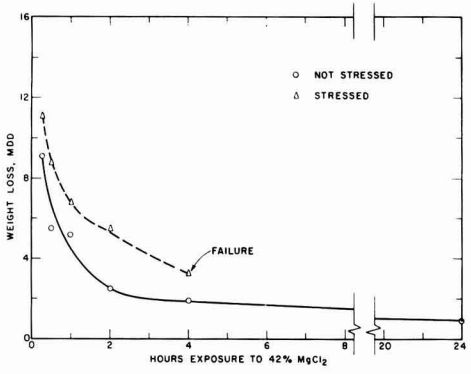

Fig. 2. Weight loss of 18-8 specimens in 42% $MgCl_2$ at 154°C (spec. previously stress relieved).

Rate of stressing on cracking time.—In order to determine effect of rate of stressing, 18-8 test specimens, stress relieved as usual after shearing, were bent to a 4-in. span in times of 10 sec, 5 min, and 10 min, and then immediately tested in $MgCl_2$. Results are summarized in Table I, showing no effect.

Additional but smaller size specimens bent at higher velocity by impact of falling weights held in a specially constructed jig also cracked within times normal for slowly deformed specimens.

Degree of bending and cold work on cracking time.—Stress-relieved specimens were bent to spans ranging from 3½ to 4⅞ in. In all cases the applied stress was above the yield strength (approx. 30,000 psi). Data of Table II show no trend, and, hence, small variations in stresses beyond the yield strength are not important. The higher average time to cracking in Table II (4.8 hr) reflects behavior of the particular batch of $MgCl_2$ employed, but this value, too, falls within the experimental variation of all tests.

Severe cold work is another story. Several as-sheared specimens were cold rolled to an average cross-sectional reduction of 30%. These specimens were then cut to a 5-in. length, pickled, bent to the usual 4-in. span, and tested in boiling 42% $MgCl_2$. The observed average time to failure for six such specimens was 1.0 ± 0.2 hr, which is significantly

Table I. Time to failure of 18-8 specimens for various rates of stressing

Rate of stressing (Time to bend specimen to 4-in. span)	No. of specimens	Time to failure (hr)	Av
10 sec	3	4.6, 4.3, 3.7	4.2
5 min	2	3.9, 4.2	4.1
10 min	2	3.6, 4.1	3.9

Table II. Time to failure of 18-8 specimens for various degrees of bending

Span of stressed specimens (in.)	No. of specimens	Time of failure (hr)	Av
3½	2	4.9, 4.8	4.9
4	3	5.8, 3.5, 4.0	4.4
4¼	2	4.6, 5.6	5.1
4½	2	6.4, 4.5	5.5
4⅝	2	4.1, 4.0	4.1
4¾	2	4.3, 5.4	4.9
4⅞	2	4.8, 4.7	4.8

less than the usual 4 hr. The decrease of cracking time, probably caused by high residual stresses or microstructural changes, is in accord with similar experiments on mild steel by Parkins (10) and on 18-8 by Franks, Binder, and Brown (11) or by Hoar and Hines (12).

Effect of adding acid or base to 42% $MgCl_2$.— Since values of pH could not be measured at the boiling temperature of 42% $MgCl_2$ test solution (154°C), known amounts of HCl and NaOH solutions were added to the $MgCl_2$ test solution without reference to measured hydrogen ion activity. A 10*N* HCl solution was added before rather than after bringing the solutions up to temperature in order to minimize volatilization of the HCl on mixing with hot $MgCl_2$. General corrosion of the stressed 18-8 test specimens became significant at 8 ml 10*N* HCl/liter, and, hence, no quantitative tests were carried out for additions of acid beyond this amount. Additions of alkali were limited to 2 ml 5*N* NaOH/liter, since it was found that further additions caused precipitation of $Mg(OH)_2$.

The plot of Fig. 3 shows time to failure vs. ml/liter of added acid or base. Additions of acid decreased the cracking time to a minimum of about ½ the normal time, whereas additions of alkali increased the time slightly. These results proved that shorter times for cracking in used test solutions did not result from decrease in acidity caused by reaction of the metal with $MgCl_2$ solution. Instead the effect is undoubtedly caused by ferric chloride accumulation (9) through corrosion of specimens and test apparatus.

Effect of anodic and cathodic polarization.—The range of anodic current densities employed was from 0.0001 to 0.01 ma/cm² based on the measured total surface area of the test specimens (28.5 cm²). The cathodic current densities ranged from 0.0017 to 0.04 ma/cm². It was necessary to start each test in freshly prepared $MgCl_2$ solution in order to obtain consistent results. Gradually accumulating impurities, e.g., ferric ion from corrosion products, potentially caused a lowering of the effective current density by continuous reduction at the cathode and oxidation at the anode. Current through the cell

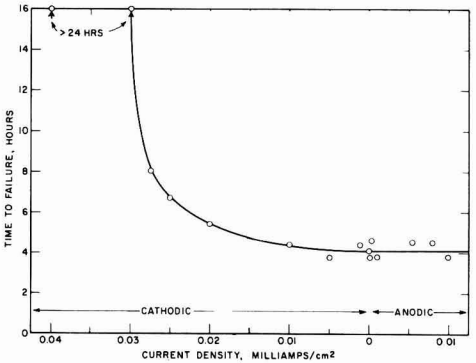

Fig. 4. Effect of anodic and cathodic polarization on time to failure of 18-8 specimens in 42% $MgCl_2$ at 154°C (spec. previously stress relieved).

varied 5% or less, which in view of the large average deviation in the time to failure (approximately ±1.0 hr) was inconsequential. A plot is provided in Fig. 4 for time to failure vs. applied current density. All points for anodic polarization are values averaged for 2-4 specimens at each current density, and similarly for 2-5 specimens for cathodic polarization, with the exception that only single runs are reported for cathodic values of 0.0017 and 0.02 ma/cm².

No cracking occurred within the maximum time of the test (24 hr) for cathodic current densities above 0.03 ma/cm². On the other hand, anodic current densities of small magnitude up to 0.01 ma/cm² had no measurable effect on cracking time. In line with the anodic polarization results, 4 separate experiments in which platinum (4 cm²) was coupled to 18-8 specimens showed normal average cracking time.

Effect of pre-exposure to 42% $MgCl_2$.—It was desirable to know whether pre-exposure of unstressed specimens to 42% $MgCl_2$ would aid in the initiation of cracks, or produce surface areas susceptible to crack formation. An effect of this kind was reported by Hoar and Hines (13). Unstressed 18-8 test specimens, previously stress relieved, with surface prepared as usual, were pre-exposed to 42% $MgCl_2$ for

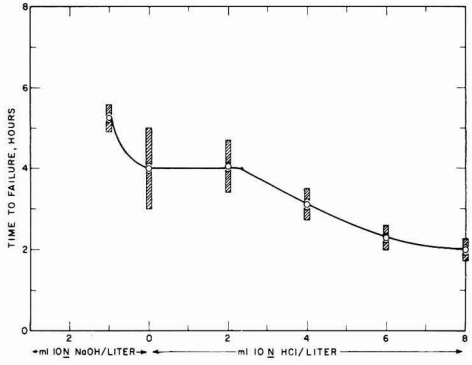

Fig. 3. Effect of acid and alkali additions to 42% $MgCl_2$ at 154°C on time to failure of stressed 18-8 specimens (spec. previously stress relieved). Spread of each point is standard deviation.

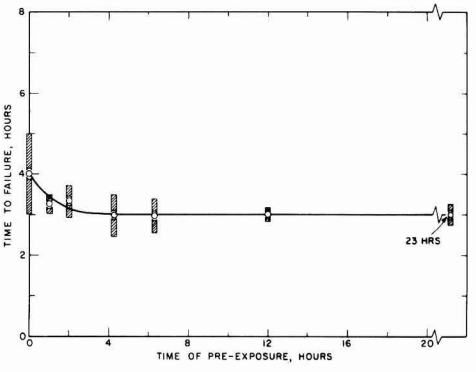

Fig. 5. Effect of pre-exposure of 18-8 specimens in unstressed condition on time to failure when stressed in 42% $MgCl_2$ at 154°C (spec. previously stress relieved). Spread of each point is standard deviation.

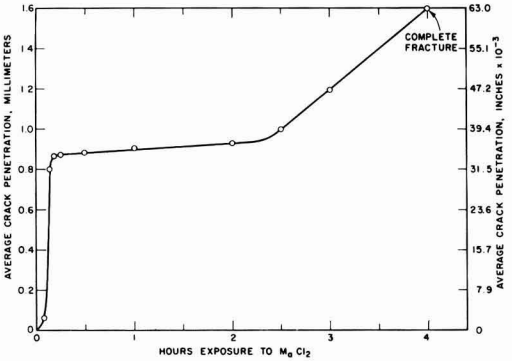

Fig. 6. Average visible rate of crack propagation for stressed 18-8 specimens in 42% $MgCl_2$. Total specimen thickness approx. 1.6 mm (spec. previously stress relieved).

various times, then immediately immersed in a beaker of distilled water. While still wet they were stressed, loaded into the test apparatus, and quickly placed in the $MgCl_2$ test solution. Times of pre-exposure varied from 0.5 to 24 hr, the corresponding cracking times being plotted in Fig. 5. The effect is one of slight decrease in the time for cracking after pre-exposure for 3 or more hours, with no further effect for longer times.

Rate of crack propagation.—In order to obtain data on the rate with which cracks propagate through stressed 18-8 test specimens, a metallographic inspection and photomicrographic study were made. Stressed specimens were immersed in the test solution for periods ranging from 5 min to 4 hr. Upon removal they were cleaned under tap water, mounted in Bakelite, polished, and etched. The average depth of cracks was measured from photomicrographs of known magnification and plotted vs. time of exposure to $MgCl_2$ in Fig. 6.

Crack propagation at the edges was very rapid (0.5-1 cm/hr) [5] through ½ the specimen thickness, corresponding to the tension side. Cracks stopped momentarily when they reached the midsection, corresponding to the compression side of the U-bend specimen. At this stage, thin cracks in the form of tortuous channels through the metal grew wider, eventually merging to produce one or more major cracks. Consolidation of thin cracks both at and away from the edges required about 2-2½ hr, whereupon one or more major cracks proceeded through the entire specimen cross section within another 1½ hr. This behavior clearly demonstrated that the alloy must be stressed in tension and not in compression in order to favor stress corrosion cracking.

No induction time for cracks to start was found. Tiny transgranular edge cracks were observed after the shortest time of exposure (5 min) to $MgCl_2$, still allowing time for thermal equilibrium. These cracks grew much deeper within a matter of additional minutes. The initial cracks began usually at the sheared edges, despite stress relief heat treatment, growing rapidly normal to the surface, and more slowly laterally from both edges toward the center of the convex surface. Hoar and Hines (13) found an induction time for initiation of cracks in 18-8 wire stressed below the elastic limit, except when they added HCl to the $MgCl_2$ solution, whereupon they stated that the induction time disappeared. No acid was added in our experiments.

The accompanying photomicrographs (Fig. 7 through 11) show the typical appearance of sheared edges of bent specimens after various times of exposure to $MgCl_2$.

Discussion

Corrosion Rates

The slightly higher weight losses of stressed specimens compared with unstressed specimens (Fig. 2) is probably accounted for by growing cracks on the convex surface of the stressed specimens, which do not develop in absence of stress. The higher cor-

Fig. 7. Sheared edge of bent, stress-relieved specimen after 8-min exposure to 42% $MgCl_2$. Electrolytic etch, 50X.

Fig. 8. Sheared edge of bent, stress-relieved specimen after 10-min exposure to 42% $MgCl_2$. Electrolytic etch, 50X.

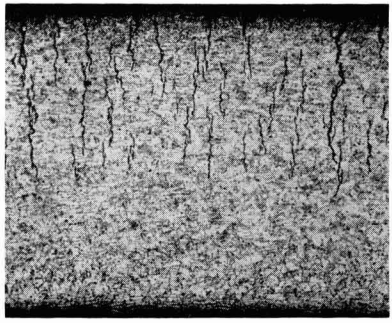

Fig. 9. Sheared edge of bent, stress-relieved specimen after 30-min exposure to 42% $MgCl_2$. Electrolytic etch, 50X.

[5] Hoar and Hines found 0.1-0.4 cm/hr (14).

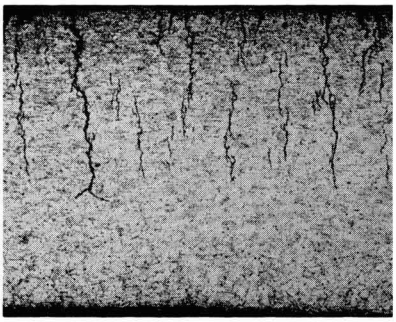

Fig. 10. Sheared edge of bent, stress-relieved specimen after 2-hr exposure to 42% $MgCl_2$. Electrolytic etch, 50X.

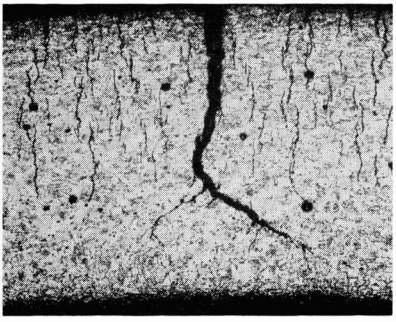

Fig. 11. Sheared edge of bent, stress-relieved specimen which failed at 3.8-hr exposure to 42% $MgCl_2$. Electrolytic etch, 50X.

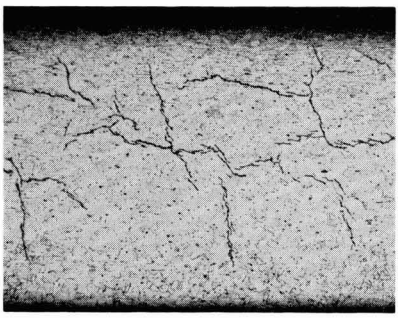

Fig. 12. Sheared edge of unbent, stress-relieved specimen exposed to 42% $MgCl_2$ for 2 hr. Electrolytic etch, 50X.

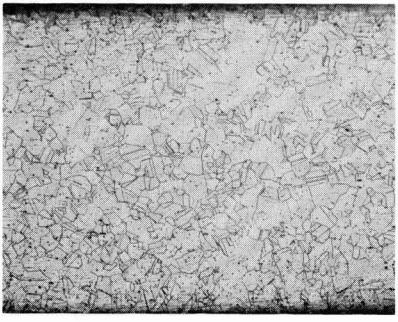

Fig. 13. Sheared edge of unbent specimen, annealed 1050°C, W.Q., exposed to 42% $MgCl_2$ for 2 hr. Electrolytic etch, 50X.

rosion rates can be explained both by formation of additional alloy surface opened up by cracks and by electrochemical action causing metal to dissolve at the apexes of opening fissures.

A high initial compared to a final constant corrosion rate, for both stressed and unstressed specimens, can be explained in part by cracks that develop rapidly at sheared edges despite stress relief heat treatment (Fig. 12), and which stop growing after tension stresses are relieved by crack formation. Such cracks indicate that heat treatment at 375°C for 2 hr is not effective in reducing residual stress to a level that precludes stress corrosion cracking.

It is also likely that oxygen dissolved in the test solution causes a high initial rate, diminishing to a final steady state as the oxygen is consumed or boiled off. A third factor is the preferential corrosion of those specific crystal faces of polycrystalline test specimens exhibiting highest corrosion rates. Examination of test specimens under the microscope confirmed that crystal facets were well developed after exposure to $MgCl_2$, these representing presumably residual crystal faces that corrode least. The effect of both dissolved oxygen and crystal orientation explains why annealed and water-quenched specimens, whose edges are not crack sensitive (Fig. 13), also show a higher initial corrosion rate.

Effect of Pre-exposure

It is plausible that cracking of sheared edges during pre-exposure, despite stress relief treatment, caused part of the observed effect of pre-exposure on cracking times. Since specimens annealed at 1050°C and water-quenched, similarly pre-exposed, showed no surface cracks at either edge, pre-exposure of specimens free of residual or applied stresses would presumably have less effect on cracking times of such specimens subsequently bent. Lack of reproducibility for annealed-quenched specimens has delayed an experimental check of this conclusion and the matter is now under further study. Absence of an effect of pre-exposure on cracking times of mild steel in nitrates has been reported by Parkins (10). The effect found by Hoar and Hines for 18-8 wires pre-exposed to $MgCl_2$ may perhaps have been the result, as in our tests, of residual surface stresses causing superficial cracks.

Relation of Pits to Cracks

There is no evidence that deep pitting must precede initiation of a crack when $MgCl_2$ is the test medium. Photomicrographs, such as those of Fig. 7, indicate that, within a time of exposure as short as 8 min, surface cracks form without evidence of surface cavities having dimensions greater than the cracks themselves.

However, there is good reason for believing that in waters containing neutral chlorides, e.g., NaCl, pit formation may always precede stress corrosion cracking.[6] The evidence for this comes from various in-

[6] Leu and Helle (15) demonstrate that small elongated pits of microscopic dimensions form on slip bands of stressed 18-8, and these act as nuclei for subsequent cracks. Locallized attack of this kind probably always precedes stress corrosion cracking of 18-8. The pits discussed above are orders of magnitude larger than the dimensions of slip bands, and occur only under specific conditions.

stances of service failures where cracks are associated with pits, for example, at welded areas where natural crevices occur, or beneath inorganic scale formations, or at other types of crevices favorable to the initial action of oxygen-concentration cells. As was shown in an earlier paper on mechanism of pitting in stainless steels (16), interior surfaces of pits are the anodes of passive-active galvanic cells, with dissolution of anodic metal serving to fill such pits with concentrated low *p*H metal chlorides, in particular ferrous chloride. Concentrated ferrous chloride is one of the active chemical media causing stress corrosion cracking, behaving in this respect like magnesium chloride. For example, two stressed commercial 18-8 specimens exposed to boiling (114°C) concentrated ferrous chloride solution in a N_2 atmosphere were found to crack transgranularly within an average of 7.4 ± 0.5 hr. (A similar specimen exposed to boiling concentrated NaCl did not pit nor crack within the maximum test period of 250 hr.)

Pits, therefore, act as reservoirs for concentrated metal chlorides, the latter in turn being directly active in causing stress corrosion cracking. With magnesium chloride, the necessary crack-inducing medium is already at hand, hence pitting is not necessary, and cracks in plastically deformed metal initiate as rapidly as the metal comes into contact with the test solution.

Dissolved oxygen is necessary for pitting to occur in NaCl (17) because the cathodic reaction occurring on the large exterior surface of alloy surrounding the pit requires presence of a depolarizer. It is significant in this regard that Williams and Eckel (2) report dissolved oxygen is also necessary for stress corrosion cracking of 18-8 in NaCl solutions at elevated temperatures, from which one can conclude that since boiling concentrated NaCl did not cause cracking, pitting always precedes cracking in this medium. Following the reasoning above, dissolved oxygen should not be necessary for cracking in $MgCl_2$ or $FeCl_2$ solution. This is confirmed for $FeCl_2$ by the previously cited experiment and for $MgCl_2$ by an experiment in which two sheared Type 304 small size test specimens were exposed to 42% $MgCl_2$ test solution, the latter being thoroughly deaerated with purified nitrogen before and during the test, and observing cracking within 3.2 ± 0.6 hr.

Effect of pH and Depolarizers

Decrease of cracking time by additions of acid may conceivably have a complex cause associated with supposed films on the metal surface, but it also seems reasonable that the effect may be no more than to increase electrical conductivity of $MgCl_2$ through additional hydrogen ions. The acid also increases the operating emf of metal electrode-hydrogen electrode cells, presumably responsible for crack propagation, to the extent of 42 mv (154°C) for every unit *p*H change. Ferric salts, on the same basis, decrease cracking time because they are active depolarizers serving to accelerate the cathode reaction. Any similar depolarizer is expected to behave in the same way. Continuous bubbling of oxygen through the $MgCl_2$ test solution, for example, was found to decrease cracking time about 40%.

Effect of Anodic and Cathodic Polarization

The minimum cathodic current density of 0.03 ma/cm² found to protect against cracking for at least 24-hr exposure is in good agreement with values reported by Hoar and Hines (14) of 0.03 ma/cm² for protection extending to 50 hr, and of 0.05 ma/cm² for protection up to at least 250 hr and probably for an indefinite period. Results of longer test periods during which cathodic protection is applied probably mean very little because of the accompanying change in test-solution composition, particularly increase of *p*H, brought about by cathodic reaction products.

The initial over-all corrosion rate for stressed specimens is about 12 mdd (Fig. 2), corresponding to a current density of 0.005 ma/cm². From electrochemical theory, the applied current density for complete cathodic protection must always be greater than the equivalent current density corresponding to the corrosion rate in a given environment, other things being equal. The present data are in line with this conclusion. Correspondingly, in a less active medium than $MgCl_2$, the required current density for protection would be less than the values cited above.

The appreciable difference in the current density for protection and that corresponding to the corrosion rate indicate that the anodic areas of electrolytic cells responsible for cracking are appreciably polarized by the prevailing small corrosion currents (Fig. 14), assuming that cathodic polarization follows a Tafel relation. For a concentrated chloride solution such as $MgCl_2$ in which anodic passivation does not occur, and for which anodic polarization per unit area, therefore, is not pronounced, this means that the effective anodic areas must be very small. Small anodic areas correspond, logically, to the relatively limited anodic areas of metal corroding at the apexes of incipient growing cracks.

Anodic polarization of specimens presumably should affect cracking time only if applied positive current leaving the metal surface is focussed mostly

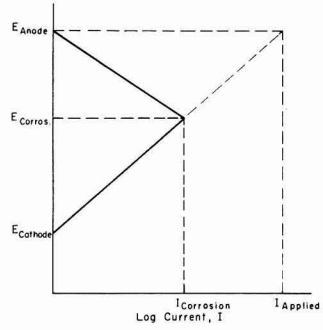

Fig. 14. Schematic polarization diagram for cell accounting for stress corrosion cracking. Applied current for cathodic protection is considerably larger than the corrosion current because of pronounced polarization of small area anode.

at nuclei for cracks.[7] This condition might obtain if supposed surface films largely exclude current from all parts of the surface except at specific defects in the film. Since an effect of anodic polarization is not found, it must be concluded that distribution of current in this manner does not occur. Lack of an effect by anodic currents does not support Edeleanu's (9) statement that coupling of platinum to stainless steel accelerates cracking, and that of Hoar and Hines (14) to the effect that anodic polarization increases rate of crack propagation. Reasons for the difference in results are not apparent.

Acknowledgment

The authors are pleased to acknowledge assistance of Louis Bogar in carrying out several supplementary experiments.

This research was supported by the United States Air Force through the Air Force Office of Scientific Research of the Air Research and Development Command, under contract No. AF 18(600)-1221. Reproduction in whole or in part is permitted for any purpose of the United States Government.

Manuscript received July 15, 1957. This paper was prepared for delivery before the Buffalo Meeting, Oct. 6-10, 1957.

Any discussion of this paper will appear in a Discussion Section to be published in the December 1958 JOURNAL.

[7] A decrease of cracking time can result indirectly from contamination of $MgCl_2$ by accumulation of anodic dissolution products.

REFERENCES

1. M. A. Scheil in "Corrosion Handbook," H. H. Uhlig, Editor, p. 174, John Wiley & Sons, Inc., New York (1948).
2. W. Williams and J. Eckel, *J. Am. Soc. Naval Engrs.*, **68**, 93 (February 1956).
3. H. Copson, *Welding J.*, Supplement, p. 3 (February 1953).
4. J. Heger, *Metal Prog.*, **69**, 109 (1955).
5. R. A. Lincoln, American Iron and Steel Inst., N.Y.C., May 26, 1954.
6. F. W. Davis, *Trans. Am. Soc. Metals*, **42**, 1233 (1950).
7. W. Rion, Jr., *Ind. Eng. Chem.*, **49**, 73A (1957).
8. M. Scheil, "Symposium on Stress Corrosion Cracking of Metals," ASTM and AIME, pp. 395-410, Philadelphia (1945).
9. C. Edeleanu, *J. Iron Steel Inst.*, **173**, 140 (1953).
10. R. N. Parkins in "Stress Corrosion Cracking and Embrittlement," p. 146-7, W. D. Robertson, Editor, John Wiley & Sons, Inc., New York (1956).
11. R. Franks, W. Binder, and C. Brown, Ref. 8, p. 411.
12. T. Hoar and J. Hines, *J. Iron Steel Inst.*, **184**, 166 (1956).
13. T. Hoar and J. Hines, *ibid.*, **182**, 124 (1956).
14. T. Hoar and J. Hines, Ref. 10, p. 107.
15. K. Leu and J. Helle, "On the Mech. of Stress Corros. of Austenitic Stainless Steels in Hot Aqueous Chloride Solutions". Koninklijke/Shell Lab., Amsterdam. Presented at Nat. Assoc. Corros. Engrs., St. Louis, Mar. 1957.
16. H. H. Uhlig, *Trans. Am. Inst. Mining Met. Engrs.*, **140**, 411 (1940).
17. H. H. Uhlig and M. Morrill, *Ind. Eng. Chem.*, **33**, 875 (1941).

A Study of the Effect of Chloride Ion on Films Formed on Iron in Sodium Nitrite Solutions

G. W. Mellors,[1] M. Cohen, and A. F. Beck[2]

Division of Applied Chemistry, National Research Council, Ottawa, Canada

ABSTRACT

The effect of chloride ion on the potential of iron in sodium nitrite solutions has been measured. This has been related to the surface composition and topography by the techniques of electron diffraction and electron microscopy. The effect of initial surface preparation has also been investigated.

It is shown that in the absence of chloride ion the potential is noble and steady and that the surface remains practically unchanged. A film of γ-Fe_2O_3 is shown to be present by electron diffraction. When chloride ion is added to the system the potential becomes unsteady and less noble. Inclusions of a second phase grow in the oxide layer. This is shown to be γ-$Fe_2O_3 \cdot H_2O$ or lepidocrocite. The lower and unsteady potential is probably due to the decrease in resistance of the anodic areas, which correspond to the inclusions in the oxide layer.

The present research was initiated to confirm the nature of the oxide film formed on iron by sodium nitrite solutions (1) and to investigate more fully the effect of chloride ions on these films. It has been shown in previous work by electron diffraction that the films formed in sodium nitrite solutions are composed of γ-Fe_2O_3 with a small amount of γ-$Fe_2O_3 \cdot H_2O$ (lepidocrocite). The films were examined *in situ* by reflection, and transmission patterns were obtained from films stripped from the metal by the method of Vernon, Wormwell, and Nurse (2).

Although electron diffraction results have been published for films stripped from iron passivated in potassium chromate solutions (3-5) and in concentrated nitric acid (4), the above work (1) constitutes the only reflection diffraction results on films formed in sodium nitrite solutions.

It was thought desirable to employ the reflection method, despite the poorer quality of the patterns

[1] Present address: National Carbon Research Laboratories, Cleveland, Ohio.

[2] Olin Mathieson Chemical Corporation, New Haven, Conn.

obtained, since reorientation and recrystallization of the film substance may occur during the process of stripping specimens for transmission work. It is also possible that inclusions in the oxide film will be removed during the process of stripping.

Potential measurements were made of iron exposed to a range of concentrations of sodium nitrite solutions containing various amounts of chloride ions. Parallel electron diffraction examinations of the surface to identify the surface composition and electron microscope pictures to determine the surface topography were made. Specimens were also passivated in de-aerated solutions in order to determine the effect of dissolved oxygen. The effect of various surface preparations on both the electrode potential and film formation was also measured.

Experimental and Results

The "Armco" iron was in the form of annealed sheet, 1.5 mm thick and had the following analysis:—C-0.012, Mn-0.015, P-0.005, S-0.025, Si-trace.

Sodium nitrite, potassium chloride, and all other chemicals used were of C. P. quality. The silver wire used in the preparation of the silver-silver chloride electrodes was of 99.999% purity. The electrodes were formed by anodizing in a dilute HCl solution.

Potential Measurements

The specimens for potential measurements were 5 cm x 1.5 cm of which 1.5 cm x 1.5 cm was exposed to the solution. The remainder was insulated with "Apiezon" W wax. All specimens were first ground flat and then polished through 4/0 emery paper. Some of these specimens were exposed for potential measurements in this condition, while others were first exposed to dry air for 24 hr or etched with *N* HCl for 1 min.

Potential measurements were made using a reference electrode of a chloridized silver wire connected to the inhibitor solution through a salt bridge. No correction was made for junction potentials. All runs were made in the presence of air. All potentials are on the saturated Ag-AgCl scale.

The effect of surface pretreatment on the potential of iron in *N*/10 sodium nitrite is shown in Fig. 1. It can be seen that the etched specimen has a much lower potential than the unetched specimens, although all are passive.

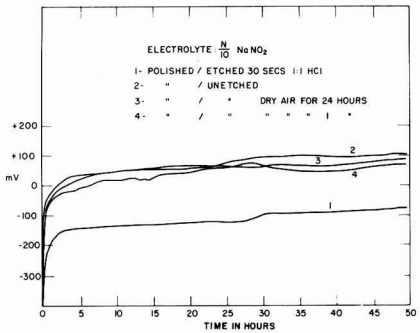

Fig. 1. Effect of pretreatment on potential of iron in N/10 $NaNO_2$ solutions.

Potentials of iron in various concentrations of nitrite solution with or without additions of chloride are shown in Fig. 2-7. Figure 8 shows the effect of small additions of "Versene" (ethylene-diamine-tetra-acetic acid) a strong complexing agent for cations, on the potentials of etched and unetched specimens in *N*/10 air-exposed solutions of sodium nitrite. In other experiments with etched iron it was noted that the time required for passivity to be attained increased with increasing Versene concentration.

The following general observations can be made:

1. In pure sodium nitrite solutions the unetched specimens attain a more positive potential than the etched specimens.

2. Differences in potential due to differing surface preparation decrease with decreasing inhibitor concentration and/or the addition of chloride.

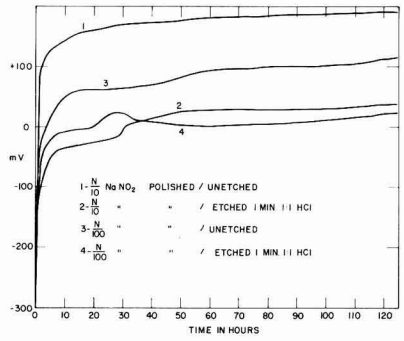

Fig. 2. Effect of concentration and etching on potential

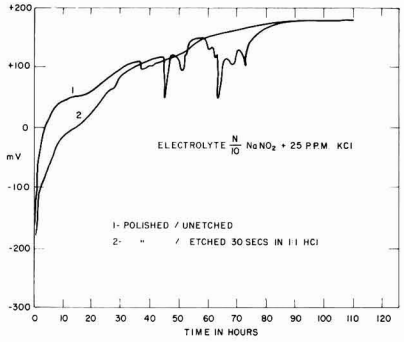

Fig. 3. Potential of iron in N/10 $NaNO_2$ + 25 ppm KCl

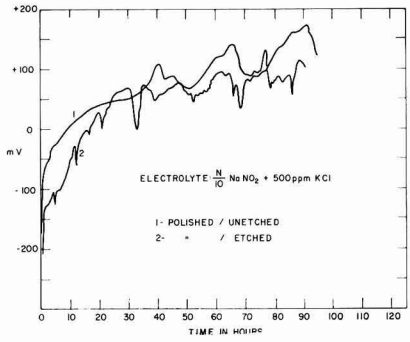

Fig. 4. Potential of iron in N/10 $NaNO_2$ + 500 ppm KCl

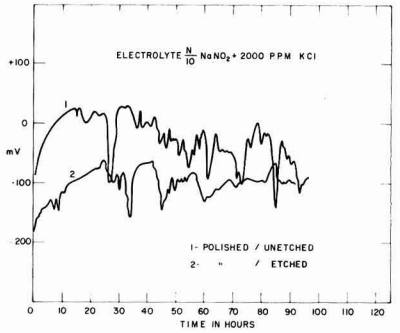

Fig. 5. Potential of iron in N/10 $NaNO_2$ + 2,000 ppm KCl

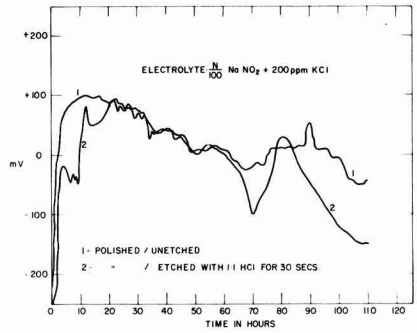

Fig. 7. Potential of iron in N/100 $NaNO_2$ + 200 ppm KCl

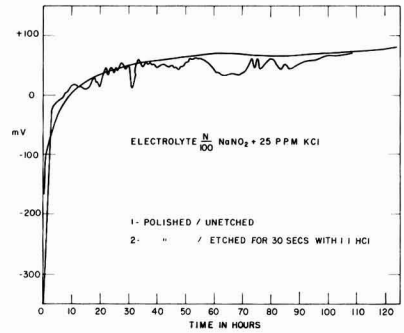

Fig. 6. Potential of iron in N/100 $NaNO_2$ + 25 ppm KCl

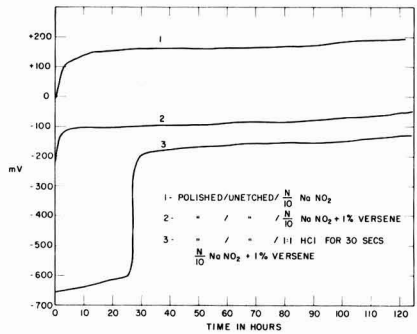

Fig. 8. Potential of iron in N/10 $NaNO_2$ + 1% Versene

3. The presence of chloride ion leads to unstable potentials. A sufficiently high concentration of chloride ion breaks down passivity completely.

4. The presence of a complexing agent (Versene) lowers the potential of etched specimens at the beginning, but after some time passivity is attained. With unetched specimens passivity is attained in the usual manner.

Electron Diffraction Experiments

All specimens for electron diffraction were ground flat on a belt grinder and then polished through 4/0 emery paper. All patterns were obtained by reflection in a General Electric electron diffraction machine Model No. G2. Finely divided magnesium oxide was used as a standard. After calculation of "d" values and estimation of line intensities, identification was made using the A.S.T.M. Card Index system.

It was found that specimen preparation was critical in obtaining measureable patterns. Specimens which had been given a fine polish only always gave diffuse patterns, probably due to a very finely crystalline or amorphous "Beilby" layer. When this amorphous layer was removed by etching good patterns characteristic of the metal could be obtained.

Electron diffraction results in aerated solutions.— A general summary of the results obtained by diffraction in aerated solutions is presented in Table I.

In Table II "d" values and relative intensities for a typical specimen are collected. The "d" values and intensities for γ-Fe_2O_3 and γ-$Fe_2O_3 \cdot H_2O$ are presented for identification. The treatment of the specimen was as follows: it was polished through 4/0 emery, etched for 2 min with N/10 HCl, and immersed in air-exposed N/100 sodium nitrite plus 200 ppm potassium chloride solution for 10 days.

The good numerical and intensity match of the observed lines with that of γ-$Fe_2O_3 \cdot H_2O$ and the absence of the 1.61 lines of γ-Fe_2O_3 leads to the conclusion that the unknown is γ-$Fe_2O_3 \cdot H_2O$ together with some γ-Fe_2O_3 since several lines can be matched to this latter substance. The diffuse 2.47 line is a combination of the 2.53 γ-Fe_2O_3 and 2.46 γ-$Fe_2O_3 \cdot H_2O$ lines.

Reproductions of some diffraction patterns obtained in air-exposed solutions are shown in Fig. 9.

The following conclusions may be drawn from the patterns:

1. Iron polished through 4/0 emery paper yields a pattern consisting of 2 or 3 diffuse haloes.

2. Iron polished through 4/0 emery and etched with N/10 or N HCl for periods of from 30 sec to 3 min, yields a pattern consisting mainly of iron plus some γ-Fe_2O_3 (Fig. 9a).

3. Iron treated as in [2] above, immersed in aerated N/10 or N/100 sodium nitrite yields γ-Fe_2O_3 together with a small amount of γ-$Fe_2O_3 \cdot H_2O$ (Fig. 9b).

4. The addition of chloride ion to sodium nitrite solutions increases the amount of γ-$Fe_2O_3 \cdot H_2O$ present. At a concentration of 25 ppm chloride ion in N/10 sodium nitrite, (Fig. 9c) the pattern is pre-

Table I

Surface cond.	Mech. pol. to 4/0	Pol. & etch.	Pol. & etch.	Pol. & etch.	Pol. & etch.	Pol. to 2/0
Conc. $NaNO_2$	—	—	N/10	N/10	N/10	N/10
Conc. KCl	—	—	—	25 ppm	2000 ppm	—
Patterns: Fe	Diffuse	Largely	—	—	—	Some
γ-Fe_2O_3	—	Some	Largely	Largely	Some	Some
γ-$Fe_2O_3 \cdot H_2O$	—	—	Very little	Some	Largely	—
Time of exposure	—	30 sec —2 min etch	3 hr —5 days	9 days	10 days	6 days

dominantly γ-Fe_2O_3, while at 2000 ppm chloride ion the pattern is almost entirely γ-$Fe_2O_3 \cdot H_2O$ (Fig. 9d).

Effect of Deaerated Solutions on Reduced Iron Specimens

The apparatus for the reduction of specimens in hydrogen and subsequent treatment consisted of a quartz tube connected to a vessel for de-aeration of the inhibitor. The hydrogen purification train consisted of a magnesium perchlorate drying tower and a platinized asbestos furnace that was operated around 450°C. The entire apparatus could be evacuated by means of a mercury diffusion pump supported by a backing pump.

The cycle of operations in the apparatus was as follows:

[1] An etched specimen, previously polished to 4/0 grade, was placed in the quartz vessel and the inhibitor in the connecting vessel frozen with liquid air.

[2] The entire apparatus, including the hydrogen purification train, was evacuated to about 10^{-4} mm Hg.

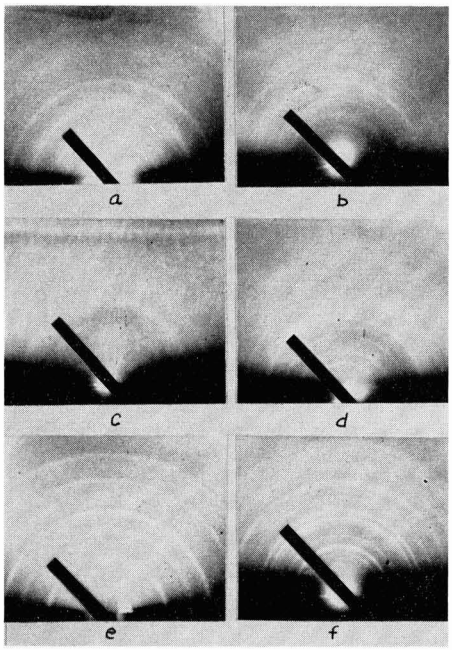

Fig. 9. Electron diffraction: (a) etched specimen; (b) etched or reduced and N/10 $NaNO_2$; (c) as (a) — N/10 $NaNO_2$ + 25 ppm KCl; (d) as (a) — N/10 $NaNO_2$ + 2000 ppm KCl; (e) reduced specimen; (f) reduced — N/100 $NaNO_2$.

Table II

"d" Exp.	I/I_1 Exp.	"d" γ-Fe_2O_3	I/I_1	"d" γ-$Fe_2O_3 \cdot H_2O$	I/I_1
3.23	80			3.29	90
2.47	90D*	2.53	100	2.46	70
2.08	10	2.08	24	2.08	20
1.90	80	—	—	1.93	70
1.71	10	1.70	12	1.73	40
1.49	100	1.48	53	—	—
1.37	20			1.37	40
1.17	50			1.19	30
1.08	v. faint	1.09	19	1.07	40

* D—Diffuse.

[3] The inhibitor solution was de-aerated by alternate freezing and melting three or four times.

[4] The inhibitor was frozen with liquid air and a slow stream of hydrogen passed through the apparatus.

[5] The temperature of the furnace around the quartz tube was raised to 550°-600°C and the specimen reduced overnight.

[6] After cooling in hydrogen, the inhibitor solution was melted and, by rotation of the solution vessel transferred into the quartz vessel, covering the reduced specimen.

[7] The specimen was allowed to stand in contact with the inhibitor for various periods of time and a reflection diffraction pattern was obtained.

To insure that the specimen was in fact reduced by operation [5], several "dry" runs (runs with no inhibitor) were conducted. The specimen was reduced and removed from the apparatus; a reflection diffraction pattern showed lines characteristic of iron, together with two weak lines due to γ-Fe_2O_3, probably formed on exposure to air. If the specimen had not been reduced completely, then α-Fe_2O_3 would be expected since this is the oxide stable at the high temperatures of reduction.

In all experiments conducted with de-aerated inhibitors the iron was reduced in hydrogen at 550°-600°C prior to treatment with the solution.

Results of diffraction experiments in de-aerated solutions.—A summary of these results is presented in Table III.

Reproductions of some diffraction patterns obtained in de-aerated solutions are shown in Fig. 9. The following conclusions may be drawn from the patterns.

(*A*) Iron polished through 4/0 emery paper, etched with *N*/10 or N HCl for from 30 sec to 3 min and reduced in hydrogen at 550°-600°C yields lines characteristic of iron with one faint line that may be ascribed to γ-Fe_2O_3 (Fig. 9e).

Table III

All specimens reduced in hydrogen at 550°-600°C. Surface cond.	40 Polish & etch.	40 Polish & etch.	40 Polish & etch.	40 Polish & etch.
Conc. $NaNO_2$	—	N/10	N/100	N/10
Conc. KCl	—	—	—	2000 ppm
Patterns: Fe	All	—	—	—
γ-Fe_2O_3	(1 faint line)	All	All	Little
γ-$Fe_2O_3 \cdot H_2O$	—	(1 faint line)	—	Largely
Time of Exposure	—	3 hr-2 days	2 days	10 days

(*B*) Iron treated as above with de-aerated N/10 or N/100 sodium nitrite yields γ-Fe_2O_3 plus a little γ-$Fe_2O_3 \cdot H_2O$ (identical with Fig. 9b).

(*C*) The addition of chloride ion to the nitrite solutions results in the production of γ-$Fe_2O_3 \cdot H_2O$, but some γ-Fe_2O_3 is present.

An experiment was made in which reduced iron was exposed to de-aerated *N*/700 (100 ppm) nitrite solution for 4 hr. A film of interference color thickness grew on the iron. A diffraction pattern (Fig. 9f) showed that this was probably Fe_3O_4, as the film pattern obtained has a sufficiently large number of sharp lines to distinguish it from γ-Fe_2O_3.

Electron Microscope Experiments

Micrographs were made using an R.C.A. Model E.M.T. transmission microscope. The negative replica technique with Formvar as described by Caule and Cohen (6) was used. Metal surfaces were washed and dried with redistilled methanol prior to the application of the 0.75% solution of Formvar. The replicas were shadowed with chromium metal uni-directionally at an angle of incidence of 9°. Direct positive paper was used in order to make the shadows look dark. The iron used in these experiments was the same as that described above. The magnification was × 6700.

The micrographs, in Fig. 10, are of the shadowed replicas of the iron subjected to the following treatment: (*a*) polished to 4/0 emery paper, under ethanol, no etch; (*b*) polished to 4/0 emery paper, under ethanol, etched with N/10 HCl for 30 sec; (*c*) as for (*a*), then immersed into a solution of air exposed N/10 $NaNO_2$ for 120 hr; (*d*) as for (*b*), then immersed into a solution of air exposed N/10 $NaNO_2$ for 120 hr; (*e*) as for (*b*), then immersed into a solution of air exposed *N*/10 $NaNO_2$ + *N*/100 KCl for time intervals of: 70 hr, 116 hr, and 133 hr; (*f*) as for (*b*), then immersed into an air-exposed solution of 100 ppm $NaNO_2$ + 100 ppm KCl for [1] 45 hr, [2] 93 hr.

In the photographs shown in Fig. 10 one can estimate the size and height of the bumps in the film from the magnification and shadowing angle. In the micrographs the width of the light areas is equivalent to the width of the inclusions, while the length of the shadows is 6.34 (shadowing angle = 9°) times the height. The large inclusion in the center of *f*[2] is therefore 2.3×10^{-4} cm wide and 0.5×10^{-4} cm high. The smaller inclusion at the top of *f*[1] is

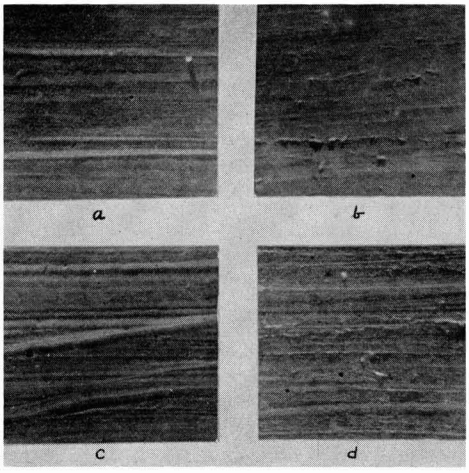

Fig. 10. Electron microscope results: (a) polished surface; (b) polished surface exposed to N/10 $NaNO_2$; (c) etched surface; (d) etched surface exposed to N/10 $NaNO_2$.

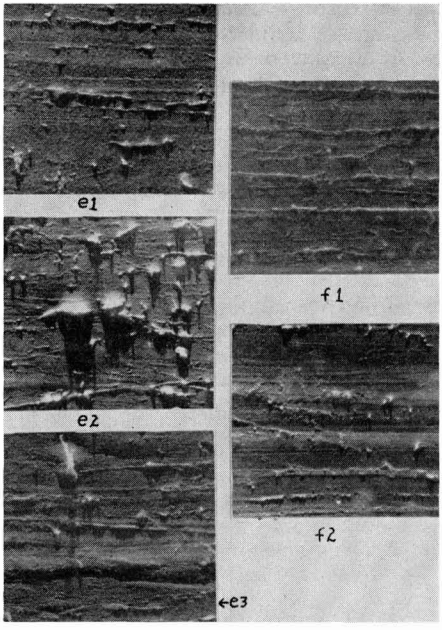

Fig. 10 (cont'd). (e) N/10 $NaNO_2$ + N/100 KCl (1) 70 hr, (2) 116 hr, (3) 333 hr; (f) 100 ppm $NaNO_2$ + 100 ppm KCl (1) 45 hr, (2) 93 hr.

0.25×10^{-4} cm wide and 0.1×10^{-4} cm high. In general the inclusions protrude well above the film and are wider than high. This would account for their fairly easy detection with the 1° reflection angle of the electron diffraction machine.

Discussion

Previous investigation had indicated that a film of γ-Fe_2O_3 is formed on iron in the presence of sodium nitrite solutions. There was also some evidence for the additional formation of a hydrated oxide. This has been confirmed and expanded in this work.

Surface preparation has a very marked effect on both the potential behavior and appearance of the

iron. Potentials tend to be more positive and more stable on polished than on polished and etched surfaces. This can be related to a difference in the surface which is shown both by the electron micrographs and electron diffraction. Specimens which were polished to 4/0 paper showed only diffuse iron patterns which were obscured by contact of the metal with nitrite solutions. However, specimens which were etched gave mainly iron patterns, and these on exposure to nitrite gave γ-Fe_2O_3 patterns. It is probable that the etched specimens, which were exposed to air before insertion into the nitrite solutions, already had a thin oxide film on them. However, this oxide film was too thin to show in the diffraction patterns and exposure to nitrite thickened the film considerably. The film after exposure to nitrite was probably at least 40Å thick.

The diffuse pattern obtained from a polished surface indicates that the metal at the surface is very finely crystalline or "amorphous." This may lead to the formation of an oxide film with very small crystals well packed together. This film would be of both small pore size and low porosity, which would lead to higher potentials than those obtained with etched specimens. The "amorphous" iron probably has a lower density than crystalline iron; this should lead to an oxide-metal interface under less strain than the interface formed on crystalline iron.[1] It should be pointed out that there is only a very small change in surface appearance as shown by the electron microscope when either polished or etched iron is exposed to $N/10$ nitrite solutions.

Intermediate air exposure or the presence of oxygen in the solution is not necessary for the formation of the γ-Fe_2O_3. This is shown in the experiments in which specimens were polished, etched, and then reduced by hydrogen and exposed in de-aerated nitrite solutions in the absence of air. A good γ-Fe_2O_3 pattern was obtained. Specimens treated in this manner without exposure to nitrite gave iron patterns, although, as stated above, there was probably a very thin oxide formed in air during transfer to the diffraction machine.

The electron microscope showed that there was very little change in the appearance of either etched or polished surfaces on exposure to nitrite solutions. This would indicate that the main function of nitrite is to thicken and repair the film.

Films in the Presence of Chloride

The presence of chloride ions in the solutions both lowered the final potential and led to unsteady potentials. The electron diffraction experiments showed that there was an increasing amount of hydrated oxide present in the films formed in these solutions when both the relative amount of chloride ion or time of exposure was increased. The electron micrographs confirmed these observations by showing that inclusions were formed in the film and that these inclusions also increased in height and area with time. It is very probable that the inclusions are composed mainly of hydrated oxide. The fact that the bumps became obscured at high relative concentrations of chloride ion would appear to indicate that under the conditions leading to very unsteady potentials some of the hydrated oxide precipitates over the whole surface, thus covering the original oxide layer. This would account for the almost complete absence of anhydrous oxide lines in the diffraction patterns of these specimens.

The behavior of the potential of iron in these solutions can be explained most easily in terms of an oxide film with inclusions (7), as observed by the electron microscope technique. Inclusions of hydrated oxide have a fairly good permeability to ferrous ions and are the sites of the anodic reaction, while the oxide covered surface provides the cathodic areas. The measured potential is determined by the relative resistances of the inclusions, the electrolyte, and the cathode film, as well as the polarization characteristics of the cathodic and anodic reactions. At low chloride ion concentration the inclusions are small and their resistance is high. This leads to high anodic polarization with consequent low current and small cathodic polarization. The observed potential is then close to that of the cathodic reaction and "noble" or passive. The effect of chloride ion on breaking down the passive potential is due to three factors. Chloride ion has a relatively high transport number and small size and tends to carry a large amount of the current to the anodes. This leads to the presence of both nitrite and chloride ions in the anodic pores, which favors the formation of ferric chloride. The hydrolysis of ferric chloride decreases the pH of the electrolyte in the anodes, leading to conditions which are conducive to either undermining or autoreduction of the oxide film. Chloride ion is also a complexing agent for iron and tends to prevent precipitation of a healing hydrate or hydrated oxide. These factors allow the pores to grow in size. Under near passive conditions, precipitate forms, but it is thicker than the oxide film because of a higher permeability for ferrous ions. The unsteady potentials in the presence of chloride indicates that there is a continuous formation and repair of pores. This explains the necessity of the continued presence of an inhibitor for maintaining passivity.

The effect of a strong complexing agent on the potential is shown in the experiments with Versene in Fig. 8. Here it can be seen that the potential remains active until a balance between iron ions in the complex and in the solution is reached, at which point the hydrated oxide precipitates in the pores and the metal becomes passive. This would indicate that the complexing ability of the chloride ion plays only a small part in the mechanism of the breakdown of the films. It is interesting to observe that the Versene has a much smaller effect on a polished surface than on one that has been both polished and etched. This is in line with other observations that the concentration of chloride required to break down a polished surface is greater than that required to break down an etched surface. Both these effects may be explained in the following manner. The

[1] The surface of "polished" iron can be considered as having a high concentration of defects, which would lead to a lower density. The oxide formed has a lower density than iron and the strain of the metal-oxide interface is in part, at least, determined by the difference in density between the oxide and metal. Because of the small crystal size (many grain boundaries) the oxide film may grow thicker than on etched metal.

metal surface is disrupted by polishing and the oxide formed on this very finely crystalline or amorphous metal has a smaller crystal size and is possibly thicker than oxide formed on the more perfect etched metal surface. The oxide film formed on the polished metal may also contain some of the oxide formed during the polishing. It was observed that the potential of polished iron in nitrite solutions is always higher than that of etched iron. This indicates that the films on polished iron have smaller pores than those on etched iron. If the effect of chloride and/or the complexing agent is to break down the film by acting at the pores, then it would be expected that the oxide film on the polished surface would be more stable than the film on the etched metal. In this connection the major effect of the chloride is to lead finally to the breakdown of the film by undermining or autoreduction while the Versene prevents the plugging of the pores by removing iron ions before they form a precipitate.

The mechanism for nitrite inhibition would appear to be much the same as that proposed in previous papers (7, 8). The nitrite solution reacts directly with the iron surface to form an oxide film which, due to nonhomogeneity of the surface, is not perfect and does not protect completely. Full protection is obtained by the formation of inclusions in the discontinuities of the film which grow somewhat thicker than the oxide film itself until reaction substantially ceases. If there is present in the solution a material which prevents the formation of inclusions or changes their physical character, such as a complexing agent or chloride ion, then the discontinuities in the film can grow by either undermining or autoreduction of the film when the anodes become sufficiently acid, and if these disruptive agents are at a sufficiently high concentration, then passivity will not be obtained.

Manuscript received Feb. 26, 1957. This paper was prepared for delivery before the Pittsburgh Meeting, Oct. 9-13, 1955.

Any discussion of this paper will appear in a Discussion Section to be published in the December 1958 JOURNAL.

REFERENCES

1. M. Cohen, *J. Phys. Chem.*, **56**, 451 (1952).
2. W. H. J. Vernon, F. Wormwell, and J. T. Nurse, *J. Chem. Soc.*, **1939**, 621.
3. I. Itaka, S. Miyake, and T. Imori, *Nature*, **139**, 156 (1937).
4. P. D. Dankov and C. R. Shushakov, *Acad. Sci. URSS*, **24**, 553 (1939).
5. J. E. O. Mayne and M. J. Pryor, *J. Chem. Soc.*, **1949**, 1831.
6. E. J. Caule and M. Cohen, *Can. J. Chem.*, **31**, 237 (1953).
7. M. J. Pryor and M. Cohen, *This Journal*, **100**, 203 (1953).
8. R. Pyke and M. Cohen, *ibid.*, **93**, 63 (1948).

The Protective Value of Tin-Nickel Alloy Deposits on Steel

F. A. Lowenheim

Metal & Thermit Corporation, Rahway, New Jersey

W. W. Sellers

Development and Research Division, International Nickel Company, New York, New York

F. X. Carlin

Research Laboratory, International Nickel Company, Bayonne, New Jersey

ABSTRACT

Outdoor exposure tests of the comparative value of the Sn-Ni alloy and conventional Ni/Cr deposits on steel, with and without a copper undercoat, are reported. It is shown that Sn-Ni is comparable in protective value to Ni/Cr, not quite so good in marine but superior in industrial atmospheres. The type of corrosion behavior of the two deposits differs considerably. In general, the protective value of the Sn-Ni deposit is of a high order.

A process for plating an alloy of tin and nickel from a chloride-fluoride electrolyte was developed by the Tin Research Institute in 1951 (1). Since that time several papers have appeared dealing with various aspects of the process and the resulting deposit: it has been shown that the deposit is an intermetallic compound of the formula SnNi (2); the function of fluoride ion in complexing the tin in solution has been elucidated (3); the throwing power of the bath has been determined (4); the electrode potential of the alloy and its resistance to many chemical reagents have been studied (5); the hardness has been measured (6); the original bath formulation has been modified (7); and the behavior of the deposit in outdoor weathering tests has been reported (8, 11).

The tin-nickel deposit is of exceptional interest, both theoretically and practically, for several reasons, among which may be mentioned:

1. The intermetallic compound SnNi (65% Sn, 35% Ni) does not appear on the thermal equilibrium diagram of the nickel-tin system and apparently

cannot be prepared by standard metallurgical techniques. It is thus in effect a new metal, so far preparable only by electrodeposition, having properties which cannot necessarily be predicted from those of its constituents.

2. The plating bath is of a relatively new type, being particularly unusual in that it is the first practical example of an acid tin-plating electrolyte which does not require organic addition agents for the production of sound deposits.

3. In spite of its acid nature the bath exhibits exceptionally good throwing and covering power.

4. The deposit possesses several unusual properties which give promise of useful applications in both the decorative-protective and industrial or engineering phases of metal finishing. It is hard, smooth, and almost bright as plated, and according to published reports shows exceptional chemical resistance to a wide variety of reagents as well as to outdoor weathering. It can be soldered with ordinary soft solder using mild (rosin-alcohol) fluxes. In ease of solderability the tin-nickel deposit is not so good as tin, tin-zinc alloy, etc., but the remarkable feature is that a hard, bright deposit can be soldered at all with noncorrosive fluxes.

5. When the process was first introduced, nickel was in extremely short supply, and the new deposit offered the possibility that one pound of nickel could be made to do the work of three, assuming that performance was equivalent. Although such considerations are of only ephemeral importance, they do help in lending impetus to the investigation of new processes.

Since corrosion resistance appeared to be one of the most interesting properties of the deposit, both of the companies represented by the present authors instituted programs to investigate it further, by means of outdoor exposure tests. These were designed to supplement the English results already published in several respects: several additional variables were included, the exposure times involved are considerably longer, and the exposures represent American rather than English conditions. The tests here reported are still in progress, but have proceeded far enough to permit conclusions to be drawn.

Scope and purpose of tests.—It was desired to investigate the performance of tin-nickel alloy deposits on steel under outdoor weathering conditions. The plating systems used in the exposure were designed to test the following variables.

Table I. Weathering of tin:nickel-alloy coatings at Kure Beach

Exposed on ASTM-type racks facing south in lot 800 ft from mean shore line; type of steel: mild, cold-rolled; size of panels: 4x6 in.; dates of exposure: Lots I-1 thru I-12 exposed 2-2-55. Lots M-1 thru M-23 exposed 3-24-55.

Lot No. (3 panels per lot)	Type and thickness (mils) of coating					Rating					
						Approximately 7 months		12 Months		24 Months	
	Total thickness exclud. Cr	Cu	Ni	Sn-Ni	Cr	Rating No.	Defects	Rating No.	Defects	Rating No.	Defects
I-1	0.75		0.75B		0.01	2	iS,xpR,xRs,xcR	0		0/0	xcR,xRs
I-11*			0.25B	0.50	0.01			7	scR,sRs,xS,xeRs	4/0†	icR,sRs,iecR
I-7*		0.25B		0.50	0.01			6	iS,icR,xeRs,sRs	6/0	icR,iRs,xecR
I-5		0.25B		0.50	—	4	xcR,xeRs,xS,iRs	4	xcR,xeRs,xS,iRs	2/0	xcR,iRs,xS,xecR
M-14	1.00		1.00B		0.01	9	vscR	6	sRs,vspR,xS		
M-4				1.00	—	1	xcR	0	xpR,xRs,xS		
M-5		0.01		1.00	—	9	vscR	6	iS,iRs,spR		
M-11		0.25B	0.75B		0.01	8	vsRs,scR	3	iRs,xS,spR		
M-3		0.25		0.75	—	5	icR	3	sS,ipR,iRs		
M-12		0.50B	0.50B		0.01	5	icR,iRs	1	xS,spR,xRs,scR		
M-2		0.50		0.50	—	3	iRs,icR	2	xS,xRs,ipR		
M-13		0.75B	0.25B		0.01	3	xcR,xRs	1	xS,icR,xRs		
M-1		0.75		0.25	—	2	xRs,xcR	1	xRs,xpR		
I-2	1.25		1.25B		0.01	6	spR,iRs,sS,icR	5	spR, iRs,sS,icR, seRs.	1/1	xpR,icR,xRs
I-12*			0.25B	1.00	0.01			8	icR,iRs,iS,xeRs	5/0†	icR,iRs,xecR
I-8*		0.25B		1.00	0.01			8	iS,xeRs	8/0	icR,iRs,xecR
I-6		0.25B		1.00	—	9	xS,vsRs,xeRs	8	xS,vsRs,sC,xeRs	6/0†	icR,iRs,xS,xecR
M-18	1.50		1.50B		0.01	9	vsRs	7	sRs,vspR,iS		
M-9				1.50	—	0	xcR	0	xRs (100%),xpR		
M-10		0.01		1.50	—	9	vscR	6	iRs,iS,spR		
M-15		0.50B	1.00B		0.01	9	vscR	7	sS,sRs,vspR		
M-8		0.50		1.00	—	7	icR	5	iS,iRs,ipR		
M-16		0.75B	0.75B		0.01	9	vscR	7	xS,sRs,spR		
M-7		0.75		0.75	—	2	xcR,iRs	2	xS,ipR		
M-17		1.00B	0.50B		0.01	9	scR	4	xS,sRs,spR		
M-6		1.00		0.50	—	4	icR,iZ	3	iS,iRs,ipR		

NOTES: * All the chromium applied to the tin-nickel coatings had completely flaked off in less than 6 months. This is not considered in rating numbers. Ratings are an average for the lot.
† = following rating indicates a spread greater than two rating numbers from average given.
B = buffed
Lots designated with prefix "I" were prepared by the International Nickel Co.
Lots with prefix "M" were prepared by the Metal and Thermit Corp.
Abbreviations used to describe defects are identified in Table III.
Ratings for 7 and 12 months were made with single-number system. Ratings for 24 months were made with two-number system. First numeral denotes protective values; second numeral general appearance.

1. Effect of total thickness of deposit. Thicknesses from 0.75 to 1.5 mils are included.

2. Effect of proportion between copper undercoat and tin-nickel. Copper undercoats from 0.25 to 1.0 mils are used.

3. Effect of type of undercoat. Tin-nickel is plated (*a*) direct on steel, (*b*) over a copper flash, (*c*) over substantial thicknesses of copper, (*d*) over nickel.

4. Direct comparison of tin-nickel vs. nickel/chromium, thickness for thickness, over various thicknesses of copper. The nickel is in all cases buffed Watts', which is generally agreed to be at least as good as and in most cases better than bright nickel in corrosion resistance.

5. Effect of chromium over tin-nickel. As will appear, this purpose of the experiment was not fulfilled because, at the time these exposures were initiated, the method used for chromium plating over tin-nickel turned out to be unsatisfactory. Panels were prepared but the chromium flaked off soon after exposure. Later tests still on exposure give preliminary indication that this problem has been solved.

6. Possible application of tin-nickel as a final flash coat, used similarly to the conventional thin chromium. Thin plates of tin-nickel (0.01 mil or so) were deposited on copper and bronze undercoats. This phase of the program is omitted from the tables and subsequent discussion; it need only be said that tin-nickel used in this way proved unsatisfactory as a decorative finish.

7. All of the foregoing comparisons and tests are conducted in the two principal types of atmospheres, marine and industrial.

The actual plating systems used are included in Tables I and II along with the results of the exposures.

Preparation of Panels for Exposure

Panels were prepared by International Nickel Company (designated in Tables I and II with an "I") and by Metal & Thermit Corporation (designated in the same tables with an "M").

This basis metal for all panels was cold-rolled mild steel cut to standard 4 x 6 in. size. Standard commercial practices for polishing, degreasing, electrolytic cleaning, and pickling the steel in preparation for plating were employed.

Nickel and copper were plated according to accepted methods (9). Nickel was deposited from a conventional low-pH Watts-type bath. Copper cyanide and copper sulfate baths were used to deposit

Table II. Weathering of tin:nickel-alloy coatings at Bayonne

Exposed on ASTM-type racks facing south; type of steel: mild, cold-rolled; size of panels: 4x6 in.; date of exposure: 3-24-55.

Lot No. (3 panels per lot)	Type and thickness of coating (mils)				Rating							
					6 Months		12 Months		24 Months		29 Months	
	Cu	Ni	Sn-Ni	Cr	Rating	Defects	Rating	Defects	Rating	Defects	Rating	Defects
I-1		0.75B		0.01	3	xpR,xRs	1	xpR,xRs	2/0	xpR,xRs	2/0	xcR,xRs,xpR
I-11*		0.25B	0.5	0.01	8	icR	7	icR,iRs	8/8	scR	6/4	icR,xLS
I-7*	0.25B		0.5	0.01	8	vsSp,icR	8	vsSp,icR	8/8	scR	9/7	scR,xLS
I-5	0.25B		0.5		7	scR,xecR	4	scR,xecR	6/6	icR,xecR	5/3	icR,xLS, vxecR.
M-14		1.0B		0.01	7	ipR,iRs	2	xRs,iSp,ipR	1/0	vxRs	1/0	vxRs,xpR
M-4			1.0		3	iRs,xcR	2	xcR,xRs	3/3	xcR,xecR	2/1	xcR,xecR, xRs,xLS.
M-5	0.01		1.0		9	vscR	9	vscR	9/9	vscR	9/7	vscR,vsSp, ieR,xLS.
M-11	0.25B	0.75B		0.01	4	xpR,iRs	4	iRs,iS,ipR	3/1	xpR,xSp,xRs	2/0	xpR,xcR,xRs
M-3	0.25		0.75		9	vscR,vsRs	8	vscR,vsRs	8/8	scR	7/5	scR,iRs,ipR, xLS.
M-12	0.5B	0.50B		0.01	3	xpR,Rs,xS	2	xS,xpR,xRs	2/0	xpR,xSp,xRs	1/0	xpR,xcR,vxRs
M-2	0.5		0.5		6	sSp,icR,sZ	6	sS,scR,sRs	4/4†	icR,xRs,ipR	3/2†	icR,xRs,xLS
M-13	0.75B	0.25B		0.01	3	xpR,xSp,scR,iRs	1	xRs,xS,xpR,icR	1/0	xpR,xSp,xRs	0/0	xcR,xRs
M-1	0.75		0.25		5	sRs,icR	4	iRs,icR	4/4†	icR,iRs,ipR	4/2†	icR,xRs,xLS
I-2		1.25B		0.01	7	ipR,xRs	7	spR,sRs	2/1	xpR,xRs	3/1	xcR,xRs,xpR
I-12*		0.25B	1.0	0.01	8	icR	7	icR,iRs	7/7	icR	5/3	icR,xLS
I-8*	0.25B		1.0	0.01	9	scR	9	vscR	9/9	vscR	10/8	xLS
I-6	0.25B		1.0		10		10		10/9	sSp	10/8	xLS
M-18		1.5B		0.01	8	iSp,spR	5	ipR,iRs	2/1	xpR,xRs	1/0	xpR,xRs,iMS
M-9			1.5		0	xRs	0	xRs	0/0	xRs	0/0	xRs
M-10	0.01		1.5		8	iZ,sRs	8	iZ,iRs	8/7	ipR,iZ,iB,sS	7/3†	icR,iZ,iRs,xLS
M-15	0.5B	1.0B		0.01	8	iSp,spR,sS	6†	iS,sRs,sSp	4/2	ipR,iZ,xS	5/2	ipR,xRs,xMS, iW
M-8	0.5		1.0		9	vspR,vsSp	9	vspR,vsSp	9/9	vspR	10/8	xLS
M-16	0.75B	0.75B		0.01	7	ipR,iSp	5	iS,sRs,ipR	3/2	xpR,xS	3/0	xpR,xRS,xSp
M-7	0.75		0.75		9	vspR,vsZ	8	iS,iZ,vscR	9/9	spR	8/6	vscR,ipR, iRs,xLS.
M-17	1.0B	0.5B		0.01	7	spR,xSp	3	xpR,sRs,iS	3/1†	xpR,xRs	4/3†	ipR,xRs,iSp
M-6	1.0		0.5		9	sSp,ipR,sS	7	vscR,vsRs,iS	8/8	spR	7/5	spR,iRs,xLS

NOTES: * All the chromium applied to the tin-nickel coatings had completely flaked off in less than 6 months. This is not considered in rating numbers. Ratings are an average for the lot.
† = following rating indicates a spread greater than two rating numbers from average given.
B = buffed.
Lots designated with prefix "I" were prepared by the International Nickel Co.
Lots with prefix "M" were prepared by the Metal and Thermit Corp.
Abbreviations used to describe defects are identified in Table III.
Ratings for 6 and 12 months were made with single-number system. Ratings for 24 months and 29 months were made with two-number system. First numeral denotes protective value; second numeral, general appearance.

copper. Thickness of coating on each panel was determined with a Magne-Gage at several predetermined points. Panels were rejected if any measurement deviated by more than 10% from the desired thickness.

Tin-nickel alloy was plated from the bath originally recommended by Parkinson (1). Thicknesses of coatings over copper were measured with a Magne-Gage. By measuring the time and current density required to deposit a prescribed thickness of the alloy over copper, a plating rate was determined. This rate was used to calculate plating times for the various thicknesses over nickel.

All nickel and copper coatings were buffed. The tin-nickel alloy required color buffing or wiping to remove a slight "haze" present in the as-plated coating.

Chromium was deposited as a final flash coating on panels of some lots. Thickness of chromium deposits was measured on trial panels by an anodic solution method. Although the chromium coatings on tin-nickel appeared sound initially, they powdered soon after exposure.

Exposure sites and conditions.—Panels were exposed at three sites, one marine and two industrial, as follows.

Kure Beach, N. C.: the test lot, 800 ft from the ocean, of the International Nickel Company's atmospheric exposure station. The atmosphere is purely marine, there being little or no industry nearby.

Bayonne, N. J.: the test lot at the laboratories of the International Nickel Company. This is a heavily industrialized area, with much chemical industry, gasoline refining, and small foundries and smelters, in the immediate neighborhood.

Pittsburgh, Pa.: the roof of a downtown office building. This area is too well-known to require description. The results of the Pittsburgh exposure are not included in the tables or discussion: trends of deterioration and relative merit of the various panels proved to be the same at Pittsburgh as at Bayonne except that Pittsburgh was less corrosive. (The I-series of panels was not included in the Pittsburgh exposure.)

All panels were exposed on standard ASTM-type racks facing south at an angle of 30° to the horizontal. The panels were not cleaned except when light brushing or rinsing became necessary during inspections to distinguish between defects and dirt.

Methods of inspection and rating.—Panels were rated as nearly as possible in accordance with methods used by ASTM Committee B-8 (10). In this system a rating number is assigned corresponding to the percentage of the area which is covered by defects (*see* Table III). In addition to the numerical rating, descriptions of the type of defect encountered are noted in shorthand abbreviations, the meanings of which are explained in the table.

During the time these panels were on exposure, one of the authors (F.A.L.) began experimenting with a modified scheme for assigning rating numbers which is now being tried out by Committee B-8. This involves the separation of defects into two categories: those which cause or are caused by basis metal corrosion (rusting) and those which affect only the coating. In the first category are all forms of rusting; in the second are such defects as surface pitting, flaking or peeling of topcoats which does not penetrate to the steel, tarnish, and the like. Two rating numbers are assigned to the panel, one for each category of defect, separated by a slash; thus 10/5 would indicate a panel free of rust (first number) but down-graded to 5 (second number) for one or another surface defect affecting its appearance.

The fact that rating methods were changed during the course of this exposure inevitably introduces a complication into the orderly interpretation of the results. Nevertheless this complication is more apparent than real: meaningful comparisons among various groups of panels can be drawn and significant conclusions reached.

A further complication is introduced by the tendency of tin-nickel coatings, unprotected by a chromium finish, to acquire in the atmosphere a film which might be variously described as light stain,

Table III. Identification of rating numbers and symbols used in Tables I and II

Numerical rating	% of Area Defective
10	0
9	0-0.1
8	0.1-0.25
7	0.25-0.5
6	0.5-1.0
5	1.0-2.5
4	2.5-5.0
3	5.0-10.0
2	10.0-25.0
1	25.0-50.0
0	over 50.0

Where two number system is used, first number denotes protective value, second number denotes general appearance.

"Shorthand" symbols used in rating exposure panels

Symbol	Meaning
R	Rusting of the basis metal (permanent or massive type of rust such as that in pinholes, bare or flaked areas, or in craters or broken blisters).
Rs	Rust staining which can be removed readily with a damp cloth or chamois and mild abrasives revealing a sound, bright surface.
S	Stains or spots other than obvious rust stains.
Sp	Surface pits (corrosion pits probably not extending through to the basis metal: i.e., absence of obvious basis metal corrosion products bleeding therefrom).
B	Blister
Z	Crazing
p	Pinpoint
c	Crater or "pustular"
e	Edge
s	Slight or small
i	Intermediate or moderate
x	Excessive or severe, or large
f	Few
m	Many
v	Very (to modify above adjectives)
L	Light } Used to denote degree of staining
M	Medium }
H	Heavy }

mild tarnish, slight discoloration, or the like. Because the tarnish is readily removable by light abrasion, this defect was arbitrarily assigned a penalty of only two points in the appearance (second number) rating, e.g., a panel otherwise perfect but exhibiting the aforesaid light stain would be rated 10/8. This property of tin-nickel is discussed further below.

A characteristic of the rating method should be borne in mind in appraising and interpreting the results. Since the numbers are based on a logarithmic scale, differences in absolute area defective are far greater between two adjacent numbers at the low than at the high end of the scale. In spite of this, however, differences at the high end of the scale are far more significant practically and commercially. This is because panels with ratings below about 5 have deteriorated beyond any practical utility, so that it is of little real interest whether they rate 3 or 1. On the other hand, there is a significant difference between a 10 and a 9: the former has no defects at all, while the latter is beginning to exhibit some failure.

Replication.—Nine panels of each lot (Tables I and II) were prepared, so that exposures at each of the three sites were in triplicate. Since it would unduly complicate the tables of results to include ratings for all panels, lot ratings were arrived at by simply averaging the individual ratings. (Where the two-number system is used, each number is treated separately.)

When the three panels were within ±2 numbers of the lot average, the figure in the tables is given without comment. When one or more panels differed by more than two numbers from the lot average, a dagger in the table so indicates. The practical significance of this notation is that too much reliance should not be placed on the particular rating: with only three replicates one is not justified in discarding any result no matter how divergent.

Results

The ratings of the lots on exposure at Kure Beach are given in Table I; those at Bayonne in Table II. As already explained, detailed results for the Pittsburgh exposure are omitted. The Kure Beach exposure has been discontinued; panels are still out at Bayonne and Pittsburgh.

The ratings given in the tables are plotted in Fig. 1 and 2. Where the two-number system was used, the value used for the plot is the second number since it corresponds closely to the rating that would result from the single-number method. The value of graphical presentation is twofold: it offers a readily assimilated summary of the results, and it enables calculation of an index of performance which is essentially more meaningful than the rating numbers themselves, viz., the useful service life of a given coating system. This may be defined as the time on exposure before a panel has deteriorated to a given rating.

As will be seen from an inspection of the graphs, occasionally panels seem to improve between inspections instead of deteriorating. This anomaly is explicable on the basis that the subjective element has, unfortunately, not been entirely eliminated from the

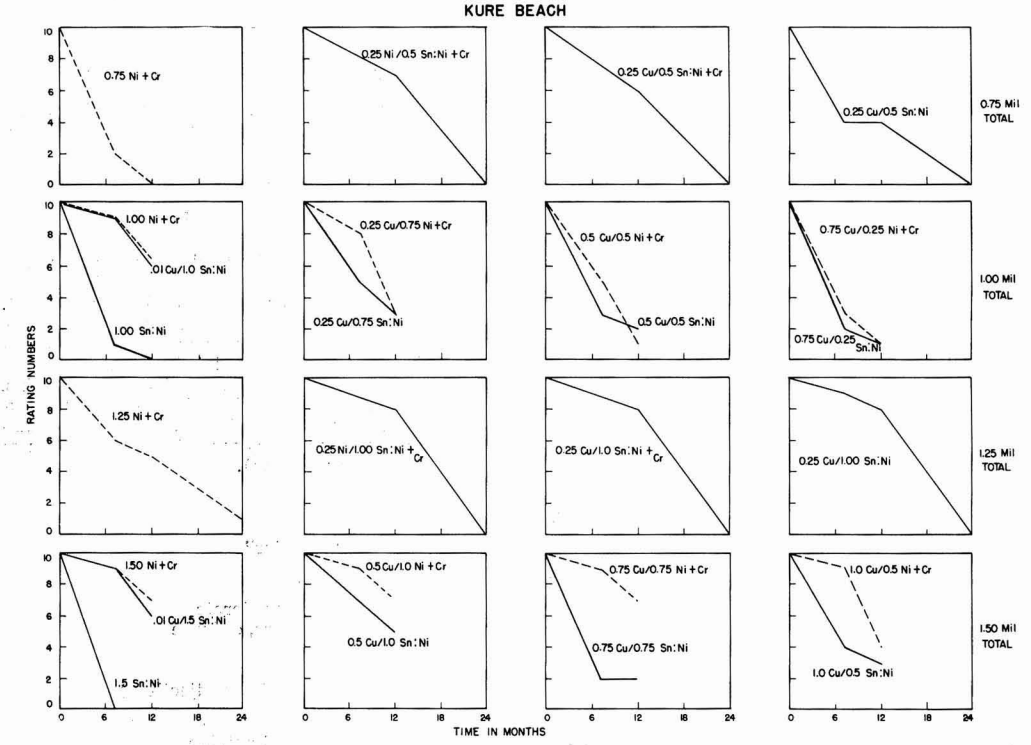

Fig. 1. Rating vs. time at Kure Beach. Solid lines, tin-nickel coatings; dashed lines, nickel/chromium coatings.

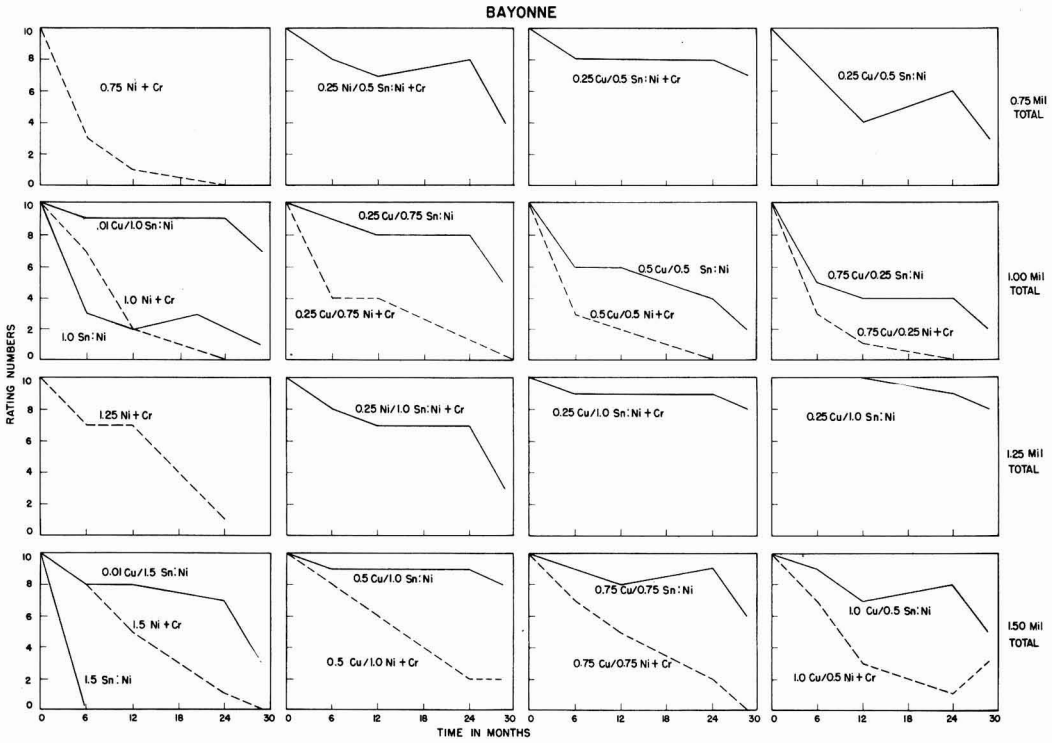

Fig. 2. Rating vs. time at Bayonne. Solid lines, tin-nickel coatings; dashed lines, nickel/chromium coatings

rating system; each inspection is independent and in many cases different inspectors were involved. Another factor may be the occurrence of heavy rain immediately before inspection, having the effect of cleaning the panels and causing them to improve in appearance.

Discussion

It is apparent that the relative merit of the various lots is quite different under the two conditions of exposure. It therefore becomes necessary to discuss the Kure Beach and the Bayonne results separately.

Marine atmosphere (Kure Beach).—All the panels in the present program deteriorated relatively rapidly. For long-time service in such a location, thicker coatings than were used in this program would be required.

Tin-nickel.—The useful service life of the tin-nickel coatings in this test was almost independent of the thickness or nature of the undercoat (with one exception noted below). In order to obtain reasonably good performance at least 1.0 mil of tin-nickel appears to be required, but it does not seem to matter appreciably whether this is plated over 0.01, 0.25, or 0.5 mils of copper (Table I, Lots M-5, I-6, M-8 and Fig. 3). Similarly 0.5 mil tin-nickel coatings failed fairly rapidly whether they were on 0.25, 0.5, or 1.0 mil of copper (Lots I-5, M-2, M-6).

In spite of the early powdering off of the chromium from the chromium-plated tin-nickel coatings, the performance of these panels was noticeably better than that of nonchromium plated ones. (This has been noted in other tests not recorded here.)

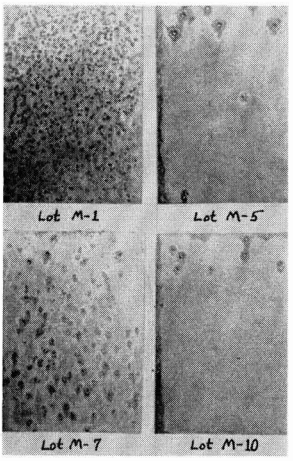

Fig. 3. Effect of thickness of tin-nickel on the protective value at Kure Beach. Total thickness of coatings: top row, 1.0 mil; bottom row, 1.5 mil. Lot M-1, 0.75 Cu/0.25 Sn:Ni; Lot M-5, 0.01 Cu/1.0 Sn:Ni; Lot M-7, 0.75 Cu/0.75 Sn:Ni; Lot M-10, 0.01 Cu/1.5 Sn:Ni.

Tin-nickel plated direct on steel failed very rapidly, but even a very thin flash of copper was sufficient to effect a dramatic improvement in performance (Lots M-4, M-5, M-9, M-10).

Tin-nickel vs. nickel/chromium.—Results for the thinner coatings are not entirely consistent, some showing tin-nickel to be superior, others showing an advantage for nickel. In the heavier coatings, the two appear to be roughly equivalent in performance.

Some further generalizations can be made which are applicable to the Bayonne results as well and are therefore considered later.

Industrial atmosphere (Bayonne).—The industrial atmosphere of Bayonne appears in these tests to be of the same order of corrosiveness toward nickel/chromium or copper/nickel/chromium coatings as is the marine atmosphere of Kure Beach. Duplicate sets of these panels failed at about the same rate in both exposures. But the industrial atmosphere was far less corrosive toward the tin-nickel coatings than was the marine. As a consequence, the tin-nickel coatings consistently outperformed the nickel/chromium coatings at Bayonne. This is illustrated in Fig. 4. This is true of all the tests, so that detailed consideration of the results is not necessary.

As at Kure Beach, for a given coating thickness performance improves as the proportion of the total which is tin-nickel increases and the proportion of the copper undercoat decreases. This statement is made principally on the basis of the data for the 1 mil coatings. Although a similar trend is observable in the 1.5 mil coatings, deterioration has not proceeded far enough to permit definite confirmation (*see* Fig. 5). The exception, as before, is the case of no undercoat at all: tin-nickel direct on steel fails very quickly; but the insertion of a mere flash of copper improves the corrosion resistance many fold. There is little to choose between nickel and copper as undercoats for tin-nickel; slight differences in comparable lots favor copper.

Results at both locations.—There remain to be discussed two differences in the behavior of tin-nickel coatings as compared with nickel/chromium coatings, which became evident at both locations and which are not obvious from the ratings and descriptions in Tables I and II.

1. Type of failure. When a nickel/chromium and a tin-nickel plated panel have failed to the same extent as measured by the rating numbers, they will in all probability not be similar in appearance. Nickel coatings normally fail in a multitude of small spots (pinhole rusting), of which more and more appear as deterioration proceeds until a typically low-rated panel is almost covered with thousands of small rust spots; some of these spots may of course become enlarged and develop into craters or pustules of rust. Pinhole rusting is, on the other hand, a relatively rare defect in tin-nickel coatings. Most often failure starts in a few spots which then gradually grow in size, so that a typically low-rated

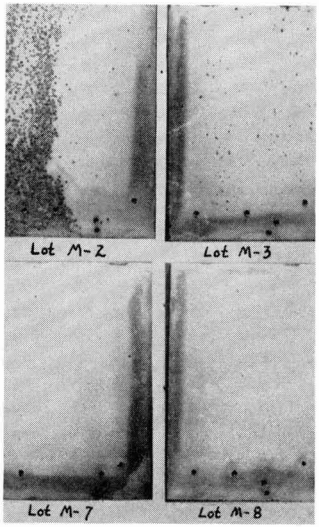

Fig. 5. Effect of thickness of tin-nickel on the protective value at Bayonne. Total thickness of coatings: top row, 1.0 mil; bottom row, 1.5 mil. Lot M-2, 0.5 Cu/0.5 Sn:Ni; Lot M-3, 0.25 Cu/0.75 Sn:Ni; Lot M-7, 0.75 Cu/0.75 Sn:Ni; Lot M-8, 0.5 Cu/1.0 Sn:Ni.

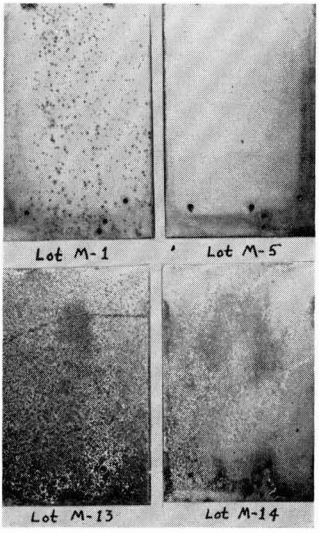

Fig. 4. Weathering of the various coatings at Bayonne. Total thickness of coatings: 1.0 mil. Lot M-1, 0.75 Cu/0.25 Sn:Ni; Lot M-5, 0.01 Cu/1.0 Sn:Ni; Lot M-13, 0.75 Cu/0.25 Ni/0.01 Cr; Lot M-14, 1.0 Ni/0.01 Cr.

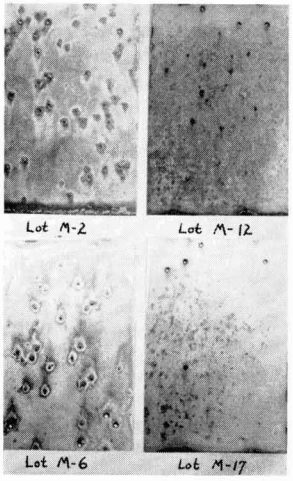

Fig. 6. Differences in the type of failure of tin-nickel and copper-nickel-chromium coatings. Kure Beach exposure. Total thickness of coatings: top row, 1.0 mil; bottom row, 1.5 mil. Lot M-2, 0.5 Cu/0.5 Sn:Ni; Lot M-12, 0.5 Cu/0.5 Ni/0.01 Cr; Lot M-6, 1.0 Cu/0.5 Sn:Ni; Lot M-17, 1.0 Cu/0.5 Ni/0.01 Cr.

tin-nickel panel may have relatively few very large rust craters, with large areas of the panel being entirely free of defects. This type of failure is illustrated in Fig. 6.

2. Stain and discoloration. If the typical "blue" color of bright chromium is taken as "standard" for a decorative finish, the tin-nickel coatings fail to meet that standard after a relatively short time of exposure. The alloy coatings, which are even as plated of a somewhat different, more reddish hue than chromium, gradually darken in color, presumably by the formation of an oxide or other film. Very soon the color difference is sufficiently obvious so that a mere glance is enough to pick out the tin-nickel panels on a rack from the chromium plated panels.

The formation of this film posed a problem in the inspection and rating of the panels, a problem which was handled differently by different inspectors. It cannot be considered a serious defect and since it usually covers the whole panel, various inspectors either ignored it entirely or penalized one or two points. It has been tentatively decided that where the tarnish film is light, two points will be attributed to this defect.

This behavior was expected from previous experience and prompted the inclusion in the present test of several lots of tin-nickel panels with a final flash coat of chromium. Unfortunately, as already stated, the chromium soon flaked off these panels so that the question whether tin-nickel can be protected from tarnishing by the conventional chromium overlay remains unanswered so far as the present test is concerned. See the remarks below on a supplementary test recently initiated.

Supplementary program.—The results above reported pose two problems:

1. The nature of the corrosion of tin-nickel strongly suggests that it is quite noble and that corrosion takes place through pores already present. If these pores can be avoided, the performance should be greatly improved.

2. Further efforts to chromium plate tin-nickel should be made in an attempt to avoid the tarnishing and discoloration already noted.

To investigate these questions, further panels were prepared and exposed at Kure Beach and Newark, N. J. The plating systems and results are shown in Tables IV and V.

This supplementary program has obviously not proceeded far enough to permit sweeping conclusions. But even at this early date the following can be said.

Lot S-1 (very similar to Lot M-5) is failing at about the same rate as M-5, so far.

Lot S-2: chromium has not flaked in 6 months; previously chromium flaked in a few weeks. The problem of chromium plating over tin-nickel appears nearer solution.

Lot S-3: so far indicates excellent performance by the use of the "double plate" technique, tending to confirm suspicions that corrosion of tin-nickel plated steel takes place principally through preexisting pores.

Table IV
Kure Beach, Exposed 2/14/57

Lot	Thickness, mils Cu	TN	Cr	4 Months	10 Months
S-1	0.1	0.9	—	8/8 vf large cR, xeR	7/4 vf large cR, iS
S-2	0.1	0.9	.01	9/9 vscR	9/9 vf large cR
S-3	0.1	0.5 + 0.4*	—	10/10	10/10

* Buffed after 0.5 TN, then replated with additional 0.4 "Double plate".

Table V
Newark, Exposed 2/28/57

Lot	7 Months	12 Months
S-1	10/10	10/8 iS
S-2	10/10	10/10
S-3	10/10	10/8 iS

Conclusions

The principal result of this exposure program is to show that the tin-nickel deposit gives excellent resistance to corrosion, in which respect it is quite comparable to Watts' nickel plus a flash of chromium. It is roughly equivalent to nickel in marine but definitely superior to it in industrial atmospheres.

The tin-nickel alloy should not be applied direct to steel for corrosion-resistant service. Copper, even if only as a flash coating, between the steel and tin-nickel, improves performance many fold. Other undercoats including nickel and bronze may be used.

The corrosion of tin-nickel alloy coated steel takes place in a different manner, probably denoting a different mechanism, from that of nickel coatings.

Although it has excellent properties as a decorative-protective coating, tin-nickel forms on outdoor exposure a tarnish film which may be considered objectionable in appearance even though it can be easily removed. Preliminary indications from a recently begun and still continuing exposure program are that this objection can be obviated by the application of a final thin chromium plate; early problems encountered in successfully plating bright chromium over tin-nickel appear to have been solved.

Acknowledgment

The authors are indebted to their respective companies for permitting publication of this paper. Particular thanks are due the Jones & Laughlin Steel Corporation for allowing use of their Pittsburgh exposure site.

Manuscript received Nov. 25, 1957. This paper was prepared for delivery before the Buffalo Meeting, Oct. 6-10, 1957.

Any discussion of this paper will appear in a Discussion Section to be published in the December 1958 JOURNAL.

REFERENCES

1. N. Parkinson, *J. Electrodepositors Tech. Soc.*, **27**, 129 (1951).
2. H. N. Rooksby, *ibid.*, **27**, 153 (1951).
3. A. E. Davies, *Trans. Inst. Met. Finishing*, **31**, 401 (1954).

4. F. A. Lowenheim, *Proc. Am. Electroplaters' Soc.*, **41**, 276 (1954).
5. S. C. Britton and R. M. Angles, *J. Electrodepositors Tech. Soc.*, **27**, 293 (1951).
6. V. R. Ramanathan, *Trans. Inst. Met. Finishing*, **34**, 1 (1957).
7. Metal & Thermit Corporation Data Sheet No. 140 (1956).
8. S. C. Britton and R. M. Angles, *Trans. Inst. Met. Finishing*, **29**, 26 (1953).
9. A. G. Gray, Editor, "Modern Electroplating," John Wiley & Sons, Inc., New York (1953).
10. H. A. Pray, *Proc. ASTM*, **49**, 231 (1949).
11. F. A. Lowenheim, *Proc. Amer. Electroplaters' Soc.*, **44**, 42 (1957).

Studies of Natural Convection at Vertical Electrodes

N. Ibl and R. H. Müller

Department of Physical Chemistry and Electrochemistry,
Swiss Federal Institute of Technology, Zurich, Switzerland

ABSTRACT

The hydrodynamic flow near vertical electrodes in electrolysis with natural convection was studied optically. The velocity distribution was measured for various experimental conditions. The flow velocities are calculated for the case of a constant current density along the electrode by the von Kármán-Pohlhausen integral method and compared with the experimental data. In the theoretical derivation various assumptions are made concerning the shape of the velocity and concentration profiles, and their influence on the computed values of the maximum flow velocities is discussed.

Mass transfer to or from the electrodes plays an important role in electrolysis. It is accomplished in general by diffusion, migration, and convection.

A hydrodynamic flow is usually present even in a solution which is not artificially stirred. This flow is called natural or free convection. It is due to the density differences between the electrode layer and the bulk of the bath, which cause, with vertical electrodes, an upward or downward flow of the solution, depending on whether the density of the electrode layer is smaller or greater than in the bulk.

Velocity distribution near the electrode is shown schematically in Fig. 1. The velocity is zero at the electrode surface, increases until a maximum is reached, then decreases again. The comparatively small region near the interface in which the upward or downward flow occurs primarily is called the hydrodynamic (or velocity) boundary layer. Similarly, the diffusion layer is defined as the region in which the concentration is significantly different from that in the bulk.

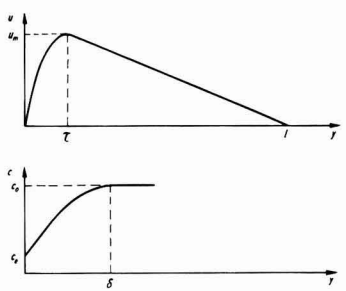

Fig. 1. Concentration and velocity distribution near the electrode (schematic).

The theory of mass transfer by natural convection to plane vertical electrodes has received much attention in recent years (1-7). The limiting current and the thickness of the diffusion layer under free convection conditions have been studied experimentally by various authors (7-13). However, no investigation of the convective flow itself has been made so far. In the present paper, measurements of the hydrodynamic boundary layer at plane vertical electrodes are reported and compared with the theory. The velocities of the flow are calculated according to the method of von Kármán-Pohlhausen (28, 27). Generalized concentration and velocity profiles are used in the calculation, and some general aspects of the application of von Kármán-Pohlhausen's method are discussed.

Theoretical

Mass transfer calculations are usually carried out along the same lines as heat transfer computations, since the basic differential equations of the problem are formally the same in both cases. In order to be able to carry out the integration of these equations, however, the boundary conditions must be known. In the case of heat transfer to a vertical plate it is usually assumed that the temperature, and therefore the density of the fluid, is the same along the surface of the plate. In the electrolysis problem a constant fluid density means that the concentration of the bath remains the same along the surface of the electrode. This condition is realized in the case of the limiting current, where, in a cathodic process, the concentration of the ions reduced at the electrode is practically zero everywhere at the surface of the electrode. It follows from the theory that under such conditions the local current density should vary from the lower to the upper edge of

a vertical electrode; this has been confirmed by the experiment (1). However, when the current density is smaller than about one half of the limiting value, the local current density (rather than the concentration) was found to remain constant from bottom to top (15, 29). These experimental results are in agreement with a recent calculation made by Wagner (2). In electrolysis problems, therefore, two typical cases may be distinguished, according to whether the liquid density or the current density is the same along the interface.

Constant Liquid Density

The velocity of the flow for a constant liquid density has been calculated by various authors (1, 5, 7). The maximum velocity u_m (*see* Fig. 1) in the direction parallel to the electrode is given by (for the case of a metal deposition from a pure salt solution, without addition of supporting electrolyte):

$$u_m = K \left(\frac{g\alpha D x (c_o - c_e)}{\nu} \right)^{1/2} \qquad (I)$$

where g is the gravitational acceleration, D the diffusion coefficient, ν the kinematic viscosity, and x the distance from the lower end of the cathode. α is the densification coefficient[1] [$\alpha = (1/\rho)(d\rho/dc)$], and $c_o - c_e$ is the concentration difference between the electrode surface (c_e) and the bulk of the solution (c_o). In the case of the limiting current, c_e is zero. K is a numerical constant, the value of which depends somewhat on the kind of the approximation used in the derivation of Eq. (I). Keulegan (5) has integrated the basic differential equations of convective mass transfer with the help of Prandtl's boundary layer simplifications in a way similar in principle to that used by Pohlhausen for heat transfer [*see* (16)], whereas Wagner (1) and Wilke, Tobias, and Eisenberg (7) employed the von Kármán-Pohlhausen integral method (22a, b). Values of K derived from the calculation of these authors are shown in Table I.

Ostrach (14) has integrated the differential equations of natural convection heat transfer by means of an IBM Card Programmed Electronic Calculator and has thus obtained the most nearly rigorous solution available at present. Owing to the analogy between heat and mass transfer Ostrach's results for high Prandtl numbers can be used to calculate the flow velocities involved in mass transfer in aqueous solutions. The value of K thus obtained has also been entered in Table I.

If the current density is smaller than the limiting one, $c_o - c_e$ is not known and must be calculated from the mean current density i over the whole electrode surface. If the relation connecting $c_o - c_e$ with i is combined with Eq. (I) the following relation is obtained

$$u_m = K' \left(\frac{g\alpha i n_A}{zF\nu} \right)^{2/5} D^{1/5} x^{1/2} h^{1/10} \qquad (II)$$

where F means Faraday's constant, z the valence of the cations reacting at the electrode, n_A the transference number of the anion, and h the total height of the electrode. The values of the numerical constant K' depend again on the method used in the integration of the basic differential equations of the problem and are also indicated in Table I.

Relation (II) is again valid for the case of a constant liquid density. This condition, as has been pointed out above, is in general not realized at current densities well below the limiting.

Constant Current Density

The case of a constant current density (in the electrolysis problem) and of a constant heat flux (in the corresponding heat transfer problem) has been considered by Wagner (2)[2] and by Sparrow (17, 18), respectively. They have not calculated, however, the velocities of the hydrodynamic flow at high Prandtl numbers.

The following derivation will be carried out for the case of a cathodic deposition from a pure salt (without addition of supporting electrolyte).[3] It can, however, be easily extended to other cases, especially to that of an anodic process.

In the derivation the von Kármán-Pohlhausen integral method (28, 27) as used by Eckert (22a, b), Wagner (2, 1), Wilke, Tobias, and Eisenberg (7) will be employed. In this method one refrains from fulfilling Prandtl's boundary layer equations for each infinitesimal volume element of the boundary layer and fulfills them instead only as a mean over the whole breadth of the boundary layer.

A volume of liquid limited by the control planes shown in Fig. 2 is considered. Plane ABCD is parallel to the electrode surface and is located at distance l from the electrode where the velocity of the flow can be assumed to be zero. The volume is further limited by the surface A'B'C'D' located at the interface electrode solution and by the two horizontal planes of unit width BCB'C' and ADA'D' separated by the small vertical distance dx (x means in the

[1] A summary of the symbols used and of the corresponding dimensions is given at the end of the paper.

Table I. Values of K and K'

K	K'	Method
1.83	1.99	Wagner (1)
0.82	0.99	Keulegan (5)
0.98	1.15	Ostrach (14)
0.77	0.90	Wilke, Tobias, and Eisenberg (7)

[2] The authors are indebted to C. Wagner for having kindly sent them the manuscript of this paper.

[3] Further assumptions, which must be made in the derivation, are discussed later, together with the possibilities to realize them experimentally.

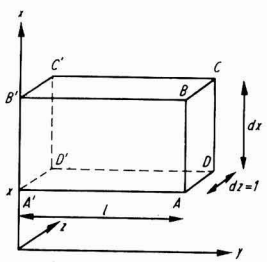

Fig. 2. Control volume for theoretical derivation

following the vertical direction, y the direction perpendicular to the electrode surface).

Under steady-state conditions the change in momentum per unit time of all the liquid particles entering and leaving the volume thus defined must be equal to the external forces acting on the volume, i.e., the buoyancy force and the shear stress at the electrode surface. This leads to the equation:

$$\frac{d}{dx}\int_0^1 u^2\,dy = \alpha g\int_0^1 \theta dy - \nu\left(\frac{du}{dy}\right)_e \qquad \text{(III)}$$

with

$$\theta = c_o - c$$

where u and c mean the velocity in the x direction and the concentration at the distance y from the electrode, respectively. $(du/dy)_e$ is the velocity gradient at the interface.

The corresponding equation for mass transfer is obtained by equating the rates at which the cations reacting at the electrode enter and leave the volume. This gives the relation:

$$\frac{d}{dx}\int_0^1 u\,\theta dy = -D\left(\frac{d\theta}{dy}\right)_e \qquad \text{(IV)}$$

where $(d\theta/dy)_e$ is equal to $-(dc/dy)_e$, i.e., to the negative concentration gradient at the interface.

To carry out the integration some assumptions must be made concerning the velocity and concentration profile. In the application of the von Kármán-Pohlhausen method to natural convection heat and mass transfer the concentration (or temperature) distribution has been usually approximated by (1, 7, 18, 22b)

$$\theta = \Theta\left(1-\frac{y}{\delta}\right)^2 \qquad \text{(V)}$$

where in our case Θ means the concentration reduction at the interface ($\Theta = c_o - c_e$). δ is the thickness of the diffusion layer, i.e., the distance at which the concentration is equal to the value in the bulk solution.

Concerning the velocity distribution the two following assumptions have been hitherto made (1, 7, 18, 22b)

$$u = U_1\left[2\frac{y}{\delta} - \left(\frac{y}{\delta}\right)^2\right] \qquad \text{for } o < y < \delta \qquad \text{(VI)}$$

$$u = U_1\frac{y}{\delta}\left(1-\frac{y}{\delta}\right)^2 \qquad \text{for } o < y < \delta \qquad \text{(VII)}$$

In the first case [Eq. (VI)] it is postulated that the velocity reaches its maximum at the outer limit of the diffusion layer (at $y = \delta$) and falls off very slowly afterward. The assumption is therefore made, that the thickness 1 of the hydrodynamic boundary layer is much greater than that of the diffusion layer. In the case of Eq. (VII) the velocity reaches its maximum at $y = \delta/3$ and is equal to zero at $y = \delta$. This means that the thicknesses of the diffusion layer and of the hydrodynamic boundary layer are now supposed to be the same.

In the case of a constant liquid density along the interface the values obtained for the maximum velocities when using Eq. (VI) ($1 >> \delta$) are more than twice as large as those computed with Eq. (VII) ($1 = \delta$).[4] The limiting current is also substantially different in both cases. Substantially different values for the maximum flow velocities are similarly obtained in the case of a constant local current density depending on whether one assumes $1 >> \delta$ or $1 = \delta$. This can be easily derived from the calculations made below.

Theoretical considerations (1) show that it is very likely that the hydrodynamic boundary layer is much thicker than the diffusion layer and this has been confirmed by the authors' experiments (19). Nevertheless, the maximum velocities (and also the limiting currents) calculated with Eq. (VII) ($1 = \delta$) fit the experimental data much better than those obtained with Eq. (VI). The unsatisfactory situation therefore arises that the wrong assumption leads to results which are in better agreement with the experiment.

In order to get a better insight into the influence exerted by the velocity and concentration profiles assumed in the derivation, the following calculation is carried out with profiles represented by more general functions than those given by Eqs. (V) to (VII). The velocity distribution is approximated by

$$u = U_1\left[\lambda\frac{y}{\tau} - \left(\frac{y}{\tau}\right)^\lambda\right] \qquad \text{for } o \leqq y \leqq \tau \qquad \text{(VIII)}$$

and

$$u = U_1\left[1-\frac{y-\tau}{\epsilon\tau}\right](\lambda-1) \quad \text{for } \tau \leqq y \leqq (\epsilon+1)\tau \qquad \text{(IX)}$$

where τ means the distance at which the maximum velocity is located (*see* Fig. 1).

The concentration profile is approximated by

$$\theta = \Theta\left(1-\frac{y}{\eta\tau}\right)^\omega \quad \text{with} \quad \eta\tau = \delta \qquad \text{(X)}$$

ϵ, η, λ, and ω are parameters whose variation allows the assumed profiles to change considerably. ω influences the shape of the concentration distribution. Variation of λ allows the shape of the velocity profile to change up to the maximum velocity [whose value is given by $u_m = U_1(\lambda-1)$]. For values of y greater than τ the velocity profile is assumed to be a straight line, whose slope depends on the value of ϵ. Finally, variation of η allows the position of the velocity maximum to change with respect to δ.

Insertion of Eqs. (VIII) to (X) into the momentum equation (III) yields upon integration[5]

$$\frac{d}{dx}(\Lambda U_1^2\tau) = \frac{\alpha g\eta\tau\Theta}{\omega+1} - \frac{\nu U_1\lambda}{\tau} \qquad \text{(XI)}$$

with

$$\Lambda = \frac{\lambda^2}{3} - \frac{2\lambda}{\lambda+2} + \frac{1}{2\lambda+1} + \frac{\epsilon}{3}(\lambda-1)^2 \qquad \text{(XIa)}$$

In the same way one obtains from Eq. (IV) (for values of $\eta \geqq 1$)

$$\Phi\frac{d}{dx}(U_1\Theta\tau) = \frac{D\omega\Theta}{\eta\tau}$$

[4] It is interesting to note that when using Eq. (VII) the von Kármán-Pohlhausen method yields values which differ by less than 10% from those calculated by Keulegan (5), who employed a more involved method, but also assumed $1 = \delta$.

[5] For details, *see* Müller (20).

with

$$\Phi = \frac{\lambda(\eta-1)^{\omega+2}}{\eta^{\omega}(\omega+1)(\omega+2)}\left[\left(\frac{\eta}{\eta-1}\right)^{\omega+2} - \frac{\lambda-1}{\lambda\epsilon} - \frac{\omega+2}{\lambda(\eta-1)} - 1\right] - \eta^{\lambda+1} B_{1/\eta}(\lambda+1,\omega+1) \quad \text{(XII)}$$

where

$$B_a(b,c) = \int_0^a t^{b-1}(1-t)^{c-1}\,dt$$

means the incomplete beta function, whose numerical values have been tabulated by Pearson (21).

Let j_D denote the mass transfer rate per unit area due to diffusion at the interface

$$j_D = -D\left(\frac{d\theta}{dy}\right)_e = \frac{\omega\Theta D}{\eta\tau} \quad \text{(XIII)}$$

Values of τ, U_1, and Θ must be determined. In a way similar to that used in the case of a constant liquid density along the interface [*see*, for instance, Eckert (22b)] we try solutions of the form

$$U_1 = C_1 x^m \quad \text{(XIV)}$$

$$\tau = C_2 x^n \quad \text{(XV)}$$

$$\Theta = C_2 \frac{j_D \eta}{\omega D} x^n \quad \text{(XVI)}$$

Equation (XVI) takes into account that in our case the local current density, and therefore j_D, is constant over the whole electrode surface.

Standard calculating procedures lead then to the result

$m = 3/5 \quad n = 1/5$

$$u_m = U_1(\lambda-1) = (\lambda-1)C_1 x^{3/5} = \underbrace{(\lambda-1)\left(\frac{\omega\eta}{\Phi^3\lambda^2(\omega+1)^2}\right)^{1/5}\left(\frac{Sc}{Sc+\frac{7\omega\Lambda}{5\eta\Phi\lambda}}\right)^{2/5}\left(\frac{g\alpha j_D}{\nu D}\right)^{2/5} D^{3/5}}_{A'} x^{3/5} \quad \text{(XVII)}$$

$$\tau = C_2 x^{1/5} = \underbrace{\left(\frac{(\omega+1)\omega^2\lambda}{\Phi\eta^3}\right)^{1/5}\left(\frac{Sc+\frac{7\omega\Lambda}{5\eta\Phi\lambda}}{Sc}\right)^{1/5}\left(\frac{\nu D^2}{g\alpha j_D}\right)^{1/5}}_{E'} x^{1/5} \quad \text{(XVII}a\text{)}$$

where $Sc = \nu/D$ = Schmidt number. Equation (XVII) relates the maximum velocity u_m to the mass transfer rate j_D and to the height x at which it is measured. It allows one to calculate u_m for various values of the parameters ϵ, η, λ, ω.

Equation (XVII) holds true too for the case of heat transfer with a uniform heat flux if α is replaced by the thermal expansion coefficient (degrees^{-1}), D by the thermal diffusivity (cm^2/sec) and j_D/D by q/k where q means the heat flux (cal/cm^2 sec) and k the thermal conductivity (cal/cm sec degree).

If Sc is greater than about 1000, as is usually the case for mass transfer in aqueous solutions (in our experiments Sc was ca. 2800) $7/5\ (\omega\Lambda)/(\eta\Phi\lambda)$ can be neglected against Sc for all the values of ϵ, η, λ, ω indicated in Table II (except for the last line).

Table II. Numerical values of A, E, and the auxiliary function ϕ for various combinations of the parameters ϵ, η, λ, ω

ω	λ	η	ϵ	ϕ	A	E
2	1.2	1.8	7	0.078	0.71	2.03
3	2	1.8	7	0.227	1.41	2.24
2	1.2	1	7	0.032	1.08	3.42
2	2	1	7	0.133	1.87	2.86
3	1.2	1.8	7	0.052	0.88	2.72
2	2	1.8	7	0.347	1.19	1.64
2	2.5	1.8	7	0.511	1.29	1.58
2	2.5	2.5	7	0.802	1.05	1.19
3	2.5	2.5	7	0.539	1.29	1.60
2.5	1.8	2.2	7	0.306	1.10	1.65
2.5	1.5	2.2	7	0.199	0.96	1.74
2.5	1.8	1.9	7	0.248	1.21	1.88
2.5	1.8	1.5	7	0.174	1.31	2.32
2	1.8	2.2	7	0.378	0.98	1.40
3	1.8	2.2	7	0.253	1.20	1.89
2.5	1.8	2.2	12	0.306	1.10	1.65
2.5	1.8	2.2	20	0.307	1.10	1.65
2.5	2.5	2.5	7	0.639	1.19	1.40
2.3	1.7	2.1	10	0.277	1.04	1.63
5	5	5	10	2.02	1.28	1.24
5	1.5	1.5	10	0.049	1.9	4.24
2	1.5	5	10	0.648	0.55	0.74
2	5	1.5	10	0.876	1.84	1.83
5	5	1	10	0.119	4.10*	6.4*

* In this case $7/5\ (\omega\lambda)/(\eta\phi\lambda)$ is not negligibly small in comparison to Sc and A' [Eq. (XVII)] instead of A [Eq. (XVIII)] is to be used to calculate u_m. The values indicated in the table are in this case A' instead of A and E' [Eq. (XVIIa)] instead of E [Eq. (XIX)], for a Schmidt number of 1000.

Furthermore, in the case of electrolysis j_D is connected with the current density i by the relation

$$j_D = \frac{i n_A}{zF}$$

where z means the valence of the cation deposited and n_A is the transference number of the anion.

Equation (XVII) thus takes the form

$$u_m = \underbrace{(\lambda-1)\left(\frac{\eta\omega}{\Phi^3\lambda^2(\omega+1)^2}\right)^{1/5}\left(\frac{g\alpha i n_A}{zF\nu}\right)^{2/5} D^{1/5}}_{A} x^{3/5} \quad \text{(XVIII)}$$

The flow velocity is proportional to the $(2/5)^{\text{th}}$ power of the current density and to the $(3/5)^{\text{th}}$ power of the height.

The distance τ from the electrode at which the velocity maximum is located is given by

$$\tau = \underbrace{\left(\frac{(\omega+1)\omega^2\lambda}{\Phi\eta^3}\right)^{1/5}}_{E}\left(\frac{zF\nu D^2}{g\alpha i n_A}\right)^{1/5} x^{1/5} \quad \text{(XIX)}$$

In Table II A and E have been calculated for various values of ϵ, η, λ, and ω. It is seen that the assumed profiles have a great influence on the results obtained by the von Kármán-Pohlhausen method. Relatively small changes in η, λ, and ω alter u_m and τ to a rather great extent. The value of ϵ, however, is not critical. Therefore it can be said that the result of the calculation is strongly affected by the relative location of the velocity maximum (η) and by the shape of the velocity profile up to the maximum (λ), but not by the slope of the profile beyond the maximum (toward the bulk solution).

The velocity profiles experimentally determined in this study (Fig. 7 and 8) are in approximate

agreement with the following values of ϵ, η, and λ: $\lambda = 1.2\text{-}2$; $\eta = 1.4\text{-}2.2$; $\epsilon = 5\text{-}15$. The interferometrically measured concentration profile corresponds to a value of ω of 2-3 (12).

Use of the following profiles is suggested in the application of the von Kármán-Pohlhausen method to the uniform mass transfer rate problem

$$\omega = 2.3 \qquad \eta = 2.1 \qquad \theta = \Theta\left(1 - \frac{y}{2.1\tau}\right)^{2.3} \qquad \text{(XX)}$$

$$\lambda = 1.7 \quad u = U_1\left[1.7\,\frac{y}{\tau} - \left(\frac{y}{\tau}\right)^{1.7}\right] \quad \text{for } o \leqq y \leqq \tau \qquad \text{(XXI)}$$

$$\epsilon = 10 \quad u = 0.7\,U_1\left(1 - \frac{y-\tau}{10\tau}\right) \quad \text{for } \tau < y < 11\tau \qquad \text{(XXII)}$$

These profiles are in reasonable agreement with the measured profiles and the values of u_m and τ calculated with Eqs. (XX) to (XXII) fit the experimental data fairly well.

For the comparison with the experiment it is convenient to write Eqs. (XVIII) and (XIX) in dimensionless form

$$\frac{u_m\,x}{D} = A\,(Sc\ \mathrm{Gr}^*)^{2/5} \qquad \text{(XXIIa)}$$

$$\frac{\tau}{x} = E\,(Sc\ \mathrm{Gr}^*)^{-1/5} \qquad \text{(XXIIb)}$$

where

$$\mathrm{Gr}^* = \frac{j_D g \alpha x^4}{\nu^2 D} = \frac{g \alpha i n_A x^4}{2zF\nu^2 D} \qquad \text{(XXIII)}$$

The dimensionless Group Gr* is the modified Grashof number, which plays the same role in the case of a uniform mass transfer rate as the usual Grashof number in the case of a uniform fluid density.

Experimental

Experimental Procedure[5]

Flow velocities were measured by means of a suspension of a suitable fraction of colophonium, whose particles hovered in the solution without sedimenting. The colophonium fraction was prepared by sedimentation analysis.

The particles dragged along by the stream were made visible by a dark field method shown in Fig. 3. Because of the small extent of the hydrodynamic boundary layer and the relatively low light-intensity of the small moving particles, lens D must provide (in plane B) an image of great brightness, good correction, and suitable magnification (about 10 times). Special care in the optical arrangement had to be given to prevent reflections of the illuminating light beam.

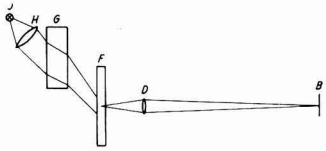

Fig. 3. Experimental arrangement for the study of the hydrodynamic boundary layer. B = image plane (camera); D = microlens (f = 46, 25, or 16 mm); F = electrolysis cell; G = liquid heat filter (6 cm $CuSO_4$ 0.1 m); H = condenser; J = light source (6 v, 6A lamp).

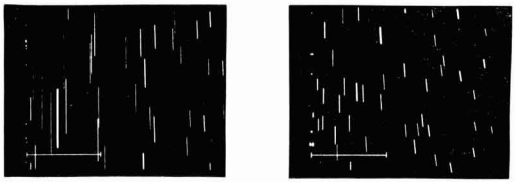

Fig. 4. Visualization of flow velocities. Both pictures were obtained with cell No. 1 4 min after the beginning of electrolysis (i = 1 ma/cm², exposure time 1 sec). Height: (a) (left) x = 7 cm; (b) (right) x = 1.5 cm.

The particles appear as bright spots on a dark background. Flow velocity can be measured either visually with the help of a suitable scale or photographically from the length of the lines obtained on the photographic plate and the exposure time (Fig. 4). Under optimum illuminating conditions the velocities in the experiments of Fig. 6 to Fig. 8 could be determined down to an electrode distance of 0.01 mm. At higher current densities the large refractivity gradient within the diffusion layer causes a blurring of the particles and a changed magnification within the diffusion layer in comparison to that of the bulk solution. The measurements in the vicinity of the electrode are then more difficult and less accurate.

Because of the friction of the liquid at the cell walls the velocities must be measured at some distance from the latter (and therefore at some distance from the edge of the electrode). The electrode position cannot then in general be precisely located on the image in B without the help of additional devices. One of these consisted of a sheet of acryl glass of suitable design whose sharp edge was pressed against the electrode surface. The glass sheet was provided with a scale which allowed, by extrapolation, the location of the electrode surface within a hundredth of a mm.

At great current densities the velocities are high and the particles disappear rapidly from the field of view, so that measurements by the visual method become tedious. This difficulty can be circumvented by the use of two cylindrical lenses with axes perpendicular to each other, instead of the spherical lens D. This allows different magnifications in the vertical and horizontal directions, permitting the use of a horizontal magnification large enough for an accurate determination of the electrode distance and reducing the vertical magnification to such an extent that the velocity can be measured conveniently.

All the experiments were carried out with pure 0.6*M* $CuSO_4$ solutions (pH = 3.35) with plane copper cathodes and anodes. The electrode arrangement and the cell form were in principle the same as in a previous study (10), but the dimensions were different (Table III). Furthermore, in cells 3 and 5 the upper and lower edge of the electrode did not reach the free liquid surface and the cell bottom, respectively.

Table III. Dimensions of electrolysis cells (in mm)

Cell No.	Inside dimensions with electrodes mounted in cell			Electrode dimensions		Electrode position
	Width	Breadth*	Height	Width	Height	
1	5	48	140	5	140	Fills whole cross section
2	18	54	140	18	140	Fills whole cross section
3	20	170	450	20	150	At mid height
4	5	3, 15, 45	30	5	30	Fills whole cross section
5	4	12	150	4	30	At various heights

* i.e., distance cathode-anode.

Some measurements were made at the anode but all the experiments reported hereafter were carried out at the cathode.

Deviations from the Ideal Flow Pattern

In the theoretical considerations, idealized flow conditions are assumed. In the first part of the authors' experimental work deviations from these idealized conditions were studied and the circumstances under which the assumptions made in the theory are fulfilled were investigated.

1. In the theory it is postulated that the electrodes are infinitely large, i.e., that the friction at the cell walls as well as the influence of the free liquid surface and of the cell bottom can be neglected. Furthermore, it is admitted that the flow at the anode does not affect that at the cathode. The influence of these factors was studied with the help of various electrode arrangements and cells of various dimensions (*see* Table III).

Figure 5 shows velocity profiles measured with cells of various widths.[6] It is seen that down to a cell width of 5 mm no significant difference is observed. Further measurements showed that at a distance from the wall of 1 mm the velocity is practically the same as in the middle of the cell.

The free liquid surface causes a backward streaming, which starts some time after the beginning of electrolysis and substantially changes the shape of the whole hydrodynamic boundary layer. This effect has been described in more detail in an earlier paper (19) [*see* also (20)].

The influence of the cell breadth was studied with cell No. 4.

2. In the theory in its present state only steady-state conditions are considered. The time which elapses after switching on the current until steady-state conditions are reached increases with height and decreases with current density. Figure 6 shows velocity profiles measured at various times after the beginning of electrolysis. In this case the steady state was reached after 2 min.

3. In the theory it is assumed that the liquid is at rest when no electric current passes through the

[6] In Fig. 5 to 10 x means the height (over the lower cathode edge) at which the velocity is measured.

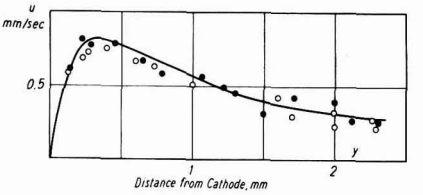

Fig. 5. Velocity profiles measured with cells of various widths with i = 1 ma/cm²; solid line, cell No. 1, x = 70 mm;[6] open circle, cell No. 2, x = 67 mm; solid circle, cell No. 3, x = 67 mm.

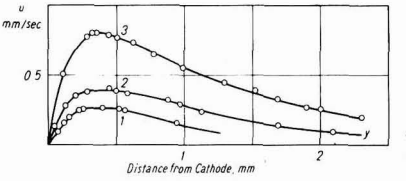

Fig. 6. Velocity profiles measured 0.5 (curve 1), 1 (curve 2), and 2 (curve 3) min after the beginning of electrolysis; cell No. 1, x = 70 mm, i = 1 ma/cm².

cell. This is not strictly realized in practice. Even hours after the solution has been filled into the cell a not negligible motion of the liquid is generally observed. It is due to small inhomogeneities in density caused by various reasons (evaporation of the solution, variations of the room temperature). Even small but rapid variations of the room temperature can give rise to flow velocities as large as 0.5 mm/sec. By careful elimination of evaporation and all causes of temperature inhomogeneities, it was possible to reduce the residual motion of the solution (i.e., the motion present without electric current) to 0.005 to 0.05 mm/sec. All the experiments reported in Fig. 5 to 10 were carried out under such conditions.

4. Finally, a laminar flow is postulated in the derivation of section on Constant Current Density. It was found that this condition is not realized at high current densities and great heights. A turbulence of the natural convective flow (clearly different from the backward streaming mentioned above) was for instance observed in cell No. 3 at a height of 80 mm, when the current density was greater than 20 ma/cm². The eddies which then form are similar to those which are described by Eckert (22c) for heat transfer to air.

Quantitative Results and Discussion

The experiments of Fig. 7 to 10 were carried out with cell No. 1. Conditions were such that the devi-

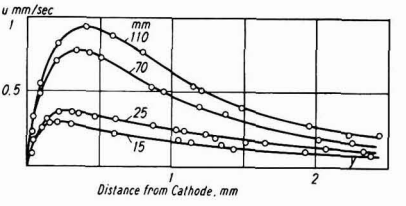

Fig. 7. Velocity profiles at heights of 15, 25, 70, and 110 mm; i = 1 ma/cm².

ations from the ideal flow pattern discussed in the preceding section were as small as possible.

Figure 7 shows the velocity profiles for various heights at a current density of 1 ma/cm² and Fig. 8 shows profiles for various current densities at a height of 70 mm.

The reproducibility of the measurements depended to some extent on the location in the cell. It was somewhat better at mid height than at the top or bottom of the electrode. It was also better near the maximum than in the outer part of the boundary layer (toward the bulk solution). In the case of the outer boundary this was probably due to the small remainders of the residual flow mentioned above.

The maximum velocity and the distance of the velocity maximum are given in Fig. 9-10 and in Table IV for various heights and current densities. The dimensionless groups $(u_m x)/D$ and τ/x are plotted logarithmically against Sc and the modified Grashof number Gr* in Fig. 9 and 10. Calculated values were computed from Eqs. (XXIIa) and (XXIIb) with A and E equal to 1.04 and 1.63, respectively (column 4 of Table IV, full lines of Fig. 9 and 10). These values of A and E are those which

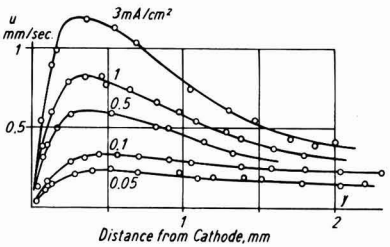

Fig. 8. Velocity profiles at current densities of 0.05, 0.1, 0.5, 1, and 3 ma/cm²; x = 70 mm.

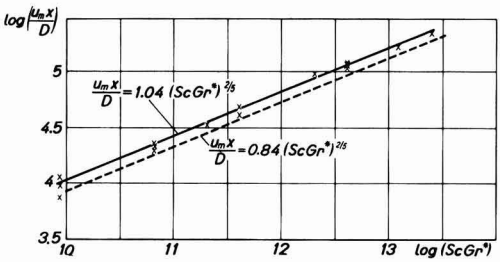

Fig. 9. General correlation of the maximum flow velocity; x = measured values.

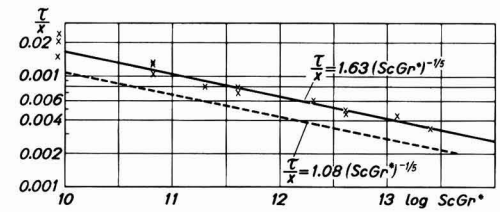

Fig. 10. General correlation of the distance of the velocity maximum from the electrode; x = measured values.

Table IV. Maximum flow velocities

i (ma/cm²)	x (cm)	u_m (mm/sec) measured	u_m (mm/sec) calculated from Eq. (XXIIa) with $A = 1.04$
0.05	7	0.22	0.24
0.1	7	0.32	0.31
0.5	7	0.60	0.59
1	7	0.83	0.78
3	7	1.2	1.21
1	1.5	0.36	0.31
1	2.5	0.44	0.42
1	11.0	1.02	1.02

Total electrode height: 14.0 cm.

are obtained when the profiles represented by Eqs. (XX) to (XXII) are used in the von Kármán-Pohlhausen's integral method. The dotted lines were calculated with A and E values of 0.84 and 1.08, respectively, which correspond to the profiles given by Eqs. (V) and (VII). It is seen that the values calculated with the profiles suggested above [Eqs. (XX) to (XXII)] fit the experimental data better.[7] Finally, a rather poor agreement is observed when the profiles of Eqs. (V) and (VI) are used in the von Kármán-Pohlhausen method. Then u_m is about two times greater and τ is about 1.7 times greater than the experimental values.

The physical properties of $CuSO_4$ 0.6 m at 20°C used in the above computations were $z = 2$, $D = 4.74 \times 10^{-6}$ cm²/sec [intrapolated from data of Oeholm (24)], $\nu = 1.33 \times 10^{-2}$ cm²/sec [intrapolated from data from (23)], $\alpha = 140$ cm³/mole [calculated from the densities given in (25)], and $n_A = 0.71$ (26).

Manuscript received Aug. 19, 1957. This paper was prepared for delivery before the Cleveland Meeting, Sept. 30-Oct. 4, 1956.

Any discussion of this paper will appear in a Discussion Section to be published in the December 1958 JOURNAL.

[7] In the case of u_m the difference, however, is not large.

Notation

A, A', E, K, K' = numerical coefficients (*see* text).
c = concentration (moles/cm³) at distance y.
c_e = concentration (moles/cm³) at the electrode surface.
c_o = concentration (moles/cm³) in the bulk solution.
D = diffusion coefficient (cm²/sec).
F = Faraday's constant (coulomb/gr. equiv.).
g = acceleration of gravity (cm/sec²).
Gr* = modified Grashof number = $\dfrac{g\,\alpha\,i\,n_A\,x^4}{z\,F\,\nu^2\,D}$.
h = total height of cathode (cm).
i = current density (amp/cm²).
j_D = mass transfer rate/cm² due to diffusion (moles/cm² sec).
l = thickness of hydrodynamic boundary layer (cm).
n_A = transference number of anion.
Sc = Schmidt number = ν/D.
u = velocity of hydrodynamic flow in x direction (cm/sec).
u_m = maximum velocity of hydrodynamic flow in x direction (cm/sec).
U_1 = proportionality factor in assumed velocity profile [Eqs. (VI) to (IX)].
x = distance from lower end of cathode (coordinate in the vertical direction) (cm).
y = distance from the electrode (coordinate in the direction perpendicular to the electrode surface) (cm).
z = valence of deposited cation (gr. equiv./mole).
α = densification coefficient (cm³/mole) = $1/\rho\ (d\rho/dc)$.
δ = thickness of diffusion layer (cm).
ν = kinematic viscosity (cm²/sec).
ρ = density (g/cm³).
θ = $c_o - c$.
Θ = $c_o - c_e$ = concentration reduction at interface.
τ = distance of velocity maximum from electrode (cm).
ϕ, Λ = auxiliary functions defined by Eq. (XIa) and (XII), respectively.
$\epsilon, \eta, \lambda, \omega$ = variable parameters (*see* text).

REFERENCES

1. C. Wagner, *J. (and Trans.) Electrochem. Soc.*, **95**, 161 (1949).
2. C. Wagner, *This Journal*, **104**, 129 (1957).
3. C. W. Tobias, M. Eisenberg, and C. R. Wilke, *ibid.*, **99**, 359C (1952).
4. J. N. Agar, *Disc. Faraday Soc.*, **1**, 31 (1947).
5. G. H. Keulegan, *J. Research Nat. Bur. Standards*, **47**, 156 (1951).
6. B. Levich, *Acta Physicochim. U.R.S.S.*, **19**, 125 (1944).
7. C. R. Wilke, C. W. Tobias, and M. Eisenberg, *Chem. Eng. Progr.*, **49**, 663 (1953).
8. C. R. Wilke, M. Eisenberg, and C. W. Tobias, *This Journal*, **100**, 513 (1953).
9. A. Brenner, *Proc. Am. Electroplaters' Soc.*, **1940**, 95; **1941**, 28.
10. N. Ibl, Y. Barrada, and G. Trümpler, *Helv. Chim. Acta*, **37**, 583 (1954).
11. N. Ibl, *ibid.*, **37**, 1149 (1954).
12. N. Ibl, R. Müller, and K. Frei, Proceedings of 8th meeting of the International Committee for Electrochemical Thermodynamics and Kinetics (in press).
13. R. E. Wilson and M. A. Youtz, *Ind. Eng. Chem.*, **15**, 603 (1923).
14. S. Ostrach, *Nat. Advisory Comm. Aeronaut: Tech. Note*, 2635 (February, 1952).
15. N. Ibl, W. Rüegg, and G. Trümpler, *Helv. Chim. Acta*, **36**, 1624 (1953).
16. H. Schlichting, "Grenzschicht-Theorie," p. 257, G. Braun, Karlsruhe (1951).
17. E. M. Sparrow and J. L. Gregg, *Trans. Am. Soc. Mech. Eng.*, **78**, 435 (1956).
18. E. M. Sparrow, *Nat. Advisory Comm. Aeronaut. Tech. Note* 3508 (July, 1955).
19. N. Ibl and R. Müller, *Z. Elektrochem.*, **59**, 671 (1955).
20. R. Müller, Dissertation, Eidgenössische Technische Hochschule, Zürich (1956).
21. K. Pearson, Tables of the Incomplete Beta-Function, Cambridge (1934).
22. E. R. G. Eckert, "Introduction to the Transfer of Heat and Mass," McGraw-Hill Book Co., New York (1950) (*a*) p. 66 ff. (*b*) p. 158 ff, (*c*) p. 169-170.
23. International Critical Tables, **5**, 14 (1929).
24. L. W. Oeholm, *Soc. Sci. Fennica, Comm. Phys.-Math.*, **12**, 1 (1943).
25. "Handbook of Chemistry and Physics," **37**, 1836 (1955).
26. Landolt-Börnstein, *Hauptwerk*, **2**, 1104.
27. Th. v. Kármán, *Z. ang. Math. Mech.*, **1**, 233 (1921).
28. K. Pohlhausen, *ibid.*, **1**, 252 (1921).
29. N. Ibl and L. Ramalhete, Proceedings of 8th meeting of the International Committee for Electrochemical Thermodynamics and Kinetics (in press).

The Preparation of Uranium Metal by the Electrolytic Reduction of Its Oxides

L. W. Niedrach[1] and B. E. Dearing

Knolls Atomic Power Laboratory,[2] General Electric Company, Schenectady, New York

ABSTRACT

The background work is described for a new continuous process for the production of uranium by electrolytic reduction of its oxides in fused salt electrolytes. Unlike past electrolytic processes for uranium production, the present one is operated at temperatures which are above the melting point of the metal. The effect of current, salt bath composition, and other variables on efficiency and cell operation are discussed.

An electrolysis bath containing 20 mole % UF_4 diluted with a 50:50 mole % mixture of BaF_2 and MgF_2 was found to be satisfactory. With this bath anode current densities as high as 3.6 amp/cm^2 are feasible without encountering "anode effect." Any of the oxides of uranium can be used as the feed, but UO_3 appears to be preferable. The advantages of the new process are outlined, and the areas requiring additional development work are indicated.

Although electrochemical reduction of uranium halides and UO_2-UF_4 mixtures was employed for the preparation of the initial U used on the Manhattan Project (1, 2), this process was soon superceded by the bomb reduction of UF_4 with Mg metal (3). The latter process is still in active use and electrochemical methods have never seriously threatened to displace it as the production method. This is at least partially related to the fact that the electrochemical procedure and other similar procedures (4-7) have been operated at temperatures below the melting point of U. The bulky, dendritic deposits, which are produced by such processes, trap large quantities of the salt bath, and a series of steps is required before the metal can be separated from the salt and compacted. These steps are inherently expensive for labor, and result in losses and considerable recycle of material to the electrolysis cell.

In spite of the success of the Hall process for producing molten Al from its oxide, no serious effort at developing a similar process for U has been reported. The attractiveness of such a process has been recognized before, but only a few isolated experiments have been reported in which UO_2 was electrolyzed successfully at temperatures above the melting point of U to produce beads of metal (8, 9). These results were never exploited further.

[1] Present Address: Research Laboratory, General Electric Co., Schenectady, N. Y.

[2] Operated by the General Electric Company for the U. S. Atomic Energy Commission under Contract No. W-31-109 Eng-52.

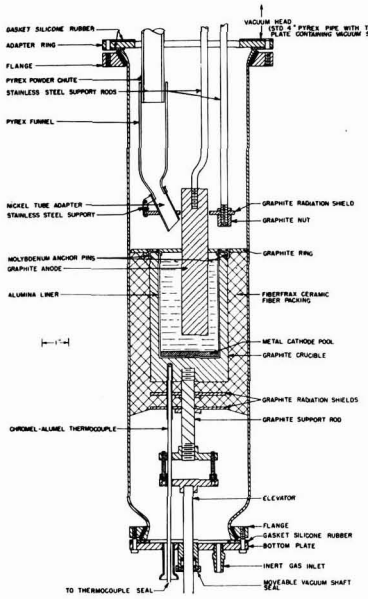

Fig. 1. Details of the electrolysis cell arrangement

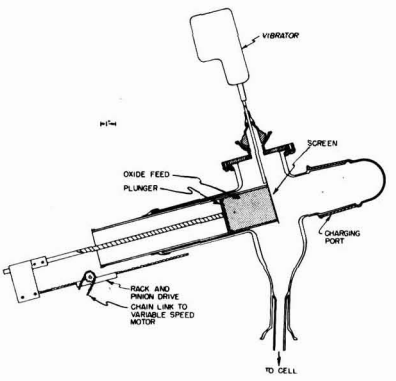

Fig. 2. Details of feed mechanism

It is with the development of a Hall-type process for U that the present work has been concerned. Studies of the variables connected with the electrolysis step itself are detailed in this paper. An engineering evaluation of the full process has been described in a separate report (10).

Experimental

Equipment and materials.—The principal features of the electrolysis cell and its enclosure are shown in Fig. 1, and additional details relating to the equipment are summarized in Table I. Not shown in detail in the drawing is the metal plate covering the top of the cell enclosure. Vacuum seals attached to this plate permitted the insertion of a powder chute for charging solids to the cell and the ¼ in. stainless steel support rods used for the electrodes, radiation shield, and other moveable parts. Cooling fans were positioned around each joint to prolong the life of the gaskets. While several alternate cell designs were employed during the course of the investigation, all were eventually discarded.

During a run inert gas was used to blanket the cell and sweep gaseous reaction products away from the cell for sampling and analysis. Flowmeters were installed in both the inlet and outlet lines, and suitable arrangements were provided for obtaining grab samples of the exhaust gases.

In some of the preliminary runs oxide was fed to the cells intermittently, but in most of the work a continuous feed was used. The positive displacement mechanism shown in Fig. 2 was employed for this purpose. When the oxide was loaded into the reservoir it was tamped frequently to insure uniform packing. Feed rates were then found to be uniform to within 5%. The vibrating screen was required across the face of the discharging oxide in order to obtain the uniform feed rate. Otherwise the oxide broke away in packed lumps and feeding was very irregular.

All chemicals other than the U compounds were standard C.P. materials. The U compounds were analyzed materials obtained from AEC sources. All salts used in the preparation of the baths were predried by heating in vacuo to about 350°C. The oxides were used without further treatment.

Operating procedure.—The graphite crucible and its liner were first degassed at 1200°C in vacuo to remove volatile products. Sufficient U was then added to form a 0.5 cm thick layer in the cell and melted at low pressure, preferably less than 10 μ. After filling the system with an inert gas, a mixture of the dry salts was sifted into the hot crucible and melted. The cell was then cooled and the system was cleaned because a thin opaque layer of salt dusted and spattered onto the walls of the furnace envelope during the salt charging procedure and interfered with observation of the cell.

The system was again evacuated and then filled with an inert gas atmosphere, the feed hopper was attached to the feed chute over the cell, and the cell was heated and placed into operation. At regular intervals during the electrolysis, grab samples of the off-gases were taken for mass spectrometric analysis.

At the completion of a run, the electrolysis circuit was opened, the electrodes were raised out of the salt bath, the feed flow was stopped, and the cell was allowed to cool slowly to room temperature. When cold, the crucible was opened, the contents

Table I. Cell Specifications

Material of construction	Graphite, National Carbon AUC Grade
Diameter of crucible, in.	3
Height of crucible, in.	4. 5
Operating temperature, °C	1200°-1250°C
Sparge gas	He or A
Sparge gas flowrate, l/min	1
Power supply	Opad selenium rectifier 0-12 v at 150 amp
Heating unit	Ajax 6 kw induction heater
Cell liner	Morganite recrystallized alumina
Cathode	Molten uranium pool
Anode	Graphite—1 in. diameter

were examined, and appropriate samples were taken for analysis.

Results and Discussion

When molten U is desired as the product, the severity of the operating conditions imposed by the high melting point and the chemical reactivity of the U metal limit the number of operating parameters that can be varied appreciably. Those which were considered important and therefore studied in detail were current, bath U content, and the properties of the oxide feed.

In addition some attention was given to the behavior of various fluorides as bath diluents. In this work NaF, LiF, BaF_2, and MgF_2 were studied. The former was unsatisfactory because of Na production, and LiF was found to be too volatile. The most satisfactory diluent material, and the one used in all of the detailed studies, was found to be a 50:50 mole % mixture of BaF_2 with MgF_2. In this system both components have low volatilities, and a wide range of liquidus compositions exists at the operating temperature of 1200°C (11).

The greatest difficulty throughout the course of the work was associated with the low solubility of UO_2 (the only important oxide in the bath because all higher oxides spontaneously decomposed) in the salt baths. Solubilities of the order of 2 wt % were measured in two widely different baths containing 9 and 84 wt % UF_4, respectively.[3] Coupled with this low solubility, the high density of the oxide resulted in rapid settling so that a dense sludge tended to form in the bottom of the cell. This interfered with coagulation of the product metal. As a result, it generally was not possible to produce a massive agglomerate. Instead, the product metal was usually in the form of small beads embedded in a matrix of salt and oxide. Typical examples of such beads are shown in Fig. 3. In addition to the material shown a considerable quantity of finer material was also always present.

In order to obtain the agglomerated product which is shown in the bottom of Fig. 3, special precautions were needed. In this case the product metal was collected in a suspended basket positioned in such a way that no unreacted oxide feed could settle in the basket. The cell design was considered too elaborate to be practical, and work with this type of cell was not pursued further.

[3] The authors are indebted to H. R. Hoekstra and I. Sheft of the Chemistry Division of Argonne National Laboratory for these analyses. Treatment of the samples with BrF_3 and $KBrF_4$ was employed to release the O_2 which was then measured manometrically (12).

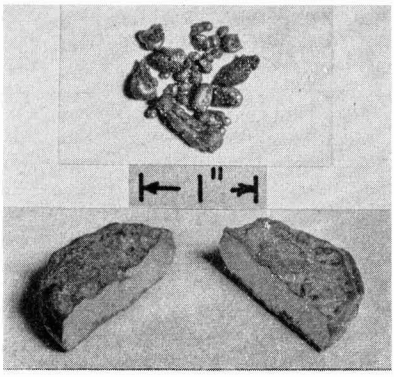

Fig. 3. Typical examples of product metal as produced in cell.

Effects of Current and Salt Bath Uranium Content

The effects of current and salt bath U content as variables were investigated concurrently. In this work the 50:50 mole % mixture of MgF_2 and BaF_2 was used as the bath diluent. The UF_4 content of the baths was varied from 10 mole % up to 40 mole %. Micronized UO_2, which was used as the feed, was added continuously. The feed was adjusted to supply oxide at a rate such that its complete electroreduction could be accomplished by 50% of the current flowing in the cell. It was hoped in this way to circumvent the oxide settling problem by driving the reduction reaction more toward completion.

A family of curves relating anode efficiency to salt-bath composition and electrolysis current (Fig. 4) shows that the efficiency increases as the UF_4 content of the bath is reduced. This may well be related to the fact that the U ion can exist in several different valence states. Then, when present at high concentrations one might expect a fair portion of the electrolysis current to be carried by cyclic oxidation and reduction between two such valence states, presumably U^{+3} and U^{+4}. The U content of the bath cannot be reduced indefinitely, however. When the U concentration becomes relatively low, one finds that it is impossible to operate with high currents because of the polarization that occurs. This is illustrated by the curves in Fig. 5 (polarization curves for 30 and 40 mole % UF_4 baths are essentially identical with that for the 20 mole % bath and were therefore omitted for clarity).

Polarization is attributed to the "anode effect" often observed during electrolysis of fluoride baths (13). Normally oxide is added to a bath to eliminate the effect, but a depolarizer such as U^{+3}, which can be oxidized to a higher valence state without production of a gaseous product, should also prevent its occurrence. It is probably through the latter mechanism that the anode effect is eliminated in the baths containing the higher concentrations of UF_4.

It is evident from Fig. 4 that the current has a somewhat lesser effect on the anode efficiency than that of the bath composition. The apparent maximum occurring at 50 amp does not appear to be real,

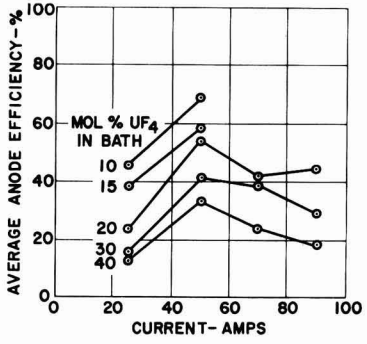

Fig. 4. Effect of current and salt bath composition on efficiency.

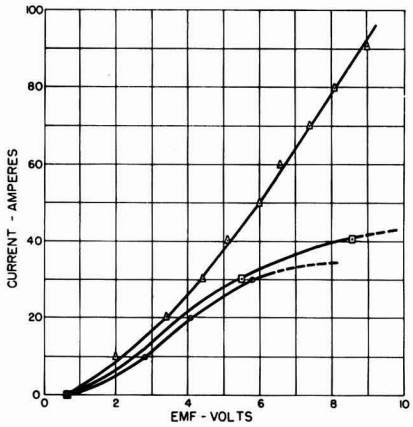

Fig. 5. Polarization curves—circle with dot 10, square with dot 15, triangle with dot 20 mole % UF_4 in bath.

but is related to the fact that the data for operation at 50 amp were always obtained at the start of a series of tests with a new bath. As a result any oxide originally present in the salt bath as an impurity was also available for reduction at that time and added to the apparent efficiency of operation. The data for the other currents are, however, reliable, and there is a real advantage to operating at the higher currents in preference to operation at 25 amp.

In addition to their effect on efficiency, the influence of current and bath composition on the composition of the off-gases was examined. In all cases, except that employing the 10 mole % UF_4 bath, CO and CO_2 were the major gaseous products with the CO content falling in the range 75-82%. In the run with the 10 mole % UF_4 bath the CO content averaged 50%. While CO_2 was again the other major constituent, in this case CF_4 contents beween 5 and 10% were also found. The CF_4 content of the gas from the run with the 15 mole % UF_4 bath averaged slightly less than 1%, and in all other cases the CF_4 content of the off-gases was equal to or less than 0.1%. Neither O_2 nor F_2 were ever detected in the off-gases.

For practical purposes, operating conditions can be optimized. In order to avoid polarization effects at the anode as well as to minimize CF_4 formation, UF_4 bath contents in excess of 15 mole % are desirable. On the other hand, because high UF_4 contents result in decreased efficiencies, it would appear that a bath containing about 20 mole % UF_4 would be a practical compromise.

Since there seemed to be no serious decrease in efficiency associated with cell operation up to 90 amp (about 1.5 amp/cm^2) and since higher current densities result in smaller cell sizes, it was of interest to determine the maximum current density that could be tolerated at the anode with a 20 mole % UF_4 bath. This was found to be 3.6 amp/cm^2.

Behavior of Several Oxides in the Process

The history of a U oxide has a marked effect on its ease of conversion to UF_4 (14). To test whether a similar effect is present in the electroreduction of U oxide, a number of runs were performed with oxide feeds having variations in physical and chemical characteristics. For this purpose various samples of UO_2, U_3O_8, and UO_3 were used. It was felt that the UO_3 might well have considerable advantage over U_3O_8 or UO_2 as a feed because it is prepared from uranyl nitrate by reactions occurring at lower temperatures than subsequent reduction operations. Reactivity would therefore be expected to be higher because there is less chance for sintering to occur.

This series of runs was made using a continuous feed of oxide to the cell. On the basis of the previous data, the bath containing MgF_2, BaF_2, and 20 mole % UF_4 was used. Operation was at 70 amp, and the oxide feed rate was again adjusted to correspond to about 50% current efficiency. With the exception of the short run with U_3O_8, all were continued for a period of about 4 hr during which time approximately 400 g of oxide was fed to the cell. A charge of U metal weighing about 250 g was added at the start of each run to serve as a molten metal cathode.

Data obtained during runs with micronized UO_2, peroxide U_3O_8, and denitration UO_3 are plotted in Fig. 6 to give an indication of the efficiencies obtained as well as the stability of operating conditions. It was observed qualitatively that the oxide settling problem persisted in all cases, and the typical sludge intermixed with metallic beads was found in the bottom of the cell at the end of each run. The CF_4 content of the off-gases was invariably less than 0.1%.

Some effort was made in these runs to determine whether gross changes in bath composition occurred during extended electrolysis. Samples of the frozen salts were therefore analyzed at the end of the runs. Because of segregation that occurred during the slow cooling of the melt, considerable scatter in the data was observed. On the average, however, the final concentrations were within 10% of those at the start for each of the cations in the bath.

In calculating the efficiencies shown in Fig. 6, a correction was first applied to the off-gas data to allow for any gases produced by thermal decomposition of the higher oxides. The remainder of the anode gases were then assumed to have been formed during the electrolytic reduction of UO_2 to metal. The efficiency then corresponds to the per cent of the feed oxide that was reduced to metal, which is the parameter of greatest interest in this work.

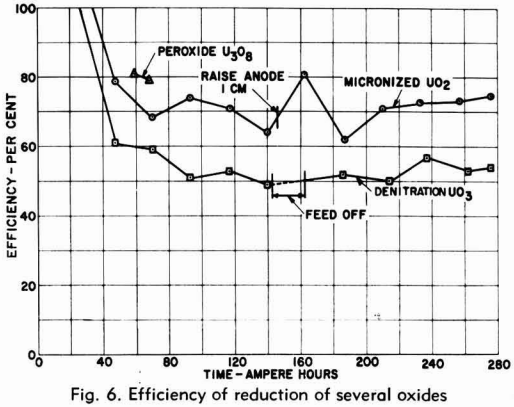

Fig. 6. Efficiency of reduction of several oxides

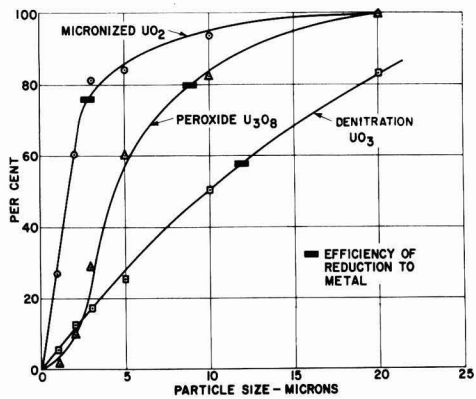

Fig. 7. Particle-size distributions for several oxides

From the results for the runs with different oxides, there does not appear to be any strong indication that one is preferable to another. If anything, the data indicate that UO_3 is a poorer feed than the other oxides. Since this was not expected, it is of interest to consider the efficiencies in the light of the particle size distributions of the three oxides. This can be done by referring to Fig. 7. On each of the curves a bar has been drawn at the percentage corresponding to the average efficiency of reduction of the feed to metal. One can then make the reasonable assumption that the smaller particles are reduced rapidly, while those above the line of demarcation are reduced more slowly and, therefore, settle out to form the sludge. When considered in this light, the UO_3 does appear to have advantages over the other oxides because much larger sized particles were present in the feed and a high percentage of the larger sized particles was actually reduced.

In view of the results obtained, it would appear desirable to perform a series of experiments employing a single feed, but with different particle size distributions. For such a series, it might be useful to feed directly from the size reducer into the cell. It might also be useful to correlate efficiencies with the reactivity of the feed as indicated by some of the common reactivity tests (15).

Purity of Product Metal

Six representative product samples were analyzed. Of greatest interest is the fact that low analyses for oxygen (4-6 ppm), barium (<200 ppm), magnesium (7-20 ppm), and hydrogen (<1 ppm) were obtained because all were macro constituents of the baths. The hydrogen was present as a small amount of water impurity in the salts and the oxide feeds. The major impurities in the samples were Al and Si (both >1000 ppm), but these were undoubtedly obtained from structural materials and could be avoided. Carbon contents of about 600 ppm were felt to be reasonable in view of the use of graphite cells.

Summary and Conclusions

This work suggests that electrolytic reduction of U oxides is feasible at temperatures above the melting point of U metal. A continuous process should therefore be possible. While U has not been produced in high yield by this method, sufficient metal has been obtained to indicate that such production is possible. Higher, more practical efficiencies should be obtainable in larger scale operations than were realized in the laboratory operations to date. This is indicated by the fact that, in the aluminum industry, efficiencies increase as one increases the spacing between electrodes (16), and such increases in spacing are possible in going to larger cells.

The major remaining problems are associated with the settling of the oxide in the electrolysis cell due to its low solubility and high density. In addition, materials of construction for the electrolysis cell must be thoroughly investigated. At present, graphite looks suitable.

The present work indicates that a bath containing MgF_2, BaF_2, and UF_4 is satisfactory as the solvent electrolyte. From an investigation of such baths in the range 10 to 40 mole % UF_4, it is concluded that a bath containing about 20 mole % UF_4 is most satisfactory. Lower UF_4 concentrations result in polarization effects at the anode which preclude the use of high currents. Higher concentrations of UF_4 in the bath have resulted in low current efficiencies for the electrolysis process of interest. With the 20 mole % bath an anode current density of 3.6 amp/cm^2 has been used without difficulty. Such high current density seems desirable for good yields. Any of the major U oxides, UO_3, U_3O_8, or UO_2, can be used as feed, but because UO_3 is the direct product of denitration of uranyl nitrate it is the most desirable for a production process.

Acknowledgments

The authors wish to acknowledge the assistance from others at the Knolls Atomic Power Laboratory. They are particularly grateful to Mr. C. F. Pachucki and Mr. L. F. Yetter who performed the many mass spectrographic analyses of gas samples that were required, to F. P. Landis for the spectrographic work, to L. M. Osika for x-ray diffraction analyses, and to E. L. Shirley for particle-size determinations. They are also grateful to Mr. C. M. Henderson of the Mallinckrodt Chemical Works and to Dr. D. S. Arnold and Dr. W. C. Manser of the National Lead Company of Ohio for valuable discussions.

Manuscript received May 29, 1957. This paper was prepared for delivery before the Washington Meeting, May 12-16, 1957.

Any discussion of this paper will appear in a Discussion Section to be published in the December 1958 JOURNAL.

REFERENCES

1. H. D. Smyth, "Atomic Energy for Military Purposes," p. 93, Princeton University Press, Princeton (1945).
2. J. W. Marden, W. C. Lilliendahl, G. Meister, R. Nagy, D. M. Wroughton, and N. C. Beese, AECD-3687 (1946).
3. H. A. Wilhelm, "The Preparation of Uranium Metal by the Reduction of Uranium Tetrafluoride with Magnesium," in "International Conference on Peaceful Uses of Atomic Energy," Vol. 8, p. 162, United Nations, New York (1955).
4. F. H. Driggs and W. C. Lilliendahl, *Ind. and Eng. Chem.*, **22**, 516 (1930).
5. F. H. Driggs and W. C. Lilliendahl, U. S. Pat. 1,861,625, June 7, 1932.

6. R. Rosen, U. S. Pat. 2,519,792, Aug. 22, 1950.
7. S. K. Kantan, N. Shreenivasan, and G. S. Tendolkar, *Chem. Eng. Prog. Symposium Ser. No. 12*, **50**, Pt. II, 63 (1954).
8. J. M. Marden, *et al.*, *op. cit.*, p. 161.
9. M. Kolodney, LA-40 (1943).
10. L. W. Niedrach and A. C. Schafer, KAPL 1668 (1957).
11. F. P. Hall and H. Insley, "Phase Diagrams for Ceramists," p. 108, American Ceramic Society, Inc., Columbus, Ohio (1947).
12. H. R. Hoekstra and J. J. Katz, *Anal. Chem.*, **25**, 1608 (1953).
13. C. L. Mantell, "Industrial Electrochemistry," 3rd ed., p. 477 and 497, McGraw-Hill Book Co., Inc., New York (1950).
14. B. A. Lister and G. M. Gillies, "The Conversion of Uranyl Nitrate to Uranium Dioxide and to Uranium Tetrafluoride," in "Progress in Nuclear Energy," Series 3, "Process Chemistry," Vol. I, Ch. 1.2, McGraw-Hill Publishing Co., Inc., New York (1956).
15. K. E. Rapp, J. S. Fox, N. C. Orrick, and E. J. Barber, TID 5295 (1956), p. 199.
16. J. Wleügel and O. C. Böckman, *This Journal*, **101**, 145C (1954).

Discussion Section

This Discussion Section includes discussion of papers appearing in the JOURNAL of the Electrochemical Society, 104, No. 4 and 7-12 (April and July-December 1957). Discussion not available for this issue will appear in the Discussion Section of the December 1958 JOURNAL.

The Potential of an Electrode of a Voltaic Cell; A New Definition with Justification for the Use of Two Sign Conventions

J. B. Ramsey (pp. 255-260, Vol. 104)

A. J. deBethune[1]: Professor Ramsey's paper does three things of value for the electrochemist: (*A*) It defines explicitly the thermodynamic state of the *electron* intended, but never previously defined, in such familiar half-cell reactions as $Fe = Fe^{++} + 2e^-$ or $Ag^+ + e^- = Ag$. In all such half-cell reactions, the thermodynamic state of the electrons is that of electrons in the metallic phase of the usual standard hydrogen electrode (S.H.E.). (*B*) It introduces the concept of the *electron chemical potential* $\mathcal{E}$ of any electrode, defined as the *partial molal electrochemical free energy (electrochemical potential)* of the electrons in the metallic phase of that electrode, divided by the faraday. This concept provides a physically meaningful and very illuminating description of what is commonly, but erroneously, known as the "American sign convention" (the Zn positive, Cu negative convention), first used by Walter Nernst in Germany in 1889. (*C*) Ramsey's paper also discusses the electrostatic properties of electrodes and of voltaic cell terminals (ignored in most chemistry texts) and thus establishes the electrostatic definition of the electrode potential, denoted by Gibbs' symbol V, which leads to the opposite "European sign convention" (the Zn negative, Cu positive convention), first used by Willard Gibbs in America in 1875-78 and by Wilhelm Ostwald in Germany in 1887, and internationally accepted by the I.U.P.A.C. at Stockholm in 1953.

The whole-cell and half-cell electromotive force E changes its sign upon a reversal of the cell reaction and cell diagram. In contrast, both $\mathcal{E}$ and V are sign invariant. The thermodynamic equations to be used in conjunction with $\mathcal{E}$ and V are worth noting. They are:

	with $\mathcal{E}$	with V
for oxidations	$\Delta F = -n\mathbf{F}\mathcal{E}$	$= +n\mathbf{F}V$
for reductions	$\Delta F = +n\mathbf{F}\mathcal{E}$	$= -n\mathbf{F}V$

For whole-cells, the free energy is given, as before, by $\Delta F = -n\mathbf{F}E(\text{cell})$, where $E(\text{cell}) = \mathcal{E}_{\text{left}} - \mathcal{E}_{\text{right}} = V_{\text{right}} - V_{\text{left}}$, for the reaction which accompanies the passage of n faradays of positive electricity through the cell (as written) from left to right. [*See* A. J. deBethune, *This Journal*, **102**, 288C (1955); T. S. Licht and A. J. deBethune, *J. Chem. Educ.*, **34**, 433 (1957)].

[1] Dept. of Chemistry, Boston College, Chestnut Hill 67, Mass.

M. O. Davies[2]: I wish to state emphatically that I do *not* use the left-right convention. This convention is *not* being taught at Western Reserve University and has not been taught here for years. Any students who wish to use it are allowed to do so. We do not feel that in the near future any one system will be used and agreed on by all scientists throughout the world.

We feel that no subject should be divorced from physical reality unless definite advantages are to be obtained by so doing. As we see it, the left-right convention tends to confuse the issue more often than it helps. Students tend to use it as a crutch to avoid thinking about what they are doing, and thus are often led unwittingly to false conclusions.

It is essential in discussing the left-right convention to consider what arbitrariness is involved when one attempts to divorce the subject of cell voltages from physical reality. Thus I feel that the illustrations presented below are not trivial criticisms of the left-right convention but, on the other hand, are essential in showing what troubles are involved with the convention.

Let us suppose that as a teacher you are introducing the subject of the experimental determination of cell voltages and have placed an electrochemical cell in front of you. Your left electrode is the right electrode to the class and thus, based on the physical picture, they would get the opposite sign for the cell voltage. In addition, if you were to turn the cell upside down and the contents of the cell did not spill out onto the table, you would get the sign that they originally obtained and vice versa. Yet the same process is still taking place inside the cell. For a cell consisting of concentric cylindrical electrodes, some additional designation is necessary. To avoid such difficulties, the left-right convention must divorce itself from physical reality; but, in so doing, it finds additional difficulties. The cell is represented on paper. Here enters the difficulty of how one looks at the paper.

Experimentally determined cell voltages (E) in our system are obtained without sign. Some of the questions that have arisen from my original comments have resulted because the words "experimentally determined cell voltages" have apparently been interpreted to mean experimentally determined open circuit cell voltages. In order to obtain currents from an experimental cell, it is essential to have spontaneous reactions taking place within the cell. A negative cell voltage would have no meaning whatsoever. An open circuit cell voltage is really nothing more than a cell voltage measured under conditions which reduce the current output to a small value. However, the cell is acting less reversibly when it is being measured (even with a potentiometer) than when it is on true open circuit.

[2] Morley Chemical Lab., Western Reserve University, Cleveland 6, Ohio.

We always measure the + and − terminals of the cell. This, plus the cell voltage (possessing no sign), is completely adequate to specify which electrode has a greater tendency to be oxidized or reduced. The absence of a sign on the experimentally determined open circuit cell voltage is not equivalent to treating a $10.00 debit as the same thing as a $10.00 credit. The − lead to the potentiometer indicates that there is an excess of electrons on the electrode to which it is connected and, thus, that its electrode reaction has a greater tendency to proceed in the oxidation sense than the electrode reaction at the electrode connected to the + lead of the potentiometer. Cell voltages are not dependent on whether some particular half-cell is being used as an anode or as a cathode. If the cell voltage is the same in magnitude and the resistances of the circuit are the same, the same amount of current will flow, whether a given half-cell is acting as an anode or as a cathode. The + lead of the cell will be hooked up to the external circuit in the same way.

It would be satisfying if all cell reactions (both at cathodes and anodes) were fully understood. This, unfortunately, is not the case. Often a cell is really nothing more than a black box with two terminals sticking out. For years, oxygen cathodes on active carbon in basic solutions were considered to be acting in accordance with the equation:

$$O_2 + 2H_2O + 4e^- \rightarrow 4OH^-$$

This misunderstanding led to many faulty interpretations of these electrodes. Actually, if the carbon does not possess a large ability to decompose peroxides, it will follow the equation:

$$O_2 + H_2O + 2e^- \rightarrow OH^- + O_2H^-$$

If the carbon is a fairly good decomposer of peroxides, its open circuit potential will lie somewhere between the expected potentials for the two reactions quoted above. Another example comes from metal-metal oxide electrodes. Their potentials often lie between the values expected for the metal-metal ion potential and the oxygen electrode potential.

Whether or not you know what cell reactions are going on inside the cell has no influence on the measurement of its voltage. As I have said before, experimentally determined cell voltages cannot be negative. Thus, in our system, no sign need be attached to them. Actually, we consider them without sign.

In our system, thermodynamically determined potentials ($\mathcal{E}$) are associated with specific reactions only, and these potentials apply only for the reaction equations as written. The thermodynamic data are used normally only for predictions of what cell voltage to expect under given conditions. In order to do so, one must know what reactions are involved, or make reasonable guesses. As stated above, this is often not simple. Only with hypothetical, thermodynamically obtained half-cell or cell reaction potentials will there be signs attached. The sign to be attached is that to be expected from the value for the free energy change for the half-cell or cell reaction, as written. In other words, if the reaction as written tends to proceed, and possesses a negative free energy change, then the reaction potential is given a positive sign and vice versa. If one obtains for the over-all cell reaction, as written, a negative value for $\mathcal{E}$, this indicates that the reaction in the cell proceeds in the opposite direction to that indicated by the written equations, and that these equations should be reversed. I agree with Dr. deBethune in stating that this aspect of electrochemistry is somewhat arbitrary. I need to define which direction a reaction is expected to follow. I feel, however, that experimentally determined cell voltages need not be divorced from physical reality as is done with the left-right convention. If experimentally determined cell voltages are treated by our system, they never need confuse the student of physical chemistry as he is confused by the multiple sign conventions for experimentally determined cell voltages. We feel that we have removed as much arbitrariness as possible by the above approach and have a sound, workable system.

It is the merits and demerits of a system that are important, not how long the system has been used or who uses it. Since I have been attempting to explain the system that I honestly believe is best, I have purposely used the symbolism that I normally use: E = the experimentally determined cell voltage; $\mathcal{E}$ = the thermodynamically determined cell or half-cell reaction potential. No confusion need arise over this symbolism so long as what it signifies is clearly indicated.

Anodic Corrosion and Hydrogen and Oxygen Overvoltage on Lead and Lead Antimony Alloys

P. Ruetschi and B. D. Cahan (pp. 406-413, Vol. 104)

Jeanne Burbank[3]: (*A*) The authors have failed to comprehend much published information, and have seriously misrepresented reported work. The following listing, by no means complete, gives a few examples of the unfortunate kind of misrepresentation profusely present in the paper.

1. Contrary to the statement of Ruetschi and Cahan (R. and C.), the x-ray diffraction peaks of published patterns for α-PbO_2[4-7] may be accounted for by the standard patterns of PbO (tetragonal), $PbSO_4$, and β-PbO_2.[8] Positive identification by diffraction techniques of α-PbO_2 in the possible presence of these other materials must be made with care; orientation effects are particularly to be avoided.

2. R. and C. state that "conventional cooling rates" produce considerable solid solution of antimony in lead, citing Hofmann.[9] The reference clearly states that very little antimony is retained in solid solution in as-cast lead antimony alloys; that interdendritic segregation is apparent in alloys as low as 0.1% Sb; and presents a micrograph to illustrate the point.

[3] Naval Research Lab., Washington 25, D. C.
[4] N. Kameyama and T. Fukumoto, *J. Soc. Chem. Ind., Japan*, 49, 154 (1946).
[5] T. Katz, *Ann. de Chim.*, 5, 5 (1950).
[6] A. I. Zaslavskii, J. D. Kondrashev, and S. S. Tolkachev, *Doklady Akad. Nauk S.S.S.R.*, 75, 559 (1950).
[7] A. I. Zaslavskii and S. S. Tolkachev, *J. Phys. Chem. (U.S.S.R.)*, 26, 743 (1952).
[8] X-ray Powder Data File, ASTM, Philadelphia, Pa.
[9] W. Hofmann, "Blei und Bleilegierungen," p. 16, Julius Springer, Berlin (1941).

3. Large hard black nodules were not observed by Burbank[10] on grids of storage batteries removed from service, and no mention of such examination appears in the reference cited by R. and C.

4. The studies of Burbank and Lander[10-12] on the anodic corrosion of lead in sulfuric acid comprise a determination of the corrosion kinetics, identification of anodic products, and coordination of thermodynamically possible reactions at defined anodic potentials. R. and C. have failed to comprehend the manner in which the work was carried out, and the importance of potential as a controlling factor in electrochemical reactions. R. and C. misrepresented the reports by stating that results were presented from experiments other than those described in the published papers.

(*B*) It is common analytical practice to decompose PbO_2 by the action of acids and H_2O_2. What "purification" was obtained by treating electroplated α-PbO_2 with such a mixture?

(*C*) Was no antimony pattern observed in the x-ray diffraction examination of the alloys? Normally a 10.98% Sb alloy would be expected to give a strong pattern for antimony, and the strongest line in the pattern of antimony metal lies very close to the strongest lines in x-ray patterns of α-PbO_2 and PbO (tetragonal).

(*D*) What potential measurements are referred to in the next-to-last paragraph in column 1, p. 408?

J. J. Lander[13]: The paper is of very great interest from both practical and theoretical viewpoints. The presence of α-PbO_2 in the corrosion product of lead and lead alloys may be particularly significant.

There are possible misconceptions which the reader might entertain without a full knowledge of some of the work referred to in the paper. Thus, in the introduction and in the discussion one might get the idea that tetragonal PbO will not be formed as a corrosion product of lead in acid solution. The works of Wolf and Bonilla,[14] and Lander[15] referred to in the paper clearly show that it can be formed under certain potential conditions which are different from those obtaining in the paper under discussion and in the work of Wynne-Jones and co-workers[16] also of reference. The authors, and Wynne-Jones and coworkers, employed constant current techniques whereby after the formation of lead sulfate the potential rose beyond that for the lead dioxide-lead sulfate couple, i.e., a condition under which tetravalent reaction products would be preferred. In my work, constant-voltage techniques were used and the voltage was held at levels below that of the lead dioxide-lead sulfate couple, a condition whereby divalent lead reaction products would be preferred, as was borne out by the application of Faraday's law to the amount of weight loss. Moreover, examination of the corrosion products showed that lead sulfate was the smaller part.

The authors point out, as I have already done,[17] that the formation of lead dioxide is thermodynamically possible at potentials well below that for the lead dioxide-lead sulfate couple. However, I have also pointed out that, if its formation occurred under such potential conditions, it would be thermodynamically unstable, which is practically attested to by the application of Faraday's law, already mentioned. The work in footnote 17 of this discussion considered reactions whereby lead-dioxide formed low potentials could go to divalent products. The tacit implication that the x-ray analysis of corrosion products in my work, which showed the presence of tetragonal PbO, resulted from confusion or ignorance of the pattern for α-PbO_2 is, therefore, unfounded.

The authors state in their discussion that α-PbO_2 occurs as a grid corrosion product and had been reported as tetragonal PbO by myself[15] and other workers. My work of the reference was concerned only with corrosion of cold-rolled lead sheet at controlled potentials.

The authors' method of determining total corrosion by accounting for the PbO_2 present by discharge, self-discharge, and titration of residual PbO_2 is no doubt good for pure lead, but must be in error for lead-antimony alloys because it can take no account of the antimony loss. This would be especially true in a constant-current system if the antimony corrosion reaction were much faster than the lead corrosion reaction. Thus, Fig. 5 in the authors' paper would indicate that the antimony exerts a protective function in the alloy; however, it is open to the very obvious interpretation that with increasing antimony concentration the corroding current went preferentially to oxidation of the antimony phase of the alloy.

Hans Bode[18]: We have found that the rhombic modification of the lead dioxide (β-PbO_2) is formed in the formation process in the positive plate.* On the surface, only the tetragonal form (α-PbO_2) is newly developed, whereas both forms (α-PbO_2 and β-PbO_2) are found inside, in a proportion of about 50:50%. It seems that the β-PbO_2 is formed from the PbO, and the α-PbO_2 from the lead sulfate or the basic lead sulfate. The beta-modification is the more stable one.

P. Ruetschi and B. D. Cahan: The authors have read the foregoing comments with great interest.

With regard to J. Burbank's remarks, the authors are aware that their list of references on x-ray data of PbO_2 is not complete. A large amount of work has been done in this field but much of the published data is unclear and contradictory.

The authors have pointed out in their paper that the major peak in the x-ray patterns of α-PbO_2 coincides with a major peak of the pattern for tetragonal PbO. Similarly, other peaks of the α-PbO_2 pattern are obscured, as J. Burbank points out, by the presence of other lead compounds like $PbSO_4$ and β-PbO_2. This is exactly the reason why α-PbO_2 has remained unknown until recently. There exist, however, as pointed out in the paper, several peaks

[10] J. Burbank, *This Journal*, **103**, 87 (1956).
[11] J. J. Lander, *This Journal*, **98**, 213 (1951).
[12] J. J. Lander, *This Journal*, **103**, 1 (1956).
[13] Electric Auto-Lite Co., Toledo 1, Ohio.
[14] E. Wolf and C. Bonilla, *Trans. Electrochem. Soc.*, **79**, 307 (1941).
[15] J. J. Lander, *This Journal*, **98**, 213 (1951).
[16] W. W. Beck, R. Lind, and W. F. K. Wynne-Jones, *Trans. Faraday Soc.*, **50**, 147 (1954).
[17] J. J. Lander, *This Journal*, **103**, 1 (1956).
[18] Research Lab., Accumulatoren-Fabrik Aktiengesellschaft, Neue Mainzer Strasse 54, Frankfurt/Main, West Germany.
* H. Bode and E. Voss, *Z. Elektrochem.*, **60**, 1053 (1956).

of the α-PbO_2 pattern which do not coincide exactly with any other known compound of Pb. Furthermore, some of the peaks, which do coincide in angular position with peaks of other compounds, can be differentiated by relative intensity measurements and by differences in profile of the diffraction peaks.

The second point of J. Burbank is not well taken for, although some segregation of Sb is indeed observed with 0.1% Sb alloys, this does not prove that with higher Sb concentrations a higher concentration of Sb does not remain in solid solution. This becomes particularly evident if, e.g., a 2% alloy is heat-treated below the eutectic temperature, at 245°C, in order to assure that all the Sb is homogeneously distributed in solid solution. Cooling this tempered alloy at "conventional" rates does not produce any precipitation of Sb. According to Hofmann "ist dies in dem Sinne zu deuten dass bei Luftabkühlung homogener Legierungen alles Sb in fester Lösung bleibt." In actual castings there exists a concentration gradient for Sb in the solidified lead grains such that the first portions to be precipitated are low in Sb, and the cast portions are rich in Sb.

With regard to J. Burbank's third point it should be mentioned that J. J. Lander [Ref. (27) in the authors' paper] describes a condition of positive plates, *which had been cycled around the* $PbO_2/PbSO_4$ *potential, as follows:* "Whenever the corrosion film had been built up for a week or so, even after long discharge periods there existed a black, shiny, hard, brittle, adherent film underneath the outer $PbSO_4$ film. This film was shown by x-ray analysis to be PbO_2 containing small amounts of PbO." No mention of the existence of an α-PbO_2 is made in the cited paper. J. J. Lander also has reported [Ref. (1) in the authors' paper] that electrodes which had been anodized between 0.7 and 1.6 v vs. H_2 (this is below the $PbO_2/PbSO_4$ potential which is at 1.7 v) had a "grayish-white surface film consisting almost entirely of $PbSO_4$. It was loosely adherent and could be wiped off with cotton, whereupon a brown to black underfilm was exposed which x-ray analysis proved to be tetragonal PbO."

We agree with J. Burbank that Ref. (4) in the authors' paper should be omitted at the particular place referred to. The authors feel that there is no reason for J. Burbank to feel that her results have been misinterpreted. The authors have pointed out that "the existence of PbO in a strong H_2SO_4 solution is difficult to picture thermodynamically or kinetically and in no case has any tetragonal PbO been detected in this laboratory by x-ray diffraction of Pb corroded in H_2SO_4."

As stated in the authors' paper, the corrosion experiments were performed at potentials above the $PbO_2/PbSO_4$ potential. However, the authors agree with J. Burbank that under certain voltage and pH conditions PbO can exist underneath a partially protecting sulfate layer. The authors are aware of the difference between constant voltage and constant current techniques.

The authors also would like to point out that in none of J. J. Lander's or J. Burbank's papers on this subject (up to the publication date of the authors' paper) has the existence of α-PbO_2 as a modification of PbO_2 been considered. In 1956, J. Burbank stated [Ref. (4) in the authors' paper] that "an unidentified material believed to be a form of lead oxide was also present in some anodic coatings. Unpublished work with several lead monoxides indicates that this may be a form of lead monoxide rather than a higher oxide." Since the publication of the authors' paper, J. Burbank has reported that this unknown material is actually α-PbO_2. With regard to points (*B*), (*C*), and (*D*) in J. Burbank's comment, the acid and peroxide treatment was applied to remove possible impurities of lower oxides. Since the α-PbO_2 plating solution at times contained a very fine crystalline precipitate of Pb_3O_4 and possibly other lead compounds, and since on washing the plating solution from the electrode some $Pb(OH)_2$ was precipitated, the nitric acid-H_2O_2 treatment was intended to remove these surface impurities. No Sb patterns were observed on the anodized Pb-Sb alloys. At the time of publication of the authors' paper, potentials for pure α- and β-PbO_2 were not yet measured successfully. Since then the authors have reported values for α-PbO_2 and β-PbO_2. According to these measurements, the potential of α-PbO_2 is 7 mv higher than that of β-PbO_2 at 30°C in 1.250 sp gr sulfuric acid.

The authors are in complete agreement with the comments of J. J. Lander with regard to constant current and constant voltage techniques. He never mentions, however, the existence of α-PbO_2 in his papers.

In reference to the last comment of J. J. Lander, it can be stated that the technique applied to determine the amount of corrosion, measures indeed the amount of PbO_2 formed. However, no error is introduced by this condition. The corrosion of Sb and Pb must be strongly coupled since corrosion occurs only at the surface of the electrode. The Sb in the alloy is enclosed by lead and can only be attacked after the surrounding lead has been oxidized. It is not conceivable that Sb moves out of unattacked bulk electrode material. The actual depth of attack can be evaluated by taking into account the density of Pb-Sb alloys, as suggested in the authors' papers. The amount of electricity, applied during the constant current oxidation (at $3ma/cm^2$) was orders of magnitude larger than the amount of electricity actually required to produce the corrosion film. Most of the current was used for gas production. If the oxidation of the Sb phase would be faster than the oxidation of the lead phase, the latter process would determine the penetration rate and the growth of the oxide film. In Fig. 5, the decrease in discharge time with increasing Sb concentration is due to an increased rate of self discharge. This is brought out in more detail in new papers which are in the course of publication.

With regard to Dr. Bode's comment, the authors are in complete agreement with his experimental findings. However, the authors have reason to suspect that (orthorhombic) α-PbO_2 is formed in the plates of storage batteries by nucleation with metallic lead particles, and (tetragonal) β-PbO_2 by oxidation of $PbSO_4$. It would be helpful if the nomenclature for the tetragonal and orthorhombic modification of

PbO_2 could be made uniform. The authors, together with Zaslavsky, *et al.*, use the term α-PbO_2 for the orthorhombic form, while Bode and Voss use the name β-PbO_2 for this modification. The respective designations for α and PbO_2 were originally chosen because of the parallelism to the orthorhombic and tetragonal modifications of MnO_2 which have been named α and β, respectively.

High Temperature Oxidation of High Purity Nickel between 750° and 1050°C

E. A. Gulbransen and K. F. Andrew (pp. 451-454, Vol. 104)

Stanislaw Mrowec and Teodor Werber[19]: The mechanism of oxidation of nickel at high temperatures has been the subject of many investigations. Applying a sensitive gravimetric method, Gulbransen and Andrew measured the rate of nickel oxidation and have found that the heat of activation of this process in the atmosphere range 750°-1050°C amounts to 41.2 cal/mole. In this region no cracks were observed in the nickel oxide layer and the parabolic rate law was obeyed. This value does not differ from the former one obtained by the same authors for the temperature range 400°-750°C.[20] Using theoretical considerations and comparing the activation energy of the oxidation process with the activation energy of diffusion of nickel in nickel oxide (which was determined by Moore[21] by aid of the tracer method), Gulbransen and Andrew as well as Moore[21] conclude that the oxidation process proceeds only by the outward diffusion of nickel ions and electrons via cation vacancies and electron holes.

The mechanism of the oxidation of nickel at high temperatures has been investigated also by the marking method.[22-24] The results of these investigations cannot be conciliated with the nickel oxidation mechanism proposed by Gulbransen and Andrew and Moore.

L. Czerski[22] used as the marker a platinum wire $\phi = 1.0 \times 10^{-2}$ cm and Ilschner and Pfeiffer[23] also a Pt-wire $\phi = 0.3 \times 10^{-2}$ cm. Czerski, Mrowec, and Werber[24] used platinum wire $\phi = 7 \times 10^{-3}$ cm and submicroscopic layers of platinum. Nickel specimens were wrapped with platinum wire and then oxidized at temperatures of 1000° and 1200°C. When submicroscopic platinum films were used as markers, the specimens before oxidizing were covered with a layer of ammonium chloroplatinate which instantaneously decomposes in the temperature of reaction, forming on the surface of the specimen an ideally dispersed platinum layer. After the reaction, the specimens were cut vertically to the wire axis, the cross sections polished and microphotographed. In the case of marking with submicroscopic platinum layers, their position in the scale was determined by spectral analysis. It was found that the position of the markers does not depend on the type of marker and on the temperature. After reaction, the marker is always situated in the middle part of the scale layer on the interface between two microscopically discernible scale layers with different structure. This position of the marker in the scale indicates that the growth of scale is a result of two simultaneous and opposite processes consisting in diffusion of both reagents: nickel and oxygen through the scale. Therefrom it results that the external layer grows owing to the outward diffusion of nickel ions and the inner one owing to the inward diffusion of oxygen. (As it was stated, the plastic flow of the scale must not be taken into account in this case.) Quantitative calculations have proved that the share of the inward diffusion of oxygen in the process of scale formation amounts to 50%. If the scale should grow owing to the outward diffusion of metal only (according to the proposition of Gulbransen and Moore) the marker would be found at the interface scale/metal.

Thus, good conformity between the activation energies of diffusion and of oxidation is not, in our opinion, a sufficient condition for drawing conclusions about the mechanism of the oxidation process of a given metal. The investigations carried out by aid of markers are very necessary since they allow one to state directly the extent of diffusion of the metal and of the oxidizing agent during the process of scale formation. The marker method makes it possible to check the correctness of the supposed oxidation mechanism which was proposed on the base of the results of indirect investigations (type of ion defect of the oxide forming the scale, parabolic course of the oxidation process, etc.)

E. A. Gulbransen and K. F. Andrew: We are very pleased to have the interesting comments of Drs. Mrowec and Werber. The role of marker experiments in oxidation processes on metals needs a thorough examination for each metal. In particular, one needs to know the thickness range over which the parabolic rate law can be applied before "breakaway" conditions occur. Many workers apply marker tests for oxidation thicknesses far past "breakaway" where submicroscopic cracking and other types of failure occur in the scale. One must realize also that oxidation is not the formation of a uniform structureless film covering the metal surface.

Let us consider the application of markers to the oxidation of nickel as presented by Drs. Mrowec and Werber. The platinum wires used ranged in size from 7×10^{-3} to 1.0×10^{-2} cm while the platinum film was of undetermined thickness. A 10^{-3} cm wire is 10^5 Å in diameter. To make experiments using a wire of such size one must oxidize the metal to a scale thickness of 10^6 to 10^7 Å. Here the wire thickness would be 1/10 to 1/100 of the oxide thickness. In our study on the oxidation of nickel, we found the parabolic rate constants to increase at temperatures above 900°C for film thickness of the order of 2×10^4 Å. We concluded that submicroscopic cracking occurred in the film at this thickness. Scales of over 7.6×10^4 Å cracked away from the metal on

[19] Dept. of General Chemistry, School of Mining and Metallurgy, Aleja Mickiewicza 30, Cracov, Poland.
[20] E. A. Gulbransen and K. F. Andrew, *This Journal*, **101**, 128 (1954).
[21] W. J. Moore and M. T. Shim, *J. Chem. Phys.*, **26**, 802 (1957).
[22] L. Czerski and F. Franik, *Arch. Górnictwa i Hutnictwa*, **3**, 43 (1955).
[23] B. Ilschner and H. Pfeiffer, *Naturwissenschaften*, **40**, 605 (1953).
[24] L. Czerski, S. Mrowec, and T. Werber, *Arch. Hutnictwa*, **3**, 25 (1958).

cooling. If submicroscopic cracks develop, oxygen penetrates to the new reacting interface.

If oxidation consists in a diffusion-controlled mechanism operating below 2×10^4 Å followed by cracking and re-oxidation, it would be impossible to study the initial reaction mechanism using wires 10^5 Å in diameter. When cracking occurs on extended oxidation, one would expect to find the platinum wire in the middle of the oxide scale no matter what the initial mechanism of oxidation.

To use marker experiments to study the initial oxidation mechanism for nickel, the marker must be of the order of 2×10^3 Å or 1/50 of the size actually used. This would require electron microscope observations to locate the marker.

The use of submicroscopic platinum films together with spectral analyses has much merit if the technique were applied to experiments at 900°C and lower and for film thicknesses of less than 2×10^4 Å. However, the analytical difficulties in sectioning a film of this thickness have not been solved. If used on thick scales at 1000° and 1200°C, the method suffers from the same criticism as given for the use of wires.

We hope that marker experiments will be tried in the thinner film range of oxidation. With present techniques, we feel the macroscopic experiments may give a false idea as to the initial mechanism of oxidation.

The Equilibrium between Titanium Metal, $TiCl_2$, and $TiCl_3$ in NaCl-KCl Melts

W. C. Kreye and H. H. Kellogg (pp. 504-508, Vol. 104)

Kai Grjotheim[25]: The mentioned paper is a welcome contribution to those engaged in a study of equilibria involving a metal and two of its salts of different valency, thus leading to the possibility of complex formation by the higher valent ion in salt melts. However, it may be of interest to comment on some of the statements made by the authors. Their calculation of the equilibrium constant for the reaction:

$$TiCl_3(\text{solution}) + 1/2\ Ti^\circ(\text{solid}) = 3/2\ TiCl_2(\text{solution}) \qquad (I)$$

on a molecular basis, by putting:

$$K_x = N_{TiCl_2}^{3/2}/N_{TiCl_3}$$

where N_i = mole fraction of (i) based on the constituents:

$$TiCl_2,\ TiCl_3,\ NaCl,\ \text{and}\ KCl$$

gives an "equilibrium constant" which varies with the total concentration of titanium dissolved in the melt.

Assuming ideal ionic melts, an equilibrium constant, K, for each of the reactions:

$$Ti^{3+} + 1/2\ Ti^\circ = 3/2\ Ti^{2+} \qquad (II)$$

$$TiCl_4^- + 1/2\ Ti^\circ = 3/2\ Ti^{2+} + 4\ Cl^- \qquad (III)$$

$$TiCl_6^{3-} + 1/2\ Ti^\circ = 3/2\ Ti^{2+} + 6\ Cl^- \qquad (IV)$$

[25] Dept. of Metallurgy, University of Toronto, Toronto, Ont., Canada.

was also calculated by Kreye and Kellogg, but the values so obtained, however, still showed the same trend with concentration displayed by K_x. [It may here be remarked that, using molar ionic-fractions, the constant for reaction (II) is numerically identical with K_x and, with the small concentrations of titanium in the melts, the constants of reactions (III) and (IV) have almost the same numerical value as for reaction (I).]

Mellgren and Opie[26] have measured the same equilibrium between $TiCl_2$, $TiCl_3$, and Ti° in the presence of $SrCl_2$-NaCl melts. Their results indicate that there might be a slight tendency for the "equilibrium constant" to increase with increasing total titanium content in the melt. Mellgren and Opie also measured the effect of varying the NaCl to $SrCl_2$ ratio, keeping the total amount of dissolved titanium fairly constant. The equilibrium was then markedly effected in a way corresponding to a decreasing K_x with increasing NaCl content in the melt.

The obvious conclusion from both these investigations must be that the solutions are not ideal when considered as simple molecular mixtures. By assuming different types of complex-molecule formation of the titanium chlorides, the authors find that relatively constant K values may be obtained.

However, it seems to be rather well established by now that molten salts may be considered as completely ionized.[27-29] The "best" ideal behavior would therefore be expected by treating the solutions as ionic mixtures. When applying the ionic point of view to these solutions, however, it must be remembered that the ionic reactions (II), (III), and (IV) are taking place in a mixed ionic milieu. The ideal ionic equilibrium constant for these reactions must therefore theoretically be expected to vary with the composition of the melts.

A qualitative explanation of the variation of this "constant" may be given in the following way. When a given reaction takes place with each component in its standard state, the change in the Gibbs function is the standard change, ΔG°. Between the thermodynamic equilibrium constant K (expressed in terms of activities of the components at equilibrium) and the standard change in Gibbs' function, one has the well-known important relationship $\Delta G^\circ = -RT \ln K$. The standard states used in equilibria involving molten salts are most conveniently selected as the pure molten salts at the given temperature. Reaction between standard states can then occur only between *neutral molecules*.

For reaction (I), therefore, the deviation from constancy of the ideal equilibrium constant calculated with use of mole fractions obviously shows that the solution is not an ideal molecular mixture.

Looking on the ionic reactions, however, the reaction between neutral molecules may be formulated in different ways for varying concentrations in the mixtures used by Kreye and Kellogg.

For the ionic reaction (III), we may assume that

[26] S. Mellgren and W. Opie, *J. Metals*, 9, 266 (1957).
[27] P. Herasymenko, *Trans. Faraday Soc.*, 34, 1245 (1938).
[28] M. Temkin, *Acta Physicochim. U.R.S.S.*, 20, 411 (1945).
[29] H. Flood, T. Förland, and K. Grjotheim, "The Physical Chemistry of Melts," p. 46, Institution of Mining and Metallurgy, London (1953).

the following reactions between neutral molecules are taking place:

$$NaTiCl_4 + 1/2\ \underline{Ti} = 3/2\ TiCl_2 + NaCl \quad (IIIa)$$

with ΔG°_{Na}, and

$$KTiCl_4 + 1/2\ \underline{Ti} = 3/2\ TiCl_2 + KCl \quad (IIIb)$$

with ΔG°_{K}, and

$$1/2\ Ti^{II}(Ti^{III}Cl_4)_2 + 1/2\ \underline{Ti} = 2\ TiCl_2 \quad (IIIc)$$

with ΔG°_{Tl}.

If either $\Delta G^\circ_{Na} \neq \Delta G^\circ_{K}$

or/and $\Delta G^\circ_{Na} \neq \Delta G^\circ_{Tl}$, two or all three of the thermodynamic equilibrium constants K_{Na}, K_K and K_{Tl} must differ for these reactions.

However, if ideal ionic solutions are assumed, the salt activities can be replaced by Temkins' activity terms for ideal ionic mixtures, as for example

$$a^{ideal}_{TiCl_2} = N_{Ti^{2+}} \cdot N^2_{Cl^-} ,$$

where the N's are the molar ionic-fractions.[28] Then

$$K = K^{ideal}_{mix}$$

for all three reactions (III, *a*, *b*, and *c*), as well as for a reaction in a mixture involving all of them, will have the same form:

$$K^{ideal}_{mix} = \frac{N^{3/2}_{Ti^{2+}} \cdot N^4_{Cl^-}}{N_{TiCl_4^-}}$$

since the cationic fractions (N_{Na^+}, N_{K^+} and partly $N_{Ti^{2+}}$) of the "inactive" cations cancel out. Thus in a mixed melt containing both Na^+, K^+, and Ti^{2+} cations, K^{ideal}_{mix} must be expected to vary with the concentrations of the cations. This is obvious due to the variation in the standard states accompanying concentration changes. A complete thermodynamic derivation of the relationship between K^{ideal}_{mix} and the composition of the mixture is to be published elsewhere.[30]

Potential-pH Diagram of the Antimony-Water System; Its Applications to Properties of the Metal, Its Compounds, Its Corrosion, and Antimony Electrodes

A. L. Pitman, Marcel Pourbaix, and Nina de Zoubov
(pp. 594-600, Vol. 104)

A. L. Pitman, M. Pourbaix, and N. de Zoubov: It has been found that errors appear in the reference to the paper of Piontelli and Fagnani (22) on p. 598, column 2, paragraph 4, lines 4-12. This material is hereby deleted from our paper; i.e., "It was concluded that metallic Sb displaces Fe in the stronger solutions and this action is in accordance with predictions which may be made from the thermodynamic emf of the process, a statement which is readily verified. They pointed out that because the overvoltage of hydrogen is higher on Sb than on Fe, corrosion is lessened as the deposited Sb film spreads."

Substitute in its place: "It was concluded that metallic iron displaces antimony from these solutions. This action is in accordance with predictions which may be made from a comparison between the equilibrium diagram for antimony (Fig. 4) and the equilibrium diagram for iron [*see loc. cit.* (1), p. 89, Fig. 20b.] Piontelli and Fagnani pointed out that the inhibiting influence is decided by the structure of the separated antimony. For a given concentration of dissolved antimony, the inhibiting action only exists in solutions sufficiently concentrated in HCl (for which the separation of Sb occurs in the form of a practically invisible but uniform film); for lower concentrations of HCl, Sb separates as a spongy coating which does not exert a protection action."

[30] K. Grjotheim and J. M. Toguri, To be published.

Optical Measurement of Film Growth on Silicon and Germanium Surfaces in Room Air

R. J. Archer, (pp. 619-622, Vol. 104)

Arthur B. Winterbottom[31]: This application of the polarimetric technique to the study of films on Si and Ge was of special interest to the discussor as the possibilities of just this kind of study had been raised some time ago by Dr. J. O'M. Bockris.[32] It was then felt that for a profitable application it would be desirable to use single crystal surfaces, as, although both base and film might be optically isotropic, the film-forming reaction might be dependent on orientation. Further, it was considered that it should be possible to compute reflection parameters $\bar{\Delta}$ and $\bar{\Psi}$ for film-free Ge surfaces from the optical constants determined by O'Bryan[33] for vacuum-evaporated coatings. From such computed parameters, together with determinations made on surfaces with growing films, it was felt that interpretation of observations in terms of optical constants and thickness of film should be feasible on the lines expounded in the discussor's papers.[34] It is therefore somewhat puzzling to note that the author's tentative values for the optical constants of Ge, apparently, based on determinations with an immersion technique, differ considerably from O'Bryan's determinations on evaporated Ge surfaces in vacuum, viz., $N = 3.47$ and $K = 0.40$. An immersion technique involving measurement on evaporated mirrors through the quartz support was used by the discussor in the case of aluminum,[34] when it gave results in fair agreement with front surface determinations in vacuo by O'Bryan and also by Hass. As the author points out, errors in optical constants of base will have a relatively minor effect on the interpretation of relative changes in Δ in terms of film thickness, but the effect on estimates of total thickness might be considerable. This all points to the necessity of

[31] Dept. of Metallurgy, Norways Institute of Technology, Trondheim, Norway.
[32] Private communication, J. O'M. Bockris, Dec. 1956.
[33] H. M. O'Bryan, *J. Opt. Soc. Am.*, **26**, 122 (1936).
[34] A. B. Winterbottom, *Kgl. Norske Videnskab. Selskabs, Skrifter*, No. 1 (1954).

reliable estimates of constants for film-free surfaces. An alternative to the immersion technique with film-covered surfaces and determinations on evaporated mirrors in vacuo might be to make measurements on clean single-crystal surfaces (of the orientation exposed by etching) while immersed in deaerated hydrofluoric acid in a plastic cell with Perspex windows. In the case of Ge it is also possible that film-free surfaces might be obtained by suitable vacuum treatments.

With regard to the curious effect of rinses in organic liquids, it seems significant that the immediate effect of the rinses gradually disappears with almost complete recovery to the original trend of the optical data. This seems rather suggestive of a gradual loss of loosely bound solvent from a swollen film.

R. J. Archer: There is in press[35] a paper by the writer which reports measurements of the optical constants of single-crystal Ge by the ellipsometric technique throughout the wave-length range of the visible. The paper compares these results with the five previous measurements in the literature, including O'Bryan's. It is concluded that O'Bryan's values represent least accurately the optical constants of single-crystal Ge. This fact is attributed to a difference between the optical properties of his evaporated films and bulk Ge.

The suggestion that reflection from Ge immersed in hydrofluoric acid would yield $\bar{\Delta}$ and $\bar{\Psi}$ is an interesting possibility but there is some evidence that an insoluble film, possibly a suboxide, forms under these conditions. The other suggestion that $\bar{\Delta}$ and $\bar{\Psi}$ could be measured on atomically clean surfaces in high vacua is a current experimental project of the writer. One problem associated with such measurements is the surface irregularities that result from the severe cleaning techniques in current use (e.g., ion bombardment). Such irregularities with dimensions small compared to the wave length of the reflected light constitute a surface film and effect a perturbation in $\bar{\Delta}$ and $\bar{\Psi}$. Further, the problem of strain double refraction in windows is a source of error when closed cells are used. Although problems of the nature mentioned here are not insurmountable, they make the direct measurement of $\bar{\Delta}$ and $\bar{\Psi}$ a difficult experimental undertaking.

Stoichiometric Numbers and Hydrogen Overpotential

A. C. Makrides (pp. 677-681, Vol. 104)

Roger Parsons[36]: It is useful to have a derivation of the stoichiometric number (ν) from the general concept of the proportionality of the rate to the affinity of the reaction. The difference between this and previous procedures[37,38] is perhaps more apparent than real, for, in the latter, the extrapolation from states far removed from equilibrium is necessary only in practical determinations of exchange current from current-voltage curves, not in the theoretical derivation of the relation equivalent to (VII) in the discussed paper.

Separation of the total work of transfer across an interface into "electrical" and "chemical" terms is possible in terms of a model[39] and causes no difficulty, provided that these quantities are used merely as an aid in the derivation of equations relating measurable quantities. This was the procedure used in the earlier paper.[38]

It is satisfying that the conclusions reached for hydrogen overpotential in the present paper confirm those of the previous paper.[38] The only exception is that of the dual mechanism 4(b). [Dual mechanisms were specifically excluded in footnote 38 and their significance was discussed elsewhere.[40]] Here an unjustified approximation appears to have been made: that the exchange velocity V^e of the over-all reaction is equal to that of each partial reaction (V^e_{I} and V^e_{III}) when these are equal. In fact, in this very special case $V^e = V^e_{\text{I}}/2 = V^e_{\text{III}}/2$. In general, the three equations at the bottom of p. 681 of the discussed paper can be solved to obtain

$$V = \frac{V^e_{\text{I}}\, V^e_{\text{III}}}{V^e_{\text{I}} + V^e_{\text{III}}} \cdot \frac{A}{RT} \qquad \text{(I)}$$

Now the quotient $V^e_{\text{I}}\, V^e_{\text{III}}/(V^e_{\text{I}} + V^e_{\text{III}})$ is the general expression for V^e for this reaction scheme[41] (compare the expression for the conductance of two conductances in series). Thus, comparison of Eq. (I) here with the general Eq. (VI) in the discussed paper shows that ν is unity for reaction scheme 4(b) whatever the relative values of V^e_{I} and V^e_{III}.

If consideration is restricted to the three partial reactions: (i) discharge, (ii) combination, and (iii) ion + atom, then nonintegral stoichiometric numbers would be obtained under equilibrium conditions when two types of dual mechanisms occur: $V^e_{\text{I}} \cong V^e_{\text{II}} >> V^e_{\text{III}}$ and $V^e_{\text{I}} >> V^e_{\text{II}} \cong V^e_{\text{III}}$. In each $1 < \nu < 2$. Neither is considered in the present paper. The fact that chain and photochemical reactions have fractional values of ν has already been recorded.[42]

A. C. Makrides: The differences between the present approach and Dr. Parsons' derivation have been noted in the paper. Briefly, our development (i) is not based on any particular reaction rate model, (ii) avoids use of quantities $\Delta\phi$, p, and q, and (iii) is applicable to competing reaction mechanisms.

(i) Dr. Parsons employed transition state theory in setting up the basic equation for the reaction rate. The two treatments are, of course, equivalent for states neighboring equilibrium since absolute reaction rate theory expressions reduce to linear relations in this region.

(ii) The difficulties encountered with $\Delta\phi$, p, and q are exemplified by Dr. Parsons' decomposition of the dependence of p and q on $\Delta\phi$ and solution composition (p. 1336 of work cited in footnote 38).

[35] R. J. Archer, *Phys. Rev.*, In press.
[36] Dept. of Physical and Inorganic Chemistry, The University, Bristol 8, England.
[37] J. Horiuti, *J. Research Inst. Catalysis, Hokkaido Univ.*, 1, 8 (1948).
[38] R. Parsons, *Trans. Faraday Soc.*, 47, 1332 (1951).
[39] R. Parsons, Chap. III, "Modern Aspects of Electrochemistry," J. O'M. Bockris, Ed., Academic Press Inc., New York (1954).
[40] R. Parsons, *J. chim. phys.*, 49, 82 (1952).
[41] *See*, for example, J. A. Christiansen, *Z. physik. Chem.*, **28B**, 303 (1935).
[42] J. Horiuti, *Proc. Japan Acad.*, 29, 160 (1953).

(iii) Dr. Parsons has examined the kinetics of "dual" mechanisms in the reference he cites. However, stoichiometric numbers for such mechanisms were not discussed. In general, it is difficult to see how Dr. Parsons' development could be modified for application to competing reaction mechanisms.

The observation in the paper that stoichiometric numbers may be smaller than unity was thought necessary in view of Dr. Parsons' definition, ". . . ν is an integer equal to or greater than unity" (p. 1333 of work cited in footnote 38).

Dr. Parsons' remarks on mechanism 4(b) are appreciated. It was assumed in the paper that the exchange velocity of the over-all reaction is equal to the exchange velocities of each partial reaction where these are equal. As Dr. Parsons notes, this is incorrect. The expression given by Dr. Parsons leads to $\nu = 1$ independently of the relative magnitude of v^e_i and v^e_{ii}. The remarks in the last paragraph of the paper should be modified by deleting reference to mechanism 4(b).

We thank Dr. Parsons for his interest and particularly for his remarks on mechanism 4(b).

The Influence of Surface Pretreatment on the Atmospheric Oxidation of 2S (U. S. Alloy 1100) Aluminum

P. M. Aziz and H. P. Godard (pp. 738-739, Vol. 104)

R. C. Plumb[43]: The studies made by Drs. Aziz and Godard are of great interest to us since we have been concerned for several years with the specific surface area or roughness factor of aluminum. In 1956[44] we described a technique for measuring the specific surface area of aluminum. Measurements were made on samples which had a variety of surface preparations, including some similar to those used by Aziz. It was found that surface areas on specimens abraded with coarse alumina or silicon carbide powders range from 2 or 3 up to as high as 20.

In a second paper which has been transmitted to Dr. Aziz in preprint form,[45] the results of a further investigation of the surface area of aluminum are described. In that work, coulometric measurements were made when barrier layer anodic oxide coatings were applied to a variety of aluminum surfaces and the apparent surface area as a function of the oxide thickness (resolution) was determined. The application of a thick barrier layer oxide on a rough surface serves to smooth the protuberances. Roughness factors measured independently on identical samples by the radiochemical technique[44] and the anodic oxidation technique[45] agreed quantitatively on samples having roughness factors as high as 20.

Aziz and Godard stated that it is hard to conceive of the geometry of a surface with a roughness factor higher than 2 or 3. A simple model for such a surface is one in which smaller asperities are built on top of large asperities. For example: One set of asperities 1000Å in size might give a specific surface area of 3. If another set of asperities 100Å in size is built upon the larger asperities, it will give a specific surface area of 9. If another set of asperities 10Å in size is added, the roughness factor will be 27.

I believe that the differences in weight gain of samples which have had different surface treatments as described by Aziz and Godard can be explained completely in terms of the specific surface area.

It is very gratifying to find that Aziz and Godard did, in fact, observe differences in weight gain which would be anticipated from our work.

P. M. Aziz and H. P. Godard: The authors agree with Dr. Plumb that there is no conceptual problem in visualizing a surface with roughness factors as high as 20-30, although we do have some difficulty in understanding how an abrasion process can produce a topography such as that presented by him. Nor do we feel that the research presented in the reference cited clarifies the problem, for the following reasons.

(*A*) In footnote 44, roughness factors as high as 19.9 were measured by a radiochemical method on aluminum surfaces abraded with 3/0 emery paper. Imbedded abrasive will certainly influence the results, as the authors state.

They feel that since no seizing or staining of the surface was noted during the abrasion process the surfaces were free of imbedded abrasive. It has been our experience that even under these conditions abrasive will be imbedded in the surface although a light metallographic polish is necessary before its presence can be detected; in fact, this was the case in our work.

(*B*) In footnote 45 roughness factors somewhat over 20 were measured by an anodizing technique. Young[46] has pointed out that the anodization of a rough surface will lead to the smoothing of the asperities, and thus the inner surface of the oxide over these asperities will be constrained to cover progressively decreasing areas, introducing local compressive stresses which can produce local failure of the film. This phenomenon will lead to high values of the roughness factor when measured by the anodizing technique, especially on surfaces containing asperities small enough to result in large roughness factors.

In view of this we feel that, while high values of the roughness are by no means excluded, their existence has not been conclusively demonstrated, and consider that contamination by abrasive particles can influence the behavior of the surface.

[43] Alcoa Research Labs., Aluminum Co. of America, New Kensington, Pa.

[44] J. E. Lewis and R. C. Plumb, *Intern. J. Appl. Radiation and Isotopes*, 1, 33 (1956).

[45] R. C. Plumb, "The Specific Surface Area of Aluminum as Determined with Continuously Variable Resolution from 20Å to 1000Å," *This Journal*, In review.

[46] L. Young, *Acta Met.*, 5, 711 (1957).

FUTURE MEETINGS OF
The Electrochemical Society

Ottawa, Canada, September 28, 29, 30, October 1, and 2, 1958

Headquarters at the Chateau Laurier

Sessions will be scheduled on

Batteries, Corrosion, Electrodeposition (including symposia on "Electrodeposition on Uncommon Metals" and "Chemical and Electropolishing"), Electronics (Semiconductors), Electrothermics and Metallurgy, and a symposium on "Films Formed in Contact with Liquids" sponsored by Theoretical Electrochemistry, Battery, and Corrosion Divisions

★ ★ ★

Philadelphia, Pa., May 3, 4, 5, 6, and 7, 1959

Headquarters at the Sheraton Hotel

Sessions probably will be scheduled on

Electric Insulation, Electronics (including Luminescence and Semiconductors), Electrothermics and Metallurgy, Industrial Electrolytics, and Theoretical Electrochemistry

★ ★ ★

Columbus, Ohio, October 18, 19, 20, 21, and 22, 1959

Headquarters at the Deshler-Hilton Hotel

★ ★ ★

Chicago, Ill., May 1, 2, 3, 4, and 5, 1960

Headquarters at the Lasalle Hotel

★ ★ ★

Houston, Texas, October 9, 10, 11, 12, and 13, 1960

Headquarters at the Shamrock Hotel

★ ★ ★

Papers are now being solicited for the meeting to be held in Philadelphia, Pa., May 3-7, 1959. Triplicate copies of each abstract (*not exceeding 75 words in length*) are due at Society Headquarters, 1860 Broadway, New York 23, N. Y., *not later than January 2, 1959* in order to be included in the program. *Please indicate on abstract for which Division's symposium the paper is to be scheduled.* Complete manuscripts should be sent in triplicate to the Managing Editor of the JOURNAL at 1860 Broadway, New York, 23, N. Y.

News Notes in the Electrochemical Field

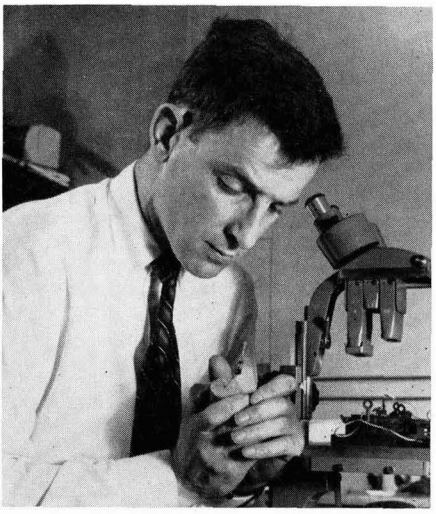

J. F. Dewald is shown inspecting a laboratory model of his newly announced transistor amplifier, based on the use of an electrolyte-semiconductor interface.

Field Effect Amplifying Device Uses Electrolyte/Semiconductor Interface

Transistor action at a semiconductor/electrolyte interface modulated by an electrical field was described by J. F. Dewald, of Bell Telephone Labs., in a paper presented to the American Physical Society in Chicago. The basic electrochemical aspects of the interface were described at the New York Meeting of The Electrochemical Society. Recent laboratory experiments have demonstrated amplifier operation at 1000 cps with gain in excess of 15 db.

Initial work on conductivity modulation at a semiconductor/electrolyte interface was carried out more than ten years ago by R. B. Gibney, W. H. Brattain, and John Bardeen, at Bell Telephone Labs., during their early studies of transistor action. In the course of their experiments, they discovered minority carrier injection at small area contacts, which led ultimately to the first point contact transistor. The electrolyte field-effect employed in the present work was all but forgotten in the ensuing rapid developments in transistor science and technology.

The experimental device described by Mr. Dewald uses a hexagonal rod-like crystal of very pure zinc oxide as the semiconductor, immersed in a highly conducting electrolyte. A platinum electrode placed nearby serves as the grid element. Because zinc oxide is a large-energy-gap semiconductor, it can be operated in a high enrichment condition, with one end of the crystal cathodically biased with respect to the solution, and the other end anodically biased. Somewhere in between is a neutral point which is unbiased, where the energy bands are flat right up to the surface of the crystal. As this neutral point shifts back and forth under the influence of varying biasing grid voltages, the resistance of the crystal changes, passing a current which follows the driving frequency very closely. A fairly extended range of linear response is obtained.

To make electrical contact to the zinc oxide crystal, the two ends are first indium plated to assume good ohmic contact. They are then copper plated to allow soldering copper wire leads. The platinized platinum grid completes the assembly. After insulating all wires and connections except the grid, the assembly is immersed in the electrolyte (5% sodium tetraborate and boric acid solution), and hermetically sealed in a small glass tube to avoid electrolyte evaporation.

Small size is required to give high frequency operation. The smallest units constructed so far use crystals about 0.3 mm long, and 0.15 mm in "diameter." It is expected that, by going to a flat plate crystal instead of the rod geometry, the present low output power levels could be raised appreciably, without any over-all increase in size, or any change in other operating characteristics.

Palladium Medal Award in 1959

The fifth Palladium Medal of The Electrochemical Society will be awarded at the Fall Meeting of the Society in Columbus, Ohio, October 18-22, 1959. The medal was established in 1951 by the Corrosion Division for distinguished contributions to fundamental knowledge of theoretical electrochemistry and of corrosion processes. It is awarded biennially to a candidate selected by a committee appointed by the Society's Board of Directors. This year the committee members are A. L. Ferguson, H. A. Liebhafsky, T. P. May, E. B. Yeager, and H. A. Laitinen, *Chairman.*

The Committee invites Sections, Divisions, and members of the Society to send suggestions for candidates, accompanied by supporting information, to *H. A. Laitinen, Dept. of Chemistry, University of Illinois, Urbana, Ill.* Candidates may be citizens of any country and need not be members of the Society. Previous medalists have been: Carl Wagner, Massachusetts Institute of Technology [now with Max Planck Institut für Physikalische Chemie]; N. H. Furman, Princeton University, U. R. Evans, Cambridge University; and K. F. Bonhoeffer, Max Planck Institut für Physikalische Chemie (posthumous award).

Society Fall 1958 Meeting, Ottawa, Canada

For the Fall Meeting of the Society, to be held Sept. 28-Oct. 2, visits are being planned to Atomic Energy (Canada) Ltd. at Chalk

River, Ont., and to Dominion Magnesium Ltd., Haley, Ont. These tours will be held on Friday, October 3, 1958, and each will be an all-day trip. The costs will be approximately $5.00 and $4.00, respectively, payable at the time of registration at the convention. As only 40 persons can be accommodated on each tour, those who are interested are asked to make their reservations at an early date.

In making a plant tour reservation, full name, address, nationality, and business affiliation should be given. Instructions for convention registration will be given at a later date.

Plant tour reservations should be addressed to Mr. J. S. McCree, Mines Branch, 552 Booth St., Ottawa, Ont., and should be received *before July 30, 1958.*

New Sustaining Members

M. Ames Chemical Works, Inc., Glens Falls, N. Y., and Ciba Pharmaceutical Products Inc., Summit, N. J., recently became Sustaining Members of The Electrochemical Society.

Conference on Magnetism and Magnetic Materials

The fourth Conference on Magnetism and Magnetic Materials will be held in Philadelphia, November 17-20, 1958, at the Sheraton Hotel. This conference is sponsored by the American Institute of Electrical Engineers in cooperation with the American Physical Society, the Institute of Radio Engineers, the Metallurgical Society of A.I.M.E., and the Office of Naval Research.

Authors should submit titles of proposed papers by August 1 and abstracts by September 1 to the Program Chairman, H. B. Callen, Dept. of Physics, University of Pennsylvania, Philadelphia, Pa. Further details may be obtained from C. J. Kriessman, Local Chairman, Remington Rand Univac, 1900 W. Allegheny Ave., Philadelphia.

Publication of Index to Scientific Journals

The Electrochemical Society JOURNAL is among the 510 periodicals that are being indexed by subject and author in a new publication announced recently.

The primary subjects included in these indexes are solid-state-physics, nucleonics, radiation, optics, mechanics, astrophysics, radio, electronics, sound, astronomy, rockets, guided missiles, artificial satellites, and space travel. These indexes, comprising several hundred thousand entries, have been compiled by the Library of the U. S. Naval Research Lab.

The original index cards are to be reproduced in book form by offset printing, 21 cards per page, 10 in. x 14 in. Author, and subject, sections, and the monthly, quarterly, and annual supplements to each, can be purchased separately.

The publication will be available only to those who subscribe in advance of printing, which will start in the third quarter of this year.

The publication is offered by Micro-Photography Co., 97 Oliver St., Boston 10, Mass.

NBS Study Shows Retardation of Copper Corrosion by Light

Sunlight or other intense light, which ordinarily accelerates the corrosion process in metals, has been found to produce an opposite effect on copper oxidation[1]—copper oxide growth is actually retarded by the irradiation. This unusual behavior was observed at the National Bureau of Standards as part of a continuing research project on the corrosion of copper over a wide range of controlled conditions.

In the present investigation, which was partially sponsored by the Corrosion Research Council, Dr. Jerome Kruger of the Bureau's corrosion laboratory immersed copper single crystals in water and found that irradiation retarded subsequent copper oxide growth. The copper crystals, which were grown from copper of 99.99% purity, were submerged in air-saturated, distilled water. All light was excluded from the highly polished copper crystal except that which shone through a small aperture in the jacket.

After 3 hr of uniform illumination at room temperature by a 3200°K tungsten lamp, the entire crystal sphere was found to be much less oxidized than when illuminated by room light. To study this effect further, one half of the crystal was illuminated with the intense white light from the tungsten lamp. It was found that the irradiated portion had oxidized at a markedly different rate than the unilluminated area. An electrometric measuring technique showed a film thickness of 120Å on the exposed side and an average film thickness of 500Å on the other side.

When similar light was allowed to impinge on part of a crystal already coated with a thick film (1000-2000Å), the oxide on the illuminated portion became considerably thinner than on the unexposed part of the crystal. X-ray diffraction studies of the films found on both the dark and the irradiated parts of the crystal showed that the films were composed of well-oriented cuprous oxide.

Although the mechanism for this behavior is not known, a possible explanation centers on the semiconductance of cuprous oxide. Irradiation would cause an electron flow from the cation-deficient semiconductor film of Cu_2O into the metal. This direction of flow is just opposite to that during oxide growth and hence could block further propagation of the oxide. Other investigators[2,3] have found that light favors oxidation of aluminum and tantalum whose oxides are cation-excess semiconductors.

[1] Inquiries concerning further information on copper corrosion should be addressed to Dr. Jerome Kruger, Corrosion Metallurgy Lab., National Bureau of Standards, Washington 25, D. C.

[2] N. Cabrera, *et al., Compt. rend.*, 224, 1558 (1947).

[3] D. A. Vermilyea, *J. Appl. Phys.*, 26, 489 (1955).

December 1958 Discussion Section

A Discussion Section, covering papers published in the January-June 1958 JOURNALS, is scheduled for publication in the December 1958 issue. Any discussion which did not reach the Editor in time for inclusion in the June 1958 Discussion Section will be included in the December 1958 issue.

Those who plan to contribute remarks for this Discussion Section should submit their comments or questions in triplicate to the Managing Editor of the JOURNAL, 1860 Broadway, New York 23, N. Y., *not later than September 1, 1958.* All discussions will be forwarded to the author(s) for reply before being printed in the JOURNAL.

Single Issues of 1956 Journals Available

A limited number of single issues of the 1956 JOURNAL of the Society, May-December, Vol. 103, No. 5-12, are available from: Librarian, Semiconductor Div., Motorola, Inc., 5005 E. McDowell Rd., Phoenix, Ariz.

"Industry Fights Corrosion"

The full "Proceedings" of the Corrosion Convention, held in London in October 1957, is now available. Organized by *Corrosion Technology*, the Convention was attended by over 500 delegates from the United Kingdom, Europe, and America. Thirteen papers dealing with different aspects of the corrosion problem were delivered and discussed over two days. Subjects covered included corrosion in the shipping, petroleum, atomic energy, and chemical industries; metals, paints, and plastics were discussed. Other subjects included packaging, water treatment, cathodic protection, fuel additives, hot galvanizing, and the protection of buried pipes.

The "Proceedings" contains over 100 pages, including full texts of all papers delivered, together with reports of the ensuing discussions. The volume is illustrated and costs 21s., post free, from *Corrosion Technology*, Leonard Hill House, 9 Eden St., London, N. W. 1.

Translation of Russian Publications

Pergamon Institute to Make Available Results of Research and Development in the U.S.S.R. and Other Soviet Orbit Countries

Pergamon Institute, a nonprofit foundation, has recently been formed in Washington, D.C., for the purpose of making available to English-speaking scientists, doctors, and engineers (from all countries that are members of the United Nations) the results of scientific, technological, and medical research and development in the Soviet Union and other countries in the Soviet orbit.

As a result of recently announced scientific and technological developments in the U.S.S.R. there is a great need, as well as pressure, from scientists, universities, government departments, and industrial firms, to overcome the language barrier and to make available rapidly in English the significant results of research and development in the U.S.S.R. in the fields of science, technology, and medicine.

It is one of the primary tasks of the Pergamon Institute to fill this need quickly by the initiation of large-scale translation programs of complete journals and books, as well as individual papers, in all the critical fields of science, technology, and medicine.

The following are the projects which have already been started or are being planned by the Institute in association with and with the financial assistance of various Government departments, learned societies, and private organizations, and some of the services which are available.

1. It is planned to hold a symposium during the summer of 1958 either in Washington or London, sponsored by the Institute and several interested universities, to examine the following problems: (*a*) how to assist with the establishment of extra-curricular courses for the teaching of Russian in the science, medical, and engineering faculties at higher seats of learning in the English-speaking world; (*b*) how to teach the reading of Russian scientific and technical texts to scientists and technologists in the minimum amount of time; (*c*) what tools of learning are required.

2. Discussions are taking place with the relevant authorities in the U.S.S.R. on the commissioning of a series of review volumes, with complete bibliographies, covering broad areas of Russian scientific, medical, and technical progress for the period 1920-56.

3. The Institute now publishes ten Russian journals in English translation. These are chiefly in the fields of medicine, physics, and metallurgy. Some of these programs have financial support from the National Institute of Health, the National Science Foundation, and the Board of Governors of *Acta Metallurgica*.

4. The Institute is also assisting with the translation and publication of important Russian books on science, technology, and medicine, and some of the titles will soon be available in English, including the work of Academician N. Semenov, who recently shared the Nobel Award for Chemistry with Sir Cyril Hinshelwood, and the classic course of Theoretical Physics by Academician Landau and his colleague, Professor Lifshitz.

For information as to these and other bibliographical and translation services, those interested should write to the Pergamon Institute, 122 E. 55 St., New York 22, N. Y.

English Translation of Abstracts of "Reports" of Fourth Conference on Electrochemistry Held in U.S.S.R.

A complete English translation of the Abstracts of the "Reports" of the Fourth Conference on Electrochemistry which took place in the U.S.S.R., October 1-5, 1956, will be published by Consultants Bureau, Inc., of New York. This monograph, running 112 pages in Russian, includes extended abstracts of 121 papers and will be sold in multilithed form for $12.00; individual abstracts will not be available. Translation was started in April and is expected to be completed this July.

Like its predecessor conferences, this meeting brought together most of the Soviet Union's most eminent electrochemists for a review of progress since the Third Conference held in 1950. The opening paper, appropriately enough, was a review by A. N. Frumkin on advances in the study of electrochemical reaction mechanisms in the period between conferences.

The following list of topics and the number of papers in each field will indicate the scope of the meeting.

General Questions of Electrochemical Kinetics and the Reaction Mechanism of Electrochemical Reactions, 22 papers.
The Mechanism of Electrode Processes in Melts, 11 papers.
Diffusion Kinetics, 8 papers.
The Mechanism of Oxidation, 8 papers.
Metal Passivity and Chemisorbed Layers, 10 papers.
Electrodeposition of Metals, 30 papers.
Chemical Current Sources (Batteries), 14 papers.
Electrolysis in Chemical Industry, 9 papers.
Electrochemical Processes in Non-Ferrous Metallurgy, 9 papers.

Titles of some of the more interesting and important abstracts are given below.

A. N. Frumkin—"Some Results of Development in the Study of Electrochemical Reaction Mechanisms in the Past Five Years."
L. I. Antropov—"The Kinetics of Electrochemical Reactions and the Zero Points of Metals."
S. I. Zhdanov and V. I. Zykov—"The Mechanism of Electrochemical Reduction of Some Oxygen-Containing Anions."
O. A. Esin—"Electrode Processes in Molten Oxides."
V. P. Mashovets—"The Mechanism of the Discharge of Oxygen-Containing Anions from Melts at a Carbon Anode."

I. D. Panchenko—"The Equation for the Polarographic Wave on Solid Electrodes in Molten Salts."

V. G. Levich—"The Diffusion Kinetics of Electrochemical Reactions."

N. D. Tomashov and Yu. N. Mikhailovsky—"The Electrochemical Kinetics of Corrosion Processes under Adsorbed Films of Moisture."

A. I. Krasilshchikov—"The Electrochemical Reactions of Oxygen."

Ya. V. Durdin, L. Kish, and B. I. Kravtsov—"The Application of the Oscillographic Method to the Study of the Kinetics of Electrode Processes Taking Place on the Surface of Dissolving Metals."

A. T. Vagramyan—"The Non-Uniformity of Cathode Surface and the Process of Metal Electrodeposition."

A. I. Levin and E. A. Ukshe—"The Role of Cathode Surface Charge in the Process of Metal Electrodeposition."

B. V. Drozdov—"The Cathodic Deposition of a Metal in a Dispersed Form."

G. A. Tsyganov, A. I. Chernilovskaya, and A. I. Iosilevich—"The Separation Coefficient in the Simultaneous Electrodeposition of Metals of the Iron Group."

E. V. Krivolapova, E. S. Weissberg, and B. N. Kabanov—The Study of the Lead Dioxide Electrode from the Potential Decay and the Evolution of Oxygen."

T. G. Lyapuntsova—"The Preparation of Oxide Electrodes by Anodic Deposition."

P. D. Lukovtsev—"The Theory of the Processes Taking Place on Oxide Electrodes in Chemical Sources of Current."

S. A. Rozentsveig and V. I. Levina—"The Mechanism of the Activation of an Iron Electrode by Means of Small Additions of Nickel Oxides."

V. S. Daniel-Bek, M. Z. Mints, V. V. Sysoeva, and M. V. Tikhonova—"The Study of Fuel Cells with Solid Electrodes."

N. A. Shurmovskaya and R. Kh. Burshtein—"The Iron-Carbon Cell."

K. G. Ilyin and V. I. Skripchenko—"The Influence of the Nature of the Electrolyte Cation on the Anodic Process in the Electrolysis of Solutions of the Chlorides of the Alkali and Alkaline Earth Metals."

V. V. Stender—"Electrolysis as a Means of Interconnecting Certain Metallurgical and Chemical Manufacturing Processes."

Yu. K. Delimarsky, B. F. Markov, E. B. Gitman, A. A. Koloty, and I. D. Panchenko—"The Electrolytic Refining of Lead from Molten Salts."

"Gas Light" for Brussels Fair

A special exhibit of a fuel cell, which produces electrical energy from the electrochemical combination of oxygen and hydrogen, assembled in the research laboratories of National Carbon Co., is among the scientific exhibits at the Brussels World's Fair. Further improvements have been made in the efficiency of the fuel cell since its announcement last September, and more compact units are now being tested. By designing the hydrogen and oxygen electrodes, made of specially treated porous carbon, as concentric cylinders to nestle within each other, researchers have produced a fuel cell that will operate on hydrogen gas and the oxygen in the air, eliminating the need for a source of pure oxygen. Although this method of operation is still far from commercial use, it is an important milestone in the development of the fuel cell into a commercial and industrial source of power.

Dr. Clarence E. Larson, National Carbon's research vice-president, examines the Brussels demonstration unit which lights up a bank of sealed beam lamps to indicate visually the power being produced.

Advance Tables of Contents, in English, of Soviet Journals Being Published in Translation

A monthly guide to current Soviet research, each issue of which will contain English titles of all papers appearing in the most recent issues of the 39 Soviet journals currently being translated into English, is to be published by Consultants Bureau, Inc., beginning in May of this year. This guide, entitled "Express Contents of Soviet Journals," will make it possible for Western researchers to know the contents of Soviet periodicals published as recently as two months previously, and from two to six months before the complete translations are published.

"Express Contents" will include the Tables of Contents of Soviet scientific and technical journals (in all fields) which are being published in English translation by Consultants Bureau, by other private agencies, or by scientific societies. Anticipation of translation needs will be made possible by a feature of Express Contents: Each Table of Contents included will cite the estimated date of publication of the specific issue in translation, as well as pertinent information as to publisher, subscription price, and individual issue/article price. This unique service, which began with a May 1958 issue, will be available on an annual subscription basis at $25.00, from Consultants Bureau, Inc., 227 W. 17 St., New York 11, N. Y. As cover-to-cover translations of other journals are undertaken, their Tables of Contents will be included.

Library of Congress Changes Titles of Two Monthlies Indexing in English New Soviet and East European Publications

Effective as of February 1958, the names of two Library of Congress monthly publications, which serve as keys to new literature coming into this country from the U.S.S.R. and East Europe, were changed from "Lists" to "Indexes."

The *Monthly List of Russian Accessions*, which entered its 11th year of publication in April 1958, becomes the *Monthly Index of Russian Accessions*. The Government Printing Of-

fice sells it for $12.00 a year ($15.00 abroad).

The *East European Accessions List*, published since 1951, becomes the *East European Accessions Index*. The GPO sells it for $10.00 a year ($12.50 abroad).

The change in the names of the two bibliographies does not mean a change in the editorial content of either one. It should also be noted that they contain information *about* the content of books and articles, *not* translations of entire books and articles.

Each index gives in English a monthly account of new material in a variety of subject fields as received from the U.S.S.R. and East Europe by the Library of Congress and by other American research libraries. The translation of all titles of books and articles into English and the elaborate subject guides in English permit a researcher who has no command of Russian or East European languages to identify easily the material important to him.

The indexes are of particular value to the scientist. For example, 54% of the books and periodicals reported in Vol. 9 (April 1956-March 1957) of the *Monthly Index of Russian Accessions* were in the field of science and technology. Scientists seeking information on current Russian achievements in this field, on which nation-wide interest has been focused by the launching of Russian and American satellites, can locate much of the related documentation through this bibliography.

New Members

In March 1958 the following were elected to membership in The Electrochemical Society by the Admissions Committee:

Active Members Sponsored by a Sustaining Member

Robert M. Brick, Continental Can Co., Inc., 7622 So. Racine Ave., Chicago 20, Ill. (Corrosion)

Donald F. Brookland, Keokuk Electro-Metals Co., 320 Concert St., Keokuk, Iowa (Electrothermics & Metallurgy)

Robert H. Dalton, Corning Glass Works, Corning, N. Y. (Electronics)

Richard W. McQuaid, Catalyst Research Corp., 6101 Falls Rd., Baltimore, Md. (Battery)

Robert A. Spurr, Hughes Aircraft Co., Culver City, Calif. (Electronics)

Donald Trevoy, Eastman Kodak Co., Kodak Park, Rochester, N. Y. (Corrosion)

By action of the Board of Directors of the Society, all prospective members must include first year's dues with their applications for membership.

Also, please note that, if sponsors sign the application form itself, processing can be expedited considerably.

Active Members

Alexis G. Basilevsky, North American Solvay, Inc., 50 Broadway, New York, N. Y. (Industrial Electrolytic, Theoretical Electrochemistry)

William R. Benn, Electro Metallurgical Co., P.O. Box 330, Niagara Falls, N. Y. (Corrosion, Electrothermics & Metallurgy, Industrial Electrolytic)

Edwin J. Bills, Joseph Lucas, Ltd.; Mail add: 17 George Frederick Rd., Sutton Coldfield, England (Battery)

Martin A. Blumenfeld, Sperry Gyroscope Co. Inc.; Mail add: 249 E. 87 St., Brooklyn 36, N. Y. (Electrodeposition)

Hans J. Borchardt, General Electric Co.; Mail add: 22 Cedar Lane, Scotia 2, N. Y. (Theoretical Electrochemistry)

Guy Dumas, S.I.L.E.C., 92, Ave. du général de Gaulle, La Garenne Colombes (Seine), France (Electronics)

K. S. G. Doss, Central Electrochemical Research Institute, Karaikudi, India (Theoretical Electrochemistry)

John F. Elliott, Rm. 8-109, Massachusetts Institute of Technology, Cambridge 39, Mass. (Electrothermics & Metallurgy, Theoretical Electrochemistry)

Herbert Epstein, Patent Dept., Philco Corp., Tioga & C Sts., Philadelphia 34, Pa. (Electrodeposition, Electronics)

William R. Eubank, Minnesota Mining & Mfg. Co., 2301 Hudson Rd., St. Paul 6, Minn. (Electronics, Electrothermics & Metallurgy)

Joseph A. Falcone, Solvay Process Div., Allied Chemical Corp.; Mail add: 609 So. Madison Ave., Glendale (Marshall County), W. Va. (Industrial Electrolytic)

Frederick H. Giles, Jr., Physics Dept., University of South Carolina, Columbia, S. C. (Corrosion, Electrodeposition, Electronics, Theoretical Electrochemistry)

Paul Goldberg, Sylvania Electric Products Inc., 35-22 Linden Place, Flushing 54, N. Y. (Electronics)

Kenneth F. Greene, I.B.M. Corp., Dept. 559, Poughkeepsie, N. Y. (Electrodeposition, Electronics)

Kalman Held, Technical Research Group, Inc., 17 Union Square West, New York, N. Y. (Electrothermics & Metallurgy, Industrial Electrolytic)

Johan B. Holte, Norsk Hydro-Elektrisk Kvaelstofaktieselskab, Solligt. 7, Oslo, Norway (Electrothermics & Metallurgy)

Brian E. Hopkinson, Research Lab., International Nickel Co., Inc., Bayonne, N. J. (Corrosion, Electrothermics & Metallurgy, Theoretical Electrochemistry)

Jiri Jansta, Research Institute for Electrotechnical Physics; Mail add: Vupef, Karlovo Namesti F, Prague 2, Czechoslovakia (Battery)

Theodore B. Johnson, Remington Arms Co., Inc., 939 Barnum Ave., Bridgeport 2, Conn. (Battery)

Herman Kerst, Dearborn Chemical Co.; Mail add: 310 Woodbridge Rd., Des Plaines, Ill. (Corrosion, Theoretical Electrochemistry)

Harold W. Kerster, University of Chicago; Mail add: 4843 So. Lake Park Ave., Chicago 15, Ill. (Electronics)

Robert A. Keyes, Robert A. Keyes Associates, 821 Franklin Ave., Garden City, N. Y. (Battery, Electronics)

Aloysius E. Knotowicz, Patent Button Co.; Mail add: 77 Hoffman St., Torrington, Conn. (Electrodeposition)

Paul A. Krasley, Chemistry Dept., National Bureau of Standards, Van Ness at Conn. Ave., N. W., Washington 25, D. C. (Electrodeposition)

John F. McCormack, Photocircuits Corp., 31 Sea Cliff Ave., Glen Cove, N. Y. (Electrodeposition)

Laurence P. McGinnis, Diamond Ordnance Fuse Labs.; Mail add: 2213 Apache St., Adelphi, Md. (Battery)

Geoffrey W. Mellors, Research Labs., National Carbon Co., P.O. Box 6116, Cleveland 1, Ohio (Battery, Electrodeposition, Electrothermics & Metallurgy, Theoretical Electrochemistry)

Paul C. Milner, Bell Telephone Labs., Inc., Murray Hill, N. J.

Correction

In the paper "Dissolution of Metals in Aqueous Solutions, II. Depolarized Dissolution of Mild Steel" by A. C. Makrides and N. Hackerman which appeared in the March 1958 JOURNAL, Vol. 105, No. 3 pp. 156-162, Eq. (VII) and (XIIb) should read:

$$k = 0.0791\, V\, (R_d)^{-0.30}\, (Pr)^{-0.644} \quad \text{(VII)}$$

and

$$k \approx 0.01\, (Pr)^{-0.644}\, V \quad \text{(XIIb)}$$

(Battery, Electrodeposition, Theoretical Electrochemistry)

Robert G. Milner, National Carbon Co., 3625 Highland Ave., Niagara Falls, N. Y. (Industrial Electrolytic)

John J. Murphy, U. S. Army Signal Engineering Labs.; Mail add: 12 Narumsunk St., Rumson, N. J. (Battery)

Ralph H. Nelson, Ray-O-Vac Co.; Mail add: 117 So. Butler St., Madison, Wis. (Electronics)

René A. Paris, Compagnie de Produits Chimiques et Electrométallurgiques Pechiney; Mail add: 23, rue Balzac, Paris, France (Electrothermics & Metallurgy, Industrial Electrolytic, Theoretical Electrochemistry)

John T. Porter, II, Corning Glass Works, Box 544, Corning, N. Y. (Theoretical Electrochemistry)

Willard J. Pugh, Jr., Cleveland Electric Illuminating Co., 75 Public Square, Cleveland, Ohio (Electrodeposition, Electrothermics & Metallurgy, Industrial Electrolytic)

Carl W. Raetzsch, Jr., Columbia Southern Chemical Corp., Box 4026, Corpus Christi, Texas (Industrial Electrolytic)

P. S. Rajasekhar, Hughes Products, M.S. 1061, 5315 W. 102 St., Los Angeles 45, Calif. (Electronics)

Maurice Rand, Ethicon, Inc., Somerville, N. J. (Corrosion, Electrodeposition)

Floyd F. Rawlings, Jr., Monmouth College, Monmouth, Ill. (Electro-Organic)

Bernd Ross, Wesson Metal Corp., Lysle Rd., Lexington, Ky. (Electronics)

Francis J. Schmidt, Reduction Research Lab., Reynolds Metals Co., P.O. Box 191, Sheffield, Ala. (Electrodeposition, Electronics, Electrothermics & Metallurgy, Industrial Electrolytic, Theoretical Electrochemistry)

Alexander G. Scobie, Shawinigan Chemicals, Ltd., Shawinigan Falls, Quebec, Canada (Electrodeposition, Electrothermics & Metallurgy, Industrial Electrolytic)

Wilfrid S. Sherk, Electro Metallurgical Co., Div. of Union Carbide Corp., Niagara Falls, N. Y. (Electrothermics & Metallurgy)

Ralph B. Soper, Sylvania Electric Products Inc.; Mail add: 28 Stanley St., North Weymouth 91, Mass. (Electrodeposition, Electronics)

Ronald W. Spafford, Electro Metallurgical Co., 805 Davenport Rd., Toronto 4, Ont., Canada (Electrothermics & Metallurgy)

Arthur W. Todd, Lincoln Electric Co., Box 3115, Cleveland 17, Ohio (Electronics)

Norval E. Toepfer, National Carbon Co., Div. of Union Carbide Corp., P.O. Box 6056, Cleveland, Ohio (Battery)

Aladar Tvarusko, Ray-O-Vac Co., 525 University Ave., Madison 10, Wis. (Electronics)

Joseph F. Wenckus, Airtron, Inc.; Mail add: 67 Lexington Rd., Concord, Mass. (Electronics, Electrothermics & Metallurgy)

Associate Members

Marion K. A. P. Poland, Ray-O-Vac Co., 525 University Ave., Madison 10, Wis. (Battery)

James C. Withers, Melpar, Inc.; Mail add: 204 Ashby Place, Fairfax, Va. (Theoretical Electrochemistry)

Student Associate Members

Seymour Lowell, New York University; Mail add: 64 Edwards St., Roslyn Heights, L. I., N. Y. (Corrosion, Theoretical Electrochemistry)

Stuart G. Meibuhr, Western Reserve University; Mail add: 15705 Chatfield Ave., Cleveland 11, Ohio (Electrodeposition, Theoretical Electrochemistry)

Arthur M. Wilson, Northwestern University; Mail add: 619 Garrett Place, Evanston, Ill. (Theoretical Electrochemistry)

Transfers from Student to Active Membership

John R. Aylward, Phillips Petroleum Co.; Mail add: 565 8th St., Idaho Falls, Idaho (Battery, Theoretical Electrochemistry)

Edward F. Duffek, Stanford Research Institute; Mail add: 182 El Carmelo St., Palo Alto, Calif. (Corrosion, Electrodeposition, Electro-Organic, Theoretical Electrochemistry)

John J. Hoekstra, Dow Chemical Co.; Mail add: 2424 Damman Dr., Apt. 202, Midland, Mich. (Battery, Electrodeposition, Theoretical Electrochemistry)

Perry Niel Yocom, RCA Labs.; Mail add: 276 Nassau St., Princeton, N. J. (Electronics, Theoretical Electrochemistry)

Transfers from Associate to Active Membership

Yeichi B. Katayama, General Electric Co.; Mail add: 1200 Wilson St., Richland, Wash. (Corrosion, Electrodeposition, Electronics, Electrothermics & Metallurgy)

Jack E. Norbeck, General Electric Co.; Mail add: 323 Bonniewood Dr., Cleveland 10, Ohio (Electronics)

James Y-N. Wang, Crane Co.; Mail add: 5547 So. Merrimac Ave., Chicago 38, Ill. (Corrosion, Electrodeposition)

Transfers from Student Associate to Associate Membership

Rajendra P. Khera, National Research Council of Canada, Sussex St., Ottawa 2, Ont., Canada (Corrosion, Theoretical Electrochemistry)

Frank J. Marasa, 34-22 Astoria Blvd., Long Island City 3, N. Y. (Electronics)

Reinstatement to Active Membership

Robert F. Cree, Foote Mineral Co.; Mail add: 16 Woodcrest Rd., West Chester, Pa. (Electronics)

Manuscripts and Abstracts for Spring 1959 Meeting

Papers are now being solicited for the Spring Meeting of the Society, to be held at the Sheraton Hotel in Philadelphia, Pa., May 3, 4, 5, 6, and 7, 1959. Technical sessions probably will be scheduled on Electric Insulation, Electronics (including Luminescence and Semiconductors), Electrothermics and Metallurgy, Industrial Electrolytics, and Theoretical Electrochemistry.

To be considered for this meeting, triplicate copies of abstracts *(not to exceed 75 words in length)* must be received at Society Headquarters, 1860 Broadway, New York 23, N. Y., *not later than January 2, 1959. Please indicate on abstract for which Division's symposium the paper is to be scheduled.* Complete manuscripts should be sent in triplicate to the Managing Editor of the JOURNAL at the same address.

★ ★ ★

The Fall 1959 Meeting will be held in Columbus, Ohio, October 18, 19, 20, 21, and 22, 1959, at the Deshler-Hilton Hotel. Sessions will be announced in a later issue.

Deceased Members

J. H. Critchett, Orleans, Mass.
P. B. Francis, Kansas City, Mo.
Arne J. Moller, Copenhagen, Denmark
W. R. Whitney, Schenectady, N. Y.

Book Reviews

Solid State Physics, Vol. 4. Frederick Seitz and David Turnbull, Ed. Published by Academic Press Inc., New York, 1957. 540 pages; $12.00

The "Solid State Physics" series is steadily becoming encyclopedic and, as no attempt is made to concentrate articles about one branch of solid-state physics in one volume, most chemists and physicists in the field will find at least one article of interest to them. In Vol. 4, two of the four articles, namely "Ferroelectrics and Antiferroelectrics," and "Theory of Mobility of Electrons in Solids," each take up more than a third of the book.

The first review article covers comprehensively the subject of Ferroelectrics and Antiferroelectrics. It is written in a clear and competent manner by Werner Känzig and is one of the most complete accounts of this subject yet to appear; it has over 400 references. The article forms a valuable reference for experimental and theoretical work prior to mid-1957, and most of the known fundamental physical properties of all the ferroelectrics and antiferroelectrics discovered by that time are included. Rightly, from the point of view of solid-state physicists, the emphasis is on the properties of single crystals with little or no mention of polycrystalline materials. After a general introduction to the subject, the author describes in detail the dielectric, electromechanical, and polarization properties of ferroelectrics together with an account of certain optical properties and phenomena closely associated with phase transitions. The properties of antiferroelectrics are satisfactorily covered and there is a brief description of the basic behavior of mixed crystals. The crystal structures and the transitions responsible for the ferroelectric and antiferroelectric properties, where known, are described in a straightforward manner. The formal thermodynamic theories of ferroelectrics and antiferroelectrics are discussed and there is a section devoted to various molecular models. The account of static domain structures

(Continued on page 112C)

ECS Membership Statistics

The following three tables give breakdown of membership as of April 1, 1958. The Secretary's Office feels that a regular accounting of membership will be very stimulating to membership committee activities. In Table I it should be noted that the totals appearing in the right-hand column are *not* the sums of the figures in that line since members belong to more than one Division and, also, because Sustaining Members are not assigned to Divisions. But the totals listed are the total membership in each Section. In Table I, Sustaining Members have been credited to the various Sections.

Table I. *ECS Membership by Sections and Divisions*

Section	Division: Battery	Corrosion	Electric Insulation	Electro-deposition	Electronics	Electro-Organic	Electrothermics & Met.	Industrial Electrolytic	Theoretical Electrochem.	No Division	Total as of 1/1/58	Total as of 4/1/58	Net Change
Boston	13	26	6	33	51	8	20	13	23	6	131	131	0
Chicago	15	35	4	44	23	10	13	14	22	12	111	124	+13
Cleveland	58	37	2	50	40	9	27	31	38	15	203	200	— 3
Columbus, Ohio	1	12	0	13	4	2	21	3	8	5	45	43	— 2
Detroit	7	19	5	47	7	7	7	6	18	20	84	85	+ 1
India	8	7	3	18	8	7	10	14	12	3	36	34	— 2
Indianapolis	11	7	3	11	11	4	5	3	5	2	40	41	+ 1
Midland	9	15	0	5	2	2	7	16	10	2	45	42	— 3
Mohawk-Hudson	5	15	13	9	12	1	6	3	12	4	51	52	+ 1
New York	82	100	23	137	126	31	66	67	93	43	482	489	+ 7
Niagara Falls	16	24	1	23	7	5	75	66	30	23	175	185	+10
Ontario-Quebec	12	24	1	16	2	3	35	27	8	15	75	78	+ 3
Pacific Northwest	5	11	0	10	2	1	8	10	9	10	47	44	— 3
Philadelphia	24	30	3	34	57	12	22	17	47	29	174	170	— 4
Pittsburgh	4	47	3	27	27	4	37	17	35	9	130	131	+ 1
San Francisco	5	13	2	20	15	4	15	22	22	4	64	68	+ 4
Southern Calif.-Nevada	14	19	2	23	26	3	14	16	20	10	95	95	0
Washington-Baltimore	36	41	8	39	22	3	9	9	30	6	128	129	+ 1
U. S. Non-Section	53	90	13	85	68	43	59	73	112	33	395	393	— 2
Foreign Non-Section	40	59	5	62	29	29	36	60	71	83	224	250	+26
Total as of Jan. 1, 1958	409	638	100	705	518	193	479	485	620	313	2735		
Total as of April 1, 1958	418	631	97	706	539	188	492	487	625	334		2784	

Table II. *ECS Membership by Grade*

	Total as of 1/1/58	Total as of 4/1/58	Net Change
Active	2448	2367	—81
Faraday (Active)	—	26	+26
Deutsche Bunsen Gesellschaft (Active)	—	9	+ 9
Delinquent	61	148	+87
Active Representative Patron Members	8	10	+ 2
Active Representative Sustaining Members	70	82	+12
Total Active Members	2587	2642	+55
Life	16	16	0
Emeritus	54	51	— 3
Associate	31	33	+ 2
Student	42	38	— 4
Honorary	5	4	— 1
	2735	2784	+49

The figures pertaining to Patron and Sustaining Member Representatives, and Faraday and Deutsche Bunsen Gesellschaft members subscribing to the JOURNAL, have been added to reflect reclassifications and changes in membership status.

Table III. *ECS Patron and Sustaining Membership*

	Total as of 1/1/58	Total as of 4/1/58	Net Change
Patron Member Companies	4	5	+ 1
Sustaining Member Companies	127	136	+ 9

is adequate but it is a pity that fuller accounts are not given of the dynamic properties of domains and the theories of domain walls. That there is no discussion of the techniques of growing the crystals may also disappoint some readers.

The second article by F. J. Blatt is a broad and very comprehensive review which has been given the catch-all title of the "Theory of Mobility of Electrons in Solids." Actually, it is a valuable review of the fundamental conduction processes which occur in metals and semiconductors, excluding the fields of ionic conductivity and superconductivity. The steady-state effects of electric and magnetic fields and thermal gradients applied to homogeneous conductors and semiconductors are treated in great detail and in an authoritative manner. The emphasis is on theory, but a good deal of attention is paid to experimental results. The reader may be surprised at the vast activity and the progress which has been made in this field recently; the 332 references are, for the most part, to work only a few years old.

The third article by Truman O. Woodruff, entitled "The Orthogonalized Plane-Wave Method," is a detailed technical description of the application of this technique for the calculation of electron-wave functions and energy eigenvalues in crystals. Following a general description of the method, a survey of its applications is given. Particular attention is given to Herman's use of the technique for diamond lattice crystals and the author's own application of the method to silicon. This last calculation is presented in some detail to illustrate the procedure.

The author's avowed purpose is to discuss the orthogonalized plane-wave method in a manner which ". . . will be particularly useful to anyone who wishes to apply (it) or appreciate its limitations." This purpose justifies the rather detailed description of the computations. The result is a pedagogical review which is perhaps too technical for the completely uninitiated. However, it should prove useful for the student with an understanding of quantum mechanical procedures who wishes to acquaint himself with an approach which has been exceedingly helpful in understanding the physical properties of metals and semiconductors.

The following article by Robert S. Knox, "Bibliography of Atomic Wave Function," consists of a listing of 117 references concerning the wave functions for 120 atoms and ions of 44 elements.

W. G. Pfann's chapter on "Techniques of Zone Melting and Crystal Growing" is a review of the principles and processes of purification, impurity control, and crystal growing by the solidification of melts. As one of the major contributors to the development of these processes, the author is well qualified to discuss them. The review is comprehensive without being overly detailed, clearly written, and summarizes in one article the numerous modifications of solidification procedures that have been used or suggested for impurity control. The subject matter and tone are somewhat more experimentally oriented than the average review in the "Solid State Physics" series. However, the topic should be of intense interest to the solid-state physicist whose experimental results can be no better defined than the material he has used.

The author begins with a definition and discussion of the distribution coefficient. The thermodynamic significance of the distribution coefficient is only sketchily treated but the reader is given a thorough exercise in its application to various procedures of solidification. This is followed by a review of the mathematical analyses of zone processes. The mathematical description of impurity motion in zone processes is sufficiently difficult so that no general equation has been derived that can be simply and exactly solved. For this reason many computational methods have been derived that give sufficiently accurate results for specialized conditions. These methods are reviewed and their limitations discussed.

The experimental techniques of zone melting are comprehensively discussed, including continuous processes, floating zone, and temperature gradient zone melting. A complete bibliography of applications to semiconductors, metals, and other chemicals is also provided. The technique of zone leveling to produce uniform impurity distributions is treated and special procedures that cause controlled changes in impurity distributions are also discussed. The application of these techniques to semiconductor technology is reviewed. The final section is devoted to the principles and techniques of crystal growth from a melt, and to a discussion of the perfection of such crystals.

This chapter presents a very complete treatment of zone techniques in their application to solids, although, in an attempt to treat all methods of impurity control in solids, diffusion from the vapor is given a one-page treatment that can contribute little more than a few additional literature references. The final section on dislocations is unfortunately too short to do the subject justice, but somewhat too long for a chapter on zone melting and crystal growing. But this criticism is minor. The author has accomplished his purpose admirably and his contribution is certain to be of continuing value to the solid-state experimentalist.

A. G. Chynoweth
T. H. Geballe
M. Tanenbaum

Gmelins Handbook of Inorganic Chemistry, 8th Ed. Published by Verlag Chemie, GMBH., Weinheim/Bergstrasse, Germany, 1957. Available in U.S.A. through any American book importer.

Systematic Subject Index; 116 pages; $17.28.—Written in English and German, this volume is the key to the Gmelin classification system, covering the entire multivolume "Handbook." Each classification is given a code number for punch card systems.

System No. 28, Calcium, Part B, Section 2; 392 pages; $52.56.—This new edition covers the first part of the material on calcium compounds. It discusses, in addition to the normal bivalent compounds, CaCl and CaF, whose free molecules in the gaseous state can probably be considered to represent a lower valence of calcium and whose nature in the condensed phase is not sufficiently explained.

The volume covers hydrides, nitrides, the azide, imide, and amide, then the Ca-NH_3 system, the compound $Ca(NH_3)_6$, the halogens, and the salts of the oxygen acids of nitrogen, as well as the corresponding addition compounds, systems, and basic salts.

System No. 60, Copper, Part B, Section 1; 624 pages; $83.76.—The substances covered here are the hydrides, and the compounds of oxygen, nitrogen, halogens, sulfur, selenium, and tellurium. Emphasis is placed on compounds such as the azides, the compounds of monovalent copper, and the basic copper(II) salts of the type $\left[Cu\left(\begin{smallmatrix}-OH\\-OH\end{smallmatrix}\!\!>Cu\right)_3\right]X_2$.

In contrast to the procedure followed previously, the properties of minerals of these compounds are presented together with the synthetically derived salts.

H. W. Salzberg

Advertiser's Index

Letters to the Editor

Dear Sir:

At the end of your "Instructions to Authors of Papers" submitted to the JOURNAL of The Electrochemical Society, you have the following: "Units of Measurement: As regards algebraic signs of potentials, the standard electrode potential for $Zn \rightarrow Zn^{++} + 2e$ is negative; for $Cu \rightarrow Cu^{++} + 2e$, positive."

I would like to make the following comments on this instruction.

1. The term "electrode potential" has two meanings: (*a*) the potential of an electrode, (*b*) the potential of a corresponding half-reaction.

2. As regards meaning (*a*), the instruction given is, of course, in agreement with experiment. The zinc electrode in an aqueous solution of zinc ions of unit activity is negatively charged with respect to a standard hydrogen electrode. Similarly, a copper electrode in a cupric solution is positively charged.

3. As regards meaning (*b*), the potential or standard potential of a half-reaction depends on the way the reaction is written. Let us take the data for aqueous solutions at 25°C.

$$\begin{cases} Zn(c) + 2H^+ \rightarrow Zn^{++} + H_2(g), \\ \Delta G^\circ = -35.18 \text{ kcal}, E^\circ = +0.7627 \text{ v} \\ Zn^{++} + H_2(g) \rightarrow Zn(c) + 2H^+, \\ \Delta G^\circ = +35.18 \text{ kcal}, E^\circ = -0.7627 \text{ v} \end{cases}$$

Here G° is the standard Gibbs free energy, and the usual relation: $\Delta G^\circ = -n\mathbf{F}E^\circ$ has been used, where **F** is Faraday's constant and n is the number of equivalents reacting. If, in addition, we use the universal convention:

$$\begin{cases} 2H^+ + 2e^- \rightarrow H_2(g), & \Delta G^\circ = 0, E^\circ = 0 \\ H_2(g) \rightarrow 2H^+ + 2e^-, & \Delta G^\circ = 0, E^\circ = 0 \end{cases}$$

we obtain for the zinc half-reaction:

$$\begin{aligned} &Zn(c) \rightarrow Zn^{++} + 2e^-, \\ &\Delta G^\circ = -35.18 \text{ kcal}, E^\circ = +0.7627 \text{ v} \\ &Zn^{++} + 2e^- \rightarrow Zn(c), \\ &\Delta G^\circ = +35.18 \text{ kcal}, E^\circ = -0.7627 \text{ v} \end{aligned}$$

This is not in agreement with the instruction cited above.

May I therefore suggest that, from the point of view of (*b*) above, the instruction be amended to read: "Units of Measurement: As regards algebraic signs of potentials, the standard electrode potential in aqueous solution for $Zn^{++} + 2e^- \rightarrow Zn$ is negative; for $Cu^{++} + 2e^- \rightarrow Cu$, positive."

M. Spiro
Chemistry Dept.
University of Melbourne
Carlton, Victoria, Australia

[We agree that the above item in the "Instructions to Authors" needs revision.—Ed.]

Dear Sir:

I read your Editorial, "Automatic Cathodic Protection," in the February issue of the JOURNAL, and with your permission I would like to make a few comments.

Experience in the United States Navy with cathodic protection of ships has shown that current requirements to maintain a protective hull polarization potential are higher for ships in motion than for ships at rest. Current requirements also vary with the speed of motion. Thus, more current is required to maintain a protective potential of 0.85 volts vs. a standard reference electrode at 20 knots than at 5 knots. The washing action that removes the polarization film from the ship's hull is more effective at higher speeds. This is an apparent contradiction of the findings by the Canadian Navy, as stated in your Editorial. The very reason for some dual cathodic protection systems installed on some U. S. Naval ships was to provide an auxiliary current supply from an impressed-current installation to augment the current supply from a galvanic anode system if and when needed. The need generally arose at high speeds and when the deterioration of the paint system set in.

The automatic control of the current supply is not a dream but a reality. Several such controls in combination with specially designed, impressed-current cathodic protection systems are now under test by the U. S. Navy.

Automatic control of current supply can also be attained with galvanic anodes, such as high purity zinc, magnesium, or aluminum-zinc alloy. A sufficient number of either of these anodes distributed over the ship's hull or strategically located in groups on the hull will supply current as demanded. However, zinc has an efficiency of about 96%; aluminum, 56%; and magnesium, 50%.

The current potential, therefore, for zinc is about 335 amp-hr/lb, 750 amp-hr/lb of aluminum, and 500 amp-hr for magnesium. The driving voltage of zinc and aluminum is about 0.2 v to a polarized hull of 0.80 v, that of magnesium is about 0.75 v. Because of this high driving potential, magnesium anodes must be mounted on dielectric shields and the ship's hull must be painted with an alkali-resistant paint system, or controlled for current output by a variable resistance.

Boris H. Tytell
Chemical Lab.
Boston Naval Shipyard
Boston, Mass.

Employment Situations

Please address replies to box shown, c/o The Electrochemical Society, Inc., 1860 Broadway, New York 23, N. Y.

Positions Available

Engineers (Aeronautical, Electrical, Electronic, Industrial, General, Mechanical, and Power Plant), **Electronic Scientists, Metallurgists, Physicists, Technologists**—Vacancies exist for professional personnel in the above positions. Starting salaries range from $4480 per annum to $8645 per annum. The Naval Air Material Center is currently engaged in an extensive program of aeronautical research, development, experimentation, and test operations for the advancement of Naval aviation. Personnel are needed for work on projects involving modification, overhauling, and testing of aeronautical equipment, materials, accessories, power plants, launching and arresting devices, and for modification and structural testing of aircraft. Also, for work involving the basic design of catapults, launchers, arresting gear and their component parts; test and development work at shore stations and on board U. S. Navy ships; evaluation of new equipment and establishment of performance parameters, and applied research on the many problems relevant to this field.

Interested persons should file an Application for Federal Employment, Standard Form 57, with the Industrial Relations Dept., Naval Air Material Center, Naval Base, Philadelphia 12, Pa. Applications may be obtained from the above address, or information as to where they are available may be obtained from any first or second class post office.

The Electrochemical Society

Patron Members

Aluminum Company of Canada, Ltd., Montreal, Que., Canada
International Nickel Company, Inc., New York, N. Y.
Olin Mathieson Chemical Corporation, Niagara Falls, N. Y.
  Industrial Chemicals Division, Research and Development Department
Union Carbide Corporation
  Divisions:
    Electro Metallurgical Company, New York, N. Y.
    National Carbon Company, New York, N. Y.
Westinghouse Electric Corporation, Pittsburgh, Pa.

Sustaining Members

Air Reduction Company, Inc., New York, N. Y.
Ajax Electro Metallurgical Corporation, Philadelphia, Pa.
Allied Chemical & Dye Corporation
  General Chemical Division, Morristown, N. J.
  Solvay Process Division, Syracuse, N. Y. (3 memberships)
Alloy Steel Products Company, Inc., Linden, N. J.
Aluminum Company of America, New Kensington, Pa.
American Machine & Foundry Company, Raleigh, N. C.
American Metal Company, Ltd., New York, N. Y.
American Platinum Works, Newark, N. J. (2 memberships)
American Potash & Chemical Corporation, Los Angeles, Calif. (2 memberships)
American Zinc Company of Illinois, East St. Louis, Ill.
American Zinc, Lead & Smelting Company, St. Louis, Mo.
American Zinc Oxide Company, Columbus, Ohio
M. Ames Chemical Works, Inc., Glens Falls, N. Y.
Auto City Plating Company Foundation, Detroit, Mich.
Bart Manufacturing Company, Bellville, N. J.
Bell Telephone Laboratories, Inc., New York, N. Y. (2 memberships)
Bethlehem Steel Company, Bethlehem, Pa. (2 memberships)
Boeing Airplane Company, Seattle, Wash.
Burgess Battery Company, Freeport, Ill. (4 memberships)
C & D Batteries, Inc., Conshohocken, Pa.
Canadian Industries Ltd., Montreal, Que., Canada
Carborundum Company, Niagara Falls, N. Y.
Catalyst Research Corporation, Baltimore, Md.
Chrysler Corporation, Detroit, Mich.
Ciba Pharmaceutical Products, Inc., Summit, N. J.
Columbian Carbon Company, New York, N. Y.
Columbia-Southern Chemical Corporation, Pittsburgh, Pa.
Consolidated Mining & Smelting Company of Canada, Ltd., Trail, B. C., Canada (2 memberships)
Continental Can Company, Inc., Chicago, Ill.
Cooper Metallurgical Associates, Cleveland, Ohio
Corning Glass Works, Corning, N. Y.
Crane Company, Chicago, Ill.
Diamond Alkali Company, Painesville, Ohio (2 memberships)
Dow Chemical Company, Midland, Mich.
Wilbur B. Driver Company, Newark, N. J. (2 memberships)
E. I. du Pont de Nemours & Company, Inc., Wilmington, Del.
Eagle-Picher Company, Chemical Division, Joplin, Mo.
Eastman Kodak Company, Rochester, N. Y.
Eaton Manufacturing Company, Stamping Division, Cleveland, Ohio
Electric Auto-Lite Company, Toledo, Ohio
Electric Storage Battery Company, Philadelphia, Pa.
The Eppley Laboratory, Inc., Newport, R. I. (2 memberships)
Federal Telecommunication Laboratories, Nutley, N. J.
Food Machinery & Chemical Corporation
  Becco Chemical Division, Buffalo, N. Y.
  Westvaco Chlor-Alkali Division, South Charleston, W. Va.
Ford Motor Company, Dearborn, Mich.
General Electric Company, Schenectady, N. Y.
  Chemistry & Chemical Engineering Component, General Engineering Laboratory
  Chemistry Research Department

(Sustaining Members cont'd)

General Electric Company (cont'd)
Metallurgy & Ceramics Research Department
General Motors Corporation
Brown-Lipe-Chapin Division, Syracuse, N. Y. (2 memberships)
Guide Lamp Division, Anderson, Ind.
Research Laboratories Division, Detroit, Mich.
Gillette Safety Razor Company, Boston, Mass.
Gould-National Batteries, Inc., Depew, N. Y.
Graham, Savage & Associates, Inc., Jenkintown, Pa.
Great Lakes Carbon Corporation, New York, N. Y.
Hanson-Van Winkle-Munning Company, Matawan, N. J. (3 memberships)
Harshaw Chemical Company, Cleveland, Ohio (2 memberships)
Hercules Powder Company, Wilmington, Del.
Hooker Electrochemical Company, Niagara Falls, N. Y. (3 memberships)
Houdaille-Hershey Corporation, Detroit, Mich.
Hughes Aircraft Company, Culver City, Calif.
International Business Machines Corporation, Poughkeepsie, N. Y.
International Minerals & Chemical Corporation, Chicago, Ill.
Jones & Laughlin Steel Corporation, Pittsburgh, Pa.
K. W. Battery Company, Skokie, Ill.
Kaiser Aluminum & Chemical Corporation
Chemical Research Department, Permanente, Calif.
Division of Metallurgical Research, Spokane, Wash.
Keokuk Electro-Metals Company, Keokuk, Iowa
Libbey-Owens-Ford Glass Company, Toledo, Ohio
P. R. Mallory & Company, Indianapolis, Ind.
McGean Chemical Company, Cleveland, Ohio
Merck & Company, Inc., Rahway, N. J.
Metal & Thermit Corporation, Detroit, Mich.
Minnesota Mining & Manufacturing Company, St. Paul, Minn.
Monsanto Chemical Company, St. Louis, Mo.
Motorola, Inc., Chicago, Ill.
National Cash Register Company, Dayton, Ohio
National Lead Company, New York, N. Y.
National Research Corporation, Cambridge, Mass.
Norton Company, Worcester, Mass.
Olin Mathieson Chemical Corporation, Niagara Falls, N. Y.
High Energy Fuels Organization (2 memberships)
Pennsalt Chemicals Corporation, Philadelphia, Pa.
Philips Laboratories, Inc., Irvington-on-Hudson, N. Y.
Pittsburgh Metallurgical Company, Inc., Niagara Falls, N. Y.
Poor & Company, Promat Division, Waukegan, Ill.
Potash Company of America, Carlsbad, N. Mex.
Radio Corporation of America, Harrison, N. J.
Ray-O-Vac Company, Madison, Wis.
Raytheon Manufacturing Company, Waltham, Mass.
Reynolds Metals Company, Richmond, Va. (2 memberships)
Shawinigan Chemicals Ltd., Montreal, Que., Canada
Speer Carbon Company
International Graphite & Electrode Division, St. Marys, Pa. (2 memberships)
Sprague Electric Company, North Adams, Mass.
Stackpole Carbon Company, St. Marys, Pa. (2 memberships)
Stauffer Chemical Company, Henderson, Nev., and New York, N. Y. (2 memberships)
Sumner Chemical Company, Division of Miles Laboratories, Inc., Elkhart, Ind.
Superior Tube Company, Norristown, Pa.
Sylvania Electric Products Inc., Bayside, N. Y. (2 memberships)
Sarkes Tarzian, Inc., Bloomington, Ind.
Tennessee Products & Chemical Corporation, Nashville, Tenn.
Texas Instruments, Inc., Dallas, Texas
Titanium Metals Corporation of America, Henderson, Nev.
Udylite Corporation, Detroit, Mich. (4 memberships)
Upjohn Company, Kalamazoo, Mich.
Victor Chemical Works, Chicago, Ill.
Wagner Brothers, Inc., Detroit, Mich.
Weirton Steel Company, Weirton, W. Va.
Western Electric Company, Inc., Chicago, Ill.
Wyandotte Chemicals Corporation, Wyandotte, Mich.
Yardney Electric Corporation, New York, N. Y.

How to make plating upon aluminum an exact science: For many years, hundreds of manufacturers have been using Alumon,® an Enthone process, to prepare aluminum alloys for electroplating. Enthone chemists work out the plating cycles, give in-the-plant assistance. Alumon is an easy process to use and it costs less than ½¢ per square foot of surface plated! Write for literature about this economical and efficient process. Also find out about Etchalume,® Weldal,® and other specialized Enthone compounds for finishing aluminum. Enthone, Inc., 442 Elm Street, New Haven 11, Connecticut.

ENTHONE

ENTHONE, INC. IS A SUBSIDIARY OF AMERICAN SMELTING AND REFINING COMPANY